UNIVERSITY OF Cincinnati

Document of Defense

Date: 7/2/2024

I, Harsha Venkat Sai Naralasetty, hereby submit this original work as a part of the requirements for the degree of Doctor of Philosophy in Materials Science.

It is entitled:

Impact of Ultrasonic Nanocrystal Surface Modification on the Corrosion Behavior of Cold Sprayed and Additive Friction Stir Deposited 304L Austenitic Stainless Steel

Student Signature: Harsha Venkat Sai Naralasetty

This work and its defense approved by:

Chair :	Vijay Vasudevan, Ph.D.
Member :	Dinc Erdeniz, Ph.D.
Member :	Ashley Paz y Puente, Ph.D.
Member :	Matthew Steiner, Ph.D.

Impact of Ultrasonic Nanocrystal Surface Modification on the Corrosion Behavior of Cold Sprayed and Additive Friction Stir Deposited 304L Austenitic Stainless Steel

A dissertation submitted to the
Graduate College
of the University of Cincinnati
in partial fulfillment of the
requirements for the degree of

Doctor of Philosophy

in Materials Science and Engineering
in the Department of Mechanical and Materials Engineering
of the College of Engineering and Applied Science, University of Cincinnati,
Cincinnati, Ohio, USA
by

Harsha Venkat Sai Naralasetty

Bachelor of Technology, Metallurgical and Materials Engineering
Mahatma Gandhi Institute of Technology, Hyderabad, India.

September 2024

Committee Chair: Vijay K. Vasudevan, Ph.D.

Abstract

The welded austenitic 304 / 304L Stainless Steel (SS) Spent Nuclear Fuel Dry Storage Canisters (SNFDSCs), either newly built or the in-service ones, are facing a looming and insidious problem of Chloride Induced Stress Corrosion Cracking (CISCC). The construction of these large structured austenitic SNFDSCs involves welding which results in them undergoing the adverse phenomenon of sensitization at the welded areas making the newly built welded austenitic SNFDSCs susceptible to intergranular stress corrosion cracking.

Furthermore, in the case of in-service canisters situated near marine environment, the presence of chloride salts in the atmosphere aided by the tensile residual stresses present at the welded areas led to crack formation at the heat affected zones of the susceptible weldments due to CISCC. Therefore, to prolong the service life of in-service SNFDSCs and to avoid the catastrophes involved in their failures, long term reliable cost-effective in-situ repair methods such as Cold Spray (CS), Laser-Assisted Cold Spray (LACS), and Additive Friction Stir (AFS) deposition techniques have been considered as plausible solutions by the nuclear industry for repairing the CISC-Cracks in the existing canisters. However, the corrosion behavior (CB) of 304L SS material deposited through these three processing techniques remains unexplored.

Hence, a part of this dissertation research work aimed at studying the microstructural, mechanical, residual stress (RS), and most importantly, the CB of 304L SS material deposited by these three processing techniques along with that of the sensitized 304L SS material, which revealed that the sensitized, CS, LACS, and AFS 304L SS materials had inferior corrosion and/or residual stress properties owing to the differences in their microstructural characteristics from that of the bulk 304L SS material.

Therefore, to improve the corrosion properties of these four different 304L SS materials having distinct microstructural characteristics, the novel cost-effective mitigation technique of Ultrasonic Nanocrystal Surface Modification (UNSM), which is well-known to improve the Stress Corrosion Cracking (SCC) resistance of a material by the introduction of very high magnitudes of compressive residual stresses (CRSs), near-surface hardening, and nano-crystallization into the material through the induction of severe plastic deformation (SPD), has been employed in the current research work.

This hypothesis driven study led to the major focus of this dissertation research work which was to investigate how distinct prior microstructural characteristics of 304L SS alloy influence the impact of UNSM on its microstructure, hardness, RS, and CB. For this purpose, the impact of UNSM on the microstructure, dislocation density (DD), phases, hardness, RS, surface topography (ST), sensitization / susceptibility corrosion behavior (SCB), and pitting corrosion behavior (PCB) of sensitized, CS, LACS, and AFS 304L SS materials has been studied extensively and the obtained results with the performed thorough analysis led to some important hypothetical driven discoveries that are presented in detail in this dissertation.

The PCB of sensitized, CS, LACS, and AFS 304L SS materials in 3.5 Wt.% NaCl solution has been improved by UNSM attributed to it introducing tremendous magnitudes of CRSs into them up to an appreciable depth. Furthermore, the SCB of lightly sensitized and oxide-free polished surface of LACS 304L SS materials in 0.5M H_2SO_4 + 0.05M KSCN solution improved by ~ 10X and 2X times respectively by UNSM. However, UNSM had some limitations with respect to improving the SCB of heavily sensitized, as-sprayed LACS, as-deposited AFS, and the CS 304L SS materials. Additionally, the CS 304L SS coating possessing inherently weak interparticle bonding (WIB) and cold work (CW), limited the degree of enhancement and/or

disallowed any improvements being made to some of its properties by UNSM.

Nevertheless, despite the differences in the prior microstructural characteristics of sensitized, LACS, and AFS 304L SS materials, UNSM induced SPD into them resulting in extreme grain refinement, near-surface nano crystallization, immense increase in DD, austenite to martensite phase-transformation, tremendous increase in near-surface and sub-surface hardness, induction of extremely high magnitudes of CRSs up to an appreciable depth, in addition to the improvements in their CB, which are all beneficial in improving the SCC resistance of 304L SS.

Overall, this dissertation research work has demonstrated that UNSM can significantly enhance the microstructural, mechanical, RS, ST, SCB, corrosion rate, and PCB of 304L SS alloy with distinct prior microstructural characteristics except when it has WIB and/or prior CW present in the material, in which case only the near-surface hardness, RS, ST, and PCB can be improved by UNSM.

Preface

This dissertation has been submitted for the degree of Doctor of Philosophy at the University of Cincinnati. The research described herein was conducted in the Department of Mechanical and Materials Engineering at the University of Cincinnati between April 2019 and July 2024.

I declare that, except where otherwise stated, this dissertation is the result of my own work. No part of this dissertation has been previously submitted to the University of Cincinnati or any other University for a degree or diploma or other qualification.

Harsha Venkat Sai Naralasetty

September 2024

Acknowledgement

I am eternally grateful to my advisor, Dr. Vijay K. Vasudevan, for giving me the opportunity to work under his invaluable guidance. I would like to sincerely thank him for his unwavering support with resources and funding, motivation during tough times, and for steering me in the right direction with his ideas and vast knowledge by always being available throughout my entire Ph.D. journey which helped me immensely in completing this work. In addition to the academic content, I have observationally learned the importance of a great many things from him, such as hard work, diligence, patience, perseverance, meticulous planning, and social skills, for which I am extremely thankful. On that note, I would like to express my heartfelt gratitude for having the privilege of having an amazing professor and person like him as my advisor.

I would like to thank Dr. Seetha R. Mannava for his constant support, encouragement, and most importantly, for pushing me to go the extra mile in everything I do. I would also like to thank him for helping me in perfecting my organizational, leadership, and management skills that would be of utmost value to me in my future endeavors.

I'm extremely grateful to Dr. Matthew A. Steiner, Dr. Ashley E. Paz Y Puente, and Dr. Dinc Erdeniz, for serving on my doctoral evaluation committee, and for their valuable suggestions and help in completing my dissertation. I would also like to thank them for taking charge of the laboratories at the University of Cincinnati after Professor Vijay's retirement and helping with everything required to keep the research work going smoothly.

I would like to sincerely thank the U.S. Department of Energy, Office of Nuclear Energy for providing the financial support of this research through Nuclear Energy University Program (NEUP) Award # DE-NE0008770 administered by the Idaho Operations Office and Dr. Kenneth Ross (PNNL) as project technical monitor. I would also like to thank Dr. Charles Bryan from

Sandia national Laboratory, for providing the 304L SS plate materials and Dr. Luke N. Brewer and Dr. Paul Allison from the University of Alabama, for providing the 304L SS coatings/cladding used in this research and for their valuable contributions and inputs to the research. I would like to thank Dr. Isabella Van Rooyen from Idaho National Laboratory, Fred Bidrawn from Holtec International, and Jonathan Tatman, Benjamin Sutton, and Nicholas Mohr from Electric Power Research Institute for their collaboration and contributions towards this research work. I would like to gratefully acknowledge the contribution of the State of Ohio, Department of Development and Third Frontier Commission (Grant # TECH 10-014), which provided funding in support of the "Ohio Center for Laser Shock Processing for Advanced Materials and Devices" and the equipment in the center that was used in this work.

I'd like to extend a special thank you to the Department Head of Mechanical and Materials Engineering at the University of Cincinnati, Dr. Ying Sun, for providing the funding to complete some of the key microscopy work performed in this research. I'm also thankful to Dr. Donglu Shi and the Department of Mechanical and Materials Engineering for giving me the opportunity to work as a Teaching Assistant for multiple semesters. I'm grateful to the College of Engineering and Applied Science at the University of Cincinnati for deeming me worthy of University Graduate Scholarship and for providing me with Graduate Student Health Insurance Awards for several years.

I would like to thank Dr. Melodie A. Fickenscher, director of Advanced Materials Characterization Center (AMCC) at the University of Cincinnati, for providing the training of X-ray Diffractometer and Electron Microscopes and for allowing the use of these sophisticated equipment when required the most, for extended hours. I'm thankful to Dr. Jie Song for his insightful contributions to my thesis work and for his technical assistance with using various

equipment. I'd also like to thank Ronald F. Hudepohl, Rhodes Hall Machine shop manager at the University of Cincinnati for his kindness and help with many nitty-gritty things on several occasions. I would like to thank Ronald Flenniken and Jeffery R. Simkins for providing training on the Optical Profilometer and allowing the use of Clean Room and OCMI facilities at the University of Cincinnati.

I would like to thank all the faculty members of the Department of Mechanical and Materials Engineering at the University of Cincinnati for teaching great courses and helping outside of class whenever required and the staff members for taking care of the tuition and assistantship offer letters, package deliveries and all the other important things. I'd like to make a special mention to the executive staff assistant, Luree A. Blythe, for her warmth smile, positivity, and kindness that lifted my spirits at the University of Cincinnati on many occasions.

I'm grateful to Barbara J. Carter, my academic advisor at the University of Cincinnati, for patiently answering all my questions and assisting me with all the required paperwork from transitioning to defending my Ph.D. that helped my journey at UC go seamlessly. I'd like to thank all the staff at UC international services for their efforts in providing awareness and assistance with maintaining the SEVIS status at and beyond the University of Cincinnati. I'd also like to thank UC libraries for providing the resources required for continued and advanced learning.

I would like to thank my friends and colleagues at the lab: Boateng Twum Donkor, Sonali Ravikumar, Anurag Sharma, Biswajit Dalai, Aruneshwar Somasundaram, Richard Chiang, Michael Kattoura, Rohit Jagtap, and Boopa Nandini for all the fun-filled conversations and gatherings that made my stay in the lab a very memorable one and I wish you all a much greater success in life.

I would also like to thank my friends that I made at the University of Cincinnati: Phani Teja Komaravolu, Atulya Dharmaraj, Manasa Rao, Pratyusha Arasu, Vamshi Krishna Kore, Rashmi Reddy, Manish Tammali, Ravi Teja Pulugurthu, Madhav Lolla, and Sathwik Reddy Toom for the many celebrations, vacation trips, and all the other precious moments that we cherished together making my experience at UC a truly memorable one. I'd like to thank my friend Rohan Dighe that I met in Cincinnati who helped me like a big brother in many situations, treating me as family at his family thanksgiving dinners and making my life in Cincinnati a much more pleasant one.

I would like to thank my Bachelors friends at Mahatma Gandhi Institute of Technology, INDIA: Sasi Kiran Tirupati, Shiva Raj Yadav, Sumeet Somani, Ashwini Kotaru, Sandeep Paka, Raghu Ram Duvvuri, Pramod Punna, Suman Prakash, Sriram Madduri, Bharath Kasibhatla, Sai Sidhardha Madireddy, Yogesh, Shashi Kiran Jonnak, Satish Eluri, Kushal, Raja Pradeep, and Nithin Kumar Kalangi who played a major part in my life at the time with whom I shared many unforgettable moments.

I would also like to thank all my family members for their love and care, with a special mention to Parvathareddy Uma Maheshwari Devi, Arun and Priya Vinnakota, Murali Kumari Jakkaraju, and Siva Nageshwar Rao Namburi who played a key role in propelling my life to where I am right now.

Finally, I would like to thank my wife Sruthi Vaka, and my parents Mr. Pardha Saradhi Naralasetty and Mrs. Lalitha Naralasetty for their unconditional love, never ending support, and for their unshakable belief in me that inspired and motivated me to do and be better in many stages of my life. I am extremely fortunate to have such reliable and steadfast pillars in my life, whose unwavering care over the years has shaped me into the person I am today. I dedicate this thesis to them, my wife and parents.

Table of Contents

List of Figures

List of Tables

List of Abbreviations

A:	Amplitude/Dynamic Load (UNSM)
AFS:	Additive Friction Stir
AM:	Additive Manufacturing
ASSs:	Austenitic Stainless Steels
BCT:	Body Centered Tetragonal
BSE:	Back Scattered Electron
CDZs:	Chromium Depleted Zones
CH-R & SA:	Conventionally Hot-Rolled and Solution Annealed
CISCC:	Chloride Induced Stress Corrosion Cracking/Cracks
CNC:	Computerized Numerical Control
CPP:	Cyclic Potentiodynamic Reactivation
CR:	Corrosion Rate
CRSs:	Compressive Residual Stresses
CS:	Cold Spray
DI:	Deionized
DLEPR:	Double Loop Electrochemical Potentiodynamic Reactivation
DOC:	Depth of Compression
DOH:	Depth of Hardening
DOM:	Depth of Martensite presence
DOS:	Degree of Sensitization / Susceptibility
DSCs:	Dry Storage Canisters
EBSD:	Electron Back Scattered Diffraction

Ecorr:	Corrosion Potential
Epp:	Passivation Potential
Epit:	Pitting Potential
EDS:	Energy Dispersive X-ray Spectroscopy
FCC:	Face Centered Cubic
FN:	Ferrite Number
FSP:	Friction Stir Processing
FSW:	Friction Stir Welding
FWHM:	Full Width Half Maximum
ECAP:	Equal Channel Angular Pressing
GBs:	Grain Boundaries
GBM:	Grain Boundary Misorientation
GS:	Grain Size
HAGBs:	High Angle Grain Boundaries
HAZ:	Heat Affected Zone
HEA:	High Entropy Alloy
HVOF:	High Velocity Oxygen Fuel
Ia:	Peak Activation Current Density
Icorr:	Corrosion Current Density
Ir:	Peak Re-Activation Current Density
IFR:	Interval Feed Rate (UNSM)
IGSCC:	Intergranular Stress Corrosion Cracking
IPF:	Inverse Pole Figure

KAM:	Kernel Average Misorientation
LACS:	Laser Assisted Cold Spray
LAGBs:	Low Angle Grain Boundaries
LPB:	Low Plasticity Burnishing
LSP:	Laser Shock Peening
LSPwC:	Laser Shock Peening without Coating
MA:	Misorientation Angle
OCP:	Open Circuit Potential
PP:	Pitting Potential
PS:	Peening Speed (UNSM)
PWR:	Primary Water Reactor
Ra:	Surface Roughness
RS:	Residual Stress
SA:	Solution Annealed
SCC:	Stress Corrosion Cracking
SCE:	Saturated Calomel Electrode
SD:	Step Direction
SE:	Secondary Electron
SEM:	Secondary Electron Micrography
SL:	Static Load (UNSM)
SMAT:	Surface Mechanical Attrition Treatment
SNF:	Spent Nuclear Fuel
SNFDSCs:	Spent Nuclear Fuel Dry Storage Canisters

SP:	Shot Peening
SPD:	Severe Plastic Deformation
SRS:	Surface Residual Stress
SSRT:	Slow Strain Rate Tests
TD:	Transverse Direction
TEM:	Transmission Electron Microscopy
TRSs:	Tensile Residual Stresses
UNSM:	Ultrasonic Nanocrystal Surface Modification
U.S. NRC:	United States Nuclear Regulatory Commission
UTS:	Ultimate Tensile Strength
VSI:	Vertical Scanning Interferometry
XRD:	X-Ray Diffraction
YS:	Yield Strength

Chapter 1. Introduction

1.1 Background

Austenitic stainless steels (ASSs) exhibit many desirable properties like high temperature mechanical strength, good corrosion resistance, ductility, cryogenic stability, weldability and are non-magnetic in annealed condition [1]–[4]. So, they find applications in several industries like energy/nuclear, architectural, automotive, food processing, aerospace etc. In nuclear industry, due to a lack of natural geologic repository, spent nuclear fuel (SNF) is being stored on-site for safe interim storage in spent nuclear fuel dry storage canisters (SNFDSCs) that are constructed from "welded" austenitic 304 SS / 304L SS / 316L SS [5], [6]. But under economic considerations, 316L SS alloy which contains molybdenum in its alloy composition, makes it an expensive choice, tending the preference to 304 SS / 304L SS as the first-choice material [7]. Even though no failures have been reported in the currently in-service SNFDSCs yet, it is highly anticipated that eventually the welded austenitic SNFDSCs situated near marine environment may undergo chloride-induced stress corrosion cracking (CISCC) failures [5], [6]. The CISCC susceptibility of ASSs is being studied extensively by many researchers from several decades [8]–[13].

Stress corrosion cracking (SCC) is a localized corrosion phenomenon which starts as pitting transforming to cracking when three criteria are met simultaneously: (1) a material susceptible to SCC, (2) presence of a sufficiently aggressive chemical environment and (3) existence of sufficient applied or residual tensile stresses for the initiation and propagation of cracking [14]. During welding, the ASSs get exposed to temperatures in the range of 450°C to 850°C due to which they undergo an adverse phenomenon called as sensitization [3], [5], [15]–[17], which involves the depletion of chromium from areas immediately adjacent to the grain boundaries that combines with carbon present in the alloy leading to the formation of chromium

carbide precipitates ($Cr_{23}C_6$ and Cr_7C_3) and chromium depleted zones (CDZs) along the grain boundaries. This formation of CDZs makes the ASSs susceptible to intergranular stress corrosion cracking (IGSCC) [3], [15], [17]–[19].

Additionally, according to research performed by different personnel, surface deposits on in-service and unused SNFDSCs situated near marine environment (Hope creek nuclear generating station in Delaware and Diablo canyon nuclear power plant in California) showed the presence of chloride rich salts deposited on the 304 SS canister surfaces which can turn into an aggressive chloride containing environment upon deliquescence [20].

Moreover, NRC modeled canister longitudinal and circumferential welds using finite element methods showed that sufficient tensile stresses to cause SCC were present through the thickness of the canister wall within the heat affected zone (HAZ) of the canister weldments that can lead to full penetration with time [21], [22].

Therefore, all the three criteria compelling the occurrence of CISCC failures in the welded austenitic SNFDSCs are present, with the welded ASSs possessing CDZs that are formed at/near the HAZs by the occurrence of sensitization phenomenon during welding, which upon getting exposed to aggressive chloride containing environment make the CDZs anodic with respect to the unaffected grain area resulting in the localized disintegration of passive chromium oxide film on the welded ASS surface by the attack of corrosive chloride species, thereby exposing the underneath metal to further accelerated chloride induced corrosion ensuing the formation of pits that can act as initiation sites for cracking, where crack initiation and propagation can occur with relative ease because of the presence of tensile residual stresses in the HAZ of ASSs that are developed during welding, ultimately leading to the possibility of welded austenitic SNFDSCs situated near marine environment to undergo CISCC failures.

So, to tackle the looming and inevitable CISCC challenge faced by these welded austenitic SNFDSCs situated near marine environment, two approaches are being considered by the nuclear industry, one with respect to the **newly built canisters** (that are not in-service yet) and the other with respect to the **in-service canisters**.

Newly Built Canisters: In the case of newly built canisters, preventative measures are being taken to mitigate their SCC susceptibility by employing laser shock peening (LSP) technique as a mitigation method to be applied on the welded areas of the SNFDSCs. However, we believe that Ultrasonic Nanocrystal Surface Modification (UNSM), which offers several advantages over the LSP technique - some of which are discussed in the following paragraphs - can be a much more effective mitigation strategy for addressing the SCC susceptibility of newly built welded austenitic SNFDSCs. Especially given its cost-effectiveness compared to LSP, UNSM would be a more suitable option for the nuclear industry.

Mitigation of SCC can be done by either modifying the microstructure or changing the environment or altering the nature of stresses present in the material. While changing the environment may not be plausible for the SNFDSCs situated near marine atmosphere, modifying the microstructure and nature of stresses in the material can be achieved by surface treatment techniques like surface mechanical attrition treatment (SMAT) [23]–[26], shot peening (SP) [27]–[29],[30], low plasticity burnishing (LPB) [31], laser shock peening (LSP) [32]–[37], equal channel angular pressing (ECAP) [38], [39], ultrasonic nanocrystal surface modification (UNSM) [40]–[51],[52] etc. The mechanical surface treatment techniques through severe plastic deformation (SPD) induce near-surface nano crystallization, near-surface hardening and compressive residual stresses (CRSs) into the material which are all proven to be beneficial in mitigating SCC [30][32][41][53][54].

When compared to other surface treatment techniques, UNSM is a relatively new novel advanced mechanical surface treatment technique that involves the application of high-frequency ultrasonic vibrations to a material's surface through the combined action of static and dynamic loads transmitted via a tungsten carbide (WC) tool tip [47]. The WC tool tip repeatedly strikes the surface of the specimen with approximately 10 to 20 thousand shots per square millimeter at a rate of several thousands of strikes per second (20-40 kHz) in a highly controlled manner through the UNSM's computerized numerical control (CNC) machine. The repeated striking of the WC tool tip subjects the specimen surface to SPD inducing beneficial near surface microstructural changes and high magnitude of CRSs into the material up to an appreciable depth. It has advantages over other surface treatment techniques like enhanced surface finish, reduced material removal, less processing time and lower energy consumption than SP; enhanced process control variables resulting in homogenously modified surface layer and reduced surface contamination by using single WC tool tip in UNSM as opposed to larger number of steel balls in SMAT; increased microstructural refinement and flexibility in component size & geometry than LPB; better surface finish, reduced heat affected zone, induction of relatively high magnitude of surface CRSs and cheaper than LSP.

Also, when compared to the other surface treatment techniques, LSP and UNSM are relatively new novel techniques with the latter technique i.e., UNSM being the newest process among the two of them as stated in the earlier paragraph. With LSP exhibiting some advantages over other surface treatment technologies (not considering UNSM), it is currently being employed by the nuclear industry to be applied on the welded areas of newly costructed austenitic SNFDSCs to mitigate the tensile residual stresses (TRSs) formed in them at their HAZs during welding [55]. Along with the traditional LSP technique which involves the application of ablative coating on the

material surface prior to its surface treatment, LSP without coating (LSPwC) has also been studied extensively for the mitigation of SCC in 304 SS / 304L SS and both these processes have been proven to improve the SCC resistance of welded or sensitized 304 SS / 304L SS alloy by the synergestic effect of grain refinement and induction of CRSs into the material [54][56][57].

However, LSP / LSPwC which involve the application of laser, can tend the material being surface treated to experience high temperatures which can have a negative impact on the sensitization behavior of 304 SS / 304L SS alloy (similar to welding) [57]. I theorize that despite this negative impact on the material's sensitization behavior by LSP / LSPwC processes, they are able to improve the SCC resistance of the 304 SS / 304L SS material due to the other advantageous factors like grain refinement and induction of high magnitude of CRSs into the material by these processes, which are outweighing their negative sensitization effect. This suggests more potential for a process like UNSM, which avoids the negative sensitization impact on the material as its processing does not involve any high temperatures. Also, UNSM process not only induces the same advantageous factors into the material like LSP / LSPwC but introduces them at even greater magnitudes which is an added benefit of the UNSM processing.

Furthermore, to evenly induce the CRSs via LSP / LSPwC peening techniques across any specimen surface, a sequencing overlap technique must be used that typically involves 4 sequence steps with some degree of overlap being applied at the same area on the specimen surface where the peening is intended to be performed. This application of 4 sequence steps at the same area constitutes to a single layer of LSP / LSPwC being applied on the specimen surface and the necessity for this sequencing process by LSP / LSPwC tends to increase their processing time significantly, especially when we think in terms of the industrial level application making these processes expensive. Moreover, the preparation of the protective ablative coating, which is a

necessary precursor for the traditional LSP technique is time-consuming and not industrially economical, particularly when it needs to be applied on the vast welded areas of the huge and numerous SNFDSC structures. Whereas in the case of LSPwC processing as well, the direct impact of high temperature laser on the naked material surface of 304 SS / 304L SS transforms its surface to a molten state which reacts with oxygen in the atmosphere resulting in the formation of an oxide film on its surface [58] which can be of a mixed nature of iron and chromium oxide that can lead to detrimental passivation and corrosion behavior to be exhibited by the LSPwC treated material at its surface. This necessiates additional steps to either prevent or remove the oxide film formed on the LSPwC processed material, which makes the LSPwC process more expensive.

Also, inconsistent results have been found with respect to the near-surface residual stress state of the LSPwC treated 304 SS / 304L SS, with a couple of studies reporting to have observed TRSs at their surface up to a depth of 25 – 50 μm from their surface beyond which they are of compressive nature. The formation of these TRSs at the surface of LSPwC treated 304 SS/304L SS has been attributed to the thermal stress relaxation effect caused by the direct high temperature laser impact on the specimen surface leading to the transformation of its near-surface to a molten state (similar to weld molten pool but to a lesser depth extent) [54][56]. As a result, during SCC testing, they observed cracks to have formed in the tensile stress state near-surface regions of the LSPwC treated 304L SS but whose growth and propogation has been arrested below 50 μm due to the combined effect of grain refinement and the presence of consistent in-depth CRSs in the material that are caused by the LSPwC peening effect [56]. On the other hand, in another study performed on 304 SS claims that laser peening without coating induced CRSs at its surface with magnitudes in the order of -600 to -800 MPa along both the orthogonal directions of the specimen which completely prohibited the initiation and propogation of SCC [58].

These discrepencies in the surface residual stress state of LSPwC treated 304 SS / 304L SS can be understood by looking at a different study performed by S. Prabhakaran et al. [59], who studied the impact of laser pulse density on the magnitude of CRSs being induced into the 304 SS material during thier LSPwC processing. They concluded that the influence of thermal stress relaxation effect of LSP without coating resulting in the decrease of CRSs being induced into the material occurs only beyond some particular laser pulse density, which in this case was beyond 2500 pulses/cm^2 i.e., upon applying a pulse density of 3900 pulses/cm^2 the magnitudes of CRSs induced into 304 SS were considerably much lower (due to thermal stress relaxation) than the magnitude of CRSs that were induced into the 304 SS matieral when pulse densities of 2500 pulses/cm^2 or 1600 pulses/cm^2 were used. Therefore, the discrepancies seen across different studies with respect to the surface residual stress state that is being imposed on the surface of 304 SS / 304L SS material by LSPwC, could be a result of different pulse densities or different LSPwC processing parameters being used across the different research studies.

However, the more general common trend that has been observed with respect to the LSPwC processing parameters being applied on 304 SS / 304L SS and comparisons being drawn from within the constrainsts of several individual studies, is that higher pulse densities resulted in higher magnitudes of CRSs at the surface or sub surface of the LSPwC treated 304 SS / 304L SS [56][59][60] which led to lowering the susceptibility of SCC [60]. But the dimples formed on the surface of LSP / LSPwC treated materials tend the material to have a rougher surface in general, which upon using higher pulse densities to attain higher CRSs, led the material to exhibit even higher surface roughness values [54][56][59] which can have a negative impact on the corrosion behavior of the material. Again, despite these several drawbacks of LSP / LSPwC process, the 304 / 304L SS material treated with these processes exhibited an improvement in their SCC resistance,

which is attributed to the synergistic effect of grain refinement and the induction of high magnitude of CRSs into the 304 SS / 304L SS material by the LSP/LSPwC peening techniques.

The presence of CRS at the surface of a material can delay crack initiation and the presence of CRS along the depth of the material can slow down the micro-crack growth. Therefore, CRSs increase the threshold of crack growth and decreases the crack growth rate which consequently increases the failure stress intensity factor while SCC testing. Also, grain refinement caused by LSP or any other surface treatment technique that induces SPD, leads to an increase in the number of triple-grain boundary junctions and the probability of arresting a crack before it reaches a critical length, indicating that a decrease in grain size can increase the probability of crack arrest thereby leading to the surface treated material exhibiting higher resistance to crack propogation. Therefore, the LSP / LSPwC peening techniques improving the SCC resistance of 304 SS / 304L SS material despite of the drawbacks exhibited by these processes as discussed in the last few paragraphs, indicates that there is still a significant degree of room for improvement in enhancing the SCC resistance of 304 SS / 304L SS material by a surface treatment technique like UNSM that has several advantages over LSP / LSPwC techniques which are described in detail in the following paragraphs.

UNSM being an ultrasonic based dynamic impact process involving direct material contact with very low to no heat input being transferred to the material surface being UNSM treated, eliminates the possibility of UNSM surface treatment negatively influencing the sensitization behavior of 304 SS / 304L SS alloy, unlike LSP / LSPwC processes which involve significant heat input. Also, unlike the traditional LSP technique, UNSM does not require any protective coating to be applied on the surface of the material being surface treated, making it a much more economical option. And unlike LSP / LSPwC techniques, it can be performed in a

single iteration i.e., UNSM does not require any sequencing technique to uniformly apply SPD or CRSs into the material, making it a much more cost-effective mitigation technique due to it requiring much less processing time than that of LSP / LSPwC. Moreover, as UNSM does not involve any heat input, it can be performed in open atmosphere without the concern of deleterious oxide film being formed on the specimen's surface during processing, which is yet another advantage over the LSPwC process. As there is no need to look for any post processing steps to remove the oxide film or pre processing care to prevent the formation of oxide film, UNSM technique can be deemed as a much more economical surface treatment technique than that of LSPwC. Therefore, in conclusion, it can be said with certainity that UNSM surface treatment technique once developed for in-situ applications can be a highly cost-effective SCC mitigating alternative technique to surface treatment technologies like LSP / LSPwC.

Furthermore, depending on the characteristics of the material being surface treated, UNSM can induce ~ 2X to 4X times greater surface CRSs into the material with a greater degree of grain refinement being imposed at its surface that would last up to a greater depth than induced by LSP / LSPwC processes, while also ensuing a surface roughness that is ~ 2X to 10X times lower than that caused by LSP / LSPwC processes [61][62], all of which would be extremely beneficial in further improving the corrosion behavior of the material being surface treated by UNSM. That is, as discussed earlier, the presence of high magnitude of CRSs at the surface of a material and the increase in the number of triple-grain boundary junctions due to grain refinement caused by the surface treatment techniques can delay the crack initiation and increase the resistance to crack propagation. Therefore, with UNSM surface treatment technique inducing greater surface CRSs and greater near-surface grain refinement in a material, and affecting the material surface roughness to an extremely lower extent than that of LSP / LSPwC processes, tends us to theorize

that UNSM can be extremely beneficial in further improving the corrosion behavior or SCC resistance of 304 SS / 304L SS than that of LSP / LSPwC peening techniques.

However, very few studies have been found in the open literature that have investigated the impact of UNSM surface treatment on the corrosion properties of ASSs. Out of which, one study focused on researching the effect of UNSM on the SCC susceptibility of as-fabricated 304 SS alloy in acidic medium of 1M H_2SO_4 solution containing 5 Wt. % NaCl [46], which reported that the corrosion behavior of 304 SS degraded after UNSM due to the higher anodic dissolution kinetics of UNSM treated 304 SS specimen in the chloride containing acidic medium. However, in a research study done by Shengxi Li et al. [45], which investigated the effect of UNSM treatment on the pitting corrosion resistance of un-sensitized / un-aged / as-fabricated 304 SS in 3.5 Wt. % NaCl solution reported that the UNSM surface treatment greatly improved the pitting corrosion resistance of 304 SS in the chloride containing environment. This improvement was attributed to the combined effect of grain refinement caused by UNSM leading to greater Cr enrichment in the formed surface passive film and to the removal of MnS inclusions from the specimen's surface by UNSM. Additionally, research performed by Chang Ye et al. [41], who studied the effect of UNSM treatment on the corrosion resistance of 304 SS welds in boiling $MgCl_2$ solution reported that no cracks were observed on the UNSM treated 304 SS specimen surface ever after 120 hours of exposure to the boiling $MgCl_2$ solution whereas in contrast, cracks were observed by them in the as-welded specimen after only 72 hours of exposure indicating that UNSM improved the corrosion resistance of 304 SS welds. Note that only one of these three studies focused on the welded or sensitized 304 SS material which is the last one by Chang Ye et al. [41] that can be representative of the welded austenitic SNFDSCs that are being considered in this study by us, whereas the other two studies focused on the as-fabricated or unsensitized 304 SS material.

However, research studies investigating the underlying factors that positively influenced the corrosion behavior of welded or sensitized 304 SS / 304L SS by UNSM surface treatment i.e., the impact of UNSM treatment on the sensitization behavior and pitting characteristics of sensitized 304L SS and the underlying mechanisms or factors that are caused by UNSM which are influencing these behaviors have not been studied or the relevant research has not been found in the open literature. Therefore, to fill the scientific gap in understanding the impact of UNSM treatment on the corrosion properties of sensitized (i.e., representative of welded specimen) 304L SS alloy, there is an imminent need for studying the impact of UNSM treatment on the sensitization behavior of sensitized 304L SS alloy (as UNSM process does not involve any heat input as well) and also for studying the impact of UNSM treatment on the pitting corrosion characteristics of sensitized 304L SS alloy in simulated seawater concentration containing chloride environment i.e., in 3.5 Wt. % NaCl solution, so as to research the effect of cl^- ions on the UNSM treated 304L SS specimen's surface, which has been fulfilled by this current dissertation research work.

Furthermore, with the majority of new SNFDSCs being constructed from 304L SS alloy, it would be beneficial to study the impact of UNSM treatment on the microstructural and mechanical properties of sensitized 304L SS alloy as well, with the ultimate idea of proposing to replace the LSP technology or provide an additional viable option to effectively deal with the SCC susceptibility of new SNFDSCs in the form of UNSM surface treatment technique, which is a cheaper SCC mitigating alternative technique that incidentally has several advantages over the traditional LSP / LSPwC peening techniques. Therefore, in the current research work, the impact of UNSM surface treatment on the microstructure, hardness, residual stress, and corrosion properties of sensitized 304L SS alloy were studied and it has been found that UNSM treatment can have a significant impact in improving the corrosion and mechanical properties of sensitized /

aged (representative of a welded specimen) 304L SS alloy. Finally, note that this is not a comparative study between LSP and UNSM treatment techniques, as the goal of this study was to first establish the possibility of improving the corrosion and mechanical properties of sensitized 304L SS alloy via UNSM surface treatment technique. And since this goal has been achieved by this study, it gives scope for a future study where the sensitization, pitting, and mechanical characteristics achieved by sensitized 304L SS alloy that is surface treated by LSP and UNSM treatment techniques could be compared and analyzed, to determine with certainty on which process is better between the two of them.

In-service Canisters: In the case of **existing or in-service canisters** which are facing the inevitable CISCC challenge, with through-wall cracks being discovered on the surface of 304L SS reactor cavity and spent fuel cooling system tanks at Koeberg Nuclear Power Station and a through-wall crack being found in 304 SS spent fuel pool cooling line at Turkey Point Nuclear Generating Station, with both the cracks being attributed to CISCC [63], demands for an immediate need for finding long term reliable cost-effective in-situ repair and mitigating methods that involve low heat input, without causing sparks and not placing high mechanical loads or causing deformation to the canister surface. And finding these methods is of utmost importance to the nuclear industry not only for prolonging the service life of the existing SNFDSCs but also for avoiding the devastating effects the release of the radioactive spent nuclear fuel by the canister failure can cause on both the environment and the human life.

Therefore, from the viewpoint of combined repair and mitigation techniques to be applied on the cracks of existing SNFDSCs, the repairing technique that is traditionally considered for treating the CISCC in welded ASS SNFDSCs is an overlay fusion weld process which involves high heat input to fix the repair area [64]. However, since this repair process involves welding as

well, it can lead to sensitization and shrinkage tensile residual stresses to appear in the repaired area/material, which upon exposure to chloride containing environment can eventually lead to the resurgence of CISCC problem in due time in the repaired SNFDSCs.

As a result, new research efforts are being focused on solid-state additive manufacturing (AM) techniques as a plausible solution to repair the CISCC in SNFDSCs, since they involve low heat input, avoid the production of sparks or melting in the process thereby avoiding sensitization and production of shrinkage tensile stresses in the repaired area. Three such repair methods based on solid-state additive manufacturing that are being considered for repairing the CISCC cracks in SNFDSCs are Cold Spray (CS), Laser Assisted Cold Spray (LACS), and Additive Friction Stir (AFS/MELD) deposition techniques.

Cold Spray: The traditional CS technique involves the solid-state deposition of metal powders that are propelled to supersonic velocities by the heating of propellant gases to extremely high temperatures and accelerating them with the help of a de laval nozzle onto a substrate material, ultimately resulting in the metal powders deforming plastically upon impact and forming a cohesive bond with the substrate or prior deposited powder particles. The plastic deformation caused in the CS coating by the bomardment of powder particles onto a substrate results in beneficial CRSs [65][66] being induced into the coating which can be useful in mitigating SCC. However, the CS coatings were also found to possess weak interparticle bonding and significant amount of porosity in them [67], [68] which can be extremely detrimental to their corrosion properties. Also, the traditional CS technique involving the solid state deposition of metal powders onto a substrate can result in the finished surface having extemely high surface roughness which can be yet another detrimental factor that can negatively influence the corrosion properties of the cold sprayed material. However, no research studies have been found in the open literature that

investigated the corrosion behavior of cold spryaed 304 SS / 304L SS alloy in particular, making the assumptions made in the last few sentences to be only theoretical. Threfore, finding out the combined effect of the factors stated in the assumptions on the corrosion properties of CS 304L SS alloy will be extremely essential for considering it as a possible method for treating the CISCC problem in the welded austenitic SNFDSCs and also, it would be very interesting to study if any one factor outweighs the others or what would the acutal case be?

Nevertheless, numerous research studies have been found in the literature which demonstrated the feasibility of depositing ASS powders onto different substrate materials using the traditional CS deposition technique with some of them aiming at improving the deposition efficiency of ASS powders by altering the temperatures, pressures, and gas types to be used during the cold spray processing to achieve enhanced particles velocites which would in turn improve their deposition efficiency [69][70][71][72][73][74][75][76][77]. Of these studies some of them focused on studying the mechanical properties of the CS - ASS coatings and their association with strain hardening and porosity present in them, along with venturing into the possibility of improving their mechnaical properties through annealing treatment [69][74][75]. The CS - ASS's were reported to result in coatings with high hardness and high yield strength (YS), but with low elastic modulus and no measurable ductility, which were attributed to the intense strain hardening and persistant presence of porosity in the CS coatings. To improve the brittle nature or ductility of the CS 304 SS, coddet et al. [69] performed an annealing treatment at 1050°C for 4h which resulted in restoring its ductility from 0 % to 9.9 % (fracture strain) but consequently leading to a reduction in its YS from 629 MPa to 422 MPa. Meng et al. [74], reported that due to the persistant presence of porosity in the CS 304 SS coatings even after annealing them at 950°C for 1h, the elongation to fracture values of annealed CS 304 SS were incredibly low with them showing values of < 4%.

Again, to add to what was stated earlier, very few research studies were found in the open literature which investigated the corrosion properties of ASS's deposited by traditional CS processing, that too only with respect to 316L SS alloy [70][78][79][80] and none with regards to 304 SS / 304L SS alloys. Therefore, there is a dire need to study the corrosion behavior of CS 304L SS to bridge the existing gap in the scientific knowledge with this regard. In a recent study as well [66], which investigated the feasibility of depositing 304L SS powders on 304 SS substrates through CS deposition process, with the view of using it as a mitigation technique for treating CISCC, looked at only the porosity levels, residual stress state, and adhesion strength of the CS 304L SS coating material, along with finding out that the cold sprayed coating was able to arrest the pre-existing population of prototypical CISCC cracks in the base material, but has not ventured into studying the surface corrosion properties of the CS 304L SS coating itself which would be incredibly useful as it will give an idea of whether the surface of the cold sprayed 304L SS material would provide enhanced corrosion resistance just like the bulk 304L SS or would it pose any corrosion problems in the present or eventually in the future? Also, with respect to the corrosion characteristics of any material, its surface state plays an important role and with typical CS deposition most likely yielding a rougher surface, there is a requirement for investigating the corrosion behavior of CS 304L SS coating in its as-deposited and polished surface state, which has not been done by anyone yet.

Therefore, there are still questions that need to be answered with regards to using or implementing the traditional CS deposition techique as a mitigation method for treating the CISCC challenge faced by the welded austenitic 304 SS SNFDSCs. This thesis aimed at finding answers for some of these questions like : What would be the corrosion behavior of as-deposited CS 304L SS? Would there be any difference in its corrosion behavior if the coating was polished? Are there

any surface characteristics that are affecting the corrosion behavior of CS 304L SS material? With the presence of porosity, weak interparticle bonding, and rougher exterior surface of CS 304L SS coating, one would anticipate it to exhibit worse corrosion properties than that of bulk 304L SS plate mateiral, but the extent of which is not known i.e., how worse would the corrosion properties of CS 304L SS material could be from that of the bulk 304L SS material? Or would this anticipation be even true or would there be any other factors like CRSs deeming our anticipation to be false? Does the beneficial CRSs produced in the CS 304L SS coating by the bombardement of powder particles during processing have a positive effect in overcoming its porosity and weak interparticle bonding with respect to its corrosion properties or not? Or if the corrosion properties of CS 304L SS material are indeed worse than the bulk 304L SS, can they be improved by surface treatment techniques like UNSM which is a direct material contact dynamic impact process that can lead to multiple advantages like densification of the CS 304L SS coating, increasing its CRS values to an even greater magnitudes and also, resulting in a decrease in the surface roughness of as-deposited CS 304L SS material? Do any of these advantages of UNSM processing performed on either as-deposited or polished CS 304L SS material result in an improvement in its corrosion properties?

Laser Assisted Cold Spray: The traditional CS deposition technique has some general limitations like coating thickness that can be deposited, requires prior surface preparation for optimal coating adhesion, and demands post heat treatment to achieve desirable mechanical properties. Most of the problems or limitations associated with the traditional CS deposition process can be overcome by simultaneously applying laser technology to the traditional CS deposition technique which is termed as laser assisted cold spray desposition technique [81], [82]. LACS is a hybrid solid-state materials deposition process that involves the combined application of laser preheating of the substrate or powder particles before or during the deposition process

accompanied by the deposition of metal powders through the traditional CS deposition technique [81].

The LACS process involving the use of laser to locally heat the substrate prior to or during deposition eliminates the need for surface preparation and also, enhances the adhesion between powder particles and the substrate [81]. Using laser technology simultaneosuly with the traditional CS deposition process (i.e., LACS) has been reported to result in heightened interparticle bonding and reduced porosity leading to improved mechanical and corrosion properties than that are exhibited by the traditionally cold sprayed coatings [67][68]. Additionally, LACS eliminates the need for post heat treatment by in-situ annealing the typical cold work generated by the bombardment of powder particles during the traditional CS deposition technique and the usage of laser technology gives the ability to control the cooling rate of the deposited particles allowing for controlled recovery and recrystallization of the LACS deposited material. Furthermore, LACS process involves partial to no melting thereby, avoiding the typical problems associated with laser based technologies like thermal stressing, distortion, dilution and other microstructural problems making it a very reliable technology for producing better coatings. LACS processing technique has been used successfully to deposit several materials like 4340 steel [67], CrMnCoFeNi based high entropy alloy [68], Fe-Ni-Zr oxide dispersion strengthened steel [83] etc.

However, because of the simultaneous application of laser during LACS processing, the beneficial compressive residual stresses produced during the traditional stand alone CS processing would be relieved due to recovery and recrystallization. Also, recrystallization tends to increase the grain size of the coating consequently decreasing its hardness. So far, with respect to 304L SS alloy, only one research study has been conducted, that investigated the effects of laser heating on the microstructure and deposition properties of cold sprayed 304L SS, in which the laser heating

was applied on the already deposited CS 304L SS. In that research conducted by C. M. Roper et al. [82], it was reported that the application of laser heating resulted in recrystallization and grain growth in the CS 304L SS coating, relieving the detrimental effects of strain hardening caused by traditional CS process but, also accompanied by a consequent decrease in its hardness due to the increase in grain size. However, they have not investigated the effect of laser treatment on the alteration of the beneficial compressive residual stress state of the CS 304L SS coatings and neither did they study the corrosion behavior of CS 304L SS or laser treated CS 304L SS coating material whose knowledge would be immensely useful in further assessing the LACS process as a possible repair method for treating the CISCC problem in the already existing welded austenitic SNFDSCs.

Some of the questions that need to be answered with regards to the LACS process for this purpose are : To what extent would the CRSs be relieved due to the simultaneous application of laser to CS technique? Can a surface treatment technique like UNSM be used on the LACS 304L SS coating, to reintroduce the relieved CRSs that are benefical to the SCC resistance of a material, and to what magnitudes could they be reintroduced and how would UNSM affect the other properties of LACS 304L SS coating? Would there be any noticeable improvement in the porosity levels of LACS deposited 304L SS coating from that of the CS 304L SS coating due to the simultaneous application of laser technology to CS? What would be the corrosion behavior of LACS 304L SS material and how different would it be from that of the CS 304L SS's corrosion behavior and why? How does the application of UNSM on the LACS 304L SS material affect its porosity and corrosion properties? Would there be any difference in the surface roughness or surface characteristics of the as-deposited LACS 304L SS material from that of the as-deposited CS 304L SS material due to the softening of the material by the use of laser during LACS processing? How would the application of UNSM on LACS 304L SS coating affect its surface

characteristics and what implications would the changes in the surface characteristics of LACS 304L SS material by UNSM would have on its corrosion behavior i.e., due to grain refinement, martensite formation etc.?

Additive Friction Stir Deposition: Another novel solid-state AM technique that is being considered for treating the CISCC in welded austenitic SNFDSCs is the additive friction stir / MELD deposition technique that is derived from friction stir welding (FSW) and friction stir processing (FSP) and is developed by Aeroprobe corporation [84]. The process of AFS/MELD involves heating a consumable powder or solid filler rod placed in the rotating tool shoulder to a semi solid state by induction or resistance heating which is then mechanically mixed by the CNC controlled rotating tool shoulder and deposited onto the substrate, layer by layer in a semi solid state under hydrostatic pressure. AFS/MELD processing technique can be used to join, repair, clad and additively manufacture similar / dissimilar / multi metals or alloys and has been used successfully to deposit several materials like IN 625 [85], 316L SS [86], Ti6Al4V [87] etc.

A very recent paper published in 2024 by B. E. T. Roper et al. [84] claimed to be the first research work to have successfully deposited 304L SS through AFS deposition technique. They studied the microstructural evolution of 304L SS cladding deposited by AFS and reported that the 304L SS cladding was fully dense, exhibiting wrought-like microstructure and mechanical properties (in terms of hardness). However, the AFS deposited 304L SS cladding's residual stress state and corrosion behavior have not been studied by them. Therefore, to further enhance the knowledge and assess the AFS deposition technique as a possible repair method that can be used effectively for treating the CISCC in the welded austenitic SNFDSCs, the AFS deposited 304L SS cladding's residual stress state at its surface and its corrosion behavior must be investigated.

The anticipation is that, since the AFS deposition technique involves the heating of feedstock material to deposit it in a semi solid state, it may result in the deposited cladding to exhibit tensile residual stresses or very low magnitude of compressive residual stresses at its surface (that could have resulted due to the deposition of the material under hydrostatic pressure by the rotating tool shoulder). But since the AFS deposition technique is being considered to repair the existing CISCC cracks on the surface of welded austenitic SNFDSCs, it would be highly desirable to have medium to high magnitude CRSs at the surface and near-surface area of AFS deposited cladding material, so as to prevent the formation of new cracks at the cladding surface and/or to prevent the probable propagation of arrested or un-arrested existing underneath cracks (that are formed due to CISCC at the welded areas of SNFDSCs) all the way to the surface, which would again cause problems in the future.

Therefore, applying a cost-effective mitigation method like UNSM on AFS 304L SS cladding would be extremely beneficial in improving the material's SCC resistance by inducing high magnitude compressive residual stresses, near-surface hardening, and nano crystallization. However, the same questions that needed answers with respect to the CS and LACS processing techniques that were being considered for treating the CISCC in welded austenitic SNFDSCs, are also posed for the AFS processing technique and the impact the UNSM treatment can have on its properties, especially on the corrosion properties of AFS deposited 304L SS cladding. That is would UNSM improve the corrosion, mechanical, and residual stress properties of AFS deposited 304L SS alloy or would there be any factors in the deposition process of AFS that would play a role in the degree of impact UNSM can have on the cladding? But first what would the corrosion properties of as-deposited or polished AFS 304L SS cladding be? Would there be any surface characteristics influencing its corrosion behavior? etc. are the questions that need to be answered.

Hence, this dissertation research study has aimed at answering all the questions that are posed in regards to investigating the corrosion behavior of CS, LACS, and AFS deposited 304L SS coatings / cladding materials and to address the anticipated shortcomings of these as-processed 304L SS coatings / claddings with the cost-effective mitigation technique of UNSM surface treatment thereby, providing a complete repair + mitigation strategy for dealing with the CISCC problem of the existing welded austenitic SNFDSCs. In addition, this dissertation research work also aims at studying the impact of UNSM surface treatment on the corrosion and mechanical properties of "sensitized" 304L SS alloy, with the intent of proposing and providing an alternate solution or additional option that is anticipated to be more efficient and cost-effective than LSP / LSPwC peening techniques for addressing the SCC susceptibility of newly built welded austenitic SNFDSCs which is the UNSM surface treatment technique.

1.2 Problem Statement

The welded austenitic 304 SS / 304L SS Spent Nuclear Fuel Dry Storage Canisters (SNFDSCs), either newly built or the already existing ones, are facing a looming and destructive problem of Chloride-Induced Stress Corrosion Cracking (CISCC). In the case of newly built canisters, which obviously do not have any cracks yet, but the material at the welded areas of these canisters has undergone sensitization phenomenon during welding, which is the formation of chromium carbide precipitates or chromium depleted zones along the grain boundaries making the welded 304L SS material susceptible to Intergranular Stress Corrosion Cracking (IGSCC). Whereas, in the case of already existing canisters, small cracks due to CISCC have been observed at the heat affected zones of the weldments, and to repair these cracks, solid state additive manufacturing techniques like Cold Spray (CS), Laser Assisted Cold Spray (LACS), and Additive Friction Stir (AFS) processing techniques are being considered by the nuclear industry.

Therefore, the initial goals of this dissertation research were three-fold as described below:

(i) To establish Ultrasonic Nanocrystal Surface Modification (UNSM) treatment as an effective method that can improve the sensitization and/or corrosion behavior of "Sensitized" 304L SS alloy, with the intent of presenting it as a cost-effective mitigation method that can effectively deal with the Stress Corrosion Cracking (SCC) susceptibility of newly built welded austenitic 304L SS SNFDSCs.

(ii) Secondly, to determine the corrosion behavior of 304L SS alloy deposited through CS, LACS, and AFS processing techniques, as these solid-state additive manufacturing techniques are being considered strongly for repairing the CISC-Cracks formed on the existing welded austenitic 304L SS SNFDSCs, and since no one has ventured into determining the corrosion behavior of 304L SS alloy deposited through these processes yet, this study would be extremely useful to the nuclear industry in assessing these processes as potential problem solvers or effective repair methods of CISCC in existing SNFDSCs.

(iii) Lastly, as stated in section 1.1, based on the data currently available in the open literature on these solid-state additive manufacturing techniques that are being considered for repairing the CISC-Cracks present in the already existing welded austenitic 304L SS SNFDSCs, we anticipate that the 304L SS alloy deposited through CS or LACS or AFS processing techniques may have inferior corrosion and/or mechanical and/or residual stress properties than that would be essential for providing a hermetic seal to the existing canisters repaired through these processes. Therefore, we strongly believe that UNSM surface treatment technique can be an effective mitigation technique that can improve the corrosion, mechanical, and

residual stress properties of 304L SS alloy deposited through CS or LACS or AFS processing techniques, and be of incredible help to restore the load carrying capacity of the existing welded austenitic 304L SS SNFDSCs by inducing high magnitudes of compressive residual stresses (CRSs), near-surface hardening, and extreme grain refinement resulting in near-surface nano crystallization in the UNSM treated CS or LACS or AFS 304L SS alloy.

It is well known that UNSM treatment can enhance the SCC resistance of conventionally hot-rolled bulk 304 SS / 304L SS alloy through the severe plastic deformation caused by UNSM resulting in the induction of high magnitudes of CRSs, near-surface hardening, and near-surface nano crystallization in the UNSM treated specimen, which were attributed to be the factors responsible for the enhancement in SCC resistance of bulk 304 SS alloy through its UNSM surface treatment. But here, in this dissertation research work, there are four different 304L SS materials being considered with distinct microstructural characteristics viz., microstructure with chromium carbide precipitates or chromium depleted zones along grain boundaries (sensitized), microstructure with porosity possessing weak interparticle bonding and cold work (CS), microstructure with porosity and improved interparticle bonding through recrystallization (LACS), and fully dense material with gradient microstructure possessing near-surface nano sized grains (AFS), whose corrosion, mechanical, and residual stress properties are aimed to be improved or enhanced by UNSM surface treatment technique. This brings us to our hypothesis: **Despite the differences in the prior microstructural characteristics of distinct 304L SS material / coatings / cladding studied in this dissertation research work, we hypothesize that UNSM surface treatment would be effective in improving the corrosion behavior, mechanical, and residual stress properties of all the distinct 304L SS materials (Sensitized, CS, LACS, and AFS 304L**

SS) by the induction of high magnitude CRSs, near-surface hardening, and near-surface nano crystallization. The goal of this research is to determine if our hypothesis is true or false, and in case it is deemed false or partially false, the goal is to find out the factors responsible.

1.3 Objectives and Scope of Thesis

The principal objective of this research is to investigate the UNSM surface treatment's ability and/or limitations in improving the mechanical, residual stress, and corrosion behavior of 304L SS with distinct microstructural characteristics viz.

- **Sensitized 304L SS** – material with austenitic microstructure having chromium carbide precipitates or chromium depleted zones segregated along its grain boundaries,
- **CS 304L SS** – material with porosity possessing weak interparticle bonding and cold work,
- **LACS 304L SS** – material with porosity and improved interparticle bonding through recrystallization, and
- **AFS 304L SS** – fully dense material like bulk 304L SS but with nanocrystalline grains at the surface or gradient microstructure.

Can a surface treatment like UNSM affect the 304L SS materials with distinct microstructural characteristics in an analogous manner or would it have a different impact and if it does have the same or different impact what would be the reason? Can UNSM improve the corrosion, mechanical, and/or residual stress behavior of all the different 304L SS materials with distinct microstructural and/or surface characteristics or would it have any limitations depending on the prior characteristics of 304L SS alloy? If UNSM can improve the corrosion, mechanical, and/or residual stress behavior of the distinct 304L SS materials, what would be the underlying mechanisms or factors responsible for the improvement? These are some of the major questions that we have set out to find the answers to initially as a part of this dissertation research work.

For this purpose, this dissertation research work has been conducted in two phases as follows:

Phase I: Initially, the microstructural, mechanical, residual stress, and corrosion properties of different 304L SS materials with distinct microstructural characteristics i.e., sensitized, CS, LACS, and AFS 304L SS have been evaluated and compared against the conventionally hot-rolled and solution annealed (CH-R & SA) 304L SS plate specimen's properties.

Phase II: Later, the mechanical, corrosion, and residual stress properties of sensitized, CS, LACS, and AFS 304L SS material / coatings / cladding have been attempted to be enhanced or improved by UNSM surface treatment, for which their microstructures, phases, hardness, residual stress, surface topography, sensitization, and pitting corrosion behaviors prior to and after UNSM treatment have been studied and compared. The underlying mechanisms or factors that were responsible to have or have not been able to improve the properties of sensitized, CS, LACS, and AFS 304L SS materials by UNSM surface treatment have been discussed extensively in this dissertation research work, giving an account of the benefits and/or limitations of the impact of UNSM treatment on these different 304L SS materials possessing distinct microstructural characteristics i.e., discussing the influence of prior microstructural features of 304L SS alloy that may or may not contribute or limit the impact, the UNSM surface treatment can have on the particular 304L SS material.

For this purpose, firstly, a UNSM parametric study was done in this phase, to determine the most optimal UNSM parameters that can be used for peening the 304L SS alloy. The UNSM surface treatment involves four different parameters for peening any specimen, namely: static load (SL), dynamic load/amplitude (A), peening speed (PS), and interval feed rate (IFR) and the after-surface-treatment material properties vary for different materials with varying UNSM processing parameters. Therefore, this UNSM parametric study was performed with 16 different parameter

combinations involving two different SLs, As, PSs, & IFRs and the most optimal UNSM parameters were chosen by comparing the after-surface treatment properties of all the 16 peens with respect to their surface roughness, CRS (surface and through-the-depth), and cross-sectional hardness depth profiles. Finally, in this phase, the obtained most optimal UNSM parameters have been applied on the sensitized, CS, LACS, and AFS 304L SS materials and further testing, analysis, and interpretations have been carried out with respect to their microstructures, hardness, residual stress, and corrosion properties by comparing them from prior to and after UNSM treatment.

The microstructures of sensitized, CS, LACS, and AFS 304L SS before and after UNSM treatment were studied using Electron Back Scattered Diffraction (EBSD) analysis performed on their respective cross-sectioned areas. X-Ray Diffraction (XRD) analysis was used to determine the near-surface phase transformations associated with the UNSM surface treatment and was also used to determine the residual stress (RS) state at the surface and through-the-depth of all the specimens before and after UNSM treatment using the conventional $Sin^2\psi$ technique to calculate the RS. The mechanical properties were analyzed with respect to nano hardness. Corrosion tests were performed in two different solutions namely: (1) 0.5M H_2SO_4 + 0.05M KSCN solution (Double Loop Electrochemical Potentiodynamic Reactivation - DLEPR tests) to evaluate the degree of sensitization / susceptibility (DOS) or the strength of the passive film formed on the material surface and (2) 3.5 Wt.% NaCl solution (Cyclic Potentiodynamic Polarization - CPP tests) to determine the corrosion rate and pitting potential (pitting corrosion characteristics) of all the differently processed 304L SS materials before and after surface treatment. The specimen's surfaces after their UNSM treatment and corrosion tests were examined using Secondary Electron (SE) / Back Scattered Electron (BSE) micrography and the compositional analysis whenever required was determined using Energy Dispersive X-Ray Spectroscopy (EDS) technique.

Chapter 2. Literature Review

This chapter is a literature review of austenitic stainless steel 304 / 304L SS alloy that is being preferentially used as a nuclear construction alloy for building Spent Nuclear Fuel Dry Storage Canisters (SNFDSCs) and about the Chloride Induced Stress Corrosion Cracking (CISCC) challenge faced by the welded austenitic 304 / 304L SS SNFDSCs situated near marine environment. It also includes a summary on the novel Cold Spray, Laser Assisted Cold Spray and Additive Friction Stir deposition techniques as possible repairing methods and Ultrasonic Nanocrystal Surface Modification treatment as a post-repair mitigation technique to be used in conjunction with each other to repair and mitigate the CISCC cracks on the surface of SNFDSCs.

2.1 Austenitic Stainless Steels – 304 / 304L SS Nuclear Alloys

Based on the crystalline structure, the stainless-steel family is divided into five types: *austenitic*, ferritic, martensitic, duplex (mixture of austenite and ferrite) and precipitation hardenable. Ferritic stainless steels typically consist of 12.5 % or 17 % chromium and iron. They are essentially nickel free. Martensitic stainless steels consist of 0.2 – 1 % carbon, 10.5 – 18 % chromium, and iron. *Austenitic stainless steels (ASSs)* consist of 16-26 % chromium, 6-12 % nickel, and iron. Other alloying elements such as molybdenum may be added or modified depending on the properties desired. The ASS group contains more grades, that are used in greater quantities, than any other category of stainless steels. ASSs make up about two-thirds of the total stainless-steel production [88]. Duplex stainless steels consist of 18 – 26 % chromium, 4 – 7 % nickel, 0 – 4 % molybdenum, copper, and iron. These stainless steels possess a microstructure consisting of both austenite and ferrite, exhibiting material characteristics of both the phases. Precipitation hardening stainless steel consists of 15 – 17.5 % chromium, 3 – 5 % nickel, along with aluminum, copper, niobium, each less than 0.5 % of the total mass of the steel, and iron.

ASSs ability to be stainless is attributed to having a minimum of 10.5 Wt.% Cr in their alloy composition. Upon exposure to atmosphere, the Cr in the ASSs reacts with oxygen in the atmosphere through a reaction called the passivation reaction and forms a thin invisible layer of chromium oxide (Cr_2O_3) film on the metal surface that acts as a barrier between the environment and the underlying metal as shown in figure 2.1. This passivation reaction can be represented as follows:

$$Cr + O_2 \rightarrow CrO_2$$

$$4CrO_2 + 2H_2O \rightarrow 2Cr_2O_3 + 4H^+ + 4e^-$$

The thickness of the passive chromium oxide film can range from a few nanometers (nm) to a few hundred nm which if disturbed by any means like scratching can automatically self-heal in the presence of oxygen. This innate quality of ASSs to self-heal in the presence of oxygen gives them the ability to have fair to good corrosion resistance in many harsh and high temperature environments [3]. Along with good corrosion resistance, ASSs have desirable properties like high temperature mechanical strength, ductility, cryogenic stability, formability, weldability and are

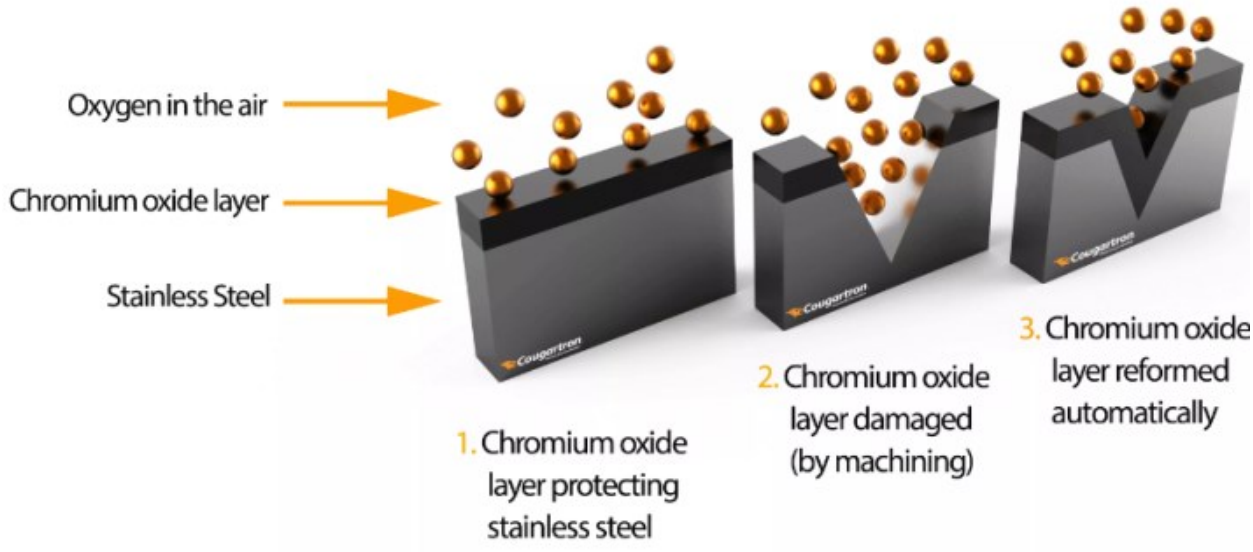

Figure 2.1: Passivation reaction of chromium in austenitic stainless steel alloy composition with oxygen in atmosphere to form protective chromium oxide layer on the surface of ASSs [Source: https://shipbuildingknowledge.wordpress.com/2017/10/25/stainless-steel-material-what-is-pickling-passivation/].

non-magnetic in annealed condition [1]–[4]. So, they find various applications in several industries like food processing, chemical, architectural, medical, energy/nuclear etc. The components made from austenitic stainless steels ranges from pots, pans, cutlery, kitchen sinks etc. used in household applications to spent nuclear fuel dry storage canisters, primary water reactor (PWR) piping and coolant systems, pressure vessels, heat exchangers etc. that are used for heavy-duty industrial applications.

Austenitic stainless steels (ASSs) are sub divided into two groups namely, 200 series (Fe-Cr-*Mn*-Ni alloys) and 300 series (Fe-Cr-Ni alloys) with the largest group being that of the latter series. Among all these ASSs, AISI grade 304 (also known as 18/8 stainless steel) / 304L SS and 316 / 316L SS are the most commonly preferred alloys for many applications, mainly because of their enhanced corrosion resistance than other ASSs, along with their other desirable mechanical properties. Furthermore, 316 / 316L SS alloy is expensive because of 2 % molybdenum addition in its alloy composition which paved way for an extensive use of 304 / 304L SS alloy as the economically preferred option for a greater number of applications that call for utilizing ASSs [1].

2.1.1 Chemical Composition and Mechanical Properties of 304 / 304L SS Alloys

304 / 304L SS alloys are predominantly made of iron with Cr and Ni as their major alloying elements, which constitute about 18 – 20 % and 8 – 10.5/12 % respectively. The typical chemical compositions of 304 SS and 304L SS alloys [4] are given in table 2.1.

Element (Wt. %)	**Cr**	**Ni**	**C**	**Mn**	**P**	**S**	**Si**	**N**	**Fe**
304 SS	18 - 20	8 – 10.5	**0.08**	2	0.045	0.03	0.75	0.1	Balance
304 "L" SS	18 - 20	8 - 12	**0.03**	2	0.045	0.03	0.75	0.1	Balance

Table 2.1: Chemical composition of 304 SS and 304L SS alloys [4], all the values are maximum unless a range is otherwise indicated.

"L" in 304L SS alloy represents it as a low carbon grade version of 304 SS alloy, containing a maximum of only 0.03% C as opposed to a maximum of 0.08% C allowed in 304 SS alloy. This restriction of percentage of carbon present in the alloy composition of 304L SS alloy was done, so as to decrease the "effect of sensitization", with the idea that upon exposure to temperatures in the sensitization range, only a fraction of chromium undergoes carbide precipitation leaving the bulk of it intact for providing better corrosion resistance than offered by 304 SS alloy [3]. Additional information on the sensitization phenomenon of ASSs is given in the introduction and section 2.2. According to L. J. Jacobs et al. [3], the sensitization effect in 304L SS alloy took three times longer than in 304 SS alloy depicting enhanced corrosion resistance by the low carbon grade version of the alloy. The effect of carbon content on the sensitization behavior of stainless steels can be seen from the time-temperature-sensitization curves shown in figure 2.2.

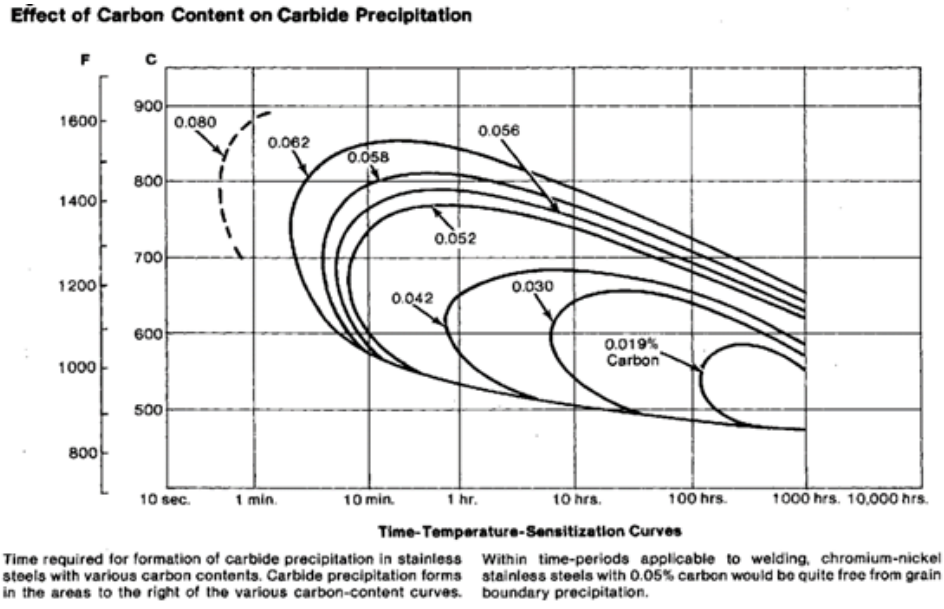

Figure 2.2: Time-Temperature-Sensitization curves showing the effect of carbon content on carbide precipitation [3].

The mechanical properties of 304 SS and 304L SS alloys [4] are given in table 2.2. Austenitic stainless steels exhibit high toughness to cryogenic temperatures, greater thermal expansion and heat capacity, with lower thermal conductivity than other types of stainless or

conventional steels [89]. Their deformation characteristics can be controlled by their chemical composition, and they are generally non-magnetic but, machining or working may turn them to slightly magnetic [89].

Mechanical Property / Alloy	0.2 % Offset Yield Strength (MPa)	Ultimate Tensile Strength (MPa)	Elongation in 2 inches (%)	Hardness, Rockwell B
304 SS	207 min.	517 min.	40 min.	92 max.
304 "L" SS	172 min.	483 min.	40 min.	92 max.
Typical for 3/8" plate	290	600	58	82

Table 2.2: Mechanical Properties of 304 SS and 304L SS alloys [4].

2.1.2 Effect of Alloying Elements of 304 / 304L SS

Chromium is by far the most important alloying element of stainless steels that prevents them from rusting. By adding a minimum of 10.5 % chromium to the alloy composition, a protective film of chromium oxide forms on the stainless-steel surface, by the reaction of chromium with oxygen in the atmosphere, thereby preventing the formation of rust because of the oxide film acting as a barrier between material and environment. With increasing chromium content in the alloy composition, the strength of the protective chromium oxide film increases. Therefore, chromium provides corrosion resistance in oxidizing conditions. Among all the alloying elements of 304 / 304L SS alloys, Cr and Si prompt the formation of ferrite within the alloy structure and are described as ferrite stabilizers. Whereas Ni, C, N, and Mn are depicted as austenite stabilizers.

Nickel is the second most important alloying element of ASSs, which along with manganese and nitrogen help maintain the austenitic microstructure of 304 / 304L SS alloys over a range of temperatures, all the way from cryogenic to their melting points. Nickel also provides

corrosion resistance in reducing conditions and empowers the ASSs with superior weldability and formability than exhibited by ferritic stainless steels, which only improve further with increasing nickel content in the alloy composition.

Carbon is an austenite stabilizer that enhances the strength of stainless steels through the formation of carbide precipitates. But, as an undesired consequence, results in decreased corrosion resistance, that deteriorates further with increasing carbon content in the alloy composition. Thus, the percentage of carbon content added to the alloy composition is varied and closely monitored according to the final application requirements.

Nitrogen increases strength and improves the localized corrosion resistance of stainless steels. *Silicon* increases their oxidation resistance. *Sulphur* and *Phosphorus* improve the machinability of stainless steels but come at a cost of reducing their corrosion resistance. Phosphorus also contributes to improving their strength. *Manganese* increases nitrogen solubility in steels.

2.1.3 Microstructure of 304 / 304L SS Alloys and Their Weldments

304 / 304L SS alloys are iron based austenitic stainless steels having face centered cubic crystal structure with chromium and nickel acting as their major alloying elements. From the iron-carbon (Fe-C) phase diagram, austenite phase gamma (ɣ), is stable only in the temperature range of 912 to 1394 °C with varying carbon content below 2.04 % C. However, as stated earlier in section 2.1.2, alloying ASSs or 304 / 304L SS with sufficient nickel and/or manganese and nitrogen (i.e., austenite stabilizers) will help the ASSs in retaining austenitic microstructure over a range of temperatures from cryogenic to their melting point. Therefore, due to the absence of phase transformations with varying temperatures, ASSs can only be hardened by work-hardening and not by heat treatment [89]. Apart from the ɣ matrix phase, the microstructure of 304 / 304L SS

consists of different carbides and nitrides, located within the matrix and along the grain boundaries. Generally, the carbides and nitrides formed are of type M_7C_3, $M_{23}C_6$ and Cr_2N depending on the amount of carbon and nitrogen present in the alloy composition. To get rid of these carbides and nitrides, annealing of 304 / 304L SS can be done in the temperature range of 950 – 1200 °C for 1 to 4 hours, which results in the complete dissolution of the carbides and nitrides into the ɣ austenite phase. Depending on the time and temperature used for the annealing treatment, the after heat treatment microstructure of 304 / 304L SS may contain uniform coarsened grains due to grain boundary migration or recrystallized grains due to coalescence of carbides, second phase particles, and grain boundary faceting [90].

The 304L SS weldments made with 308L filler rod were found to exhibit duplex microstructures according to G. Suresh et al. [91], showing a minor amount of residual primary delta (δ) ferrite phase distributed in the austenite matrix phase, as shown in figure 2.3 (a). As commonly known, during welding, two similar or dissimilar base metals are fused together by means of heat, with the help of a compatible filler rod, and the entire weldment is then allowed to cool relatively quickly generally in air medium. Depending on the filler rod composition and the welding process employed, δ ferrite could be present in the weld zone and during solidification of the 304L SS weldment, δ ferrite transformation to ɣ austenite would occur. However, since cooling of the weldment after welding process occurs relatively quickly, not enough time is present for the complete transformation of δ to ɣ, thereby resulting in some residual primary δ ferrite phase to be present in the 304L SS weldments.

According to G. Suresh et al. [91], residual δ ferrite of 8 – 15 % with different morphologies such as vermicular, lacy, and acicular was present in the 304L SS weldment as shown in figure 2.3 (b), (c), and (d). The formation of different morphological δ ferrite was attributed to the dissolution

of ferrite, resulting from thermal cycles during subsequent weld passes and variation in modes of secondary crystallization. It was also reported that the amount of ferrite was found to be maximum at the weld bead center, and gradually decreased along both the sides of the weld bead till its base. In figure 2.3 (e), the heat affected zone of 304L SS weldment exhibiting coarse austenite grains with ferrite at the grain boundaries can be observed.

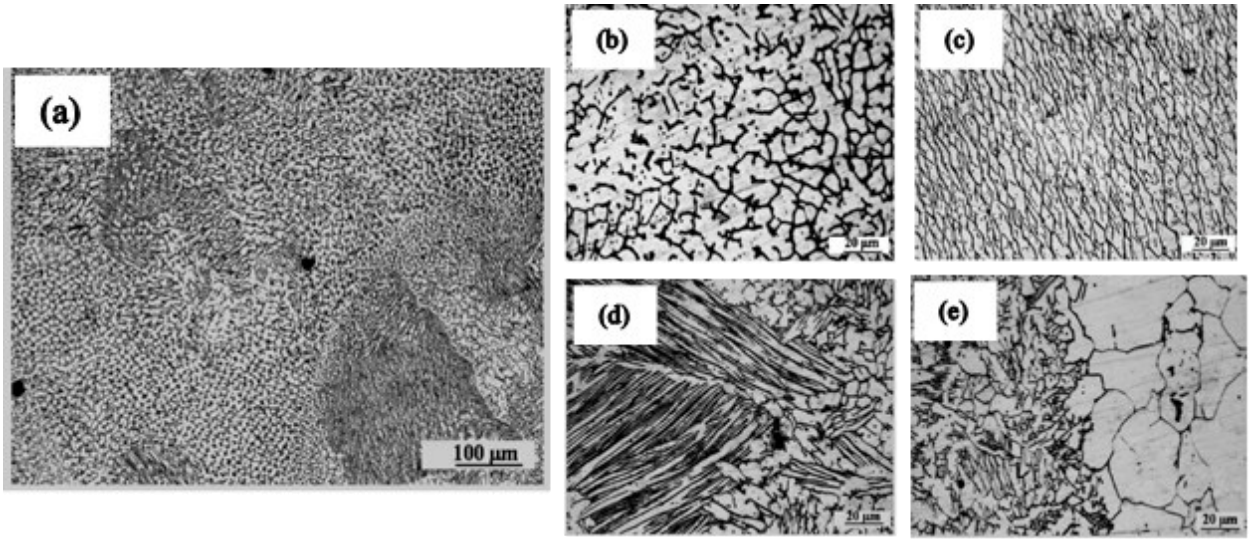

Figure 2.3:Optical micrographs of (a) weld region, (b) vermicular, (c) lacy, (d) acicular δ ferrite morphologies, and (e) heat affected zone of 304L SS weldment [66].

An austenite matrix with δ ferrite is said to have more resistance to hot cracking or micro-fissuring than a pure austenite matrix. A minimum of 5 FN (ferrite number) is required for welding consumables used in nuclear industry and a minimum of 3 FN for any multi-pass weld to prevent fissuring [92]. However, having residual δ ferrite in ASSs is not always desirable and largely depends on the nature of the final application. Especially when the final application requires good corrosion resistance, the presence of *greater amounts* of δ ferrite in the material is highly detrimental to the pitting corrosion resistance of ASSs, as the δ ferrite acts as a microstructural inhomogeneity, where pits can initiate readily. Additionally, at the δ ferrite – austenite interface galvanic cells can form with the depletion of chromium at the austenite side, leading to the initiation of pits at the interface that grow towards austenite phase [91].

Nevertheless, according to S. Krishnan et al. [93], the presence of less than 5 % δ ferrite in the material composition is beneficial to the pitting corrosion resistance of 304L SS and any percentage greater than that is considered deleterious to it. The benefit to having a small fraction of δ ferrite in the material composition is that it can help trap MnS inclusions present in the 304L SS alloy [91], which are believed to be the major pit initiation sites in the alloy [46][94][45]. As sulfur is more soluble in δ ferrite phase than in austenite phase, the MnS inclusions get entrapped by the δ ferrite, thereby decreasing the total number of pit initiation sites, consequently resulting in an increase in the pitting corrosion resistance of 304L SS [91]. But as stated earlier greater amounts of δ ferrite i.e., > 5 % is not desirable as it tends to decrease the pitting corrosion resistance of 304L SS alloy. Therefore, utmost care must be taken when choosing the filler rod and the type of welding process being employed, so that the % of δ ferrite seen in the final product is contained to a maximum of only 5 %. However, welding of ASSs results in an adverse phenomenon called as sensitization which is detrimental to their stress corrosion cracking resistance, and its causes and effects are discussed in the following section.

2.2 Chloride Induced Stress Corrosion Cracking of SNFDSCs

Chloride Induced Stress Corrosion Cracking (CISCC) is a type of intergranular corrosion, involving the selective attack of metal along its grain boundaries. It occurs in ASSs under tensile stress in the presence of O_2, chloride ions, and high temperature. More precisely, CISCC or stress corrosion cracking (SCC) in general, is a localized corrosion phenomenon like pitting and crevice corrosion, which initiates as pits and transforms to cracks when three criteria are met simultaneously as shown in figure 2.4. The three criteria are as follows: (1) a material susceptible to SCC, (2) presence of a sufficiently aggressive corrosive environment such as an environment with chlorides, O^2 and high temperature for CISCC, and (3) sufficient applied or residual tensile stresses present in the material, that can lead to the initiation and propagation of cracks [14].

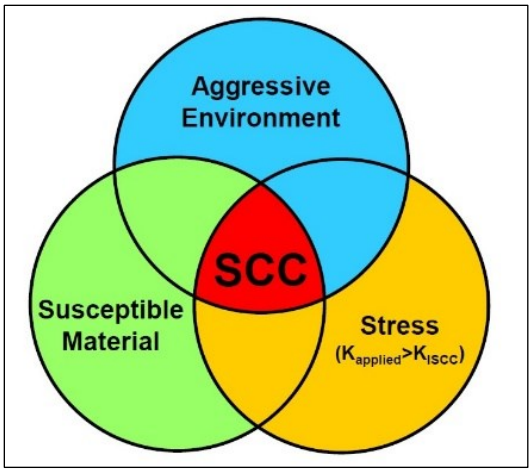

Figure 2.4: The three simultaneous criteria required for the SCC initiation and propagation.

The spent nuclear fuel (SNF) generated as a radioactive waste in the nuclear power generation plants is transferred to dry storage canisters (DSCs) for longer term safe interim storage at the reactor sites or independent spent fuel storage installation sites, as the United States does not currently have a final disposal pathway such as a natural geologic repository for the safe disposal of the SNF. Initially, these DSCs were intended as temporary storage until a more permanent disposal site was developed and were given licenses of up to 20 years with possible renewals of up to another 20 years. In 2011, 10 CFR 72.42 (a) was modified to allow for initial licenses to be up to 40 years with possible extensions to be available for another 40 years [95]. However, due to a lack of natural geologic repository as of now, these SNFDSCs may be required to continue their operation of storing the SNF waste for many decades beyond their original design intent. These SNFDSCs are predominantly made from *welded* austenitic stainless steels like 304 SS / 304L SS / 316L SS with most of them being made from 304 SS / 304L SS due to economic considerations, and the containers are enclosed within a *ventilated* concrete or steel overpack. Because of welding of ASSs and the ventilation of the SNFDSCs, it was found from several recent studies [5][6][20][21][22] that all the three criteria required for SCC to occur were present in the welded austenitic SNFDSCs situated near marine environment and if left unattended, they may undergo

catastrophic CISCC failures in the future. The presence of these three CISCC criteria in the welded austenitic SNFDSCs is discussed in the following paragraphs.

Upon welding or during high temperature operational service, the ASSs like 304 SS / 304L SS / 316L SS get exposed to temperatures in the range of 450°C to 850°C, due to which they undergo an adverse phenomenon called as sensitization [3][5][15][16][17]. Sensitization involves the depletion of Cr from areas immediately adjacent to the grain boundaries that combines with carbon present in the alloy, leading to the formation of chromium carbide precipitates ($Cr_{23}C_6$ and Cr_7C_3) and chromium depleted zones (CDZs) along the grain boundaries as shown in figure 2.5.

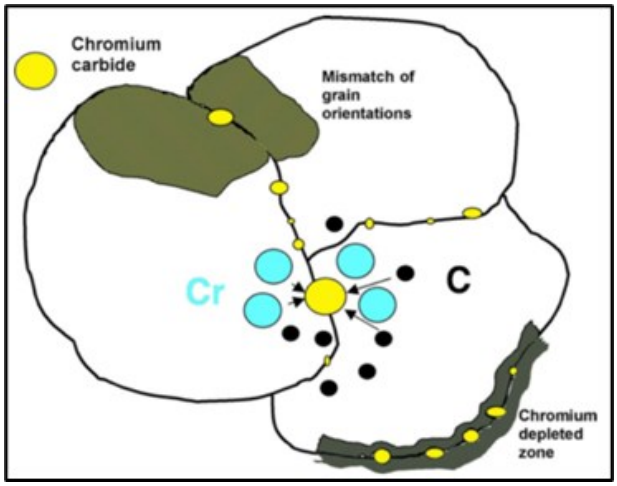

Figure 2.5: Sensitization phenomenon showing chromium carbide segregation / chromium depletion at the grain boundaries. [Source: https://www.ssina.com/education/corrosion/intergranular-corrosion/].

The ASS that has undergone the sensitization phenomenon is termed as "sensitized" austenitic stainless steel and the 304 SS specimen's microstructures prior to and after sensitization are given in figure 2.6 (a) and (b) respectively. The microstructure of non-sensitized 304 SS specimen seen in figure 2.6 (a) shows the absence of chromium carbide precipitates along the grain boundaries. Whereas the chromium carbide precipitates at the grain boundaries of completely sensitized 304 SS specimen appear as thick dark lines in its microstructure seen from figure 2.6 (b), with almost every grain boundary containing chromium carbide precipitates and chromium depleted zones. These CDZs contain less amount of chromium than the unaffected areas, and since

Cr is primarily responsible for the corrosion resistance of ASSs, the passive chromium oxide film formed at the CDZs will be weaker, making the sensitized ASS susceptible to intergranular stress corrosion cracking (IGSCC) [3][15][17][18][19]. Therefore, the austenitic SNFDSCs that are welded together, can be considered as components that are strongly susceptible to stress corrosion cracking and hence, it can be said that they exhibit the presence of the first out of the three criteria that lead to SCC.

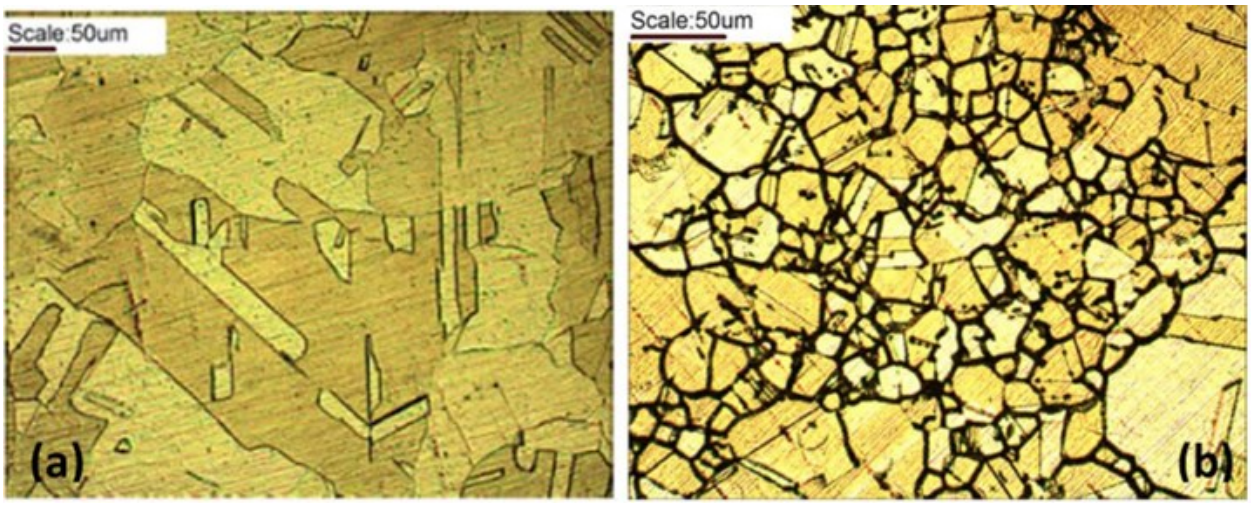

Figure 2.6: Optical micrographs of (a) non-sensitized and (b) sensitized 304 SS specimen [3].

According to Bryan and Enos [20], analysis of surface deposits on in-service and unused SNFDSCs situated near marine environment (Hope creek nuclear generating station in Delaware and Diablo canyon nuclear power plant in California) showed the presence of chloride rich salts deposited on the 304 SS canister surface. From the United States nuclear regulatory commission (U.S.NRC) results published in 2014 (NUREG/CR-7170) [5], it is anticipated that when spent nuclear fuel heat release slows down to the level where deliquescence of deposited chloride rich salts like $CaCl_2$, $MgCl_2$ and $NaCl_2$ occur at temperatures < 65°C, <52°C and <36°C respectively at a relative humidity of $30g/m^3$ and a surface concentration as low as $100mg/m^2$, an aqueous chloride-rich brine layer can form on the surface of the canisters, creating a sufficiently aggressive environment that can tend to the occurrence of SCC failures in the welded austenitic SNFDSCs.

Therefore, the second criteria for SCC to occur in the canisters is also present when these SNFDSCs are situated near marine environment.

When it comes to the third criteria for SCC, the external/applied loads on the SNFDSCs are only a small fraction of the 304 SS's yield stress, thereby lacking sufficient driving force for crack initiation/propagation [14]. However, NRC modeled canister longitudinal and circumferential welds using finite element methods showed that sufficient tensile stresses to cause SCC were present through the thickness of the canister wall within the heat affected zone (HAZ) of the canister weldments that can lead to full penetration with time [21][22]. Therefore, all the three criteria that lead to the occurrence of SCC or CISCC failures are present in the welded austenitic SNFDSCs that are situated near marine environment.

Replacing the SNFDSCs will be very expensive and their potential failure due to chloride induced stress corrosion cracking (CISCC) would be catastrophic to both human life and the environment. Hence, prolonging their service life by long term reliable cost-effective in-situ repair and mitigation methods is of immediate and utmost importance for the nuclear industry. Moreover, these repair methods must involve low heat input, should not cause sparks or place high mechanical loads on the canister surface. Three such promising repair methods are cold spary (CS), laser assisted cold spray (LACS), and additive friction stir (AFS/MELD) which have already been used to successfully deposit several materials and can be used in conjuction with ultrasonic nanocrystal surface modification (UNSM) treatment as a cost-effective mitigation technique.

Mitigation of SCC can be done by either modifying the microstructure or changing the environment or altering the nature of stresses present in the material. While changing the environment may not be plausible for most applications, modifying the microstructure and nature of stresses in the material can be done by surface treatment techniques like surface mechanical

attrition treatment, shot peening, laser shock peeing, low plasticity burnishing, ultrasonic nanocrystal surface modification etc., by inducing near-surface nano crystallization, near-surface hardening and compressive residual stresses into the material which are all beneficial in mitigating SCC. It is well known that laser shock peening (LSP) technique is already being employed by the nuclear industry in the production of new canisters, to mitigate the tensile residual stresses formed at the heat affected zone during welding [55]. UNSM is a relatively new novel technique which once developed for in-situ applications can be a cost-effective SCC mitigating alternative technique to other surface treatment technologies like LSP. More on CS, LACS, AFS, and UNSM are discussed further in the following sections.

2.3 Laser Assisted Cold Spray (LACS) and Cold Spray (CS)

LACS is a hybrid solid-state materials deposition process that involves the combined application of laser preheating of the substrate or powder particles before or during the deposition process accompanied by the deposition of metal powders through the traditional CS deposition technique [81]. The main components involved in the LACS system and the schematic demonstrating the LACS deposition process are given in figure 2.7.

It was first developed by Bray et al. [96] in the year 2009, who coupled a laser diode of 980 nm wavelength to a CS gun and used the system to deposit Ti powders of < 45 µm onto a mild

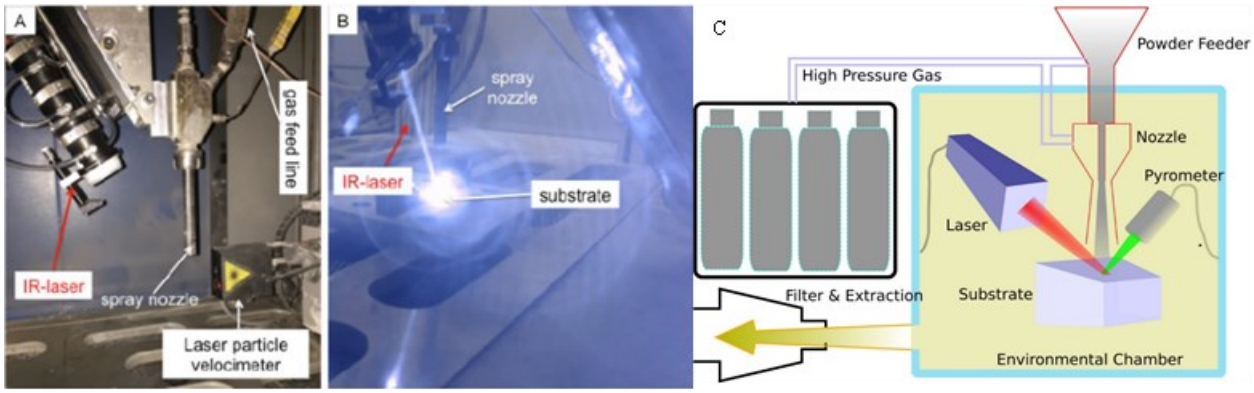

Figure 2.7: (a) Main components of LACS system, (b) LACS system during operation and (c) Schematic of LACS deposition technique [71].

steel substrate. They found that as the substrate temperature increased by the irradiation of the tlaser laser diode, the deposition efficiency of the Ti coatings increased, while the coatings porosity decreased. Since 2009, LACS deposition technique has been used successfully to deposit materials like Co-based stellite [97][98][99], Fe-Ni-Zr oxide dispersion strengthened alloy [83], 4340 steel [67], Al – 12 Wt. % Si coatings [100], CrMnCoFeNi base high entropy alloy (HEA) [68] etc.

The traditional cold gas dynamic spraying (or cold spray - CS) from which the LACS was developed, is a type of thermal spraying technique. It was initially developed in the mid - 1980s at the Institute for Theoretical and Applied Mechanics of the Siberian Division of the Russian Academy of Science [101] and later, was introduced at the laboratory level in the 2000s to the North America and Europe. The CS technique involves the solid-state deposition of metal powders, that are propelled at supersonic velocities with the help of a de laval nozzle onto a substrate material, resulting in the metal powders to deform plastically upon impact forming a cohesive bond with the substrate or prior deposited particles. The supersonic velocities of 300 – 1200 m/s during CS are achieved by a combination of two factors, (1) by the geometry of de lavale nozzle of the CS gun and (2) by heating propellent gases like N_2, He, air or a mixture of them to high temperatures in the range of 200 to 850°C, both of which aid in accelerating the powder particles brought into the CS gun [81]. The powder particles are brought into the CS gun by a high pressure carrier gas that is usually of the same nature as that of the propellent gas. The schematic of the CS gun is given in figure 2.8. The gas temperature may seem high at first glance but, the divergence of the nozzle causes expansion of gases resulting in a significant lowering of their temperatrue. Also, the powder particles have a very limited residence time in the hot gas flow due to which they remain in a solid or slightly viscous state. Generally, fine powders in the range of 5 – 50 μm are used for CS but, under appropriate conditions coarser powders can also be cold sprayed.

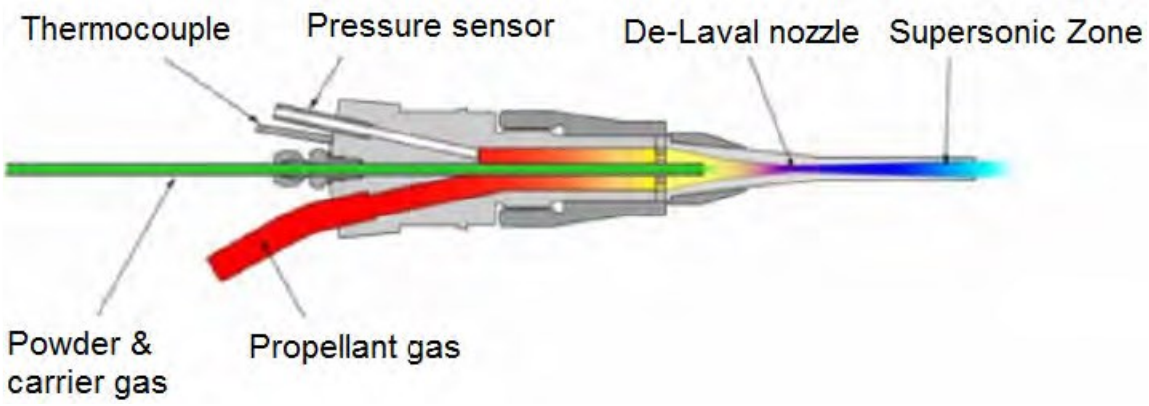

Figure 2.8: Schematic of Cold Spray gun.

Compared to the conventional thermal spraying technologies like plasma spraying, high velocity oxygen fuel (HVOF), arc spraying etc., cold spray is characterized with a low spraying particle temperature and high spraying particle velocity - figure 2.9. The major advantage of cold spray technique over other conventional thermal spraying technologies is that CS does not involve any macroscopic melting of the spraying particles since, the spraying powder particles are heated to temperatures much below their melting point. Therefore, the common problems associated with the conventional thermal spraying technologies, like high temperature oxidation, evaporation, melting, crystallization, tensile residual stresses, debonding, gas release, etc. are minimized or eliminated. However, cold spray technique faces other challenges that are discussed in the following paragraphs.

A study performed by X. M. Meng et al. [74], in which cold spray deposition of 304 SS powder particles using N_2 gas was done, have reported that the cold sprayed coating exhibited an ultimate tensile strength (UTS) and elongation after fracture of only 65 MPa and 0.1 % respectively. To improve the coating properties, they performed a post heat-treatment on the coating by annealing it at 950°C for 1hr which resulted in an increase in elongation after fracture and UTS by up to 3 % and 357 MPa, respectively. However, the UTS of cold sprayed + annealed 304 SS was still considerably lower than the UTS of bulk conventionally processed 304 SS's value

of 709 MPa [102]. The much lower UTS of cold sprayed + annealed 304 SS coating was attributed to the defects present in its microstructure like the pores and the agglomerated oxide particles which would induce the fracture taking place much in advance than the bulk 304 SS specimen.

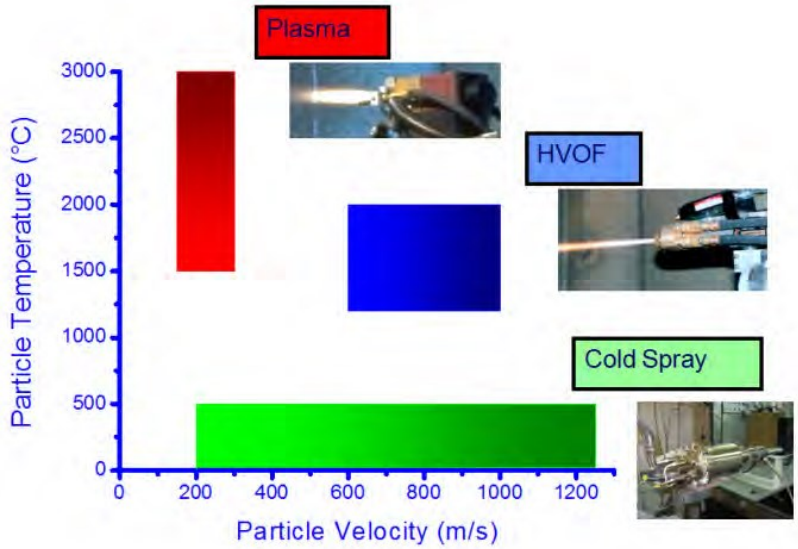

Figure 2.9: Comparison of particle temperature and particle velocity of cold spray technology with that of the other conventional thermal spray techniques.

In a different study performed by P. Coddet et al. [69], He gas was used as the propellent gas during the cold spray deposition of 304L SS powder particles, and they have reported that the deposited coating exhibited a very high UTS and yield strength (YS) of 629 MPa along with a higher hardness value of 440 $Hv_{0.2}$, but with very little measurable ductility, showing 0% fracture strain during the tensile tests, that ended up in brittle fracture as shown in figure 2.10. It was also noted that the inter-particle bonding characteristics of CS coatings sprayed with He gas showed significant improvent than the coatings sprayed with N_2 gas. However, the brittle nature of the cold spryaed 304L SS coatings sprayed with He gas, suggests that the improvement in inter-particle bonding was not sufficient enough to use the coatings without any post heat-treatment. Therefore, even in this study, to restore ductility in the CS coating, post annelaing heat-treatment was done at 1050°C for 4 hours, due to which they observed an improvement in fracture strain up to 9.9 % but,

with a consequent decrease in UTS, YS and hardness values to 422 MPa, 310 MPa and 144 $Hv_{0.2}$ respectively. The simultaneous increase in fracture strain and decrease in UTS, YS, and hardness was attributed to the microstructural reorganization and reduction in rate of stacking dislocations by annealing treatment.

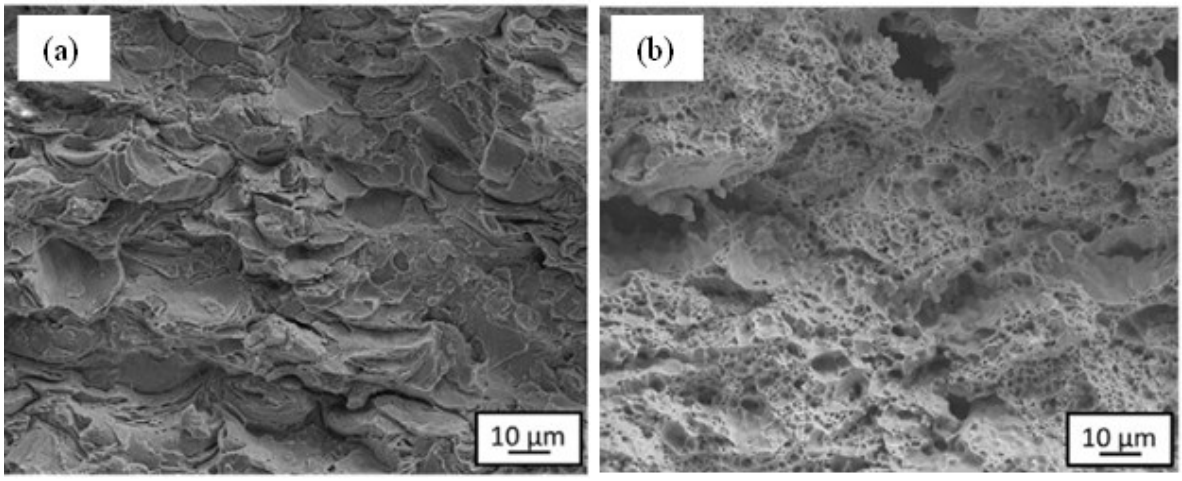

Figure 2.10: SEM micrographs showing after tensile test fracture surfaces of specimens in (a) as cold-sprayed condition exhibiting brittle fracture and (b) annealed at 1050°C for 4 hours condition exhibiting ductile fracture [79].

According to a few studies, the corrosion behavior of cold sprayed ASSs was observed to exhibit mixed behavior [76][70], with it being largely dependent on the coating thickness, powder particle size and their distribution, nature of carrier and propellant gases, inter-particle bonding achieved, post heat treatment etc. The corrosion resistance has been reported to improve with an increase in coating thickness. Also, it was stated that using He gas during CS deposition process resulted in denser coatings that exhibited better corrosion resistance than the coatings cold sprayed with N_2 gas [70]. The conclusion, as reported by several authors [69][70][103], is that during the traditional CS process, the supersonic velocites achieved by heating He gas were significantly higher than those achieved by heating N_2 gas, consequently resulting in denser coatings with better mechanical and corrosion properties, due to the slightly better interparticle bonding achieved by the coatings that are sprayed with He gas rather than with N_2 gas.

However, the cost of He gas is significantly greater than the cost of N_2 gas, making the usage of He gas over N_2 gas, a very expensive option. Even when CS coatings were sprayed with He gas, they were not 100% dense, still possessed a significant amount of porosity and needed much more improvement in their inter-particle bonding characteristics thereby, exhibiting inferior mechanical and corrosion properties than the bulk metal that is conventionally processed. Moreover, CS deposition process has limitations on coating thickness that can be deposited, requires surface preparation for optimal coating adhesion, and demands post heat treatment to achieve desirable properties. Hence, it can be said that the CS deposition process by itself has many drawbacks that need to be addressed for attaining better coatings. And most of these problems associated with the CS deposition process can be solved by simultaneously applying laser technology to the traditional CS deposition technique which is termed as laser assisted cold spray desposition technique.

LACS process involving the use of laser to locally heat the substrate prior to or during deposition eliminates the need for surface preparation and also, enhances the adhesion between powder particles and the substrate [81]. Using laser technology simultaneosuly with the traditional CS deposition process can result in heightened interparticle bonding and reduced porosity, leading to improved mechanical and corrosion properties than exhibited by the traditionally cold sprayed coatings. R. Nikbakht et al. [68], made a comparitive study on the CS and LACS deposition of CrMnCoFeNi high entropy alloy (note that its properties are comparable to that of 304 SS alloy) using N_2 as the propellent gas. They reported that deposition with traditional CS technique resulted in dense coatings but with inferior inter-particle bonding. Whereas deposition with LACS technique resulted in much denser coatings with significantly improved inter-particle bonding characteristics. The SEM micrographs, showing the inter-particle bonding characteristics of

CrMnCoFeNi high entropy alloy (HEA) deposited using both CS and LACS deposition techniques are given in figure 2.11. The micro-hardness values of HEA coatings sprayed with CS and LACS deposition techniques were reported to be 361 Hv_{100gf} and 391 Hv_{100gf} respectively which were both significantly higher than the atomized powder hardness value of 166 Hv_{10gf}. The higher hardness values of both the coatings was attributed to the high dislocation density and grain refinement that was observed by them from the XRD analysis, which was showing wider full width half maximum (FWHM) for the coatings than the FWHM of powder feed particles. Also, the EDS map analysis performed by them on the LACS deposited HEA alloy coating revealed a homogenous microstructure with no localized segregation.

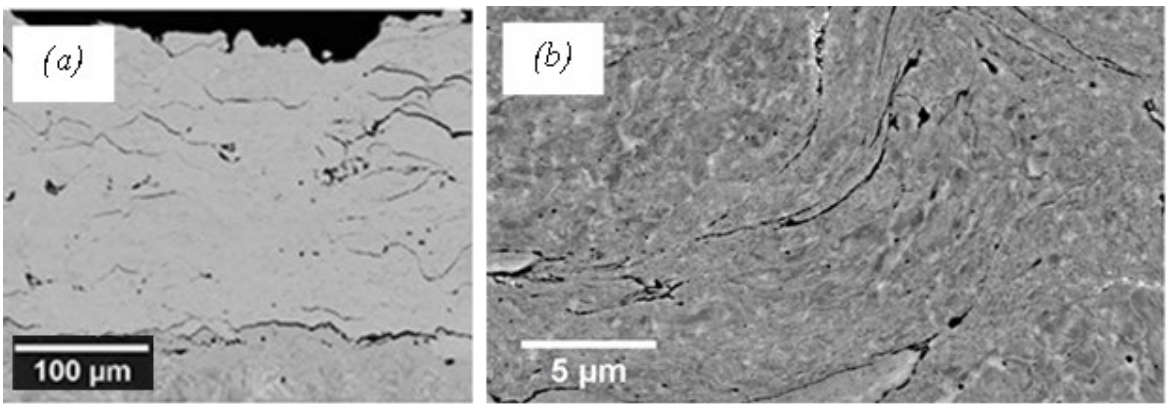

Figure 2.11: SEM micrographs of CrMnCoFeNi high entropy alloy deposited with (a) CS process showing inferior inter-particle bonding and (b) LACS process showing better inter-particle bonding [55].

In another study performed by Luke N. Brewer et al. [67], the deposition of 4340 steel with CS and LACS techniques was compared with each other and it was reported that the depostion efficiency achieved by CS coatings was 48% which improved notably to 72% in LACS coatings sprayed with a laser heat of 950°C. Similar to HEA, 4340 steel coatings deposited with both CS and LACS deposition techniques showed higher hardness values than the atomized powder, with LACS exhibiting slightly higher hardness value of 592 Hv than CS coating's measured hardness of 561 Hv. The higher hardness of CS 4340 steel coating was attributed to the strain hardening

upon impact while that of the LACS coating was attributed to the martensite phase formation at the higher temperature that arises due to laser application. The porosity levels in both the coatings were measured to be less than 1% but the inter-particle bonding characteristics were found to be significantly better in the case of LACS 4340 steel coating.

The quality of properties attained and the rate of deposition of coatings are directly related to the amount and the rate at which the heat is applied and removed from the impact zone which can be controlled with high precision by using laser technology. Also, controlling the impact temperature through laser heating eliminates the need for gas heating which is an essential part of the traditional CS deposition technique thereby, avoiding dangerous problems associated with the use of high process gas temperatures [96]. Additionally, LACS can eliminate the need for post heat treatment by in-situ annealing the typical cold work generated by the bombardment of powder particles during the traditional CS deposition technique and controlling the cooling rate of the deposited particles can allow for controlled recovery and recrystallization. Furthermore, LACS process involves partial to no melting thereby, avoiding the typical problems associated with laser based technologies like thermal stressing, distortion, dilution and other microstructural problems making it a very reliable technology for producing better coatings. However, because of the simultaneous application of laser, the beneficial compressive residual stresses produced during traditional CS can be relieved by recovery and recrystallization. Also, recrystallization tends to increase the grain size of the coating consequently decreasing its hardness. Hence, a cost-effective mitigating technique such as UNSM treatment can be applied on the LACS coatings to induce nano crystallization, CRSs and near surface hardening in them that are all proven to beneficially improve the SCC resistance of a material [1][48][49][50][40][41][44].

2.4 Additive Friction Stir (AFS / MELD) Deposition

Additive Friction Stir (AFS) / MELD manufacturing technique derived from friction stir welding (FSW) and friction stir processing (FSP) [104] was developed by Aeroprobe corporation. AFS/MELD technique designed to create fully dense metal parts by combining additive manufacturing, friction stir welding, and computerized numerical control (CNC) machining evolved into an enhanced and unique manufacturing technology of its own. The schematic of AFS/MELD manufacturing and the finished product of a pressure vessel made by AFS/MELD are presented in figure 2.12. The distinguishable feature of AFS/MELD processing from that of FSW and FSP processes is that there is no contact between the rotating tool shoulder and the substrate or the previously deposited layer. AFS/MELD can be used to join, repair, clad and additively manufacture similar/dissimilar/multi metals or alloys and it has been used successfully to deposit alloys of IN 625 [85], 316L SS [86], AA219 [105], Ti-6Al-4V [87] etc.

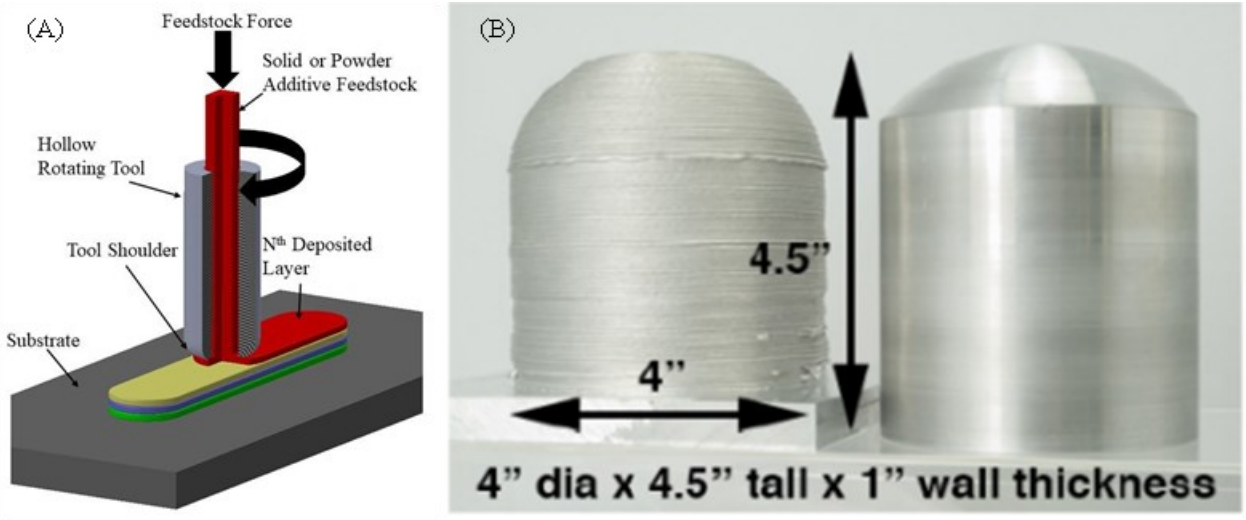

Figure 2.12: (a) Schematic of AFS/MELD manufacturing technique and (b) pressure vessel produced by AFS/MELD technique.

The process of AFS/MELD involves heating a consumable powder or solid filler rod placed in the rotating tool shoulder to a semi solid state by induction or resistance heating which is then mechanically mixed by the CNC controlled rotating tool shoulder and deposited onto the substrate

layer by layer in a semi solid state under hydrostatic pressure. The height of the rotating tool shoulder will be raised to accommodate successive material layer deposition forcing the material into the former layer ensuing a strong metallurgical bond between layers. Also, by design, the heat affected zone (HAZ) in AFS/MELD manufacturing will be limited to the regions of filler rod and the substrate directly below the tool. Furthermore, the combined action of mechanical mixing by CNC controlled rotating tool shoulder and the applied hydrostatic pressure on the semi solid feedstock material results in a fully dense defect free part eliminating the general problems encountered in fusion-based techniques such as porosity, elemental segregation, hot cracking, dilution, and distortion in finished parts [85].

P.G. Allison et al. [85], reported that deposition of IN 625 through AFS/MELD resulted in a refined, equiaxed grain structure as shown in figure 2.13 with excellent mechanical properties exhibiting an YS and UTS of 730 MPa and 1072 MPa respectively, whereas other fusion based additive manufacturing processes showed a columnar preferred orientation with comparatively inferior mechanical properties.

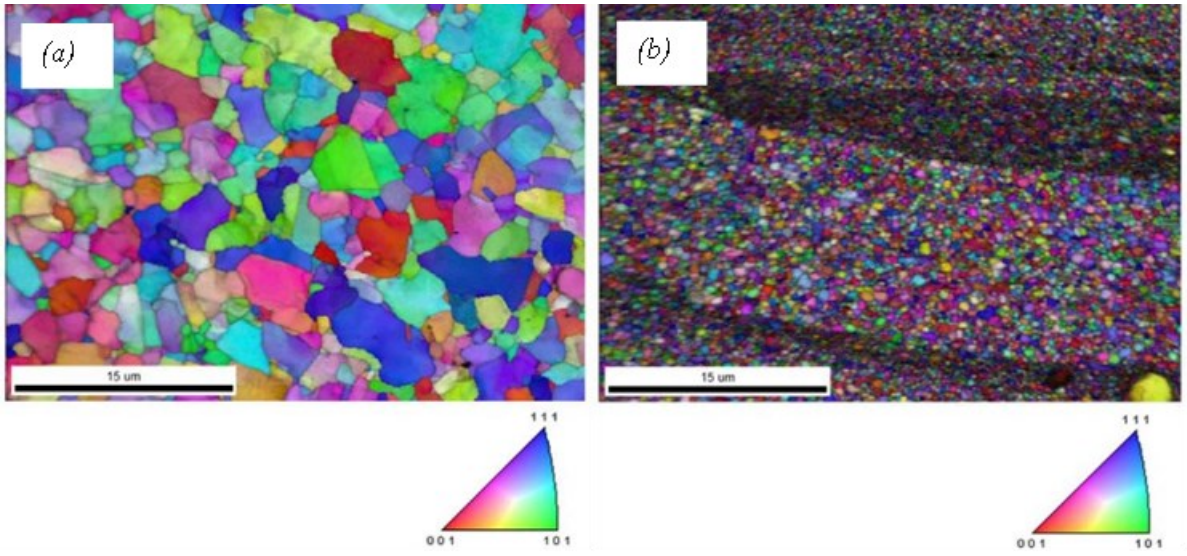

Figure 2.13: EBSD maps of AFS deposited IN 625 (a) in the middle of the layer showing equiaxed grains and (b) layers interface showing fine size equiaxed grains [60].

Also, E. Farabi et al. [87], deposited Ti-6Al-4V in the form of plates using AFS/MELD deposition technique and reported a homogenous microstructure with negligible porosity and mechanical properties of 20% ductility, 1010 MPa YS and 1233MPa UTS which were noted to be superior than the properties obtained with other conventional wrought and melt-based additive manufacturing techniques. Therefore, AFS/MELD being a solid-state deposition process with minimal HAZ can be applied locally on a large scale in open atmosphere with high deposition rates to similar/dissimilar metals and alloys resulting in near-wrought refined homogenous microstructure having excellent mechanical properties throughout the 3D build.

2.5 Ultrasonic Nanocrystal Surface Modification (UNSM)

The UNSM treatment technique is a patented technology developed for commercial applications by DesignMecha Co., Ltd. [47][49]. It is a methodology for improving the characteristics of metals by utilizing ultrasonic energy. The UNSM technique controls the quality, properties, and surface characteristics of a material by modifying the material properties at the near-surface of the treated area, improving the fatigue, wear, and corrosion resistance of a material, by inducing compressive residual stresses, near-surface nano crystallization, and near-surface hardening into the material through severe plastic deformation during UNSM.

UNSM is an advanced mechanical surface treatment technique that involves the application of high-frequency ultrasonic vibrations to a material's surface through the combined action of static and dynamic loads transmitted via a tungsten carbide tool tip [47]. The WC tool tip repeatedly strikes the surface of the specimen with approximately 10 to 20 thousand shots per square millimeter at a rate of several thousands of strikes per second (20-40 kHz) in a highly controlled manner through the UNSM's computerized numerical control (CNC) machine. The UNSM machine consists of three main components as seen in figure 2.14 (a): (1) generator and piezoelectric transducer generating the ultrasonic vibrations at 20 kHz, (2) acoustic booster holding

the single/double horn (used for soft/hard materials respectively) amplifying the generated ultrasonic vibrations and (3) tungsten carbide tool tip physically transmitting the ultrasonic energy to the surface of the material through the combined application of static and dynamic loads. The dimension of the vibrating part, which contacts the surface, allows vibration amplitudes of 10 – 100 µm to be attained. A homogenous treatment is obtained on the treated surface. The principle of UNSM is based on the instrumental conversion of harmonic oscillations produced by acoustically tuned body into resonant impulses of ultrasonic frequency by energizing an ultrasonic transducer [49].

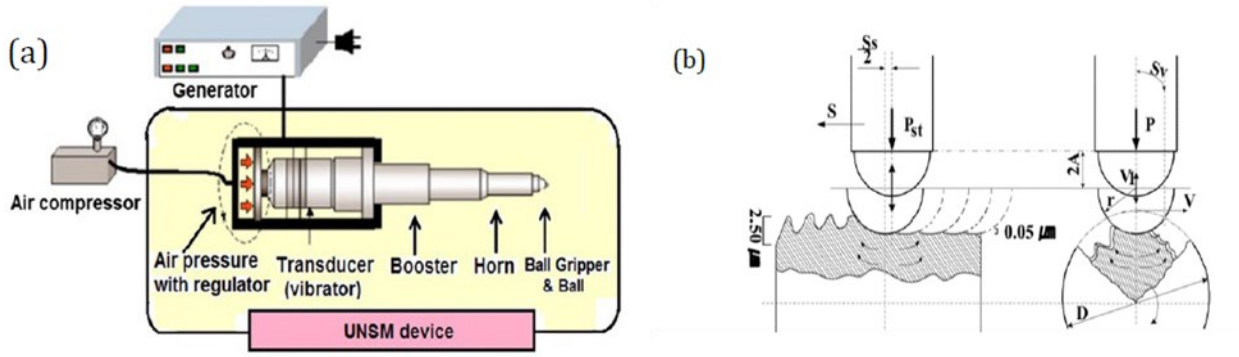

Figure 2.14: (a) Schematic representation of UNSM setup and (b) motion of WC tip / impact of static and dynamic loads during UNSM treatment [46][47].

The energy generated from the transducer impacts the surface of the work piece with a total striking force of $F = Pst + P \sin 2\pi ft$ where Pst is static load (N), P is the amplitude (µm), f is frequency (Hz), and t is time (s), as seen in figure 2.14 (b) (i.e., with combined static (Pst) and dynamic loads ($P \sin 2\pi ft$)) [48][49]. The number of strikes per unit area (mm^2) through UNSM treatment is given by $N = (60*f) / (v*s)$ where f is frequency (Hz), v is peening speed (mm/min) and s is interval feed rate (mm); and the associated strain energy density (J/mm^3) is given by $E = (F * N * A) / d$ where F is the load applied (N), N is the number of strikes per mm^2, A is amplitude (µm) and d is the ball tip diameter (mm) [50].

The tool tip produces innumerable micro-dimples on a specimen surface causing severe

plastic deformation at and near-surface of the specimen leading to the formation of nano crystal microstructure at its immediate surface. Each of the micro-dimples can function either as a micro-hydrodynamic bearing in cases of full or mixed lubrication and as a micro-reservoir for wear debris in lubricated conditions. Traditionally, silicon nitride ceramic (Si_3N_4) and/or tungsten carbide (WC) balls and pins, having high spherical accuracy and smoother surface are used as the striking media by attaching them to a single/double horn as shown in figure 2.14 (a). The sizes of pins and balls typically range in between 1.2 – 6 mm in diameter. The choice between material and size of pins and balls to be used as tool tip, strongly depends upon the material and mechanical properties of the specimen being UNSM treated and on the final effects desired from the UNSM treatment. The UNSM treatment induces severe plastic deformation on the surface of a specimen, resulting in high compressive residual stresses both at the surface and through the depth of the material, near surface nano crystallization and appreciable near surface hardening [51] which are all beneficial in mitigating SCC. UNSM has been used successfully to enhance performance of materials like ATI 718 alloy [40], stainless steels [41][44][45][46][50], tool steel [48], Ti-6Al-4V [42], and magnesium alloys [43][52] by improving their properties.

Amanov et al. [49], reported the formation of nanostructured surface layer in SAE 52100 bearing steel through UNSM treatment up to a depth of 100μm as seen in figure 2.15. Refined grains of size 50nm were reported up to 10μm depth from the surface, followed by 100nm grains up to 30μm and 500nm grains up to a depth of 100μm before reaching their original grain size, resulting in a gradient nanostructure near the material's surface. The surface hardness after UNSM was reported to have increased to 840 Hv due to nano crystallization at the surface, following the Hall-Petch relationship of showcasing higher hardness with a decrease in grain size. They also reported that CRSs of up to -900 MPa were observed in the UNSM treated bearing steel.

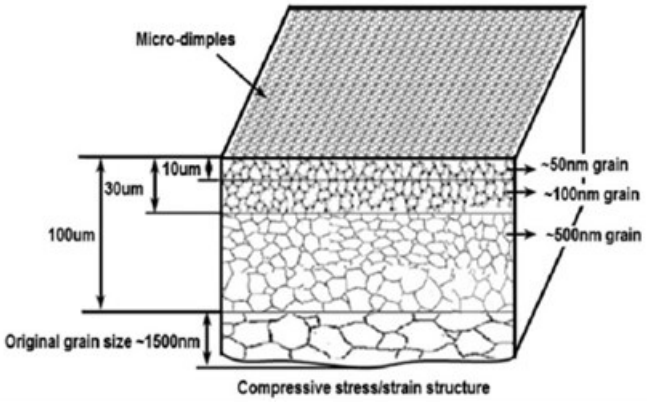

Figure 2.15: Grain size distribution at the surface of bearing steel subjected to UNSM treatment [47].

Chang Ye et al. [44], also reported gradient nanograined microstructure observed in austenitic 304 SS with a 100% austenite to martensite phase transformation occurring at the surface due to the SPD induced in the material by UNSM. The amount of martensite transformation was said to have decreased through the depth of the material and was observed by them up to a depth of approximately 80 – 100 μm from the specimen surface as shown in figure 2.16.

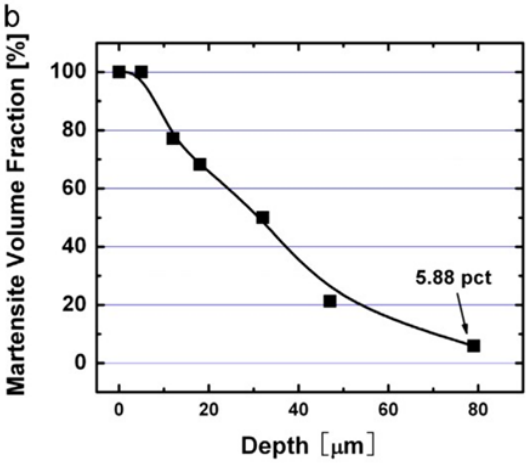

Figure 2.16: Through the depth martensite volume fraction present in UNSM treated 304 SS [42].

In another study performed by Chang Ye et al. [41], it was reported that UNSM treatment of 304 SS weldments resulted in an increase in their near surface hardness and a surface residual stress transformation in the weldments from tensile to compressive in nature as seen in figure 2.17 (a). Compressive residual stresses of -200 to -300 MPa were reported to be present up to a depth

of ~ 250µm as seen in figure 2.17 (b). Surface hardness of the UNSM treated 304 SS weldment was reported to have nearly doubled from 210 Hv to 400 Hv and the increase in hardness was seen by them up to a depth of ~ 400µm from the surface of the weldment before reaching the as-welded hardness values. And the through-the-depth micro-hardness profile observed by them is given in figure 2.17 (c).

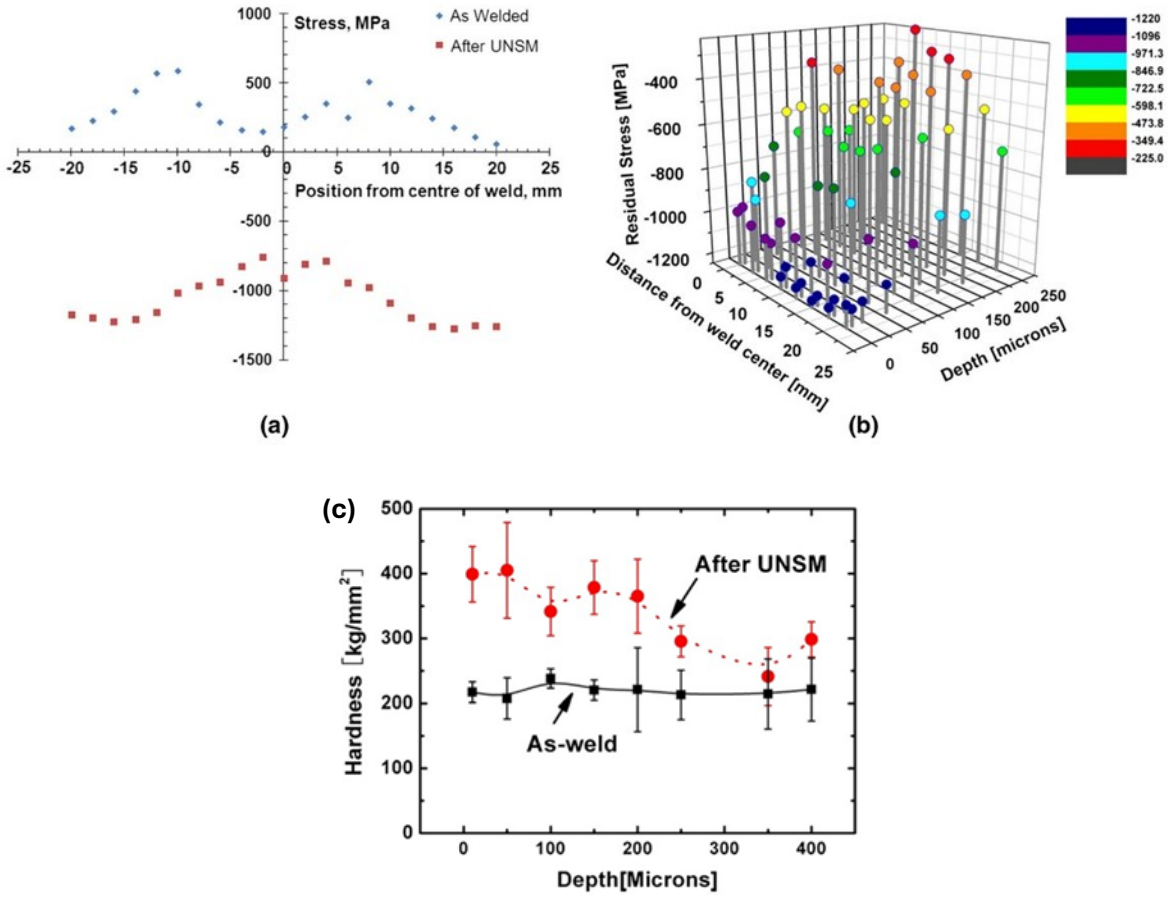

Figure 2.17: (a) Surface residual stress distribution across the weldment before and after UNSM, (b) through the depth residual stress distribution across the weldment after UNSM, and (c) through the depth microhardness values of 304 SS weldment before and after UNSM [39].

Corrosion behavior of 304 SS weldments with and without UNSM treatment were determined by them through boiling MgCl2 tests. Upon exposure to boiling MgCl2 solution, cracks were reported to be observed on the surface of as-welded samples after 72 hours of exposure whereas no cracks were said to be found in UNSM treated 304 SS weldments even after 120 hours

of exposure. The cracking was attributed to the tensile stresses present in the weldments prior to UNSM treatment leading to SCC in the as-welded specimens. Finally, it was concluded that UNSM treatment improved the corrosion resistance of 304 SS weldments in chloride containing environment. Shengxi li et al. [45], studied the pitting resistance of UNSM treated 304 SS in 3.5 Wt.% NaCl solution and found that surface re-passivation improved by UNSM due to the grain refinement of the surface layer. They also reported that the MnS inclusions that were primarily responsible for the pitting corrosion in 304 SS were broken-down and completely removed by UNSM treatment.

Therefore, it can be said that UNSM treatment can beneficially impact the factors that influence the SCC resistance of a material. Moreover, research studies investigating the effects of UNSM treatment on the microstructure, mechanical and corrosion properties of "sensitized" (i.e., representative of welded specimen) 304 "L" SS alloy (i.e., the low carbon grade version of 304 SS alloy), especially corrosion properties in simulated seawater concentration containing chloride environment i.e., in 3.5 Wt. % NaCl solution were not found in the open literature. Furthermore, the effects of UNSM treatment on the properties of LACS and AFS deposited 304L SS alloy have not been studied yet, with the successful deposition of 304L SS alloy through LACS, AFS techniques being reported very recently. Hence, in this thesis work the effects of UNSM on the microstructure, hardness, residual stress, and corrosion properties of sensitized, CS, LACS and AFS deposited 304L SS alloy have been studied thoroughly and the observed results are discussed extensively, whose knowledge would be extremely important to the nuclear industry in tackling the CISCC challenge faced by the SNFDSCs situated near marine environment.

Chapter 3. Experimental Methodology

This chapter provides a detailed description of the 304L SS materials processed in different ways, their surface preparation for the surface and heat treatments, along with details on the ultrasonic nanocrystal surface modification (UNSM) treatment parameters used in this research work to surface treat the differently processed 304L SS alloy, and the various characterization techniques used, to evaluate the impact of UNSM treatment on the material properties of sensitized, cold sprayed, laser assisted cold sprayed, and additive friction stir deposited 304L SS.

3.1 Materials and Specimen Preparation

3.1.1 Baseline (Conventionally Hot-Rolled & Solution Annealed – CH-R & SA) and Sensitized 304L SS Materials

A 3 mm thick conventionally hot rolled 304L SS plate having the chemical composition as shown in table 3.1, that is solution annealed (SA) at 1080°C followed by water cooling was obtained for this research from Sandia National Laboratory. To study the sensitization behavior of 304L SS alloy, coupons of 30 mm x 30 mm x 3 mm dimensions were aged/sensitized in a conventional Thermolyne Type 48000 furnace at 600°C, 650°C, 675°C and 700°C for 5 h & 24 h followed by air cooling. The furnace temperature was measured using a K-type thermocouple.

Element	C	Ni	Cr	Mn	P	S	Si	N	Mo	Cu	Fe
Wt. %	0.024	8.02	18.2	1.33	0.028	0.001	0.31	0.068	0.29	0.45	Balance

Table 3.1: Chemical composition of conventionally hot rolled & solution annealed 304L SS plate material that is obtained from Sandia National Laboratory.

3.1.2 Cold Sprayed (CS) & Laser Assisted Cold Sprayed (LACS) 304L SS Coatings

Multiple 304L SS coatings processed through CS and LACS deposition techniques as shown in figure 3.1 were obtained from The University of Alabama. These coatings were made by the deposition of 304L SS powder particles onto a 3 mm thick 304L SS substrate material, using

the processing parameters given in table 3.2. The obtained coating's thickness and area dimensions were measured to be 3 mm and 27 mm x 34 mm respectively for both the CS and LACS 304L SS coatings.

Process	Gas	Pressure (Psi)	Temperature (°C)	Laser Heat (°C)	Laser speed (mm/s)	Coating Thickness (mm)	Number of Passes	Sample size
CS	He	600	350	N/A	N/A	3	4	27 mm x 34 mm
LACS	He	600	350	950	10	3	4	27 mm x 34 mm

Table 3.2: Processing parameters used for depositing the 304L SS powder particles onto the 304L SS substrate material using the CS and LACS deposition techniques.

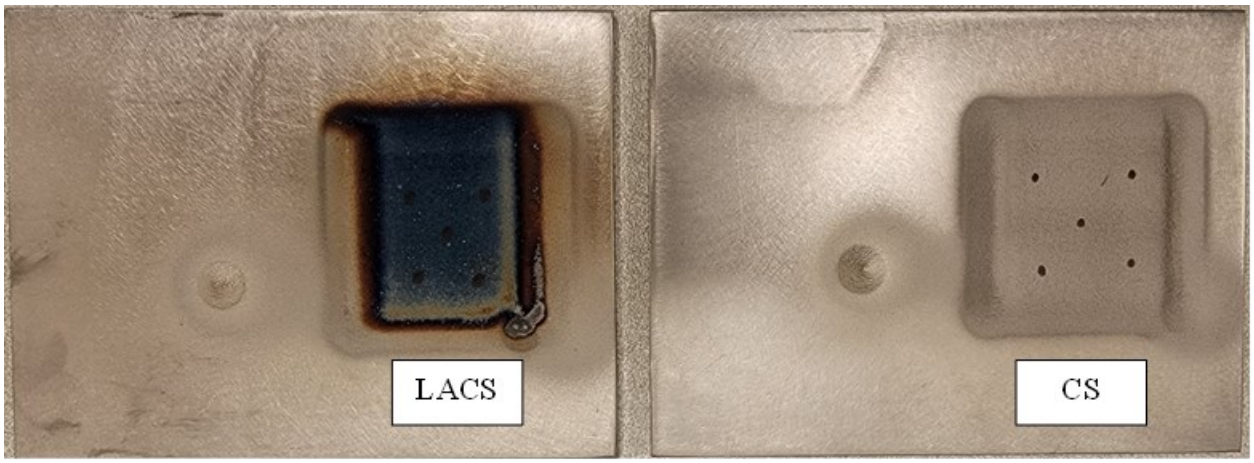

Figure 3.1: Top view of as-CS and as-LACS 304L SS coatings made on 304L SS substrate.

3.1.3 Additive Friction Stir (AFS / MELD) Deposited 304L SS Cladding

An AFS / MELD processed 304L SS cladding deposited onto a stainless-steel substrate material, which was processed with suitable processing parameters was obtained from The University of Alabama. The image of as processed AFS / MELD 304L SS cladding that was obtained and used for this study, along with its nomenclature defining the build and line directions of its deposition are given in figure 3.2. The thickness and the area dimensions of the obtained cladding were measured to be 7 mm and 17 mm x 76 mm, respectively.

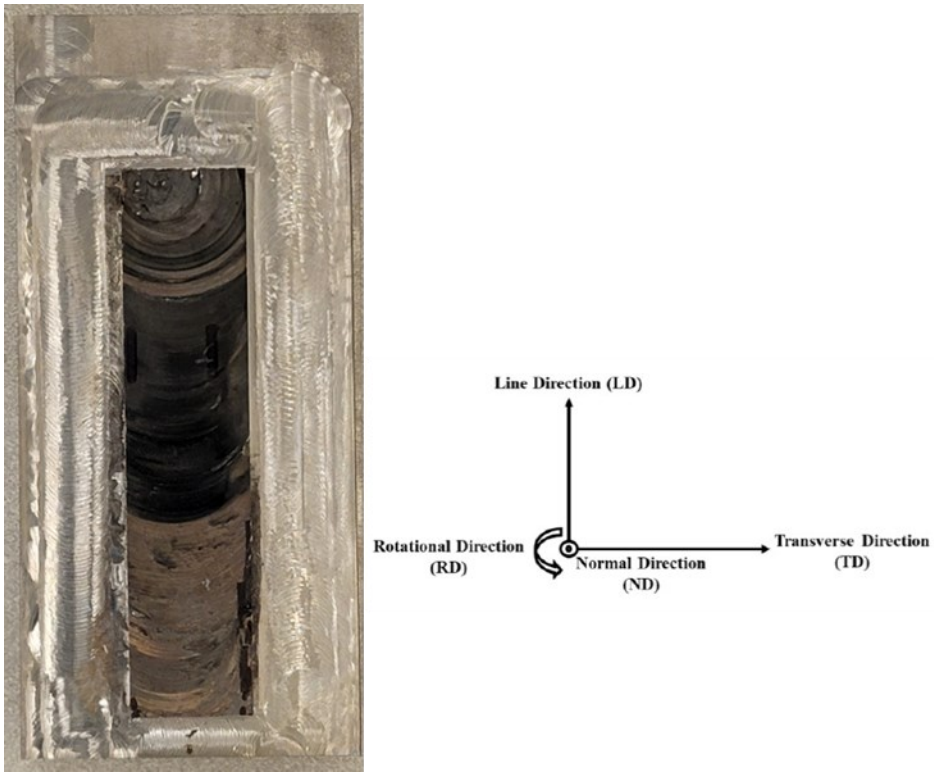

Figure 3.2: Top view of as-AFS/MELD deposited 304L SS cladding.

3.1.4 Surface Preparation

Prior to performing the corrosion tests on the untreated - SA and sensitized 304L SS specimens - while studying the alloy's sensitization behavior, for performing the corrosion tests on the CS, LACS, and AFS 304L SS specimens in their polished surface condition, and prior to the application of UNSM treatment on the surface of SA, sensitized, CS, LACS, and AFS 304L SS materials, polishing of the specimen surfaces has been done. However, it must also be noted that in the case of CS, LACS, and AFS 304L SS specimens, UNSM treatment has been done on their as-is surface condition as well, for studying the impact of UNSM treatment on both of their as-is and polished surface conditions, for reasons stated later in this dissertation research work.

Nevertheless, whenever polishing action was required, it was performed on the several different 304L SS specimen surfaces studied in this research work in a similar manner as follows, it was performed by gradually grinding the respective 304L SS material surface on the silicon

carbide – SiC emery papers, by first grinding it on 180 grit paper followed by 320 grit, 600 grit, 800 grit, and finally finishing with or obtaining the final surface finish on 1200 grit emery paper. The polished 304L SS specimens were then cleaned with de-ionized water and dried thoroughly, prior to subjecting them to either corrosion tests or UNSM surface treatment. The polishing was done manually on Buehler Ecomet 250 system that is shown in figure 3.3.

Figure 3.3: Buehler Ecomet 250 system used for polishing the distinct 304L SS specimens studied in this dissertation research work.

3.1.5 Sectioning of Test Specimens

The CH-R & SA, CS, LACS, and AFS 304L SS plate / coatings / cladding materials were sectioned to the dimensions required by the various tests performed on them, using Accutex SP-300I electric discharge machine shown in figure 3.4.

Figure 3.4: Accutex SP-300I electric discharge machine used for sectioning the various 304L SS specimens.

3.2 Ultrasonic Nanocrystal Surface Modification (UNSM)

The UNSM surface treatment involves four different processing parameters namely, static load (SL), dynamic load / amplitude (A), peening speed (PS), and pitch / interval feed rate (IFR) as shown in figures 2.14 (b) and 3.5. The UNSM surface treatment is generally performed in a zig zag manner as represented by the direction of arrows in figure 3.5. The longer arrows and shorter (shown as pitch) arrows shown in figure 3.5 correspond to the transverse direction (TD) and step direction (SD) of UNSM surface treatment respectively.

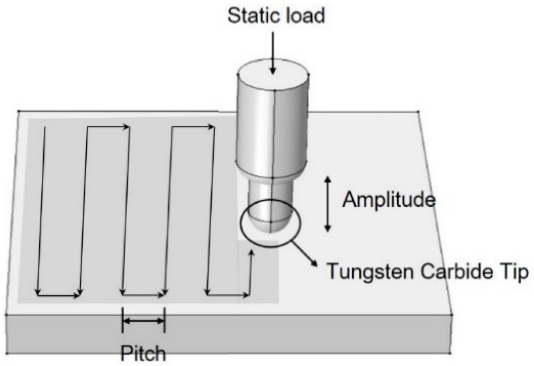

Figure 3.5: Schematic of UNSM process showing its various parameters.

The UNSM surface treatment performed with different combinations of parameters yields different results for different materials. Therefore, firstly, a UNSM parametric study was done to determine the most beneficial UNSM parameters that can be used for surface treating the 304L SS alloy. For this purpose, a total of 16 UNSM parameter combinations involving two static loads (20 N and 40 N), two amplitudes (8 µm and 20 µm), two peening speeds (2000 mm/min and 3000 mm/min) and two interval feed rates (30 µm and 70 µm) were employed. The combination of parameters used in this parametric study are shown in table 3.3.

The UNSM surface treatments were performed on LM-520 system at a frequency of 20kHz and the load transfer to the material surface was made with a WC tool tip of 2.38mm in diameter. The set up of LM-520 system located at University of Cincinnati, which is utilized for this study is shown in figure 3.6 (a). Oil spray was used for cooling the specimens during UNSM treatment

as shown in figure 3.6 (b) and the oil residue on the surface treated specimens was cleaned thoroughly with high pressure deionized (DI) water followed by ultrasonic cleaning in DI water for 10 minutes at room temperature. UNSM peens of 20 mm x 20 mm dimensions were made on 16 different 304L SS specimens of 30 mm x 30 mm x 3 mm dimensions (that were cut from the CH-R & SA plate specimen) using the UNSM parameter combinations shown in table 3.3.

Peen Number	Static Load (N)	Amplitude (µm)	Peening Speed (mm/min)	Interval Feed Rate (µm)	Number of shots per mm^2
1	20	20	2000	30	20000
2	20	20	2000	70	8571
3	20	20	3000	30	13333
4	20	20	3000	70	5714
5	20	8	2000	30	20000
6	20	8	2000	70	8571
7	20	8	3000	30	13333
8	20	8	3000	70	5714
9	40	20	2000	30	20000
10	40	20	2000	70	8571
11	40	20	3000	30	13333
12	40	20	3000	70	5714
13	40	8	2000	30	20000
14	40	8	2000	70	8571
15	40	8	3000	30	13333
16	40	8	3000	70	5714
2.38mm diameter WC tool tip.					

Table 3.3: Combination of UNSM parameters employed for performing the UNSM parametric study.

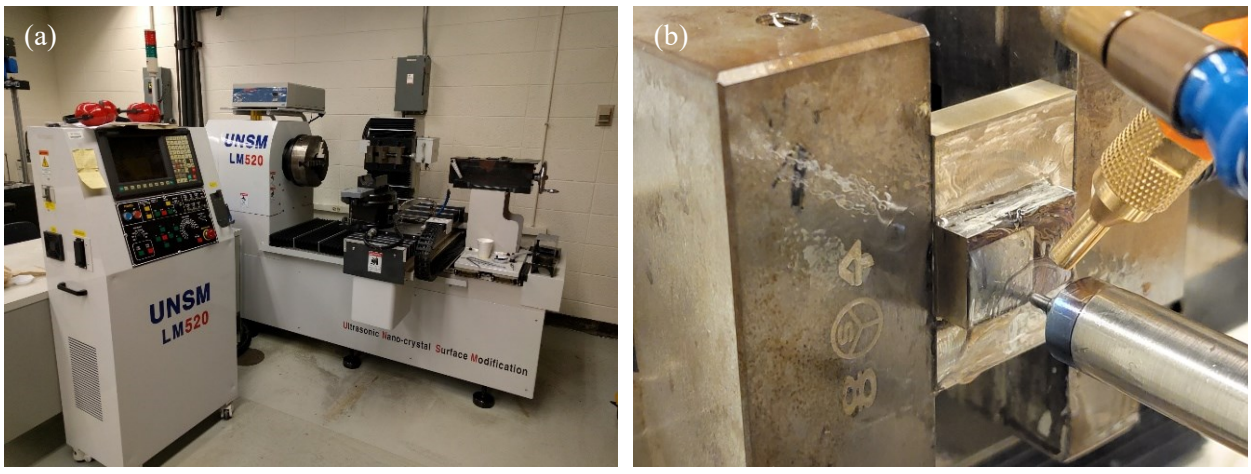

Figure 3.6: (a) LM-520 Ultrasonic Nanocrystal Surface Modification system at University of Cincinnati and (b) the image showing the application of oil spray during the UNSM surface treatment.

The material properties considered for determining the most optimal UNSM parameters - that will be used in further studies, for surface treating the distinct 304L SS materials studied in this dissertation research work (sensitized, CS, LACS, and AFS) - were surface roughness, surface residual stress, through-the-depth residual stress and near-surface & sub-surface hardness. These properties were chosen as the criteria because of the positive impact they have on the stress corrosion cracking resistance of a material. The UNSM parameter combination that yields the best combination of low surface roughness, high surface compressive residual stress (CRS), greater depth of CRS induction, high near-surface hardness, and deeper hardness penetration depth results, will be used in further studies for surface treating and studying the impact of UNSM on the several properties of sensitized, CS, LACS, and AFS 304L SS materials.

For studying the impact of UNSM treatment on the properties of sensitized 304L SS alloy, the two preliminary studies i.e., the sensitization study and the UNSM parametric study of 304L SS alloy were put together i.e., the impact of UNSM treatment on the properties of sensitized 304L SS alloy were studied by peening the most sensitized 304L SS specimen with the most optimal UNSM parameter combination obtained from the UNSM parametric study. Also, as mentioned in the previous paragraph, the UNSM surface treatment on CS, LACS, and AFS 304L SS specimens was performed using the same optimal UNSM parameters, which comprise of *40 N static load, 8 μm amplitude, 2000 mm/min peening speed and 0.03mm interval feed rate/pitch*.

In the case of SA and sensitized 304L SS specimens, the UNSM treatment was performed on them, only after polishing them to a 1200 grit surface finish. But in the case of CS, LACS, and AFS 304L SS specimens, the UNSM surface treatment was performed on them, when they were in two different surface conditions: (1) in as sprayed / as deposited surface condition and (2) in polished to 1200 grit surface finish condition. This was done this way, so as to study the corrosion

behavior of the 304L SS coatings / cladding with respect to their surface finish, since their surface roughness values were extremely high, and also, as LACS and AFS processing techniques involve semi-high to high temperatures, their surface characteristics could be different from that of the CH-R & SA specimen, which could impact their corrosion behavior and these different surface characteristics might also influence the impact, the UNSM surface treatment can have on the properties of CS, LACS, and AFS 304L SS specimens, with a dependence on them being in their as-is or polished surface conditions. Therefore, the UNSM surface treatment was performed on the CS, LACS, and AFS 304L SS specimens, in both of their as-is and polished surface conditions.

Accommodating the initial dimensions of differently processed 304L SS specimens, UNSM peens of varying dimensions were made on them as follows: 20 mm x 20 mm peens on 30 mm x 30 mm x 3 mm sensitized specimens; 25 mm x 25 mm peens on CS & LACS coatings; and 28 mm x 16 mm peens on AFS cladding. All these UNSM peens of different dimensions made on the distinct 304L SS specimens are presented in figure 3.7. Finally, the impact of UNSM treatment on several properties such as the microstructures, phases, hardness, surface topography, residual stress, and corrosion properties of sensitized, CS, LACS, and AFS 304L SS materials were investigated in this research work, and the obtained results are presented and thoroughly discussed in Chapter 5 of this dissertation.

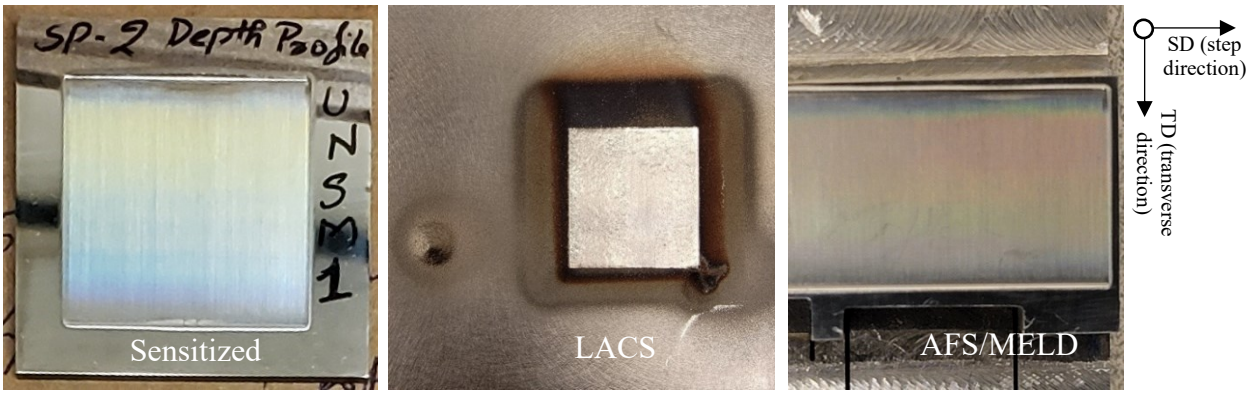

Figure 3.7: UNSM peens performed on sensitized, CS/LACS, and AFS/MELD 304L SS alloy.

3.3 Surface Topography Analysis

Surface roughness (Ra) measurements were measured with a non-contact optical profilometer - Bruker contour GT equipped with vision 64 software. The optical profilometer used for this dissertation research work is given in figure 3.8. During the Ra measurements, the surface of the specimen was scanned using white light illumination in vertical scanning interferometry (VSI) mode using 5X objective lens at 1X speed. The length of the scan was adjusted according to the surface being measured. For every specimen a minimum of five scans were taken, and their average surface roughness values are presented in the current dissertation research work.

Figure 3.8: Bruker contour GT optical profilometer.

3.4 X-Ray Diffraction Phase Analysis

UNSM surface treatment induces severe plastic deformation (SPD) into a material that can result in phase transformations. Especially in CH-R & SA 304L SS specimen, it is well known that near-surface austenite to martensite phase transformation occurs due to its UNSM surface treatment. However, as this dissertation research work involves different 304L SS materials possessing distinct prior microstructural characteristics, the phase changes associated with UNSM treating these differently processed 304L SS specimens were studied using Rigaku X-ray

Diffraction (XRD) system, to evaluate any dissimilarities in the phase transformations involved in these distinct 304L SS specimens by their UNSM treatment. The Rigaku XRD system used for this research work is shown in figure 3.9. The XRD scans were performed using Cu-Kα radiation at 40kV and 44mA, employing Bragg-Brentano focusing method. A 2θ scan range of 20°-110° was measured for every specimen with a step size of 0.02° at a speed of 0.5s per step. The obtained raw XRD pattern data was processed using MDI/JADE software.

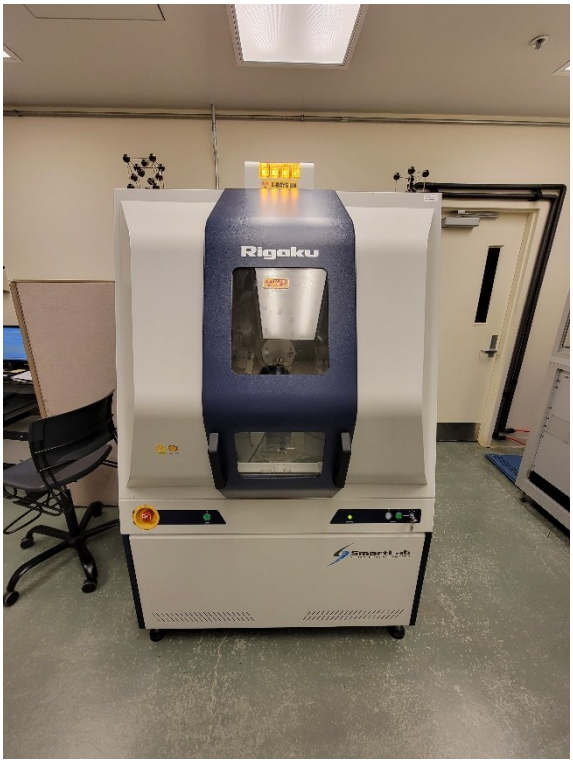

Figure 3.9: Rigaku X-Ray Diffraction system.

3.5 Residual Stress Analysis

The residual stresses (RS) present in the differently processed 304L SS specimens before and after UNSM surface treatment were determined through X-Ray diffraction technique utilizing the Proto LXRD system employing the conventional $Sin^2\psi$ technique. The Proto LXRD system at UC, the principles of x-ray diffraction stress measurement, and the specimen placement in the proto LXRD system, along with the measurement's directional indices (0° and 90°) are shown in figure 3.10. While measuring the residual stress via X-Ray diffraction technique, the strain in the

crystal lattice is measured and the residual stress corresponding to that strain is calculated, assuming a linear elastic distortion of the crystal lattice [106]. The severe plastic deformation produced in the specimen by the surface treatment leads to changes in the spacing of the lattice planes that causes a change in their stress-free value to that of a new value which then corresponds to the magnitude of residual stress present in the specimen at that point of measurement.

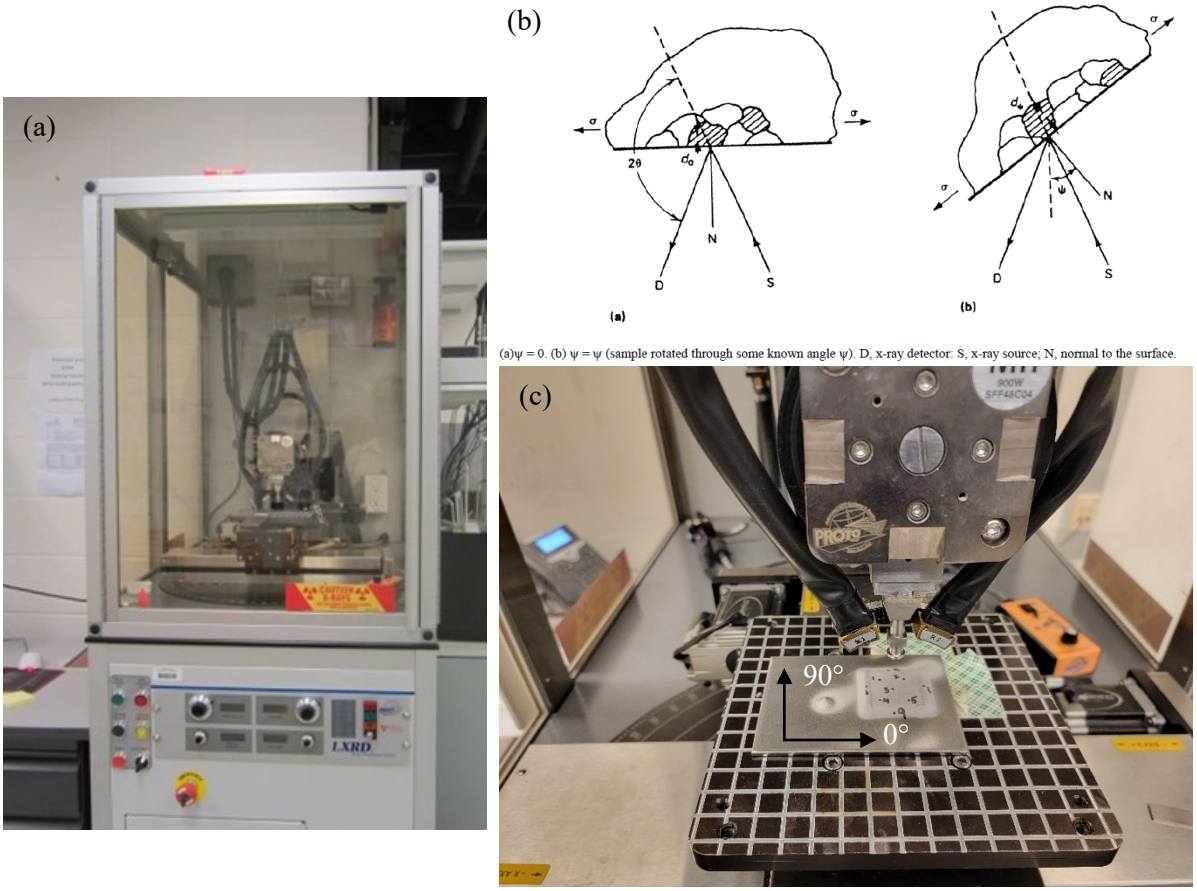

Figure 3.10: (a) Proto LXRD system at UC, (b) principles of x-ray diffraction stress measurement [85], and (c) specimen placed in the proto LXRD system showing the residual stress measurement's directional indices.

To determine the RS pertaining to the austenite phase of 304L SS alloy, Mn X-ray tube with a wavelength of 2.103A° was used to acquire the {311} peak at a 2θ value of 155.10° whereas to determine the RS pertaining to the martensite phase induced by UNSM in 304L SS alloy, Cr X-ray tube with a wavelength of 2.2897A° was used to acquire the {211} peak at a 2θ of 152.80°. The X-ray detectors were equipped with vanadium filters while using Cr tube and no filters were

used for Mn tube as recommended by the manufacturer of proto LXRD system. The X-ray $S_2/2$ elastic constants used for austenite and martensite phases were 7.18 x 10^{-6} MPa^{-1} and 5.67 x 10^{-6} MPa^{-1} respectively and a round aperture of 2 mm diameter was used for X-ray beam emission. The residual stress on the surface of every specimen was measured at five different locations in both of its orthogonal directions (0° and 90°) and their respective average values are presented in this thesis work.

Through-the-depth residual stress profiles along both the orthogonal directions of all the differently processed 304L SS specimens after their UNSM treatment were obtained, by measuring residual stress at the center of the specimens at different depth intervals via layer-by-layer material removal method using electropolishing technique on Buehler Electromet 4 system. The Buehler Electromet 4 system used for material removal in the current research work, which is located at UC is presented in figure 3.11.

Figure 3.11: Buehler Electromet 4 electro-polisher at UC.

Electropolishing technique was used for material removal in this research work because it prevents stress alteration in the specimens while removing material, unlike the mechanical material removal methods. The electropolishing solution used for material removal comprises of 87.5 % methanol and 12.5 % sulfuric acid. To prevent the specimen surface from overheating, each electropolishing cycle was limited to less than 90 s. During the electropolishing cycle, the solution

was kept at room temperature and the system voltage was adjusted accordingly so as to maintain the current generated during electropolishing withing the range of 2.2 A – 2.6 A.

The depth intervals used for the residual stress measurements up to a depth of ~ 100 μm from the surface of any of the specimens studied in this research work, were kept to a small range of 10 μm – 30 μm, because the variance in the residual stress near the surface of a UNSM treated specimen would be significantly higher, due to the gradient nature of the microstructure that is generally obtained due to its UNSM surface treatment, with nano crystals being present at its absolute near-surface. The depth intervals used beyond the 100μm depth from the specimen surface, were gradually increased to 50 μm - 80 μm, with the intent of determining the depth up to which the compressive residual stresses were induced into the different 304L SS materials researched in this dissertation work by their UNSM surface treatment. Strain and depth gradient corrections were applied to the measured residual stress values in accordance with SAE J784a standard using the standard Moore and Evans software available with the Proto LXRD system.

3.6 Nano Hardness Analysis

Nanoindentation hardness testing was performed using Anton Paar's CSM indentation system equipped with Berkovich indenter having a trigonal pyramid profile. The hardness tester setup used for this research, which is located at UC is given in figure 3.12. To determine the depth hardening impact induced by UNSM in all the different 304L SS specimens studied in this research work, through-the-depth nano hardness profiles of all the specimens with and without UNSM treatment were obtained on their respective cross-sectioned areas.

The cross-sectioned 304L SS specimens that are required for performing the hardness depth profiles were sectioned by EDM, and their cross-sectional areas were cold mounted in epoxy resin. The mounted specimen's surface was prepared for hardness testing, by gradually grinding them on SiC emery papers starting from 180 grit to 1200 grit. During nano hardness testing, a maximum

load of 100 mN was applied on the specimen's surface, at a loading / unloading rate of 200 mN/min per indentation, with a holding time of 5 s at the maximum load. To avoid indentation-overlap, the distance between adjacent indentations was maintained at 30 μm. Three sets of hardness depth profiles per specimen were performed, to check for discrepancies and repeatability of results. Their average values are presented in this dissertation.

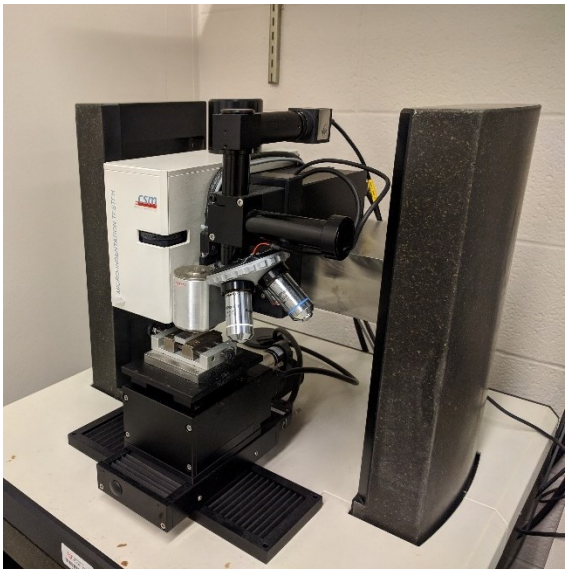

Figure 3.12: Anton Paar's CSM nano / micro hardness indentation system at UC.

3.7 Corrosion Tests

Corrosion tests of sensitized, CS, LACS, and AFS 304L SS specimens prior to and after UNSM treatment were performed in two different solutions: (1) in 0.5M H_2SO_4 + 0.05M KSCN solution, which are called as the double loop electrochemical potentiodynamic reactivation (DLEPR) tests, which help in determining the degree of sensitization or degree of susceptibility (DOS) of a material i.e., the strength of the passive film formed on the material surface, depending on which the material proportionally resists / undergoes corrosion and (2) in 3.5 Wt.% NaCl solution - simulating seawater containing environment, which are called as the cyclic potentiodynamic polarization (CPP) tests, which help to determine the corrosion rate and pitting corrosion behavior of a material in chloride containing environment. However, it must be noted

that during the initial sensitization study performed on the 304L SS specimens, in which the alloy's sensitization behavior was determined, only DLEPR tests were performed.

The corrosion tests were executed in a gamry paracell connected to a gamry instruments reference 600 potentiostat as shown in figure 3.13 (a). The test setup involves a conventional three-electrode system with saturated calomel electrode (SCE) as the reference electrode, graphite as the counter electrode and the metal specimen as the working electrode (anode). The graphite electrode and the metal specimens were thoroughly cleaned with de-ionized water and dried before performing the corrosion tests. Electrochemical sample masks of $1cm^2$ area were used to keep the area of metal exposed to corrosive solution constant among all the specimens, as shown in figure 3.13 (b), whose purpose was also to reduce crevice corrosion.

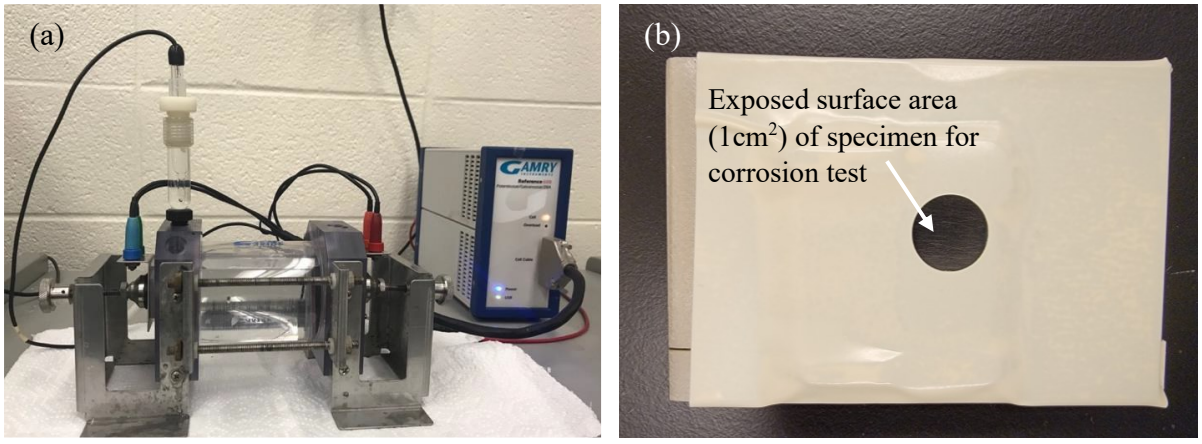

Figure 3.13: (a) Gamry Reference 600 Potentiostat and the corrosion tests setup, and (b) specimen masked with electrochemical sample mask for carrying out the corrosion test.

Prior to performing the open circuit potential (OCP), the paracell with the test solution was de-aerated with compressed Ar gas for 1 hour followed by sealing the paracell chamber with ace threaded nylon plugs. The cyclic corrosion tests were initiated only after a near steady state OCP was achieved, followed by a potential (vs SCE) sweep from -500mV (vs SCE) to 1000mV (vs SCE) at a rate of 2V/h (0.56mV/s) during the forward scan. At the apex voltage the scanning direction was reversed, and the reverse scan was performed at the same rate of 2V/h (0.56mV/s)

until the initial voltage of -500mV (vs SCE) was reached. Both the corrosion tests (i.e., DLEPR and CPP), carried out on all the different 304L SS specimens studied in this research work, were performed at room temperature following the same procedure as outlined above.

DLEPR corrosion tests generate a curve that is plotted between potential vs logarithmic current density comprising of a loop with anodic/forward scan and reactivation/reverse scan. A typical curve obtained as a result of the DLEPR test is presented in figure 3.14. During a DLEPR test, a passive film forms on the surface of the test specimen during the forward scan, and depending on the strength / weakness of the passive film formed on the specimen surface, a proportional amount of metal dissolution occurs in the material during the reverse scan, which occurs by the local disintegration of the passive film by the corrosive test solution, leading to a localized and/or uniform corrosive attack on the metal specimen surface, depending on the microstructural characteristics of the specimen being tested.

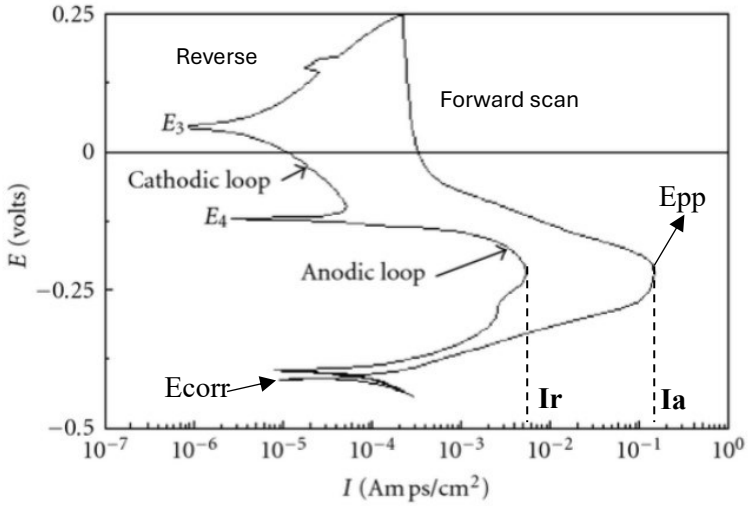

Figure 3.14: Typical DLEPR test curve showing the forward and reverse scans along with various potentials and current densities that can be obtained from it.

The current density at which the passive film starts to form during the forward scan is known as the peak activation current density (Ia). The degree of metal dissolution occurring by the breakdown of passive film during the reverse scan is represented by the peak reactivation current

density (Ir). Finally, the degree of sensitization or susceptibility (DOS) of a specimen or the strength of the passive film formed by the material on its surface, can be determined quantitively from the following formula, % DOS ratio = (Ir/Ia) * 100. Other useful data such as the corrosion potential (Ecorr) and passivation potential (Epp) can also be obtained from the DLEPR test curves. The location of Ia, Ir, Ecorr, and Epp on a typical DLEPR test curve are shown in figure 3.14.

The corrosion potential - Ecorr is the electrochemical potential at which the oxidation and reduction reactions that are occurring at the metal-electrolyte interface are in equilibrium with each other and the metal / alloy is said to be in a stable / equilibrium corrosion state at this potential. Passivation potential - Epp is the potential at which the passive film starts to form during the forward scan i.e., it is the potential at Ia.

During the forward scan, between the potentials Ecorr and Epp, the material surface gets into an active state undergoing uniform anodic metal dissolution. At potential Epp during the forward scan, the material surface transforms to a passive state, which is represented by the sudden drop in current density values seen in figure 3.14. Potential - E4 in figure 3.14 is the potential at which the initial breakdown of passive film occurs during the reverse scan, beyond which the current density increases to a peak value (Ir) depending on the DOS of the material. That is, if a material is heavily sensitized i.e., having more chromium depleted zones (CDZs) due to extensive chromium carbide precipitation - as in during prolonged exposure to temperatures in the range of 450°C to 850°C - the passive film formed on the specimen surface will be extremely weaker at the CDZs, where it will locally breakdown with relative ease during the reverse scan, leading to greater localized metal dissolution, yielding a greater Ir value and a higher DOS ratio and vice versa. Therefore, by finding the strength of the passive film forming on a material surface through DOS ratio, the material's strength to resist / undergo corrosion could be determined.

The CPP corrosion tests were performed in a similar manner as that of the DLEPR corrosion tests, which also yield a curve plotted between potential on the x-axis and logarithmic current density on the y-axis. However, the majority of the relevant / required test result data from the CPP corrosion tests, like the corrosion potential (Ecorr), pitting potential (Epit), and corrosion current density (Icorr) are obtained from the forward scan itself. Whereas the reverse scan gives an indication of whether there is any re-passivation ability shown by the material being tested, by re-passivating the pits formed during the forward / anodic scan.

The potential Ecorr, is the potential at which the oxidation and reduction reactions occur at equilibrium and the potential Epit, is the potential at which the onset of pitting occurs and is represented by the rapid increase in current density with a constant increase in potential on the CPP test curve. The location of Epit and Ecorr on a typical CPP test curve are shown by arrows in figure 3.15. Whereas the corrosion current density - Icorr, was measured from the cyclic polarization curves using Tafel extrapolation method as shown in figure 3.15. Using the Icorr value, the corrosion rate (CR) of a material / specimen being tested, can be calculated using the formula: CR (mpy) = (0.13*Icorr*EW)/(d*A) where Icorr is in $\mu A/cm^2$, EW is the equivalent weight in grams/equivalent, d is density in $grams/cm^3$, and A is area of metal exposed to corrosive solution in cm^2. Therefore, the CPP corrosion tests performed in 3.5 Wt.% NaCl solution, give a representation of the CR of a material and its pitting corrosion behavior (determined from the pitting potential shown by a material) in chloride containing environment.

Hence, by performing the DLEPR and CPP corrosion tests on the prior and after UNSM surface treatment surfaces of the different 304L SS specimens with distinct microstructural characteristics that are being studied in this research work, the impact of UNSM treatment on the degree of sensitization / susceptibility, corrosion rate, and pitting corrosion behavior of the

sensitized, CS, LACS, and AFS 304L SS materials has been determined and thoroughly analyzed, whose results and analysis are presented in detail in the following chapters of this dissertation.

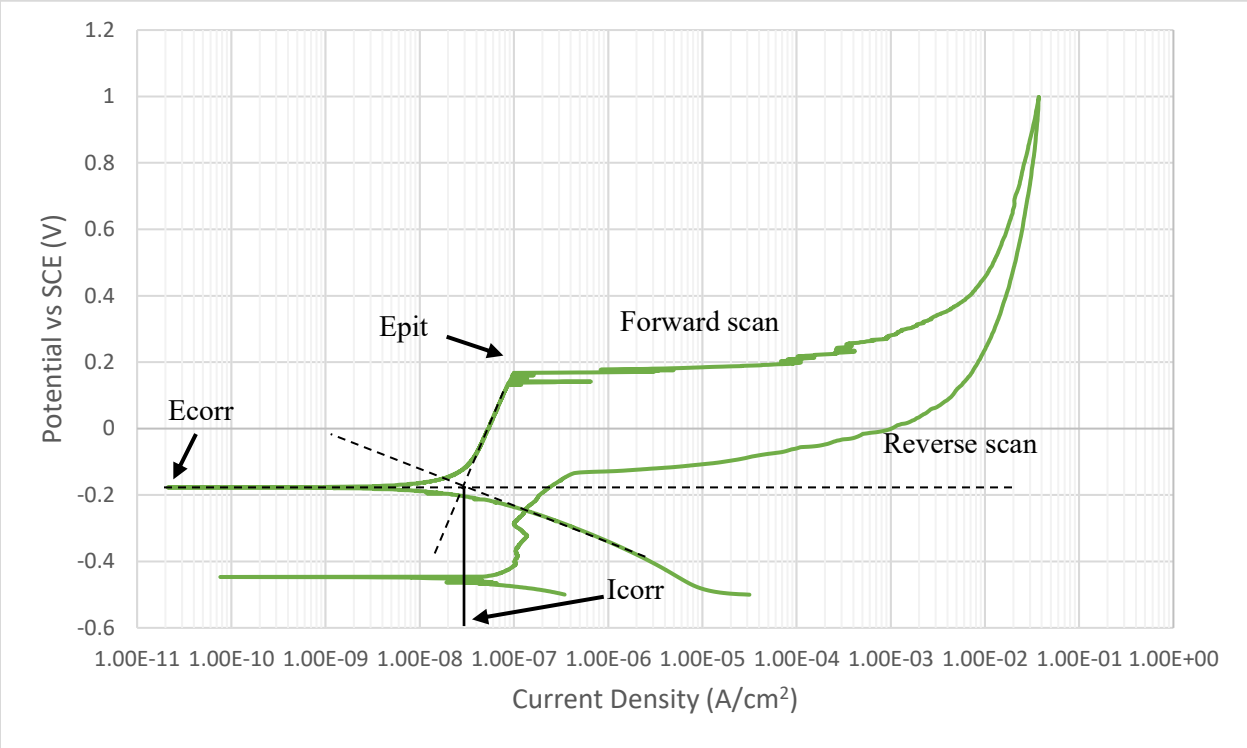

Figure 3.15: Typical CPP test curve showing the forward and reverse scans along with various potentials and current densities that can be obtained from it.

3.8 Microstructural Characterization

Secondary Electron (SE) / Back Scattered Electron (BSE) micrography, Electron Back Scattered Diffraction (EBSD), and Energy Dispersive X-ray Spectroscopy (EDS) techniques were employed as needed throughout the course of this research work, to analyze the various 304L SS specimens with distinct microstructural characteristics studied in this dissertation research work. These analyses were performed using the ThermoFisher SCIOS equipment shown in figure 3.16.

EBSD was performed on the ThermoFisher SCIOS equipment equipped with EDAX EBSD detector, to analyze the cross-sectioned areas of all the differently processed 304L SS specimens studied in this research work, with respect to before and after their UNSM treatment, to determine the changes in microstructure, dislocation density, grain boundary misorientation and

the extent of plastic deformation embedded in the specimens through their UNSM treatment.

Figure 3.16: ThermoFisher SCIOS equipment at UC.

The specimens required for cross-sectional EBSD analysis, were prepared by cold mounting them in epoxy resin with a curing time of 8 – 12 hours, followed by mechanical grinding with SiC emery papers ranging from 180 grit to 1200 grit, followed by fine polishing with 1 μm diamond suspension and final polishing with 0.05 μm colloidal silica suspension, to ultimately obtain specimens with a mirror finish. The specimens were then thoroughly cleaned with deionized water and ethanol followed by drying with an electric heater gun. Furthermore, to avoid charging issue in the SCIOS machine, a thin layer of gold coating was applied on the cleaned specimen's surface using timed sputter coating method.

Finally, to obtain the respective specimens inverse pole figure (IPF) maps that determine their crystallographic orientation and texture, the EBSD scans were performed at an operating voltage of 30 kV and a current of 13 nA with varying step sizes in accordance with the magnification at which the scans were performed.

Further analysis of EBSD data was done using EDAX/TSL OIM Analysis 7 software, to obtain the grain boundary misorientation (GBM) maps, kernel average misorientation (KAM) maps and their distribution charts, grain size (GS) and misorientation angle (MA) distribution charts, which are all presented in the following chapters of this dissertation document.

SE/BSE micrography was used to examine the surface characteristics of various 304L SS specimens after their UNSM treatment and to analyze the post-corrosion test surfaces of all the distinct 304L SS specimens studied in this research work, with the corrosion tests performed in different solutions on their untreated and UNSM treated surfaces. Very minimal cleaning was applied to the UNSM treated and corrosion tested specimens, to preserve their surface integrity and observe the unaltered effects of UNSM and corrosion tests on the various 304L SS specimen surfaces studied here.

When necessary, the elemental composition of the various 304L SS specimens was determined using the EDS technique, with the help of EDAX EDS detector mounted on the ThermoFisher SCIOS system.

Keyence VHX-600 digital microscope shown in figure 3.17 was used to observe the basic optical microstructures of some of the UNSM treated 304L SS specimens.

Figure 3.17: Keyence VHX – 600 digital microscope.

Chapter 4. Evaluating the Properties of Sensitized, CS, LACS and AFS 304L SS with respect to the Conventionally Hot-Rolled and Solution Annealed 304L SS

In this chapter, various properties that can have an influence on the SCC resistance of a material like the microstructure, hardness, surface roughness, residual stress, degree of sensitization or susceptibility, and pitting corrosion behavior of sensitized, CS, LACS, and AFS 304L SS materials have been studied extensively and whenever appropriate these properties have been evaluated by comparing them with the properties of conventionally hot-rolled and solution annealed (CH-R & SA) 304L SS plate material.

4.1 Determining the Sensitization Behavior of 304L SS Alloy using Double Loop Electrochemical Potentiodynamic Reactivation (DLEPR) Tests

Firstly, a preliminary study was done for determining the sensitization temperature at which the greatest degree of sensitization (DOS) occurs in the CH-R & SA 304L SS plate specimen when it is subjected to sensitization temperatures in the range of 600°C - 700°C. This preliminary study was performed to further evaluate the various properties of sensitized 304L SS with respect to the properties of unsensitized or as-received CH-R & SA 304L SS specimen and for studying the impact of UNSM treatment on the sensitization behavior and other properties of "sensitized" 304L SS material. For this purpose, the sensitization / aging parameters used in the current research work are, temperatures → 600°C, 650°C, 675°C & 700°C and durations → 5h & 24h followed by air cooling (culminating in 8 sensitization parameter combinations). The sensitized 304L SS specimens were polished and subjected to DLEPR corrosion tests following the procedures outlined in sections 3.1.4 and 3.7 of Chapter 3 in this thesis, respectively. From the obtained DLEPR corrosion test curves for the various sensitized 304L SS specimens studied here, the degree of sensitization (DOS) ratios for each individual specimen were calculated using the formula %

DOS ratio = (Ir/Ia)*100 where Ia and Ir are the peak activation and peak reactivation current densities respectively, which were obtained from the respective specimen's DLEPR corrosion test curve, whose typical location is given in figure 3.14.

The obtained DLEPR curves and the calculated DOS ratios of all the 304L SS specimens aged / sensitized at 600°C, 650°C, 675°C and 700°C for (a) 5h and (b) 24h, are compared against the CH-R & SA or baseline 304L SS specimen in figure 4.1. And the data obtained from all these DLEPR test curves such as the peak activation current density (Ia), peak re-activation current density (Ir), corrosion potential (Ecorr), passivation potential (Epp) and the calculated DOS ratios are presented in table 4.1. Whereas the Back Scattered Electron (BSE) micrographs showing the after DLEPR test surfaces of the SA and all the sensitized 304L SS specimens studied in this research work are presented in figure 4.2.

No relevant trends could be drawn from the corrosion and passivation potentials obtained for the SA and sensitized 304L SS specimens. The DOS ratio of SA specimen was found to be 0.003 %, which is representative of an unsensitized material that is significantly resisting corrosion by the formation of a strong passive oxide film on its surface. This is evident in the BSE micrograph showing its surface after the DLEPR test in figure 4.2 (i), which exhibits a surface unaffected by the DLEPR test solution.

The sensitization behavior of the 304L SS specimens aged for 5h, appears to be severe when aged at 650°C & 675°C, displaying DOS ratios of 2.95 % and 2.1 % respectively, as opposed to 0.15 % and 0.09 % shown by the 304L SS specimens aged at 600°C & 700°C respectively. The difference in-between the DOS ratios of specimens aged for 5h at {650°C & 675°C} and specimens aged for 5h at {600°C & 700°C} appears to be small. Especially with the difference between DOS ratios of specimens aged for 5h at 650°C & 675°C being small, a clear indication of the temperature

at which the sensitization behavior in 304L SS alloy is most dominant could not be determined with enough confidence from the specimens aged for only 5h.

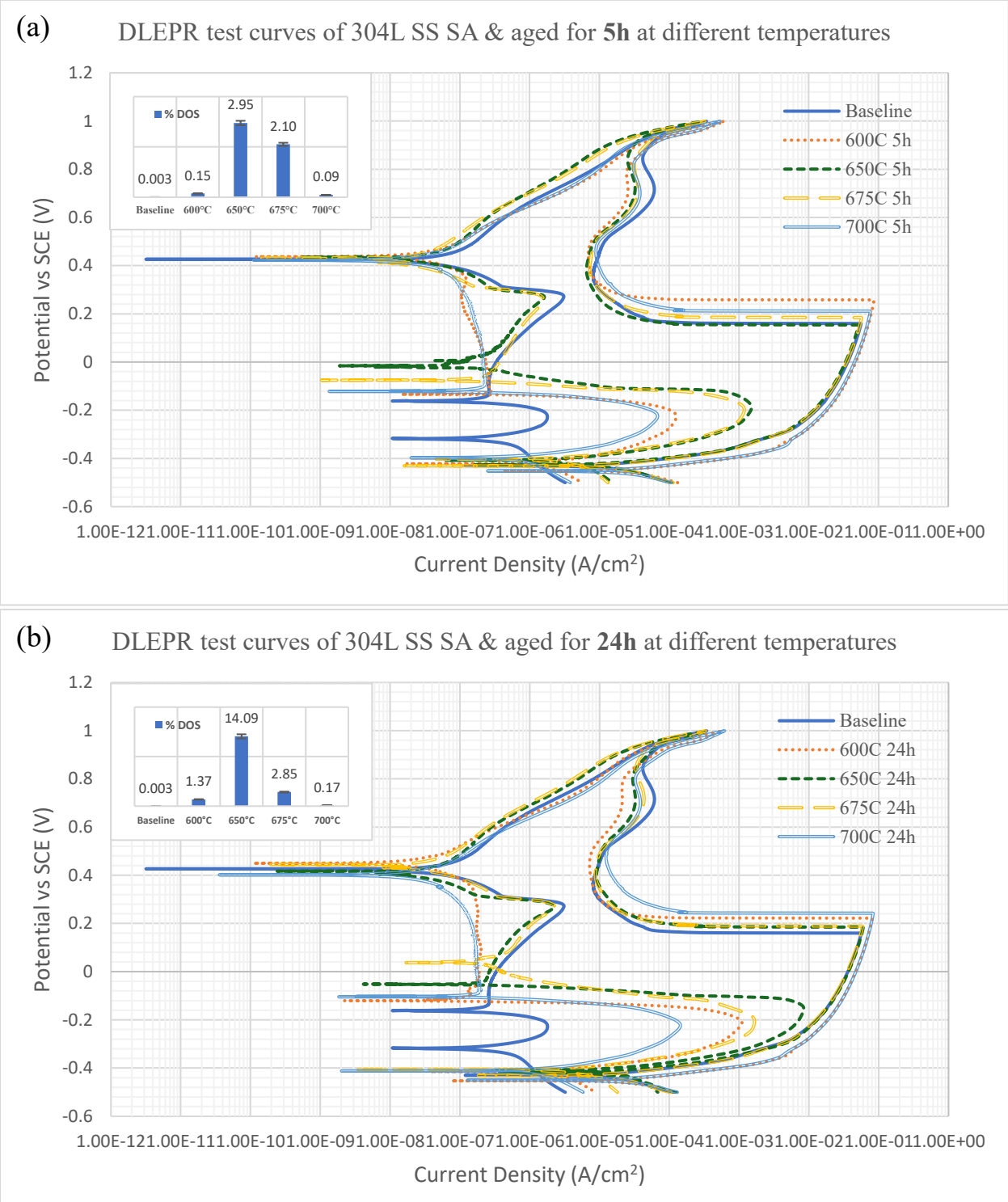

Figure 4.1: DLEPR curves of SA 304L SS sample compared with sensitized 304L SS specimens aged for (a) 5h and (b) 24h, at 600°C, 650°C, 675°C and 700°C that are tested in 0.5M H2SO4 + 0.05M KSCN solution.

However, when the 304L SS specimens were aged for 24h, a clear distinction in their sensitization behavior was apparent with respect to the different aging temperatures studied here. The specimen aged at 650°C for 24h showed a significantly higher DOS ratio of 14.09 % than when compared to the DOS ratios of the other three specimens aged for 24h at the other three temperatures studied here. The DOS ratios of these 304L SS specimens aged for 24h at 600°C, 675°C, and 700°C were measured to be only 1.37 %, 2.85 %, & 0.17 %, respectively. Nevertheless, the relationship between the DOS ratios exhibited by the 304L SS specimens sensitized at the four different temperatures studied here that are either aged for 5h or 24h exhibit the same trend as follows: the DOS ratio of 304L SS specimen sensitized at 650°C > 675°C > 600°C > 700°C.

Aging time	Aging temperature	Peak Activation Current Density Ia ($_{f}$A/cm^2)	Peak Re-Activation Current Density Ir (A/cm^2)	Degree of Sensitization, %DOS = ((Ir/Ia) * 100)	Corrosion potential, Ecorr (mV)	Passivation potential, Epp (mV)
Baseline/Solution Annealed		0.056010	0.000002	0.003	-430	158
5h	600°C	0.086030	0.000128	0.15	-451	255
	650°C	0.051440	0.001518	2.95	-426	151
	675°C	0.056860	0.001196	2.10	-431	183
	700°C	0.075920	0.000068	0.09	-452	208
24h	600°C	0.080630	0.001102	1.37	-453	219
	650°C	0.059890	0.008441	14.09	-420	183
	675°C	0.058420	0.001663	2.85	-431	187
	700°C	0.083240	0.000144	0.17	-450	240

Table 4.1: Data obtained from the DLEPR test curves of solution annealed and sensitized 304L SS specimens that are tested in 0.5M H2SO4 + 0.05M KSCN solution.

During aging / sensitization treatment of 304L SS specimens, depletion of chromium occurs from areas immediately adjacent to the grain boundaries which then combines with carbon present in the alloy composition leading to the simultaneous formation of chromium carbide precipitates and chromium depleted zones (CDZs) along the grain boundaries. Such depletion of Cr by sensitization phenomenon is deleterious because it adversely affects the formation of passive

chromium oxide film on the austenitic stainless steel (ASS) specimen's surface whose purpose is to act as a barrier between the metal and the surrounding environment providing corrosion resistance to ASSs. During the DLEPR tests, the sulfides in the corrosive test solution uniformly attack the passive chromium oxide film formed on the 304L SS specimen's surface. And the weaker passive film formed at the CDZs due to a lack of Cr content will quickly disintegrate with relative ease and will not be able to regenerate at a pace that is required for providing further corrosion resistance thereby, leading to heavy metal dissolution at these CDZs. This loss of material to corrosion during DLEPR tests at the CDZs appears as ditches in the BSE micrographs as can be seen from figures 4.2 (a) – (h), which are displaying the after DLEPR test surfaces of all the sensitized 304L SS specimens studied in this research work. Depending on the degree of sensitization occurring in the material / specimen during the different aging / sensitization treatments, the number and size of ditches formed during the DLEPR tests will vary, giving a direct qualitative measure of the CDZs formed during the 304L SS specimen's respective sensitization treatments performed with different sensitization parameters.

The ditches seen in the BSE micrographs of all the differently aged 304L SS specimens in figure 4.2 and their obtained DOS ratios align proportionally well with each other. Upon comparing the micrographs of 304L SS specimens aged at different temperatures for the same duration (i.e., comparing all the 304L SS specimens aged at 5h or 24h among themselves), it can be observed that the number and size of the ditches formed along the grain boundaries is substantially greater in 304L SS specimens aged at 650°C than the specimens aged at the other three temperatures studied in this research. Hence, from both the DOS ratios and the BSE micrographs of sensitized 304L SS specimens, it can be concluded with certainty that among the sensitization temperatures studied in the current research work, the DOS / chromium depletion or

the kinetics of nucleation and growth of chromium carbide precipitates in 304L SS alloy occurs most profoundly at 650°C.

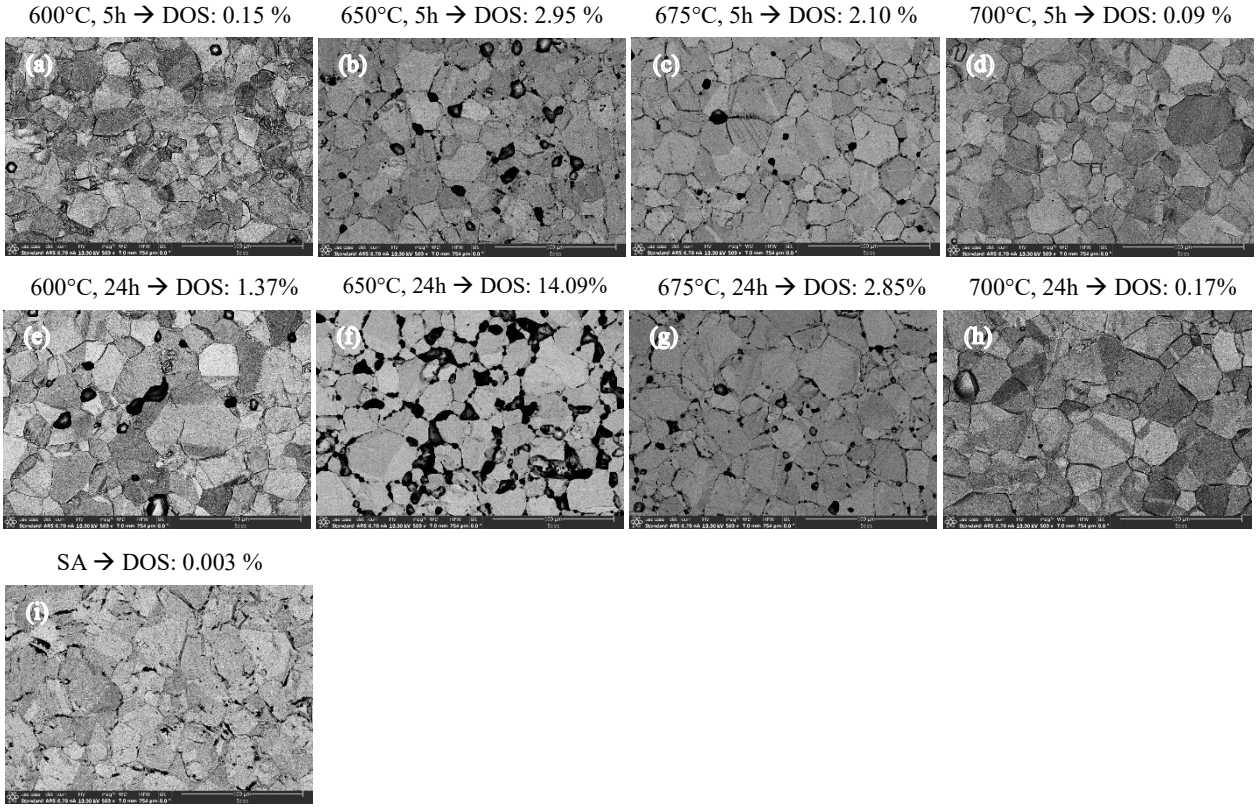

Figure 4.2: Back scattered electron (BSE) micrographs showing after DLEPR test surfaces of (i) solution annealed (SA), and (a-h) differently aged 304L SS specimens tested in 0.5M H2SO4 + 0.05M KSCN test solution. The sensitization parameters and the obtained DOS ratios for all the 304L SS specimens are presented at the top of their respective micrographs.

4.2 Evaluating the Microstructure, Phases, Hardness, Residual stress and Corrosion Properties of Sensitized, CS, LACS and AFS 304L SS w.r.t the CH-R and SA 304L SS Plate Specimen

From the research study performed in section 4.1, where the temperature at which the highest degree of sensitization occurring in 304L SS plate material was determined to be at 650°C among the four different temperatures studied there, gives a baseline sensitization temperature of 650°C with aging durations of 5h and 24h to be used for further studies where several properties of sensitized 304L SS specimen will be evaluated and compared with respect to the properties of unsensitized or as-received CH-R & SA 304L SS plate specimen. As described in sections 4.1 and

3.1, the sensitized 304L SS specimens for further testing were obtained by sectioning them from the CH-R & SA 304L SS plate specimen and subjecting them to the appropriate sensitization parameters (temperature: 650°C, durations: 5h & 24h) using the conventional Thermolyne Type 48000 furnace located at The University of Cincinnati itself. Whereas the CS, LACS, and AFS 304L SS coatings / cladding deposited using appropriate parameters were obtained from The University of Alabama as described in section 3.1.

In order to thoroughly evaluate and compare the Sensitized, CS, LACS, and AFS 304L SS material / coatings / cladding with that of the as-received CH-R & SA 304L SS plate specimen, their properties such as microstructure, phases, hardness, residual stress, surface topography, degree of sensitization / susceptibility, and pitting corrosion behavior have been studied in the current research work, whose results and analysis have been discussed thoroughly in the following sections of this chapter.

But first, the designations used for conveniently representing the different 304L SS specimens studied in this research work pertaining to this chapter are as follows:

304L SS Specimen's Surface Condition	**Designation**
As-received Conventionally Hot-Rolled & Solution Annealed specimen	**SA**
Sensitized at 650°C for 5h specimen	**S5**
Sensitized at 650°C for 24h specimen	**S24**
As Cold Sprayed specimen	**As-CS**
As Laser Assisted Cold Sprayed specimen	**As-LACS**
As AFS/MELD deposited specimen	**As-AFS**
Polished to 1200grit CS specimen	**CS + P**
Polished to 1200grit LACS specimen	**LACS + P**
Polished to 1200grit AFS specimen	**AFS + P**

Table 4.2: Designations used for representing the different 304L SS specimens studied in this Ph.D. Dissertation research work.

4.2.1 Microstructural Analysis using Electron Back Scattered Diffraction (EBSD) Technique

The EBSD analysis of the SA and Sensitized 304L SS specimens was performed at two magnifications - 250X and 1000X using a step size of 0.7 μm and 0.15 μm respectively. For different analysis, the EBSD images captured at the magnification most appropriate for accurately representing the relevant data have been used accordingly. Whereas the EBSD analysis of CS, LACS, and AFS 304L SS coatings / cladding were performed at a higher magnification of 2500X using a step size ranging from 65 nm – 80 nm as required by different specimen's microstructure.

The EBSD analysis of SA, Sensitized, CS, LACS, and AFS 304L SS specimens performed at the different magnifications using the step sizes that are appropriate to the magnification being used results in acquiring the respective specimen's inverse pole figure (IPF) maps which show their crystallographic orientation and texture. Using the EDAX/TSL OIM Analysis 7 software, other relevant data such as the grain boundary misorientation (GBM) maps showing low angle grain boundaries (LAGBs i.e., 2°-15°) and high angle grain boundaries (HAGBs i.e., > 15°); grain size (GS) and misorientation angle (MA) distribution charts; kernel average misorientation (KAM) maps and their kernel distribution charts have been obtained for all the different 304L SS specimens and the obtained data is presented here in this section.

Note that the black area seen at the top of the microstructures (e.g. figure 4.3 (a-f), figure 4.4 (a-c) etc.) represents the void space above the specimen surface i.e., the interface between the black area and the colored grains seen here represents the actual surface of the specimen. Moreover, the color scheme used in the KAM maps (e.g. figure 4.5 (a-c) or figure 4.6 (b) etc.) which represent the plastic strain present in the material follows the relationship: blue < green < yellow < red. Whereas, the white color seen in the KAM maps (e.g. figure 4.6(b)) represents the

0-point kernels which are either heavily deformed or signify very tiny grains that are difficult for EBSD detection.

Sensitized 304L SS:

Figure 4.3 (a), (b), (c) show the inverse pole figures (IPF) maps and (d), (e), (f) show the phase distribution maps of SA, S5, and S24 304L SS specimens respectively that are obtained using the EBSD technique. The IPF maps of SA, S5, and S24 specimens indicate that all the specimens have random crystallographic orientation and no texture.

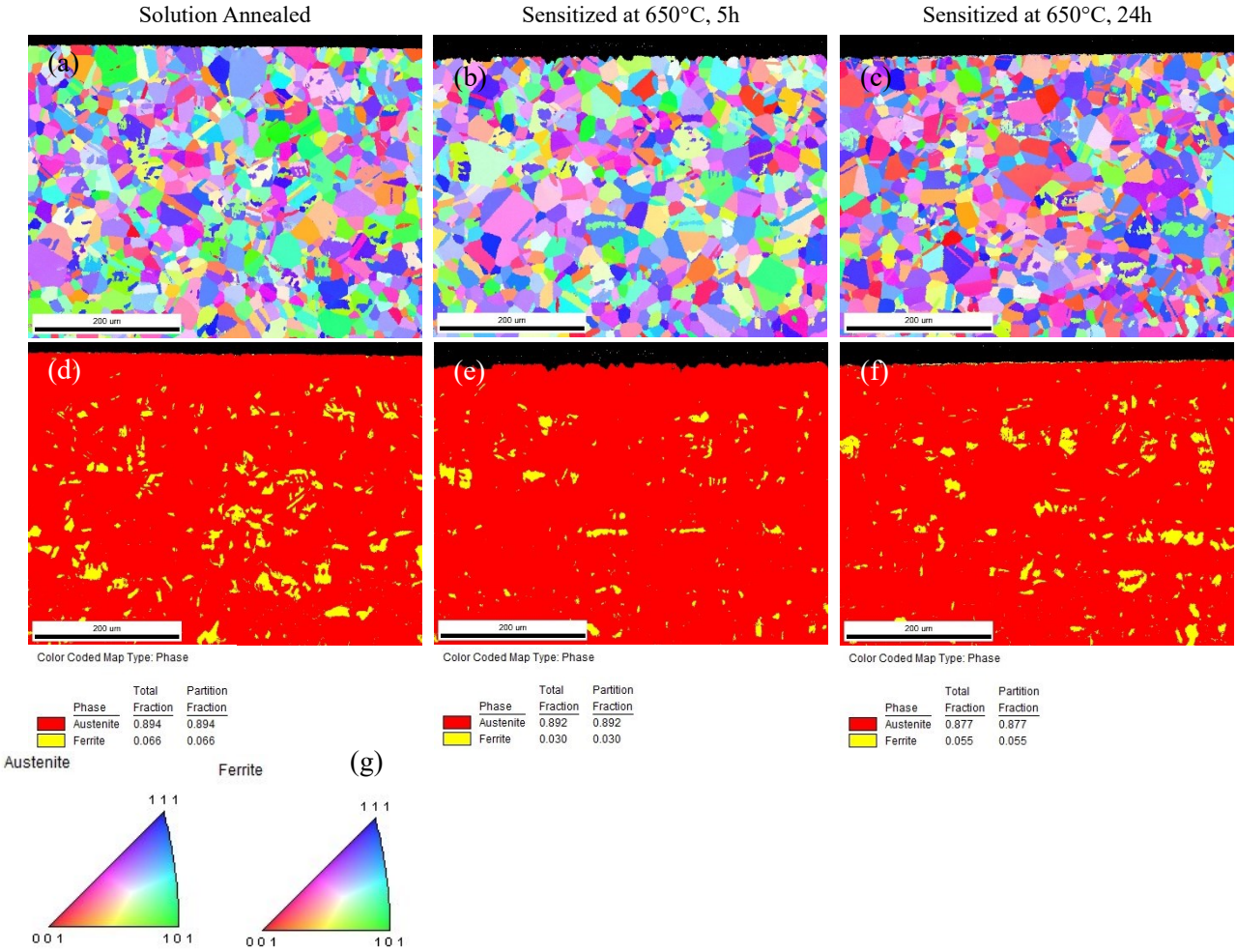

Figure 4.3: Maps obtained from EBSD analysis with (a), (b) & (c) representing the Inverse Pole Figures (IPF); (d), (e) & (f) representing the Phase distribution maps (red-austenite, yellow-delta ferrite) of cross-sectioned 304L SS specimens SA, aged at 650°C for 5h & 24h respectively, (g) represents the legend of IPF maps in (a-c). The top black edge seen at the top of all the images (a-f) is the respective specimen's surface.

Observing the phase distribution maps in figure 4.3 (d-f), a small fraction of delta ferrite (yellow) stringers can be seen in the austenite (red) matrix of SA, S5, and S24 specimens. Also, it can be observed that there are very few to no delta ferrite stringers up to a depth of ~ 50 μm from their surface beyond which the delta ferrite content increased and is randomly dispersed throughout the material in all the three specimens.

GBM maps obtained from the EBSD analysis of SA, S5, and S24 304L SS specimens are presented in figure 4.4 (a), (b), and (c) respectively and their corresponding GS vs area fraction and MA vs number fraction charts are presented in figure 4.4 (d-f) and (g-i) respectively. On comparing the SA and S5 specimens, the following observations can be made: the total length of grain boundaries (GBs) i.e., both LAGBs and HAGBs decreased tremendously in S5 specimen (3.4 mm) from that of SA specimen (6.03 mm); whereas the GS increased from 3.7 μm in SA to 7.2 μm in S5 specimen along with a higher average MA value noticed for the S5 specimen (43.4°) than that of SA specimen (35.2°), all of which indicate that grain boundary migration or grain coarsening is occurring in the S5 specimen during its aging / sensitization treatment.

Now, on comparing the EBSD data obtained for the S5 specimen with that of the S24 specimen, the following observations were made: the total length of GBs increased tremendously in S24 specimen (8.5 mm) from that of the S5 specimen (3.4 mm); whereas the GS decreased from 7.2 μm in S5 specimen to 3.8 μm in S24 specimen along with a decrease in average MA value of 43.4° in S5 specimen to 37.9° in S24 specimen. Additionally, it must be noted that the total length of GBs, average GS, and average MA values of S24 specimen have reverted closer to that of the SA specimen's values from that of the S5 specimen's values. These changes observed in the EBSD data of S24 specimen from that of S5 specimen indicates that recrystallization phenomenon is occurring in the 304L SS alloy between the aging durations of 5h and 24h. The

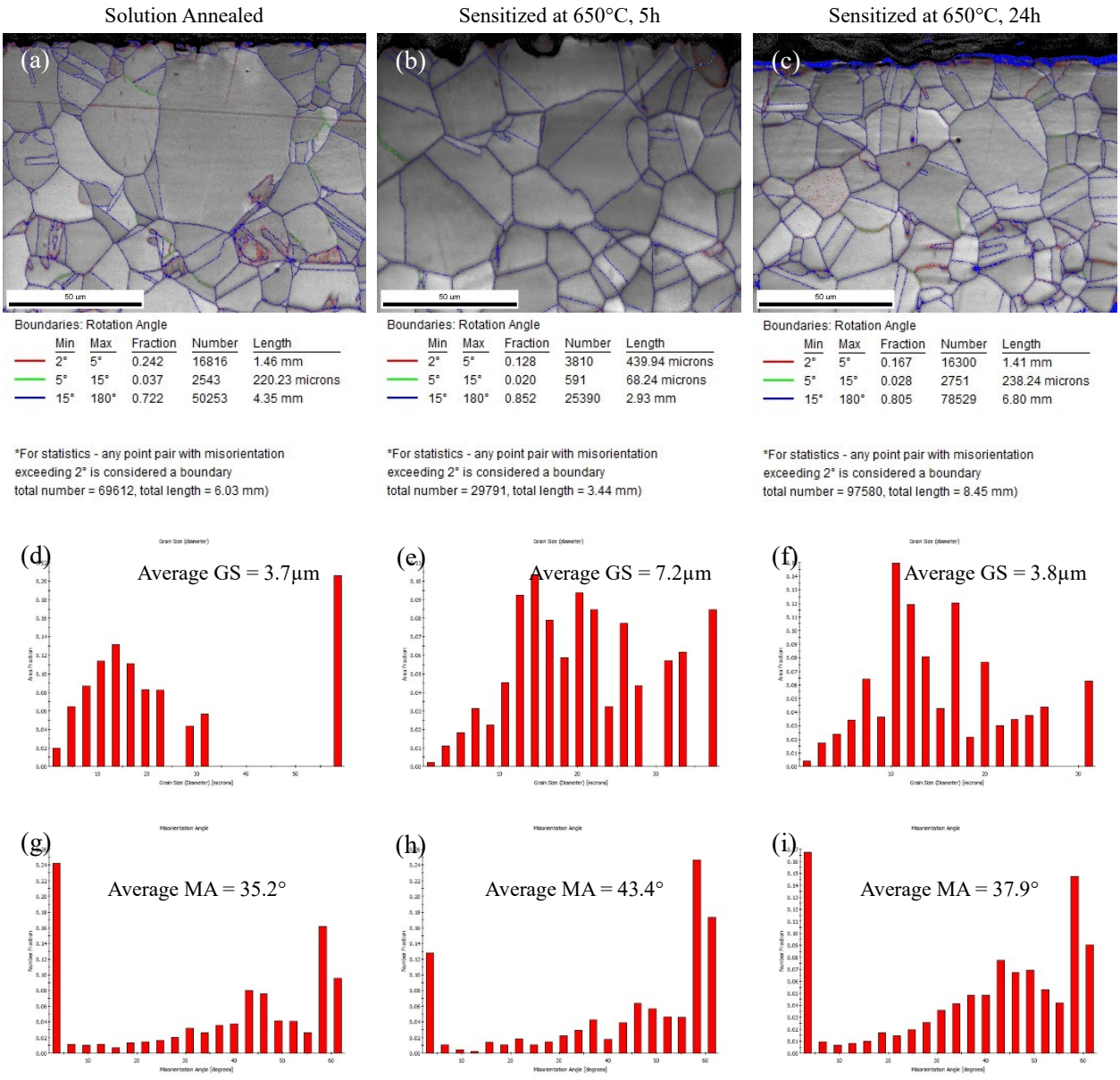

Figure 4.4: Maps obtained from EBSD analysis with (a), (b) & (c) representing the Grain Boundary Misorientation (GBM) maps, (d), (e) & (f) representing the grain size diameter vs area fraction charts, and (g), (h) & (i) representing the misorientation angle vs number fraction charts of cross-sectioned 304L SS specimens SA, aged at 650°C for 5h & 24h respectively. The top black edge in images (a-c) is the specimen's surface.

same is reflected clearly in a visual manner from (b) and (c) in figure 4.4, which show that there are many twins appearing in the S24 specimen from that of S5 specimen and the GS of S24 specimen decreased from that of S5 specimen as well which would increase the total length of GBs in the former specimen from that of the latter. Furthermore, the significant increase in

HAGBs of S24 specimen from that of S5 specimen which are also considerably higher than the HAGBs present in SA specimen could be an indication of enhanced chromium carbide segregation occurring at the grain boundaries of S24 specimen which would make it highly susceptible to intergranular stress corrosion cracking (IGSCC). The change in the degree of sensitization behavior of S5 to S24 specimen has been clearly observed in the DLEPR corrosion test results presented in section 4.2.6.

Figure 4.5 (a), (b), (c) represent the Kernel Average Misorientation (KAM) maps of SA, S5, and S24 304L SS specimens respectively and (d-f) represent their corresponding KAM distribution charts showing the average kernel average misorientation in degrees vs number fraction. The average KAM value gives information regarding the local lattice distortion or plastic strain present within the material. The obtained average KAM values of SA (0.76), S5 (0.64), and S24 (0.73) specimens seen in figure 4.5 (d-f), indicate that the S5 specimen has slightly lower

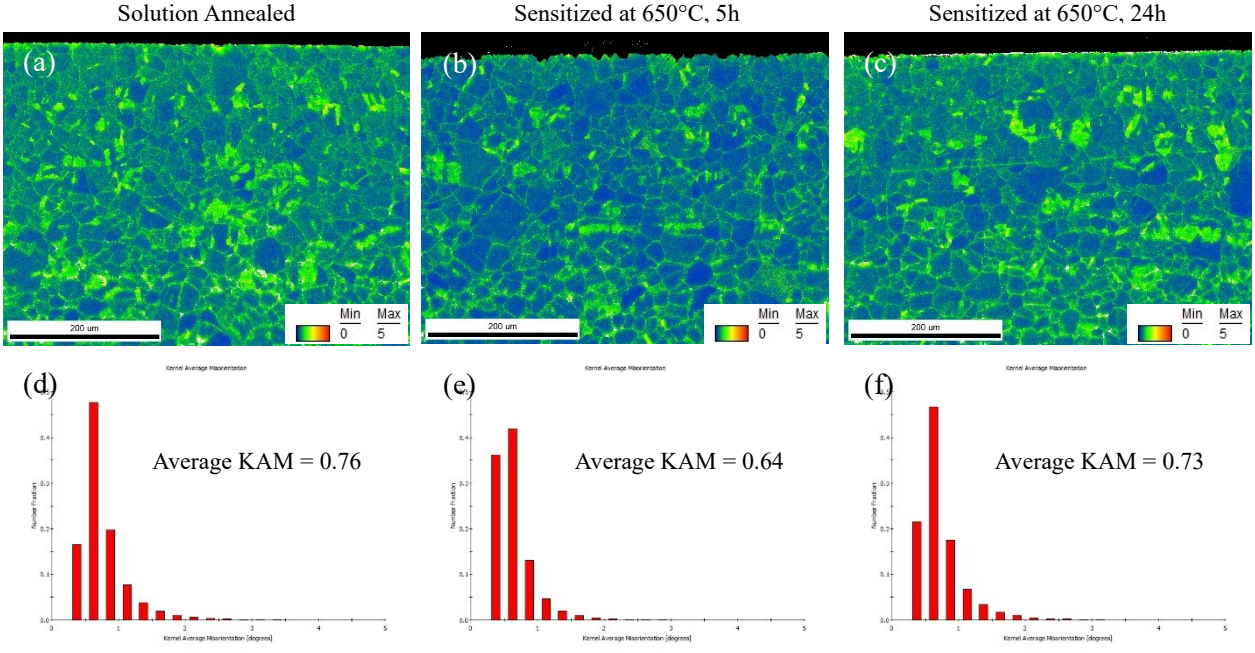

Figure 4.5: Maps obtained from EBSD analysis with (a), (b) & (c) representing the Kernel Average Misorientation (KAM) maps of cross-sectioned 304L SS specimens SA, aged at 650°C for 5h & 24h respectively and (d), (e) & (f) representing their respective KAM charts showing the kernels misorientation in degrees with respect to number fraction. The top black edge in images (a-c) is the specimen's surface.

plastic strain in it when compared to the SA and S24 specimens, which could be attributed to grain coarsening occurring by the grain boundary migration in S5 specimen during its aging/sensitization treatment. Whereas the increase in chromium carbide segregation at the grain boundaries and/or the increase in total number of grain boundaries itself due to recrystallization in the S24 specimen, could have caused an increase in its lattice distortion yielding an average KAM value greater than that of the S5 specimen and one that is closer to that of the SA specimen.

CS & LACS 304L SS:

Figures 4.6 and 4.7 represent the EBSD microstructures and data pertaining to the near-surface cross-sectional areas of CS and LACS 304L SS coatings respectively. The IPF map in figure 4.6 (a) belonging to the CS 304L SS specimen exhibits an extremely deformed microstructure possessing very tiny, deformed grains. Its average KAM value of 2.6 is extremely high and indicates the presence of high amount of plastic strain in the CS coating that could have resulted from the extreme plastic deformation undergone by the 304L SS powder particles during their CS deposition / coating process. The total length of LAGBs and HAGBs present in the CS 304L SS specimen were determined to be 3.47 mm and 35.5 mm respectively.

Whereas its average values of GS and MA were found to be 0.24 μm and 38.3° respectively. Also, from observing (a) or (b) or (d) in figure 4.6, it can be said that the CS coatings have porosity in them with pores being represented by the black areas within the material's EBSD microstructures where no EBSD patterns were detected. These porous areas are represented by white arrows in figure 4.6 (a).

The IPF map in figure 4.7 (a) belonging to the LACS 304L SS specimen exhibits a homogenous grain structure with random crystallographic orientation (or without texture). Although the processing technique of LACS involving the simultaneous application of laser to the

Near-surface area of cross-sectioned **as-CS** 304L SS Coating – 2500X magnification.

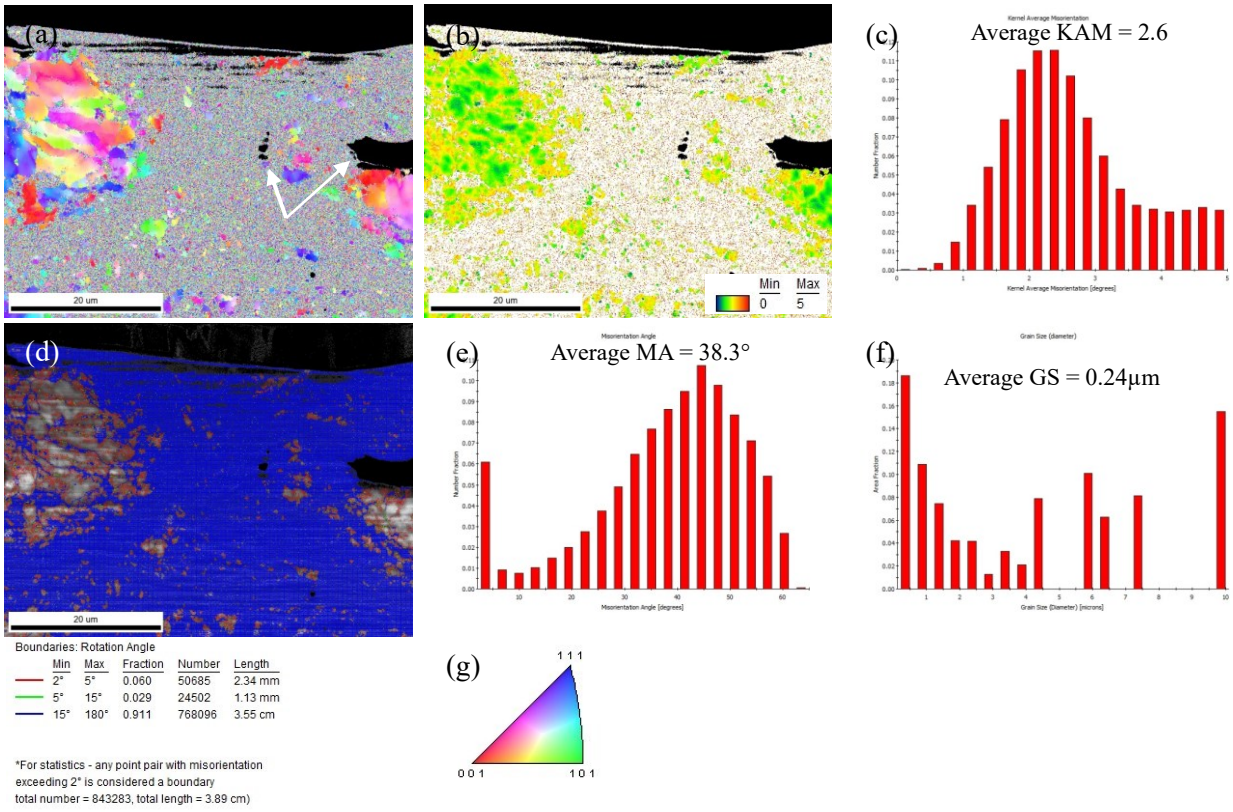

Figure 4.6: Maps obtained by EBSD analysis performed on the near-surface area of cross-sectioned as-CS deposited 304L SS coating representing its (a) Inverse Pole Figure (IPF) map, (b) Kernel Average Misorientation (KAM) map, (c) KAM distribution chart (d) Grain Boundary Misorientation (GBM) map, (e) Misorientation Angle (MA) distribution chart, (f) Grain Size (GS) distribution chart, and (g) legend of IPF map in (a).

solid-state deposition of powder particles aims to produce a completely dense product, some voids/ porosity can be observed within the microstructure of LACS 304L SS specimen represented by the small lamellar black areas in figure 4.7 (a, b & d). The near-surface average values of GS and MA were found to be 1.0 µm and 44.7° respectively. Whereas the total length of the LAGBs and HAGBs present in the LACS 304L SS specimen were determined to be 0.49 mm and 3.54 mm respectively. Also, its average KAM value was discovered to be 0.6 representing that of a less strained material with strain present only at the grain boundaries whereas the grains themselves appear to be strain free as can be seen from figure 4.7 (b). The lower KAM value of the LACS deposited 304L SS coating from that of the CS 304L SS coating's value of 2.6 could be attributed

to the simultaneous application of laser to the traditional cold spray technique resulting in the in-situ annealing of the material (i.e., recrystallization) thereby, relieving the typical cold work that is generated by the bombardment of powder particles during cold spray, leading to a coating / material with strain free grains.

Near-surface area of cross-sectioned **as-LACS** 304L SS Coating – 2500X magnification.

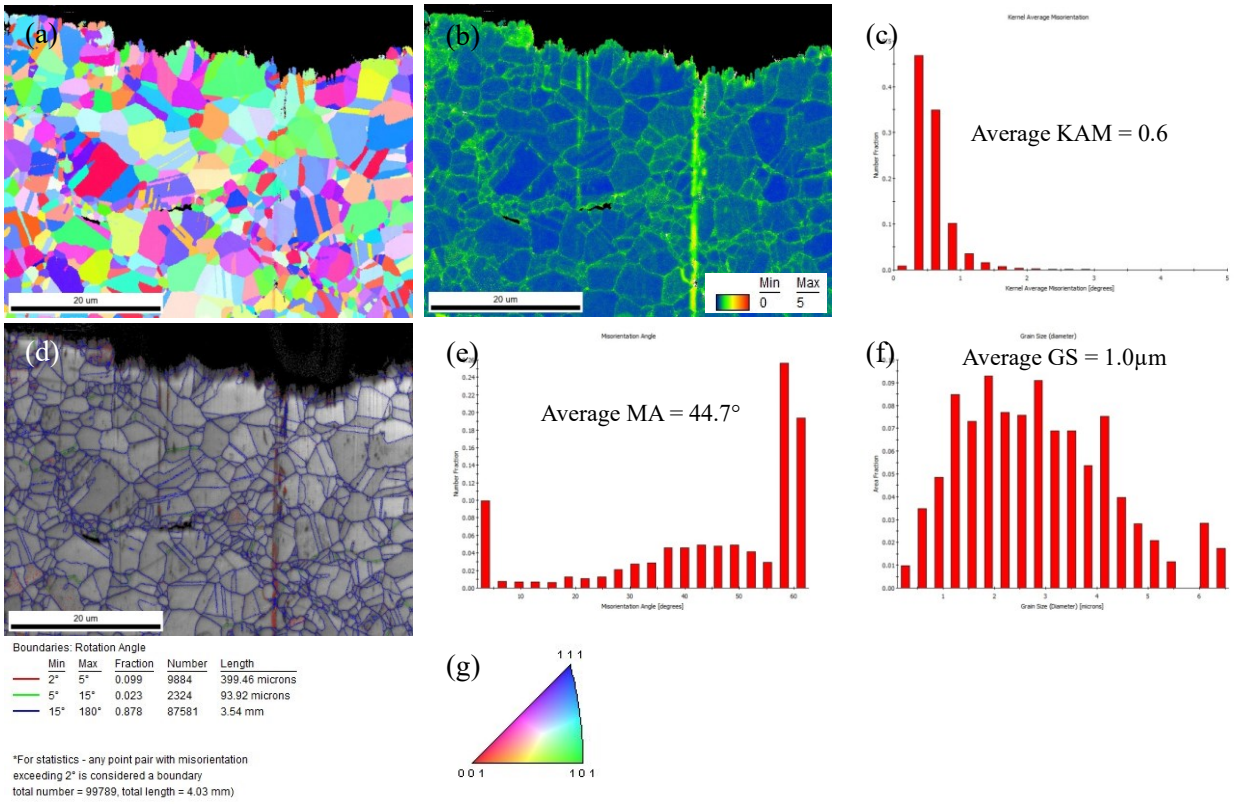

Figure 4.7: Maps obtained by EBSD analysis performed on the near-surface area of cross-sectioned as-LACS deposited 304L SS coating representing its (a) Inverse Pole Figure (IPF) map, (b) Kernel Average Misorientation (KAM) map, (c) KAM distribution chart (d) Grain Boundary Misorientation (GBM) map, (e) Misorientation Angle (MA) distribution chart, (f) Grain Size (GS) distribution chart, and (g) legend of IPF map in (a).

<u>AFS 304L SS</u>:

Figures 4.8 and 4.9 represent the EBSD analysis performed at the top-edge and center area of cross-sectioned AFS/MELD 304L SS respectively. The top-edge and center areas in this analysis are representative of a single layer of AFS deposit. As the AFS layers have repetitive characteristics only the top layer is analyzed where the subsequent UNSM treatment will be performed.

Top-Edge of cross-sectioned **as-AFS** Coating – 2500X magnification.

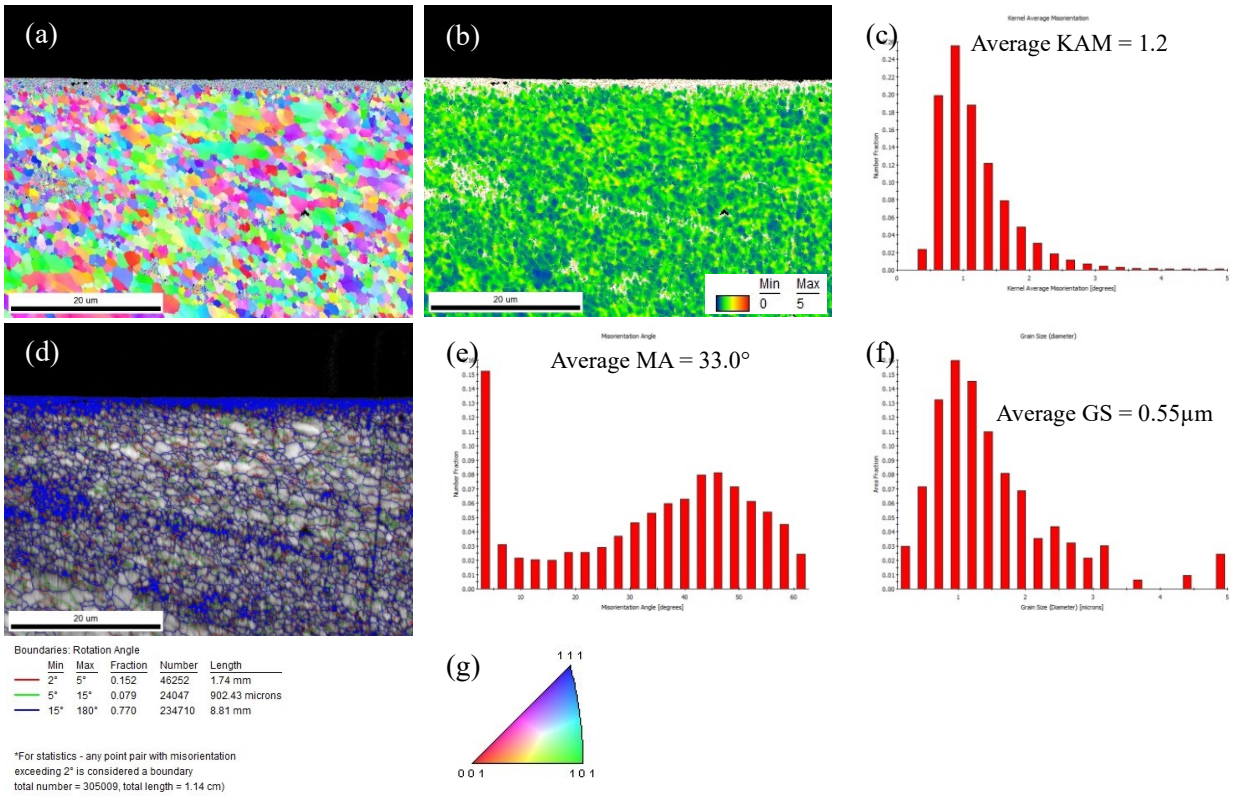

Figure 4.8: Maps obtained by EBSD analysis from the top-edge of cross-sectioned 304L SS as-AFS coating representing its (a) Inverse Pole Figure (IPF) map, (b) Kernel Average Misorientation (KAM) map, (c) KAM distribution chart (d) Grain Boundary Misorientation (GBM) map, (e) Misorientation Angle (MA) distribution chart, (f) Grain Size (GS) distribution chart, and (g) legend of IPF map in (a).

Looking at the IPF maps in figures 4.8 and 4.9, a large difference in the grain size can be observed at the center of the AFS layer from that of its top edge. The average GS at the top and the center of the layer were measured to be 0.55 µm and 2.38 µm respectively. Also, both the LAGBs and HAGBs decreased significantly from the top layer to its center area combined with an increase in average MA from 33° to 39.8°. Therefore, with all these observations it can be said that considerable amount of grain growth has occurred at the center of the AFS layer. The grain growth at the center of the AFS layer can be attributed to the differences in cooling rate of an individual layer from its top edge to its center. AFS being an open atmosphere process that is occurring in a semi solid state, the cooling of an individual layer will commence from the top proceeding to the

bottom as the top of the AFS layer will be exposed to the atmosphere. Therefore, the top layer will cool faster resulting in very fine recrystallized grains at the very top followed by a gradient increase in grain size as the cooling progresses to the bottom of the AFS layer allowing the grains to grow for longer through the depth of the AFS layer.

Center Area of cross-sectioned **AFS** Coating – 2500X magnification.

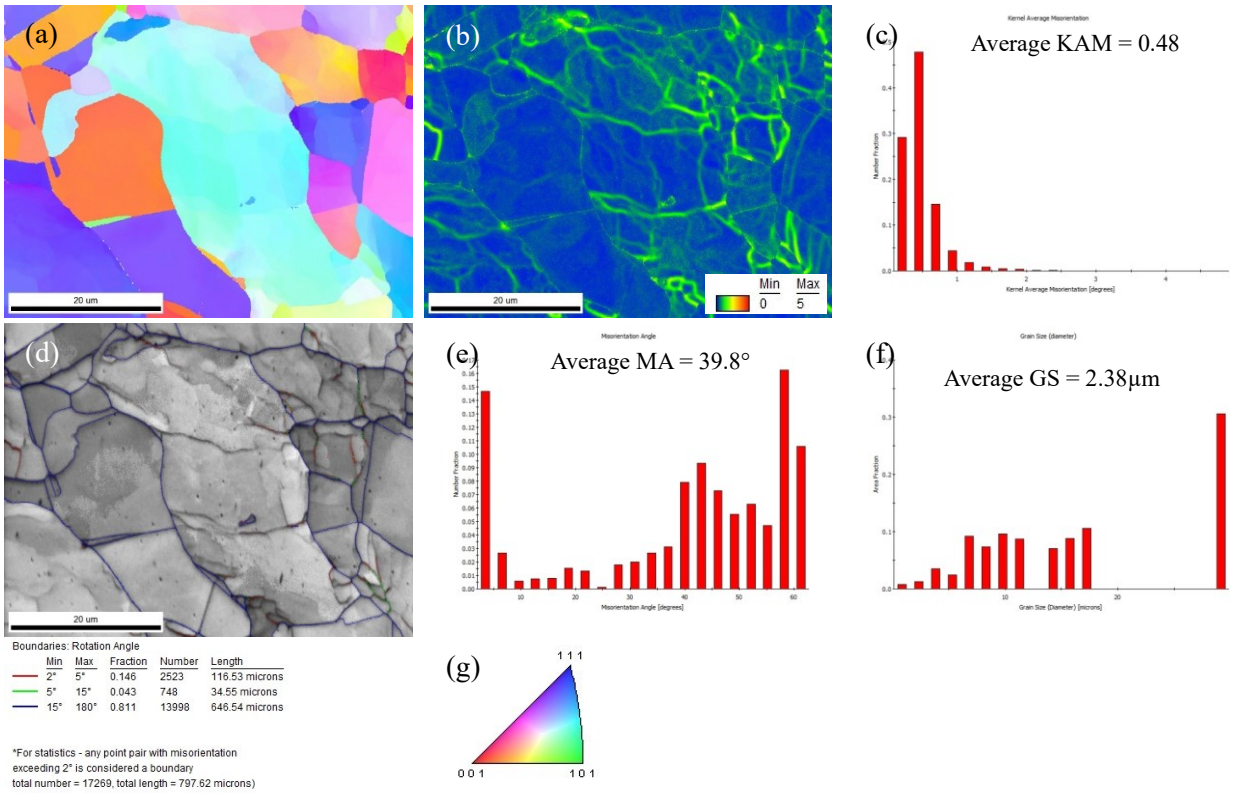

Figure 4.9: Maps obtained by EBSD analysis from the center area of cross-sectioned 304L SS AFS coating representing its (a) Inverse Pole Figure (IPF) map, (b) Kernel Average Misorientation (KAM) map, (c) KAM distribution chart (d) Grain Boundary Misorientation (GBM) map, (e) Misorientation Angle (MA) distribution chart, (f) Grain Size (GS) distribution chart, and (g) legend of IPF map in (a).

The KAM map and its distribution chart representing the plastic strain present in a material are given in (b) and (c) of figures 4.8 and 4.9 respectively. The average KAM values obtained from the top edge and center of the AFS layer are found to be 1.2 and 0.48 respectively. The KAM map of the top AFS layer and its average KAM value show that some degree of plastic strain is present at the top of AFS layer. This plastic strain could be a result of the rotating tool shoulder and the hydrostatic pressure under which the feedstock material is deposited during MELD processing.

However, due to the grain growth observed at the center of the AFS layer, strain relief occurs resulting in a decrease in the plastic strain as observed from its KAM map and its lower average KAM value. Therefore, it can be conveyed that through the depth of an AFS layer the grain size increases accommodated by a consequent decrease in grain boundary area and plastic strain.

4.2.2 X-Ray Diffraction Phase Analysis

Sensitized 304L SS:

Figure 4.10 (a) and (b) shows the XRD scans of SA and sensitized 304L SS specimens respectively with different surface conditions. In both (a) and (b) the blue scan represents the as-is specimen surface condition, and the orange scan represents the polished to 1200 grit specimen surface condition. The XRD scan of as-SA 304L SS specimen reveals it to be predominantly made of austenite phase with the presence of a small amount of delta (δ) ferrite. The presence of δ ferrite is indicated by the minor peak of δ ferrite seen at a 2θ of 44.5°. When the SA specimen was polished to 1200 grit surface condition, its XRD scan appears to be similar to that of the as-SA specimen's XRD scan with a minor difference, which is that the δ ferrite peak intensity seen at the 2θ of 44.5° increased considerably.

When it comes to the XRD scan of as-sensitized 304L SS specimen, it shows an oxidized surface with peaks corresponding to both iron and chromium oxides. However, upon polishing the sensitized specimen, its XRD scan revealed it to be similar to that of the polished SA specimen's XRD scan, exhibiting it to be made of predominantly austenite phase with a high intensity δ ferrite peak at the 2θ of 44.5°. Therefore, it can be said that the sensitization treatment of 304L SS specimen led to its surface oxidation which was then removed by polishing.

From the phase maps of SA and sensitized 304L SS specimens seen in figure 4.3 (d-f), it was inferred that very minimal delta ferrite stringers were present up to a depth of ~ 50 μm from

their surface beyond which their presence increased notably. Typically, upon polishing a specimen to 1200 grit surface condition, ~ 50 – 100 µm of material is removed from the surface. Therefore, the notably higher δ ferrite peak intensities of polished SA and sensitized specimens seen in their respective XRD scans can be attributed to the polishing action removing the material from their

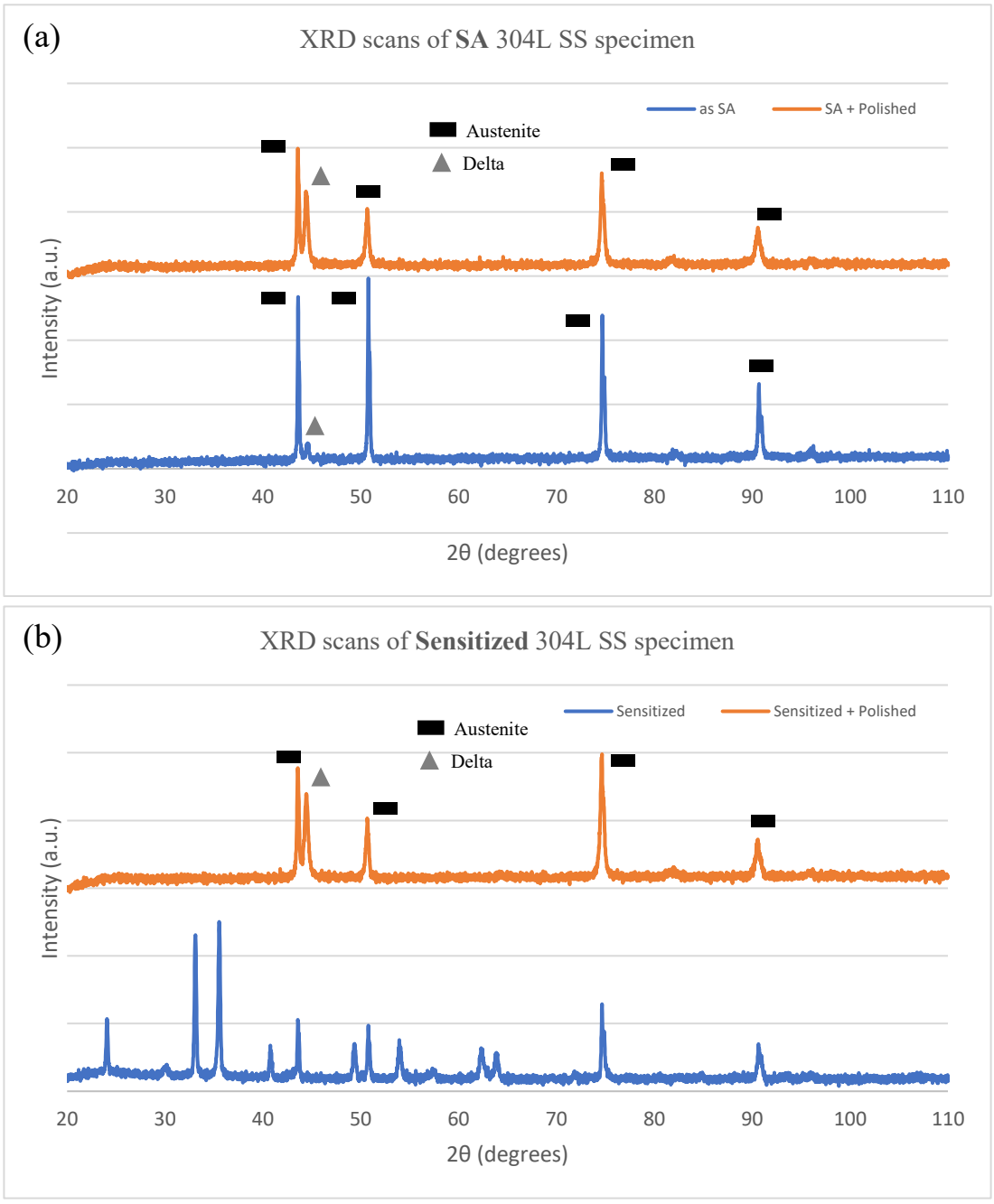

Figure 4.10: XRD scans of (a) SA and (b) sensitized 304L SS specimens in as-is and polished to 1200 grit surface conditions.

surface thereby, exposing a surface with higher δ ferrite content (i.e., surface beyond 50 μm depth seen in figure 4.3 (d-f)) to the X-rays while performing their X-ray diffraction scans. Hence, from both the phase maps and the XRD scans it can be said with certainty that the acquired 304L SS plate has some amount of δ ferrite in it.

CS & LACS 304L SS:

Figure 4.11 (a) represents the XRD scans performed on SA, CS, and LACS 304L SS specimens in as-is condition i.e., before polishing. The XRD scans of as-CS and as-LACS coatings reveal to be just like as-SA specimen having completely austenitic phase with a very weak delta ferrite peak located at a 2θ of 44.5°.

Figure 4.11 (b) represents the XRD scans performed on SA, CS, and LACS 304L SS specimens after polishing them to 1200 grit surface finish. Like SA specimen, the polished CS and LACS coatings show an increase in the delta ferrite peak intensity at a 2θ of 44.5°. Therefore, all the specimens seem to be predominantly austenitic but, with a very small amount of delta ferrite present in the material.

AFS 304L SS:

The XRD patterns obtained from the as-AFS specimen surface are presented in figure 4.12 (a) along with the XRD patterns of as-SA 304L SS and as-sensitized at 650°C for 24h 304L SS specimens for comparison. The XRD pattern of as-AFS specimen reveals that it has oxidized surface with peaks similar to the as-sensitized 304L SS specimen. The 304L SS specimen was aged in a conventional open atmosphere furnace which resulted in an oxidized surface. Similarly, the AFS/MELD processing being an open atmosphere process resulted in the oxidation of the outer surface layer. From the XRD pattern of as-AFS deposit the nature of the oxide film on its surface could not be deduced precisely but they contain peaks from both iron and chromium oxides.

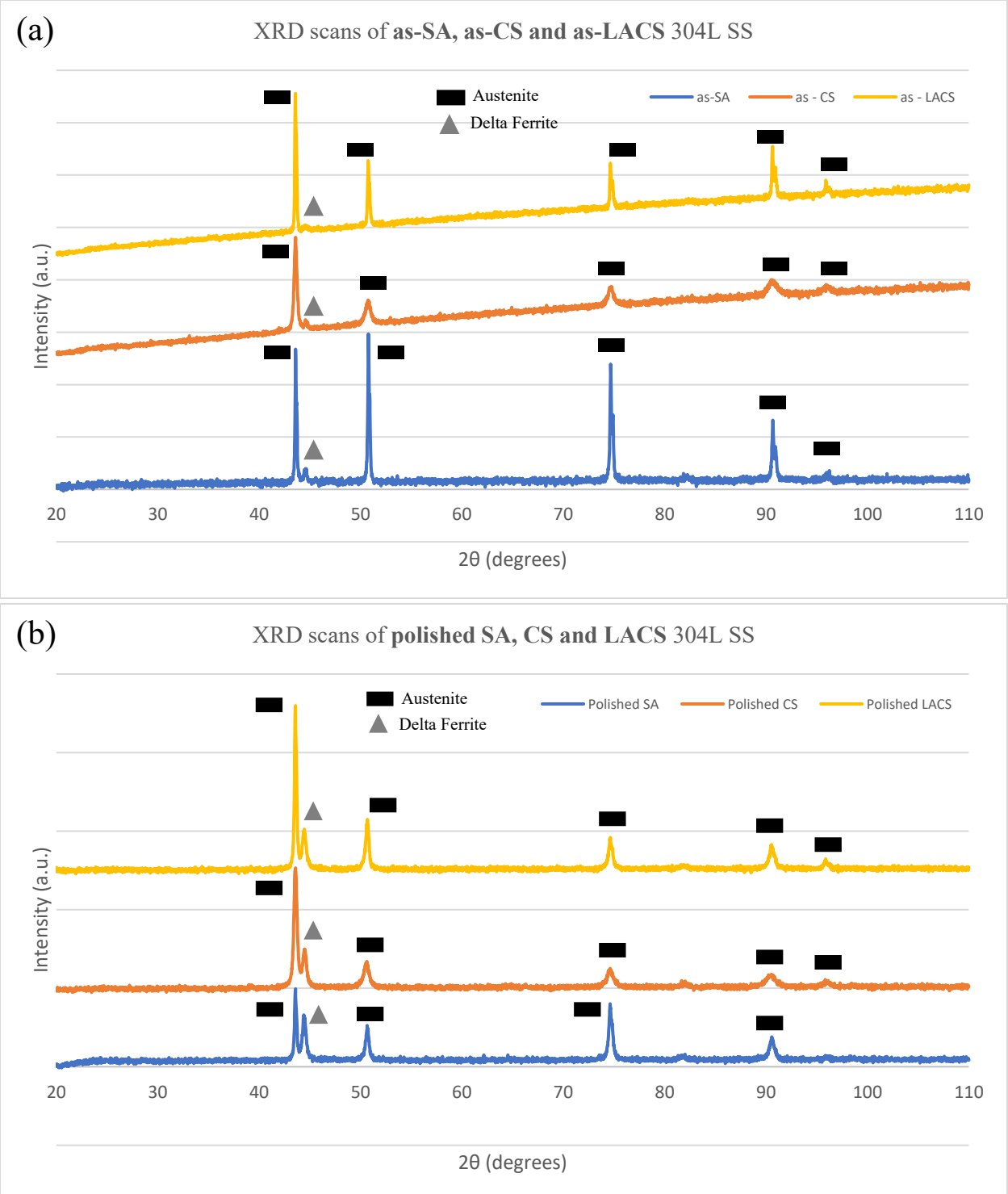

Figure 4.11: Comparing the XRD scans of rolled SA 304L SS, CS and LACS deposited 304L SS coatings in their (a) as-is surface condition and (b) polished to 1200 grit surface condition.

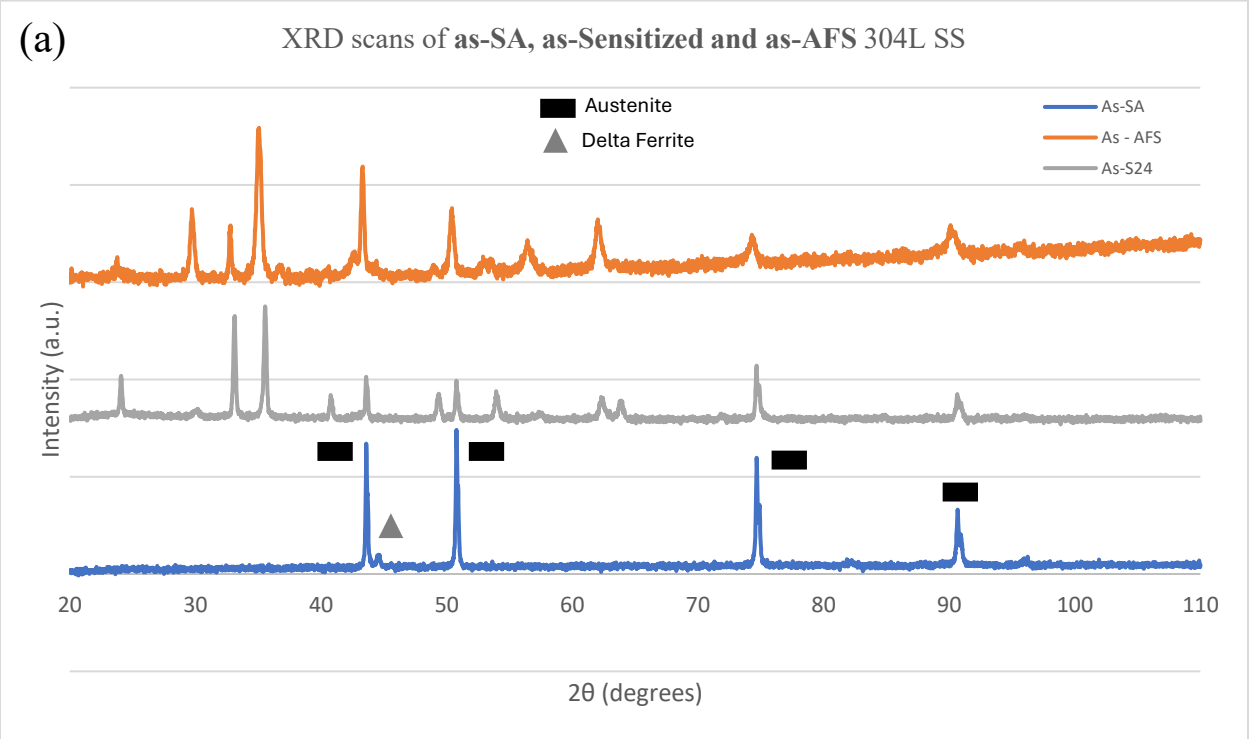

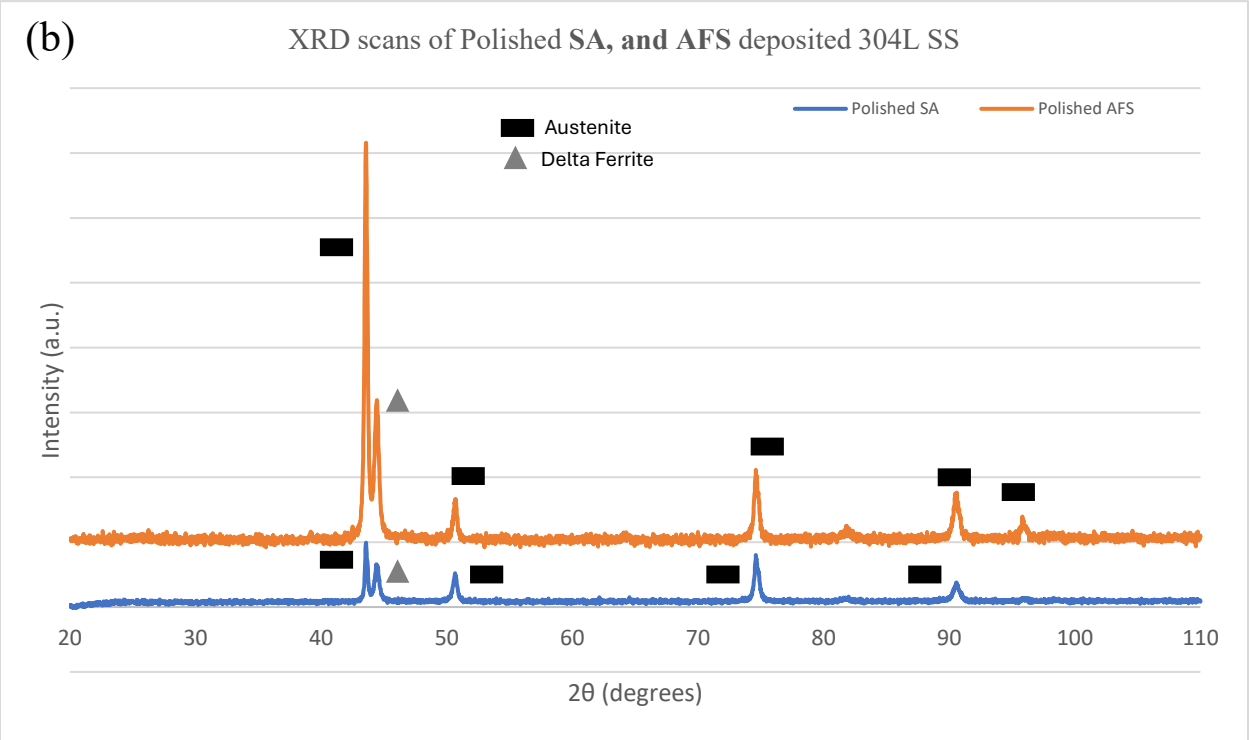

Figure 4.12: XRD patterns of (a) rolled SA, sensitized at 650°C for 24h, and as-AFS deposited 304L SS and (b) polished SA and polished AFS deposited 304L SS (polished to 1200 grit surface finish).

The as-AFS specimen was polished with SiC emery papers until all the surface oxide was removed to acquire the XRD pattern of polished AFS specimen surface which is presented in figure 4.12 (b). It revealed that the AFS deposit is predominantly austenitic but has a small amount of delta ferrite in it. The delta ferrite peak can be observed in the XRD scan at a 2θ of 44.5° like that of the polished SA specimen.

4.2.3 Nano Hardness Analysis

The nano hardness measurements of all the SA, Sensitized, CS, LACS, and AFS 304L SS specimens were made on their cross-sectioned areas, at 30 μm intervals up to a depth of ~ 600 μm from their surface. The nano hardness measurements for these different as-received or untreated 304L SS specimens have been obtained in the form of depth profiles for two reasons (1) to observe for any variations in hardness throughout the depth of these specimens which especially evaluates the processing of 304L SS powder particles deposited through CS, LACS, and AFS techniques and (2) to use these depth profiles in the next chapter to make an assessment on the impact of UNSM surface treatment on the hardness characteristics of these different 304L SS specimens along their depth.

Sensitized 304L SS:

The nano hardness depth profiles of SA (green), S5 (blue), and S24 (red) 304L SS specimens are presented in figure 4.13. The average hardness values of SA, S5, and S24 specimens that are calculated by averaging all their respective through-the-depth hardness values are found to be 297 Hv, 238 Hv, and 264 Hv respectively. The Hall-Petch relationship states that an increase in grain size leads to a consequent decrease in hardness and vice versa. Therefore, the decrease in the average hardness value of S5 specimen from that of the SA specimen can be attributed to the increase in grain size of S5 specimen from that of the SA specimen. The increase in GS of S5

specimen is a result of the grain growth phenomenon occurring in it during its sensitization treatment as observed from figure 4.4 (d) & (e). Similarly, the increase in the average hardness value of S24 specimen from that of the S5 specimen can be attributed to the recrystallization phenomenon occurring in the 304L SS alloy between the 5h and 24h of sensitization treatment as observed from figure 4.4 (b) & (c).

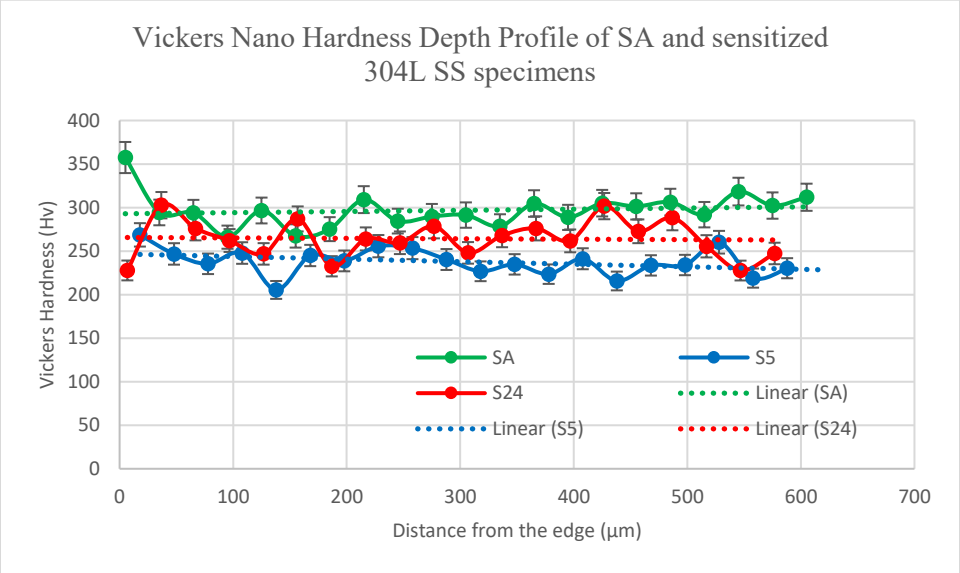

Figure 4.13: Nano Hardness Depth Profile comparison of SA and sensitized at 650°C for 5h and 24h 304L SS specimens.

The average GS of SA and S24 specimens were measured to be almost the same with values of 3.7 µm and 3.8 µm respectively. Therefore, minding the Hall-Petch relationship, it would be expected that the average hardness values of SA and S24 specimens would be very close to each other. However, this is not the case with SA and S24 specimens exhibiting quite the variance in their average hardness values. So, to explain this contradictory behavior exhibited by the SA and S24 specimens with respect to their hardness values, we need to look closely at their hardness depth profiles where they appear to be close to each other but the hardness values of S24 specimen exhibit much larger deviations when compared to the deviations in the SA specimen's hardness values. These larger deviations in the hardness values of S24 specimen can be due to the enhanced

chromium carbide segregation occurring at the grain boundaries of S24 specimen during its sensitization treatment which would consequently increase the area of chromium depleted zones (CDZs) formed in the material. The CDZs having less amount of chromium exhibit lower hardness than the unaffected areas thereby, creating localized regions with reduced hardness. Therefore, when the indentation during hardness testing falls at or close to these CDZs the material reciprocates a lower hardness value than the unaffected area which explains the larger deviations in the hardness values of S24 specimen and its lower average hardness than that of SA specimen.

CS & LACS 304L SS:

Figure 4.14 compares the nano hardness values that were obtained along the depth of SA, CS, and LACS 304L SS specimens. The average hardness values of SA, CS, and LACS 304L SS specimens that were measured by averaging all their obtained through-the-depth hardness values were found to be 297 Hv, 594 Hv, and 378 Hv respectively. The hardness values of both CS and LACS coatings appear to be higher throughout their depth than when compared to the hardness values of the SA specimen which can be attributed to the plastic deformation the 304L SS powder particles undergo during their deposition by CS and LACS processing techniques.

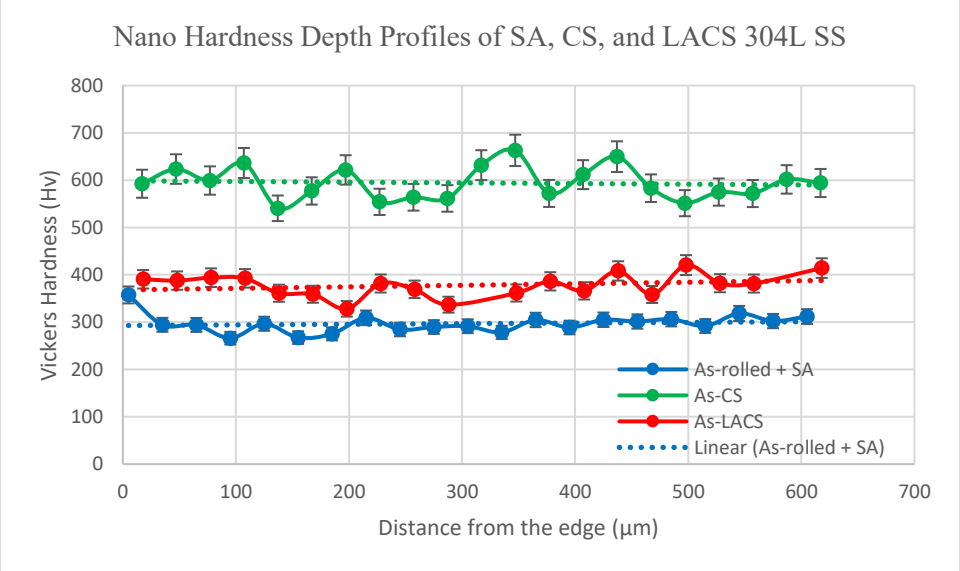

Figure 4.14: Nano Hardness depth profiles of SA, CS, and LACS 304L SS specimens.

On comparing the obtained hardness values of CS and LACS coatings with each other, it can be observed that the hardness values throughout the depth of LACS coating exhibited significantly lower values than when compared to the hardness values of CS coating which can be attributed to the simultaneous application of laser with CS resulting in the in-situ annealing of the LACS 304L SS coating leading to recrystallization phenomenon in the LACS coating as can be seen by comparing the EBSD micrographs in figures 4.6 and 4.7. The recrystallization in LACS coating results in increased grain size than that of the CS coating and consequently decreases its hardness from that of the CS coating satisfying the Hall-Petch relationship.

AFS 304L SS:

Figure 4.15 compares the nano hardness values along the depth of SA, as-AFS and AFS + P 304L SS specimens. The near-surface hardness of the as-AFS deposit exhibits a considerably higher value of ~ 530 Hv that is maintained up to a depth of 50 – 60 μm. Beyond which the hardness decreases drastically within one interval followed by a gradual decrease eventually reaching closer to the hardness values of SA specimen. The higher near-surface hardness values of as-AFS specimen are because of the very fine grains present at the very top surface of the as-AFS deposited layer as seen in figure 4.8.

As expected, after polishing the as-AFS deposit down to 1200 grit surface finish and performing the hardness depth profile on the AFS + P deposit, the near-surface hardness values of AFS + P specimen exhibited lower hardness values than the values exhibited by the as-AFS specimen near its surface. This is due to the polishing action performed on the as-AFS specimen resulting in the removal of the very fine grains at its surface that were contributing to the higher near-surface hardness values of as-AFS specimen. Also, looking at the AFS + P specimen's hardness depth profile, we can observe that the hardness values at its tail cross over to values that

are of lower magnitude than that of the SA specimen's hardness values. Additionally, it can also be seen from the trendlines of both the as-AFS and polished AFS specimens that they exhibit a steep decline in the hardness values. This is because of the gradient microstructure observed in the AFS deposit during EBSD analysis (figure 4.8 and 4.9) i.e., affected by the difference in cooling rate the grain size increased gradually through the depth of the AFS deposit. Therefore, the gradual increase in grain size through the depth of the AFS specimen resulted in a consequent gradual decrease in hardness satisfying the Hall Petch relationship.

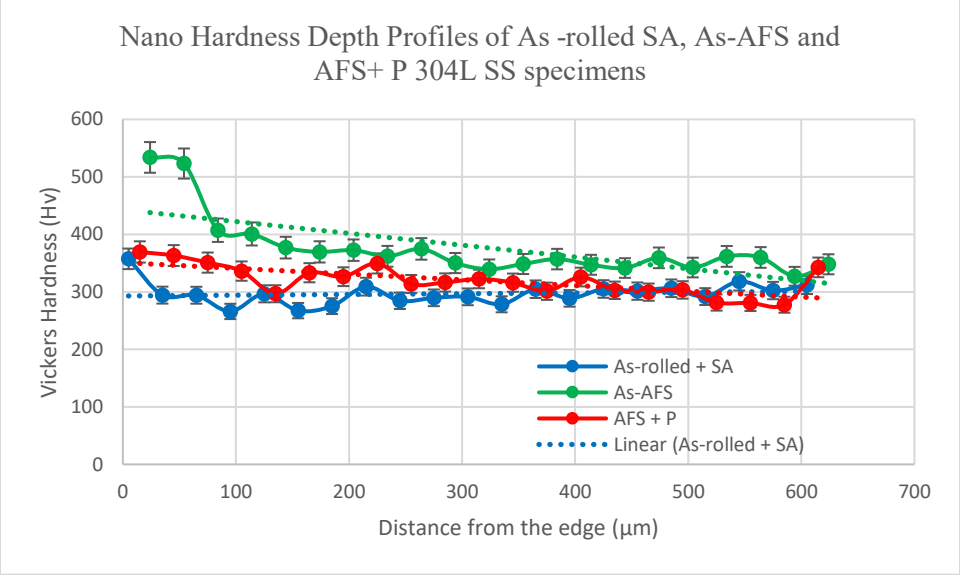

Figure 4.15: Nano Hardness depth profiles of SA, and AFS deposited 304L SS specimens.

4.2.4 Surface Topography Analysis

As both the SA and Sensitized 304L SS specimens have been sectioned from the same CH-R & SA 304L SS plate specimen, there would not be any notable difference in their as received or polished surface roughness values. With no notable difference in their surface topography, there will not be any relevance of the surface roughness properties of SA and Sensitized 304L SS specimens with that of their other properties especially their corrosion properties. Therefore, it was deemed unnecessary to perform the surface topography analysis of as received or untreated SA and Sensitized 304L SS specimens and hence, no such data is presented here.

However, the surfaces of CS, LACS, and AFS deposited 304L SS coatings/cladding appear to be extremely rough even to the naked eye as seen in figures 3.1 and 3.2. And as surface roughness of a specimen can have a significant impact on the corrosion properties of a material because of the surface inhomogeneities acting as preferential sites for localized corrosion phenomenon such as pitting and crevice corrosion and also, as it impacts the strength of the beneficial passive oxide film formed on the surface of 304L SS alloy, the surface topography of as-deposited and polished to 1200 grit CS, LACS, and AFS 304L SS coatings/cladding has been studied and the obtained results are presented and discussed here.

CS & LACS 304L SS:

The average surface roughness (Ra) values of as-CS, as-LACS, CS + P, and LACS + P 304L SS specimens that are obtained using Bruker contour GT profilometer are depicted graphically with the help of a bar chart in figure 4.16 (a) and the obtained surface profile scans that visually depict their surface topography are given in figure 4.16 (b), (c), (d), & (e) respectively. From figure 4.16, it can be seen that both CS and LACS processes resulted in as-CS and as-LACS 304L SS specimens to possess a significantly rougher surface, and intriguingly both of them exhibiting a very similar average Ra value of ~ 16 ± 1.9 μm, whose value was obviously reduced by polishing the as-CS and as-LACS specimens with SiC emery papers to 1200 grit surface finish, resulting in the CS + P and LACS + P 304L SS specimens exhibiting an average Ra value of 0.03 ± 0.006 μm and 0.02 ± 0.003 μm respectively.

The surface scans of as-CS and as-LACS 304L SS specimens depict a very irregular surface capable of developing several annihilating concentration cells (i.e., the driving force for the occurrence / acceleration of corrosion would be the existence of concentration gradience from one area to another area on the same specimen surface) by corrosive species either during corrosion

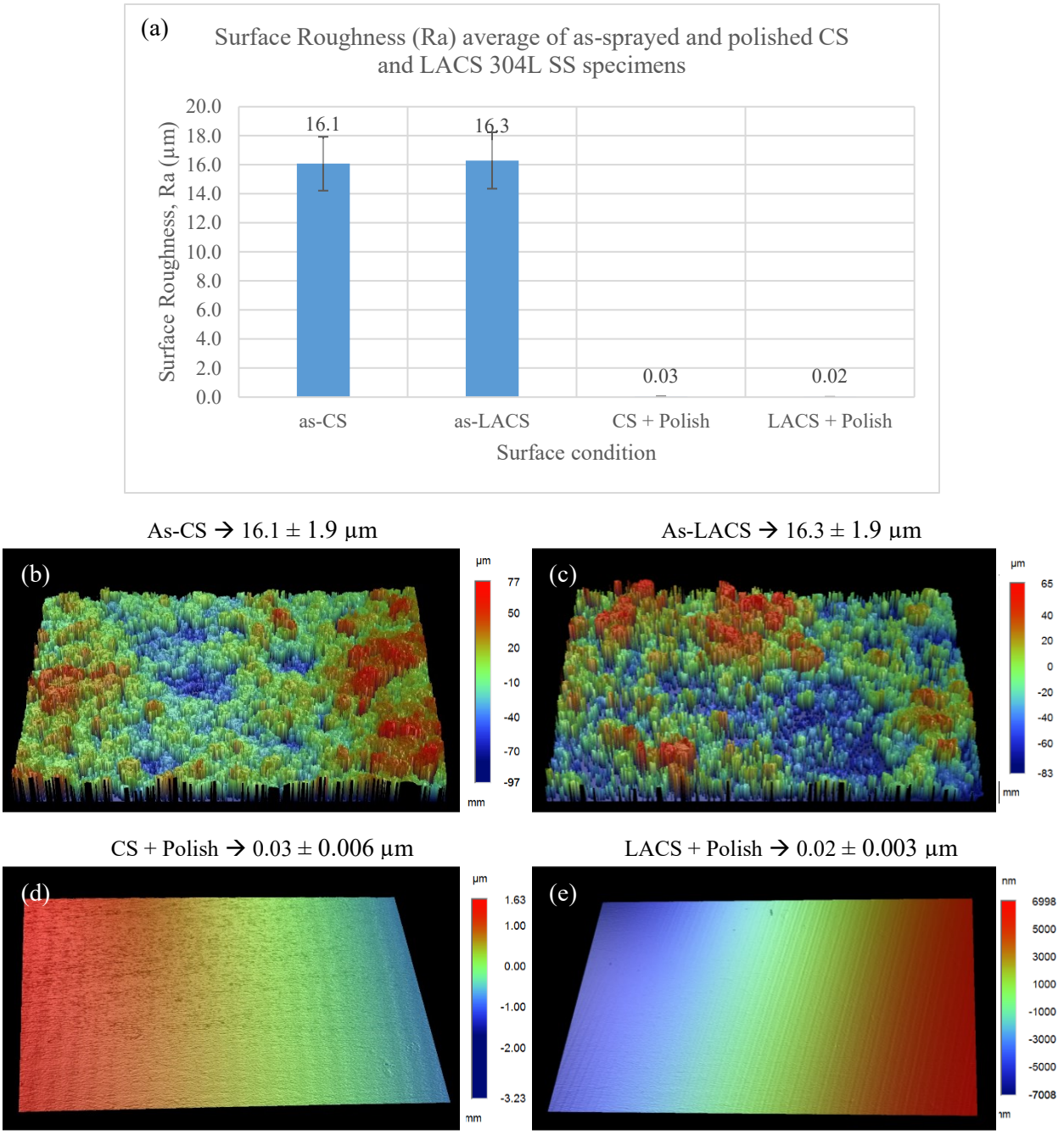

Figure 4.16: Surface topography analysis of as-sprayed and polished to 1200 grit CS and LACS 304L SS specimens with (a) representing their average surface roughness values in a bar graph, and (b), (c), (d), & (e) representing the surface profile scans of as-CS, as-LACS, CS + P , and LACS + P 304L SS specimens respectively.

tests or during real time applications of these coatings. Whereas the surface scans of CS + P and LACS + P 304L SS specimens show a very smooth surface on which the setup of concentration cells could be difficult, lethargic, and possibly confined to the mere porosity sites on these

specimen's surface which were seen in their EBSD micrographs given in figures 4.6 and 4.7.

AFS 304L SS:

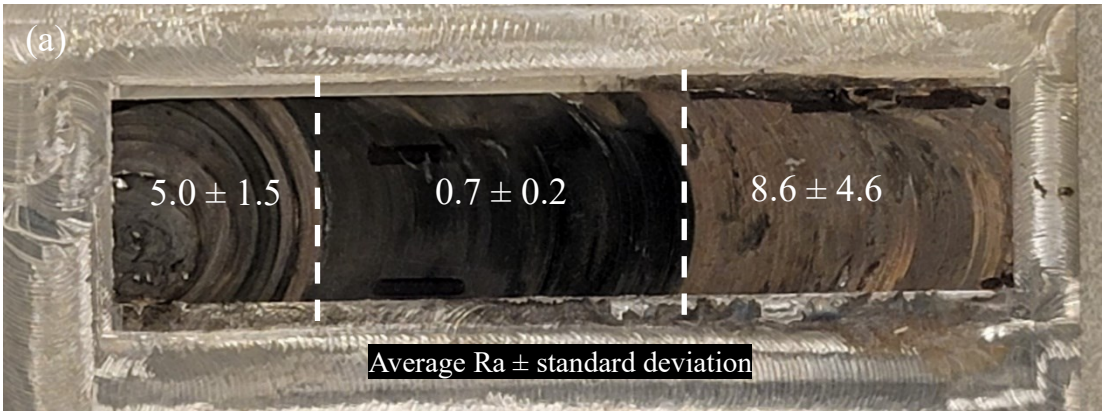

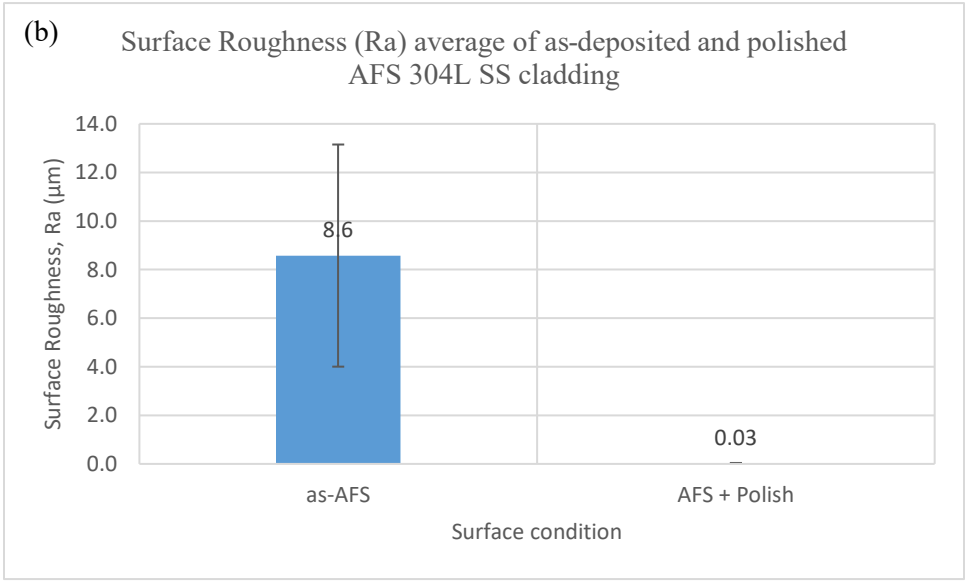

As-AFS → 8.6 ± 4.6 µm

AFS + Polish → 0.03 ± 0.012 µm

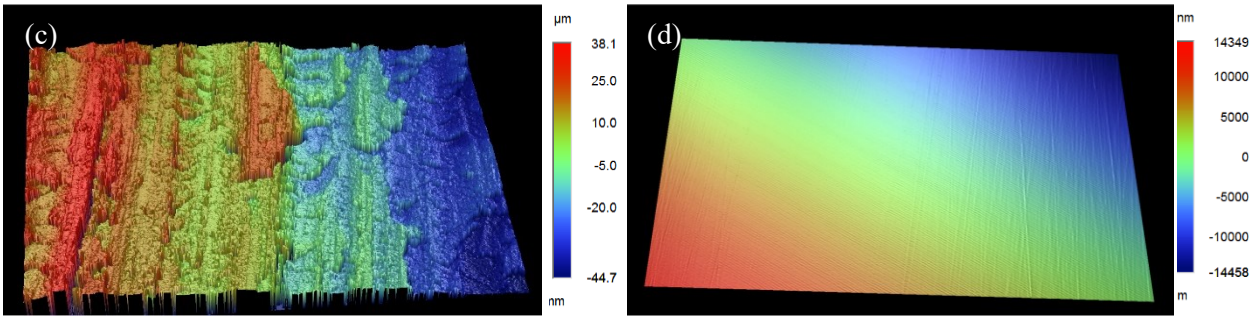

Figure 4.17: (a) Surface roughness average (along with standard deviations) of as-AFS specimen surface showing vastly different values in different regions, and Surface topography analysis of as-deposited and polished to 1200 grit AFS 304L SS specimens with (b) representing their average surface roughness values in a bar graph, and (c) & (d) representing the surface profile scans of as-AFS and AFS + P 304L SS specimens respectively.

When viewed with naked eye itself, it could be seen that the surface roughness of as-AFS/MELD deposited 304L SS varied greatly along its surface from figure 3.1 or figure 4.17 (a). Therefore, the as-AFS specimen surface was divided into three sections as shown in figure 4.17 (a) and multiple surface roughness measurements were performed per section and the average Ra values representing each section in figure 4.17 (a) are presented in it. Also, the attained average Ra values for as-AFS and AFS + P 304L SS specimens are presented graphically using a bar chart in figure 4.17 (b) along with their surface profile scans in figure 4.17 (c) & (d) respectively. The average Ra of the roughest region on as-AFS specimen surface was measured to be 8.6 ± 4.6 µm. Whereas the average Ra value of the AFS + P specimen was measured to be 0.03 ± 0.012 µm.

4.2.5 Residual Stress Analysis

Sensitized 304L SS:

The surface residual stress (SRS) of polished SA, S5, and S24 304L SS specimens were measured to be in the compressive residual stress (CRS) state along both their orthogonal directions (i.e., step direction (SD) and transverse direction (TD) of the specimen or UNSM treatment direction to be used in the later chapter) exhibiting magnitudes ranging between -140 MPa & -230 MPa as shown in figure 4.18. These low magnitude CRSs at their surfaces are due to the mechanical stress placed on the specimen's surface during polishing with SiC emery papers.

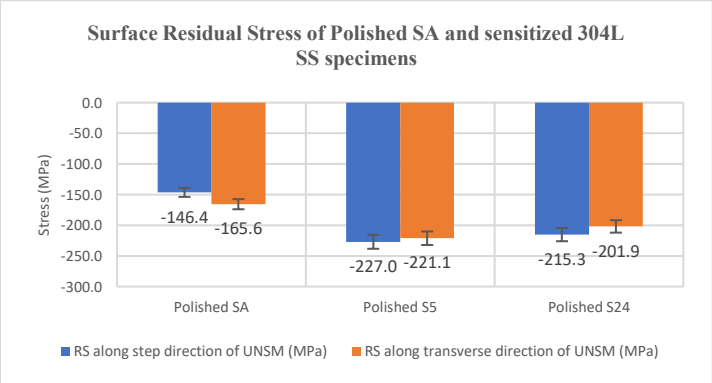

Figure 4.18: Surface residual stress comparison along both the orthogonal directions of Polished SA and sensitized 304L SS specimens.

CS & LACS 304L SS:

The SRS measurements obtained for the as sprayed and polished to 1200 grit surface finish CS and LACS coatings are presented graphically in figure 4.19. The SRSs of as-CS specimen were measured to be of compressive nature (i.e., having a negative magnitude) with magnitudes of -109 MPa and -123 MPa along its SD and TD respectively. Whereas the SRSs of as-LACS specimen were found to have a mixed nature of stress state with CRS of -24 MPa along its SD and tensile residual stress (TRS) i.e., having a positive magnitude of 42 MPa along its TD.

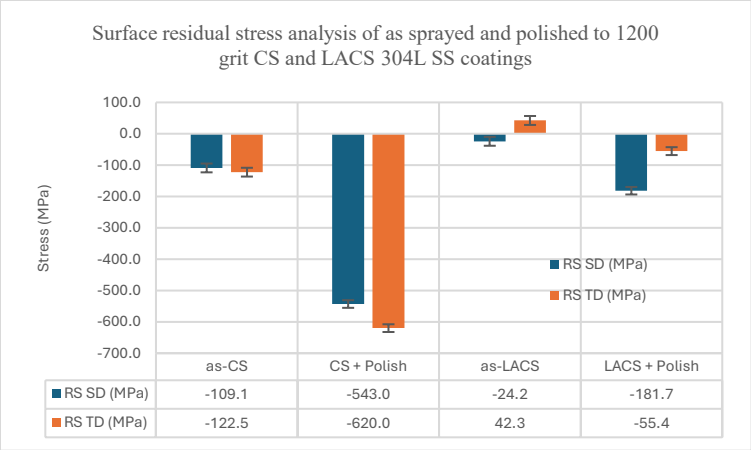

Figure 4.19: Surface residual stress measurements of as sprayed and polished CS and LACS 304L SS coatings.

Generally, due to the mechanical stress placed on a specimen's surface during polishing, the SRSs along both the orthogonal directions of a specimen increase by a magnitude of -150 MPa to -200 MPa on top of the values that are existing in them prior to their polishing. Also, these CRSs induced in a specimen due to polishing would be confined to the topmost surface up to a depth of approximately less than 5 µm to 10 µm. Therefore, the CRSs obtained for the polished LACS specimen that are seen in figure 4.19 are typical of a specimen surface that has undergone a slight amount of stress during polishing. However, the CRSs measured with respect to the polished CS specimen exhibiting magnitudes of -543 MPa and -620 MPa along its SD and TD directions respectively are not typical of mechanical polishing action. These high CRSs obtained for the polished CS specimen represent the extensive plastic deformation that was embedded in the CS

coating during its processing due to the bombardment of 304L SS powders onto the substrate material generating cold work in it. Therefore, to determine the extent and the behavior of the CRSs seen at the surface of both the as-sprayed CS and LACS 304L SS coatings along their depth, through-the-depth residual stress analysis along both the orthogonal directions of these coatings was performed.

Through-the-depth residual stress profiles of as-sprayed CS and LACS 304L SS coatings:

The residual stress depth profiles of as-CS and as-LACS coatings and their corresponding full width half maximum (FWHM) profiles are given in figure 4.20. Note that the RS depth profiles of as sprayed CS and LACS coatings would be inclusive of the RS depth profiles of polished CS and LACS coatings and hence, RS depth profiles pertaining to only as sprayed CS and LACS coatings have been performed and presented here.

The RS depth profile of as-CS coating has been done along both of its orthogonal directions up to a depth of 1mm from its surface and the obtained profiles are presented in figure 4.20 (a). The RS depth profile performed on as-CS coating revealed that CRSs were present consistently throughout the coating confirming the induction of cold work in the CS coating due to the bombardment of 304L SS powder particles onto the substrate material during the CS processing.

The RS depth profile of as-LACS coating has been performed up to a depth where the CRS that was present along its SD transformed to be of a tensile nature. Nevertheless, the RS behavior along both the orthogonal directions of the untreated LACS specimen as a function of its depth was measured and documented in figure 4.20 (b). The low magnitude surface CRS present along the SD of the untreated LACS coating lasted up to a depth of ~ 150 μm before transforming to tensile stress state whereas the surface TRS present along its TD increased notably in magnitude in the tensile direction with increasing depth.

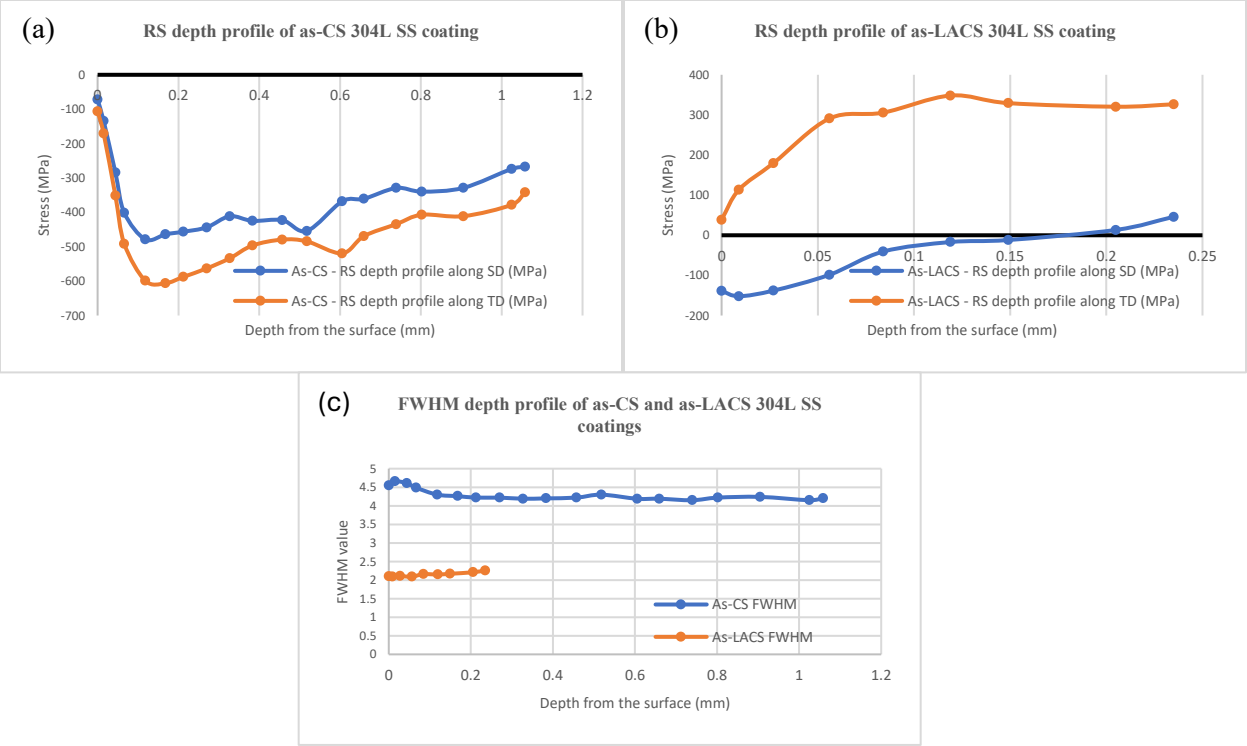

Figure 4.20: Residual stress depth profiles of (a) as-CS, and (b) as-LACS 304L SS coatings and (c) their corresponding FWHM depth profiles.

The mixed nature of RS state along the orthogonal directions observed up to a certain depth of the LACS coating could be due to the thermal gradience existing only along the SD of the deposited coating that leads to the locking of thermal stresses along this direction at the near-surface of the coating. This phenomenon can be explained as follows: LACS process involves the simultaneous application of laser with the deposition of powder particles onto a substrate. The use of laser heats up the depositing powder particles to higher temperatures resulting in the in-situ annealing of the deposited aggregate coating which is typically expected to produce strain free grains exhibiting tensile residual stresses along both the orthogonal directions of the coating. However, LACS processing involves the stepwise progression of the application of laser + deposition of powder particles with an overlap in the steps i.e., overlap between subsequent passes of powder particle deposition + laser application. This creates some thermal gradients to exist between subsequent passes of deposited powder particles along the SD of the deposit whereas the

temperature remains uniform along its TD. This should not be of much concern since the aggregate deposit undergoes recrystallization before the deposit is completely cooled. However, since LACS is an open atmosphere process, the rate of cooling at the surface of the coating would be much faster compared to its internal area. Therefore, the near surface thermal stresses along the SD of the coating get locked in place before recrystallization could relieve them. So, the very near surface RS of the LACS coating along its SD was compressive (i.e., up to ~ 150µm from the surface in this case) which transforms to tensile at subsurface whereas the RS along its TD was always tensile in nature.

The FWHM depth profiles of as-CS and as-LACS coatings given in figure 4.20 (c) represent the amount of plasticity present in a material. They show that as-CS coating had significantly higher degree of plasticity or strain in the material than compared to the as-LACS coating which aligns well with the observations made from their EBSD analysis in figures 4.6 and 4.7. As stated earlier, the high plastic strain seen in CS coating is due to cold work and the decrease in plastic strain of LACS coating is because of its in-situ annealing due to the application of laser that is resulting in recovery and recrystallization in the LACS 304L SS coating.

AFS 304L SS:

The SRS measurements of as deposited and polished AFS 304L SS specimens are given in figure 4.21. The SRS measurements for all the specimens were performed at nine different areas on their surface along both their orthogonal directions represented as step direction (SD) and transverse direction (TD), and the average SRS is presented here. The SD of AFS specimens is along the direction of movement of rotating tool shoulder depositing material during MELD processing. The TD of AFS specimen is perpendicular to its SD. The SRS of as-AFS specimen was measured to be in the compressive state (i.e., having a negative magnitude) with values of -

208 and -295 MPa along its SD and TD respectively. After polishing the AFS specimen to 1200 grit surface finish no notable changes in SRS values could be observed in either of the orthogonal directions.

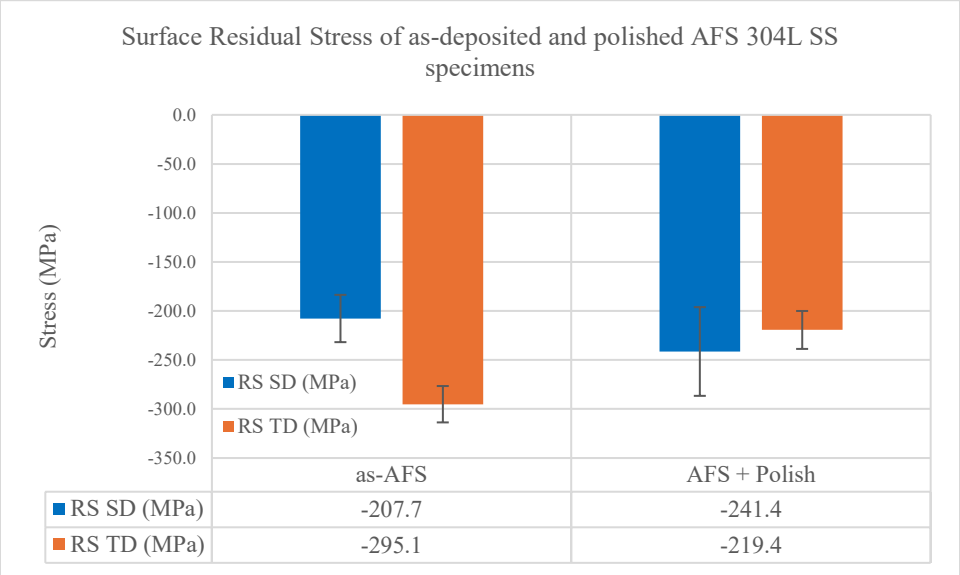

Figure 4.21: Surface residual stress measurements of as deposited and polished AFS 304L SS specimens.

4.2.6 Corrosion Analysis – Sensitization / Susceptibility Behavior

Sensitized 304L SS:

The results of the DLEPR tests performed to determine the degree of sensitization (DOS) in SA, S5, and S24 304L SS specimens which give an account of the chromium carbide precipitates / chromium depleted zones (CDZs) present in a particular material / specimen that make the material susceptible to IGSCC have already been presented in section 4.1 of this chapter in figure 4.1 along with the pertinent data in table 4.1 and their after DLEPR test surface micrographs in figure 4.2. However, in section 4.1, the DLEPR curves, data, and micrographs pertaining to SA, S5, and S24 specimens have been presented along with the curves, data, and micrographs of other 304L SS specimens as well that are sensitized at the other three temperatures, since the goal of that study was to determine the sensitization temperature at which the greatest DOS occurs in 304L SS specimens that are sensitized at the four different temperatures considered in that study. Therefore,

to exclusively study and compare the sensitization behavior of CH-R & SA 304L SS specimen with the most sensitized 304L SS specimen that is the specimens sensitized at 650°C for 5h and 24h, the DLEPR curves, the pertinent data, and the after DLEPR test surface micrographs of SA, S5, and S24 specimens have been pulled separately from section 4.1 and the results exclusive to these three specimens are presented, compared, and the analysis is discussed here in the following paragraphs of this section.

Figure 4.22 (a) presents the obtained DLEPR test curves depicting the effect of sensitization treatments of S5, S24 on 304L SS alloy by comparing them with the DLEPR curve of SA 304L SS specimen and all their corresponding values of corrosion potential (Ecorr), passivation potential (Epp), peak activation current density (Ia) and peak reactivation current density (Ir) obtained from the DLEPR curves, and the DOS calculated as a ratio from the formula % DOS = (Ir/Ia) * 100, along with the Epp - Ecorr values, which depict the passivation behavior of a specimen are tabulated in table 4.3.

Specimen condition	Peak Activation Current Density, Ia (A/cm^2)	Peak Re-Activation Current Density, Ir (A/cm^2)	Degree of Sensitization, %DOS = ((Ir/Ia) *100)	Corrosion potential, Ecorr (mV)	Passivation potential, Epp (mV)	Epp - Ecorr
SA	5.60E-02	1.80E-06	**0.003**	-430	159	589
S5	5.14E-02	1.52E-03	**2.95**	-426	153	580
S24	5.99E-02	8.44E-03	**14.1**	-420	184	604

Table 4.3: Degree of sensitization ratios and the relevant corrosion data obtained from the DLEPR curves in figure 4.22 (a).

Firstly, no significant differences were observed in the passivation behavior of SA, S5, & S24 specimens with them showing very close Epp-Ecorr values of 589 mV, 580 mV, and 604mV respectively. However, a DOS ratio of 0.003% was obtained for the SA specimen, representing it to be an unsensitzed material, with its small DOS ratio being contributed by the presence of δ ferrite or other inclusions in the material that can act as initiation sites for passive film breakdown.

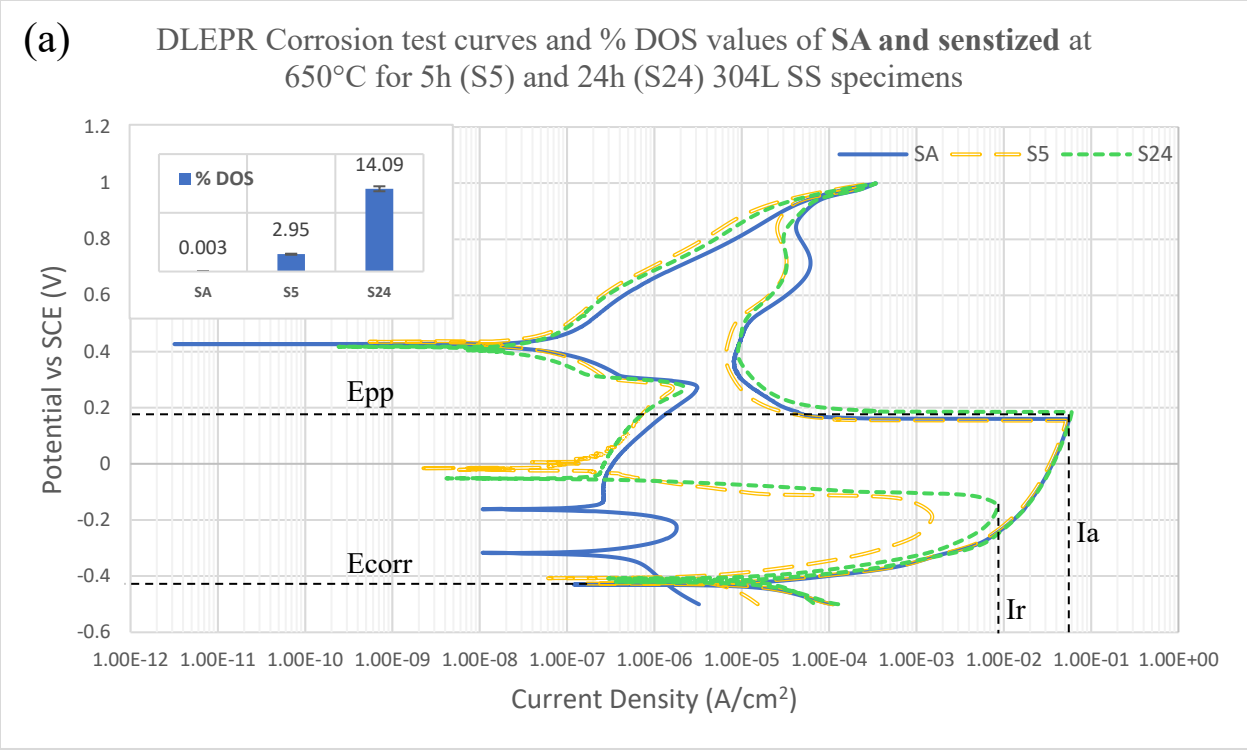

SA → DOS: 0.003 %

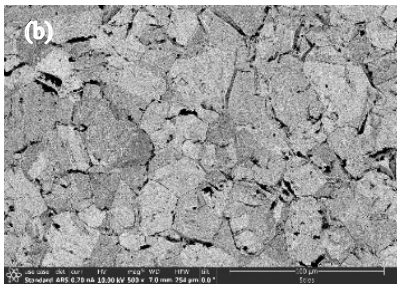

650°C, 5h → DOS: 2.95 %

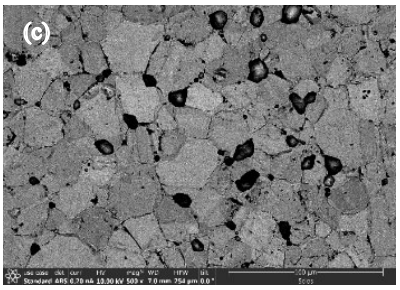

650°C, 24h → DOS: 14.09%

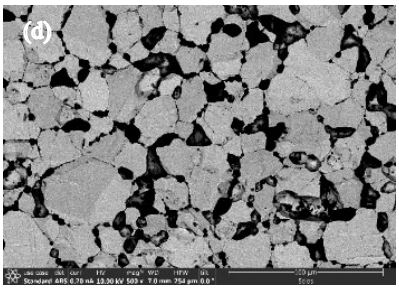

Figure 4.22: (a) DLEPR Corrosion test curves and their corresponding % degree of sensitization values of SA and sensitized for 5h and 24h at 650°C 304L SS specimens, and (b), (c), & (d) represent the corresponding BSE micrographs showing the surface after DLEPR testing of SA and sensitized for 5h and 24h at 650°C 304L SS specimens respectively.

Whereas the DOS ratios of S5 & S24 specimens were found to be 2.95 % & 14.09 % respectively giving a direct qualitative measure on the degree of chromium carbide segregation or CDZ formation happening in the 304L SS alloy at the respective aging durations upon subjecting it to sensitization / aging treatment at 650°C. Therefore, from the respective DOS ratios of the sensitized 304L SS specimens, it can be said that upon aging 304L SS alloy at 650°C for 5h a few CDZs form which increased signficantly upon aging for a longer duration of 24h.

The same is reflected visually in figure 4.22 (b), (c), & (d) which are showing the BSE micrographs of SA, S5, and S24 specimens after DLEPR test surfaces respectively. That is with respect to the BSE micrograph showing the after DLERP test surface of SA specimen, no effect of DLEPR test solution could be observed on its surface reflecting well with its extremly low DOS ratio. Whereas with respect to the S5 specimen surface, considerable number of isolated ditches varying in size can be seen and with respect to the S24 specimen surface, an even greater number of ditches that are much larger in size and well connected with each other can be observed. Futhermore, the ditches in both the S5 and S24 specimens could be seen to have formed predominantly at their grain boundaries.

The ditches that are seen forming in the sensitized 304L SS specimens in figure 4.22 (c) & (d), form by the loss of material through oxidation during their DLEPR tests. This material loss majorly occurs because of the presence of CDZs in the sensitized 304L SS speicmens. The CDZs form along the grain boundaries of 304L SS alloy duirng its sensitization treatment or more generally during its welding. And during DLEPR tests, the corrosive test solution uniformly attacks the passive film that is formed on the specimen's surface. This passive film forms on the 304L SS alloy surface with the help of the Cr content available in its composition as discussed in the literature review chapter presented in this thesis. However, the passive film that forms at the CDZs of sensitized 304L SS specimens will be weaker compared to the unaffected areas due to a lack of chromium content and therefore, it will quickly disintegrate locally at the CDZs due to the attack of DLEPR corrosive test solution. Additionally, because of the low Cr content at the CDZs, the passive film will not be able to regenerate quickly within time to provide further protection leading to continuous heavy metal dissolution at the CDZs, ultimately resulting in the formation of ditches at the CDZs as seen in figure 4.22 (c) & (d).

CS & LACS 304L SS:

The DLEPR test curves of as sprayed and polished CS & LACS 304L SS coatings are compared with the DLEPR curve of as-SA 304L SS specimen in figure 4.23 and all of their corresponding data such as Ecorr, Epp, Ia, Ir, % DOS, and Epp – Ecorr values are consolidated in table 4.4. Note that the abbreviation DOS in the case of SA, CS, LACS, and AFS 304L SS specimens denotes their degree of "susceptibility" and not degree of sensitization, as these specimens have not undergone any sensitization phenomenon like the S5 and S24 304L SS specimens. Also, note that the SA + P specimen's data from table 4.3 is added in table 4.4 for comparison purposes but its DLEPR curve is not shown in figure 4.23 as there is not much difference between the as-SA and SA + P 304L SS specimens % DOS ratios.

Specimen designation	Peak Activation Current Density Ia (A/cm2)	Peak Re-Activation Current Density I_r (A/cm^2)	Degree of Susceptibility, %DOS = ((I_r/I_a) *100)	Corrosion potential, Ecorr (mV)	Passivation potential, Epp (mV)	Epp - Ecorr
As-SA	6.63E-02	1.11E-06	**0.002**	-369	175	544
SA + P	5.60E-02	1.80E-06	**0.003**	-430	159	589
As-CS	1.11E-01	1.34E-02	**12.1**	-428	502	930
CS + P	1.00E-01	1.38E-02	**13.8**	-445	353	798
As-LACS	9.28E-02	1.83E-02	**19.7**	-410	258	668
LACS + P	9.94E-02	3.14E-03	**3.2**	-450	352	802

Table 4.4: Degree of susceptibility and corrosion data obtained from the DLEPR curves in figure 4.23.

The DOS ratios of as-SA and SA + P 304L SS specimens were found to be 0.002 % and 0.003 % respectively, representing that of an unsensitized material that is greatly resisting corrosion signifying the formation of a strong passive film on their surface. Additionally, the potential difference between Epp and Ecorr (i.e., Epp - Ecorr) which determines the kinetics of the passive film formation on a specimen's surface was measured to be 544 mV in the case of the as-SA 304L SS specimen.

As-CS 304L SS coating: The Epp – Ecorr value obtained for the as-CS coating is extremely

high exhibiting a value of 930 mV when compared to the Epp – Ecorr value of 544 mV for the as-SA specimen. This extremely high Epp – Ecorr value of as-CS specimen indicates that its passivation behavior is lethargic compared to the SA specimen which can be attributed to its extremely high surface roughness (figure 4.16 (a) & (b)), giving it difficulty to form a stable passive film on its surface during its DLEPR test. Moreover, the DOS ratio of as-CS coating was also measured to be extremely high exhibiting a value of 12.1 % indicating that a very weak passive film formed on its surface which could not effectively resist corrosion during the reverse scan of its DLEPR test. The high DOS ratio of as-CS coating can be attributed to it having persistent presence of porosity (figure 5.18) and large number of grain boundaries (figure 4.6) with the typical weak interparticle bonding that exists in the CS coatings [67][68]. Because the porous sites present in the CS coating can act as chromium depleted zones (CDZs) where the corrosive test solution can attack preferentially thereby, weakening the passive film locally at these areas and

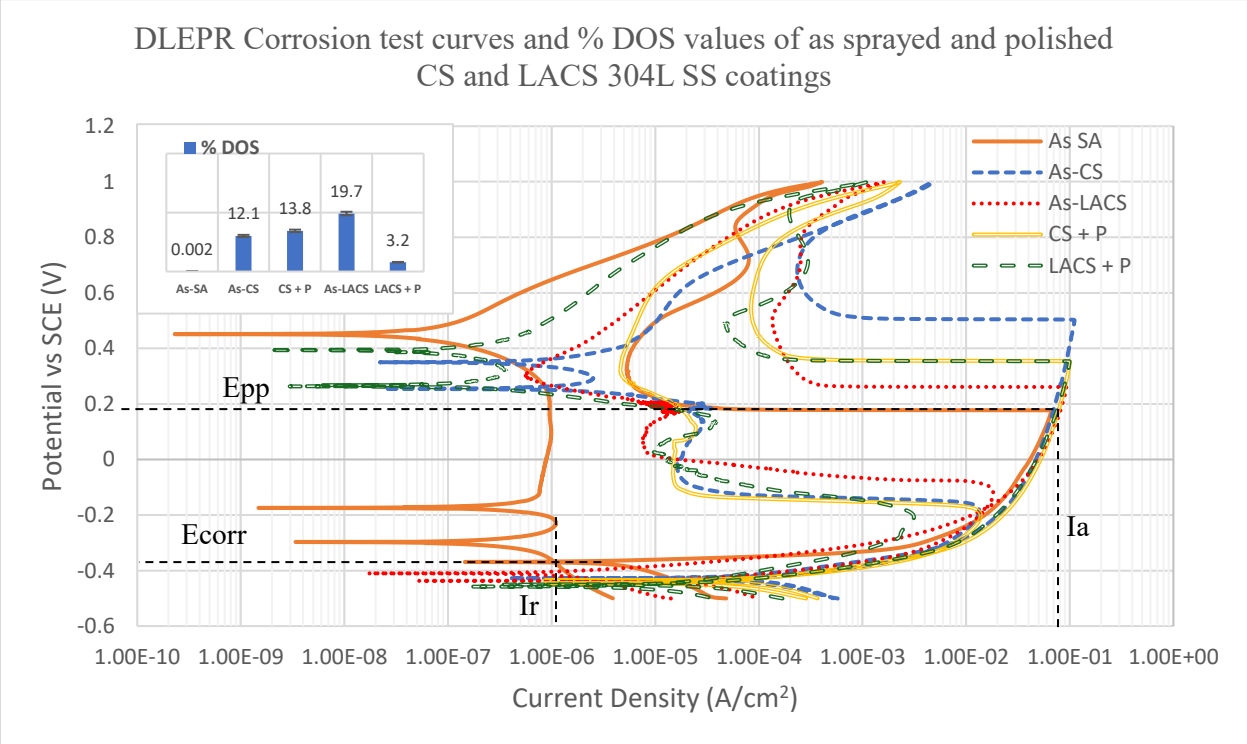

Figure 4.23: DLEPR Corrosion test curves and their corresponding % degree of susceptibility values of as sprayed and polished CS and LACS 304L SS coatings compared with as-SA 304L SS specimen.

exposing the underneath metal to accelerated corrosion. And since the CS coating has very small grains and large number of grain boundaries possessing weak interparticle bonding which can act as preferential pathways for the corrosive test solution to attack ultimately resulting in heavy metal dissolution during its DLEPR corrosion test.

As-LACS 304L SS coating: The Epp - Ecorr value acquired for the as-LACS coating is 668 mV which is significantly lower than the as-CS coating's Epp – Ecorr value of 930 mV. But the DOS ratio of as-LACS coating is measured to be 19.7 % showing that the corrosion experienced by the as-LACS coating is far worse than the corrosion experienced by as-CS coating during their respective DLPER tests.

Despite both the as sprayed coatings exhibiting similar surface roughness values (figure 4.16 (a)) of ~ 16 ± 1.9 μm, the Epp - Ecorr value of as-LACS coating is contradictorily considerably lower than the as-CS coating's Epp – Ecorr value. Additionally, the porosity seen in both the CS and LACS coatings from figure 5.18 showed that they have very similar levels of porous sites, and in research performed by different authors [67][68], it was reported that the interparticle bonding of coatings made with LACS process improved significantly from that of the coatings made with the traditional CS process.

Therefore, due to the improvement in the interparticle bonding, it would be expected that the DOS ratio of as-LACS coating would be much better than the DOS ratio of as-CS coating along with both the as sprayed coatings exhibiting very close Epp – Ecorr values because of their similar surface roughness values. However, this is not the case, and they exhibit contradictory behavior showing that while something is positively influencing the passivation behavior of as-LACS coating from that of the as-CS coating (despite similar Ra values), the corrosion behavior of as-LACS coating is worsening than that of the as-CS coating.

So, to determine this mixed behavior observed between the passivation and corrosion behaviors of as sprayed CS and LACS coatings, EDS analysis was performed on both their surfaces and the obtained results are presented in figure 4.24. The EDS analysis revealed that the as-LACS coating has oxidized surface. The LACS processing technique, which is typically performed in an open atmosphere involving the use of high-temperature laser could be the reason for the surface oxidation seen in the as sprayed LACS coating. Also, this oxide film would have to be thin and confined to the very near surface of the coating because no oxygen peaks were detected during the XRD phase analysis performed on the as-LACS coating using Rigaku XRD machine (figure 4.11 (a)) in which the X-rays penetrate deeper into the material.

As-CS coating

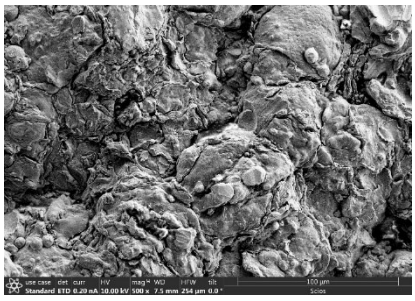

As-LACS coating

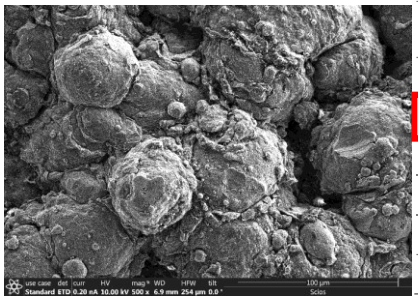

Element (Wt.%)	As-CS	As-LACS
C K	6.31	4.43
O K	**-**	**4.78**
CrK	21.29	22.32
MnK	1.4	2.74
FeK	63.84	60.32
NiK	7.16	5.42

Figure 4.24: SE images of as-CS and as-LACS coatings and their corresponding EDS analysis results.

Nevertheless, the oxidized surface of as sprayed LACS coating clearly explains the contradictory passivation and corrosion behaviors exhibited by the as-LACS coating in comparison with the as-CS coating. The prior oxidized surface of as-LACS coating assists it during the forward scan of its DLEPR test to form a passive film on its surface quicker than the unoxidized surface of as-CS coating. Therefore, the Epp – Ecorr value of as-LACS coating was significantly lower suggesting that its passivation behavior was better than that of the as-CS coating despite both the coatings having a similar surface roughness.

However, it must be noted that because of the prior oxidized surface of as-LACS coating, the passive film that forms on the surface of as-LACS coating during its DLEPR test would not be

entirely made of the beneficial homogenous chromium oxide film that is primarily responsible for the corrosion resistance of ASSs. Instead, it will have compositional irregularities which along with the porous sites and high surface roughness of the as-LACS coating can act as localized concentration sites which can be preferentially attacked by the DLEPR corrosion test solution leading to a relatively quicker breakdown of the passive film during the reverse scan of its DLEPR test. Also, these numerous localized concentration sites make it difficult for the rapid regeneration of the passive oxide film during the reverse scan of its DLEPR test leading to continuous accelerated corrosion in the as-LACS coating that ultimately results in a very high DOS ratio of 19.7 %. Therefore, the high DOS ratio of as-LACS coating can be attributed to the combined effect of its surface oxide film formed during processing, persistent presence of porosity in the coating and its high surface roughness and the huge difference between the DOS ratios of as-CS and as-LACS being attributed to the presence of surface oxide film on the latter specimen.

CS + P and LACS + P 304L SS coatings: The Epp – Ecorr values of polished CS and LACS coatings were measured to be of almost the same values with them exhibiting 798 mV and 802 mV respectively. The Epp - Ecorr values of both the polished CS and LACS coatings are worse than the SA specimen's Epp – Ecorr value indicating that there was a delay in the formation of a stable passive film on their surface during their DLEPR corrosion tests which can be attributed to the porosity present in the coatings. Additionally, in a hypothetical manner, the similarity in the Epp – Ecorr values obtained for the polished CS and LACS coatings can indicate that the porosity levels present in both the coatings could roughly be the same.

The passivation behavior (Epp - Ecorr) of CS coating improves by polishing because of the decrease in its surface roughness enabling the coating to passivate quicker. Whereas the passivation behavior of LACS coating appears to be contradictorily aggravated by polishing. But

this is not the reality because the deleterious surface oxide film formed on the surface of as-LACS coating during its processing was removed by polishing and therefore, will not be meddling with the formation of passive film on the surface of polished LACS coating during its DLEPR test. Therefore, the passivation behavior of as-LACS and LACS + P must not be compared with each other and the passivation behavior of LACS + P coating must be considered as the true passivation behavior of 304L SS material deposited by LACS process. Also, the passive film formed on the LACS + P specimen surface will be made of the beneficial homogenous chromium oxide film that is stronger than the passive film formed on the as-LACS coating surface.

The elemental composition peaks obtained from the EDS analysis performed on the as-LACS and LACS + P coating surfaces are presented in figure 4.25. The presence and absence of detected oxygen peak in the EDS scans of as-LACS and LACS + P coating surfaces respectively indicates that the oxide film on the as-LACS coating surface was removed by polishing. The oxygen peak detected in the EDS scan of as-LACS coating is represented by the black arrow in figure 4.25.

Coming to the DOS ratios of polished CS and LACS 304L SS coatings, they were found to exhibit values of 13.8 % and 3.2 % respectively. Despite the improvement seen in the passivation behavior of CS coating by polishing, no improvement could be observed in its sensitization behavior due to polishing. Because the CS coating has very tiny grains with inherently weak interparticle bonding, LACS + P specimen tends to suffer heavy metal dissolution during its DLEPR test even though its extremely rougher surface has been smoothened by polishing.

In the case of the polished LACS coating, its DOS ratio decreased tremendously from 19.1 % to 3.2 % showing an outstanding improvement of nearly 6X after polishing. This improvement seen in the DOS ratio of LACS coating by polishing can be explained as follows - with no

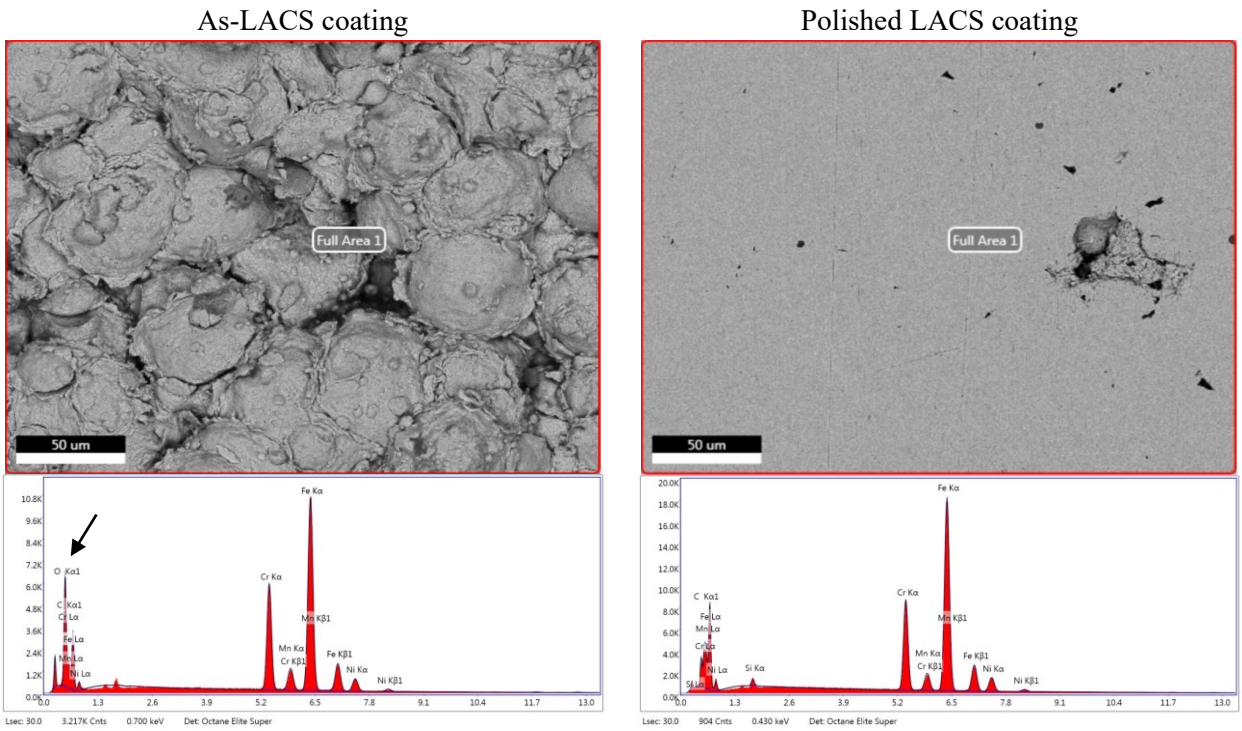

Figure 4.25: BSE micrographs and the corresponding EDS analysis results of as-LACS and LACS + P 304L SS coatings.

compositional irregularities in the passive oxide film formed on the surface of LACS + P coating during its DLERP test due to the removal of oxide film on its surface by polishing along with the significant reduction in its surface roughness by polishing, reduces / limits the number of localized concentration sites present in the LACS + P coating to its lone porosity sites. This significant reduction in the number of localized concentration sites by polishing will result in an improvement in the passive film characteristics of LACS + P coating during the reverse scan of its DLEPR test making it to experience reduced corrosion than that of the as-LACS coating during their respective corrosion tests. Therefore, in conclusion, it can be said that the significant improvement seen in the DOS ratio of LACS + P coating from that of the as-LACS coating's DOS ratio can be attributed to the removal of the deleterious surface oxide film and the significant decrease in surface roughness of as-LACS coating by polishing. Hence, the DOS ratio obtained for the LACS + P coating can be regarded as the true DOS ratio of LACS processed 304L SS material.

Additionally, on comparing the DOS ratios of both the polished CS (13.8 %) and LACS (3.2%) coatings it can be said that due to the application of laser simultaneously with CS increases the corrosion resistance of 304L SS coating despite both the coatings exhibiting roughly the same degree of porosity. Therefore, the betterment in the DOS ratio of polished LACS coating from that of the polished CS coating can be attributed to the enhancement in the interparticle bonding of LACS coating by recrystallization (figures 4.6 and 4.7) of the 304L SS powder particles during their LACS processing.

AFS 304L SS:

The DLEPR test curves of as-AFS and AFS + P specimens are compared with the DLEPR curve of as-SA 304L SS specimen in figure 4.26 and all their corresponding data such as Ecorr, Epp, Ia, Ir, % DOS, and Epp – Ecorr values are consolidated in table 4.5. Repeating the statement from earlier section, note that the SA + P specimen's data from table 4.3 is added in table 4.5 for comparison purposes but its DLEPR curve is not shown in figure 4.26 as there is not much difference between the as-SA and SA + P 304L SS specimens % DOS ratios.

Specimen designation	Peak Activation Current Density Ia (A/cm2)	Peak Re-Activation Current Density I_r (A/cm^2)	Degree of susceptibility, %DOS = ((I_r/I_a) *100)	Corrosion potential, Ecorr (mV)	Passivation potential, Epp (mV)	Epp - Ecorr
As-SA	6.63E-02	1.11E-06	**0.002**	-369	175	544
SA + P	5.60E-02	1.80E-06	**0.003**	-430	159	589
As-AFS	2.45E-02	2.64E-02	**107.8**	-337	7.9	345
AFS + P	7.00E-02	6.48E-06	**0.009**	-441	187.2	628

Table 4.5: Degree of susceptibility and corrosion data obtained from the DLEPR curves in figure 4.26.

As-AFS: The Epp – Ecorr and DOS ratio obtained for the as deposited AFS specimen are 345 mV and 107.8 % respectively. Upon comparing with as-SA specimen, the low Epp – Ecorr value of as-AFS specimen deceives us into thinking that its passivation behavior is better than SA specimen, but it is due to the already present oxide film on its surface influencing its passivation.

The presence of oxide film on as-AFS specimen was revealed by the XRD analysis shown in figure 4.12 (a). It was also observed from its XRD pattern that the oxide film on the as-AFS specimen had mixed peaks of chromium and iron oxides. Therefore, the oxide film forming on the as-AFS specimen during the forward scan of DLEPR test will not be made entirely of the beneficial chromium oxide which is the primary source for corrosion resistance in ASSs like 304L SS. Hence, the oxide film formed during the DLEPR test of as-AFS specimen will contain irregularities/defects that develop into localized corrosion sites being preferentially attacked by the corrosive test solution during the reverse scan of DLEPR test.

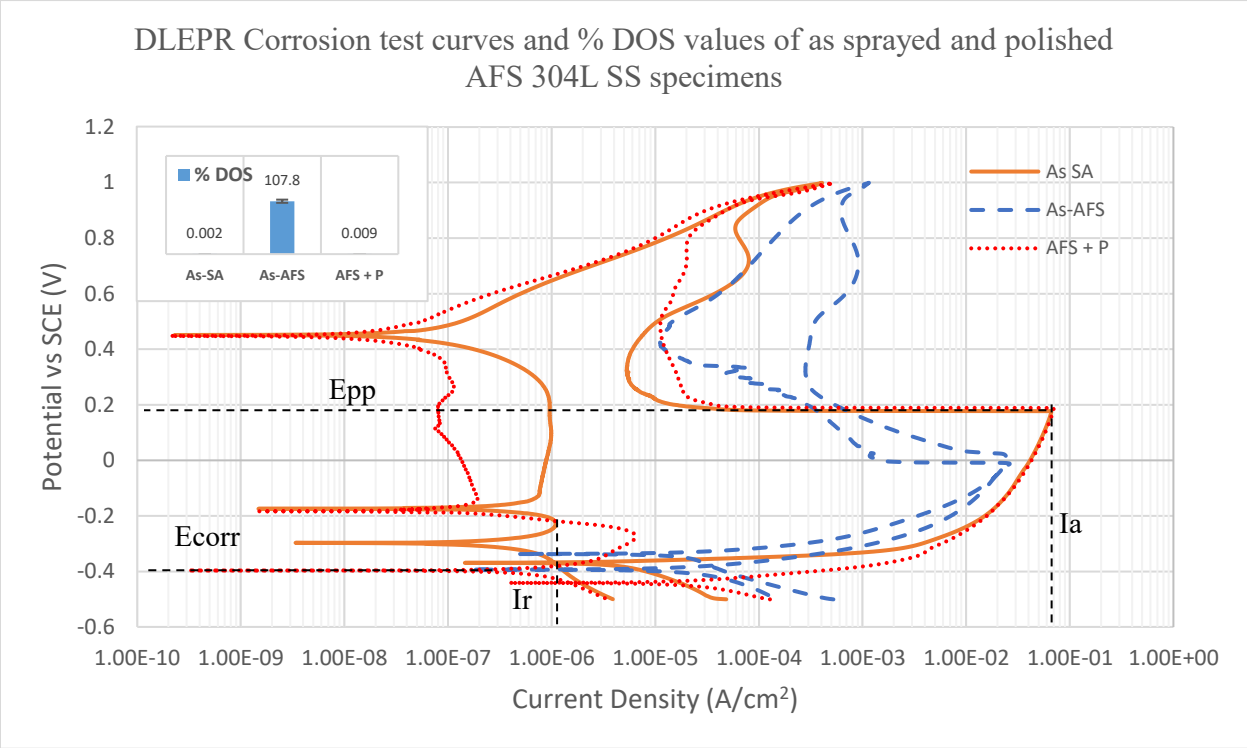

Figure 4.26: DLEPR Corrosion test curves and their corresponding % degree of susceptibility values of as deposited and polished AFS 304L SS claddings compared with as-SA 304L SS specimen.

The SE micrographs of as-AFS specimen before and after DLEPR test along with the EDS analysis performed on their surface are presented in figure 4.27. The EDS analysis performed on as-AFS specimen surface showed a very high intensity O_2 peak as expected. And the O_2 peak intensity on after-DLEPR test surface decreased considerably but still shows that significant oxide

levels were still present on the surface. Also, observing the SE micrographs we can see that corrosion has occurred on the oxide film of as-AFS specimen without exposing the underneath AFS metal to the test solution during the course of the DLEPR test. Thus, the humongous DOS ratio obtained for the as-AFS tested surface is attributed to the oxide film and does not represent the AFS deposited 304L SS. However, it can be deduced from this test that the oxide film formed on the as-AFS surface is not made of the beneficial chromium oxide and therefore is detrimental for corrosion resistance. Nevertheless, further study would be required to determine how this oxide film on the as-AFS surface can impact the underneath metal if the DLEPR test were to be performed for longer i.e., until the oxide film is completely eroded exposing the underneath metal to the altered test solution containing the eroded oxide film.

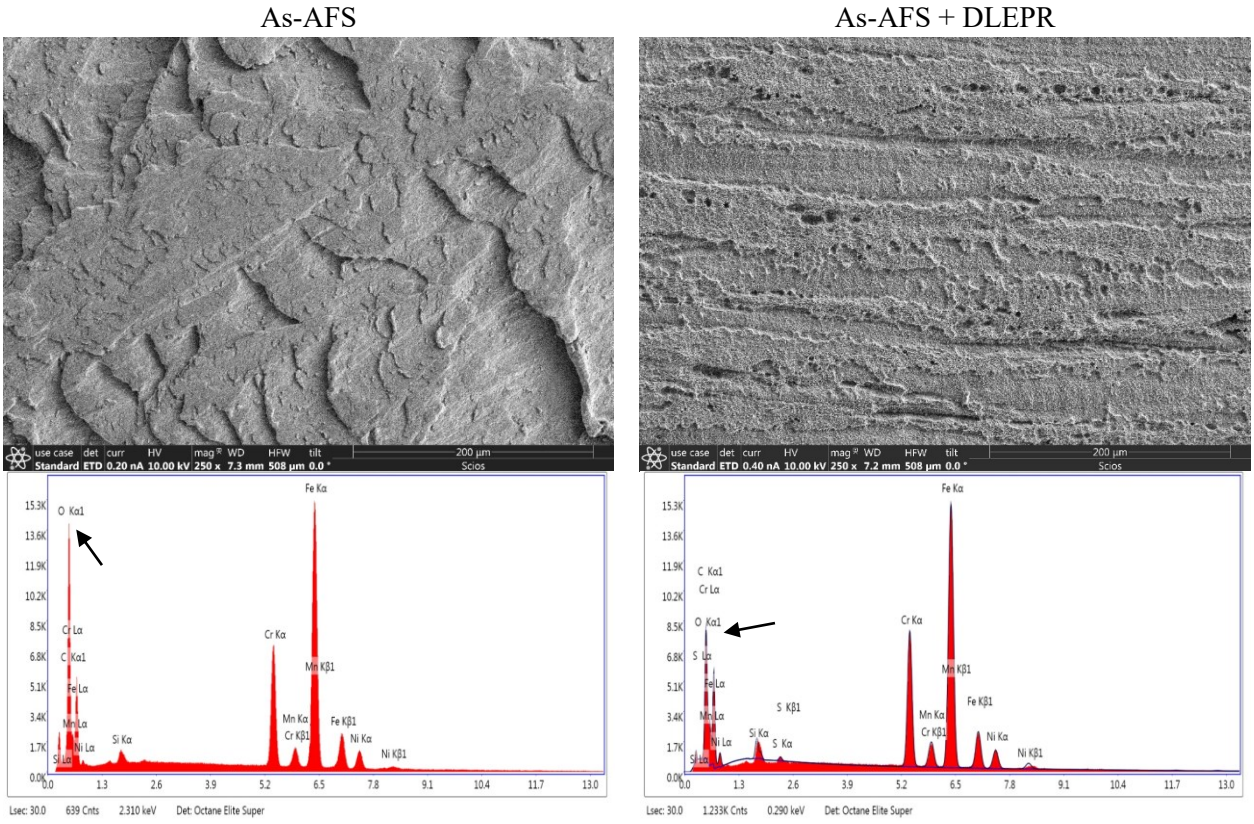

Figure 4.27: SE micrographs of as deposited AFS surface before and after DLEPR test and the results of the EDS analysis performed on their surface.

Polished AFS: The Epp – Ecorr of polished AFS specimen was found to be 628 mV which is slightly higher than the SA specimen. Moreover, the increased Epp – Ecorr of polished AFS from that of the as-AFS specimen represents the removal of the oxide film showing the true passivation potential difference of AFS deposited 304L SS material. The DOS ratio of polished AFS specimen was measured to be 0.009% which is extremely close to the SA specimen representing that the 304L SS deposited by AFS/MELD processing exhibits a great ability to resist corrosion and the passive film formed on its surface is stable, strong, and protective like that of the conventionally hot-rolled SA specimen's. The SE micrographs of polished AFS surface before and after DLEPR test are shown in figure 4.28 which show only light uniform corrosion occurring on its surface, reflecting proportionally well with its low DOS ratio.

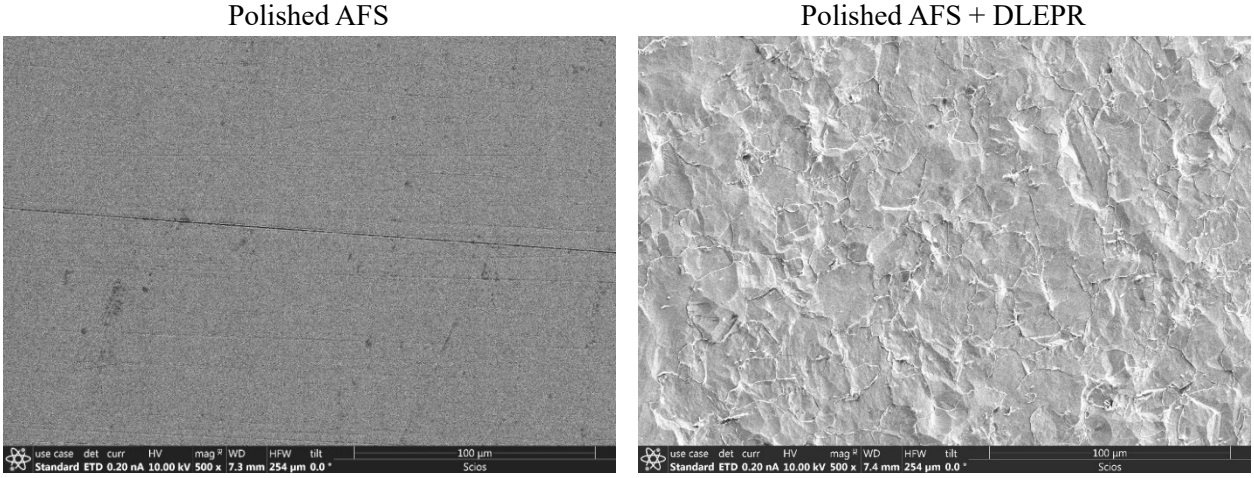

Figure 4.28: SE micrographs of polished AFS surface before and after DLEPR test.

4.3 Discussion

In this chapter, the microstructures, phases, hardness, surface topography, residual stress, and corrosion behavior of Sensitized, CS, LACS, and AFS 304L SS have been evaluated and compared with respect to the conventionally hot-rolled and solution annealed 304L SS alloy. The only similarity between the distinct 304L SS materials studied in this research work, was revealed by the XRD phase analysis, which showed that all the distinct 304L SS material / coatings /

cladding i.e., Sensitized, CS, LACS, and AFS 304L SS had predominantly austenitic microstructure with the presence of a small amount of delta ferrite.

Although the peak intensity of delta ferrite varied with the specimen's surface condition i.e., if it was in as-is surface condition or in polished surface condition, with the delta ferrite peak intensity increasing for the polished specimen surface condition from that of the as-is specimen surface condition for the SA, Sensitized, CS, and LACS 304L SS specimens. This increase in delta ferrite peak intensity of SA and Sensitized 304L SS specimens upon polishing, is attributed to the polishing action removing the top surface area, and exposing the underneath area with increased density of delta ferrite stringers that are present below the 50 μm depth level from the specimen surface, as evidenced by the phase maps obtained during their EBSD analysis, to the X-rays during their XRD phase scans.

Whereas in the case of CS and LACS 304L SS coatings as well, the increase in delta ferrite peak intensity upon polishing is attributed to the removal of their extremely rougher surfaces by polishing, thereby allowing the XRD phase scans to be performed on the flat surfaces of polished CS and LACS 304L SS coatings yielding increased delta ferrite peak intensities. However, in the case of as-deposited AFS 304L SS cladding, its XRD scan revealed it to have oxidized surface, and when the surface oxide film was removed by polishing, its subsequent XRD phase scan i.e., of polished AFS 304L SS cladding revealed it to exhibit a scan very similar to that of the other 304L SS materials studied here.

The EBSD analysis performed on the cross-sectional areas of SA, S5, S24, CS, LACS, and AFS 304L SS specimens, helped to determine the plasticity present in the particular material, that is derived from the Kernel Average Misorientation (KAM) value, which revealed that the plastic strain in the SA, S5, S24, and LACS 304L SS specimens appeared to be within close proximity of

each other with their KAM values ranging between 0.6 – 0.76, which is attributed to the plastic strain present at the grain boundaries of these specimens. Whereas the KAM value obtained for the CS 304L SS specimen is ~ 3X to 4X times greater exhibiting a value of 2.6, and the KAM value obtained for the AFS cladding specimen varied significantly from its top edge to its center exhibiting a value of 1.2 and 0.48 respectively.

The higher plastic strain present at the top edge of the AFS cladding, could be a result of the rotating tool shoulder and the hydrostatic pressure under which the feedstock material is deposited during MELD processing. And with AFS being an open atmosphere process, a difference in the cooling rates will exist between the top edge and the center area of a single AFS deposited layer, resulting in a faster cooling of the top edge and allowing the center area of an AFS layer to cool slowly leading to grain coarsening and strain relief at the center area of the AFS layer, due to which a large difference in the KAM values of the top edge and center areas of an AFS layer is observed. Therefore, the lower KAM value obtained for the center area of the AFS layer indicates the occurrence of strain relief due to grain coarsening.

Whereas the greater KAM value of CS 304L SS coating is attributed to the cold work generated in the coating during its traditional CS processing, which involves the bombardment of 304L SS powder particles onto a substrate material, resulting in heavily deformed grains or the embedment of plastic strain into the material, as evidenced from its inverse pole figure map showing a microstructure with heavily deformed grains. With the simultaneous application of laser to CS processing as in during LACS, in-situ annealing of the coating occurs resulting in recrystallization and grain growth phenomenon which tends the material to undergo strain relief as opposed to the solely CS material, yielding an LACS 304L SS coating with extremely lower KAM value than when compared to the CS 304L SS coating.

This viewpoint is also supported by the full width half maximum (FWHM) profiles obtained during the residual stress (RS) depth profiles of CS and LACS 304L SS coatings. The FWHM profiles or values give a quantitative measure of the plastic strain present in the material at its surface or at the particular depth of the specimen where the RS measurement is being done and the FWHM profile of CS and LACS 304L SS coatings reveal that high and low degree of plastic strain is present in these specimens respectively, supporting the obtained KAM values of these specimens. Additionally, the RS depth profiles performed on the CS and LACS 304L SS coatings, showed that compressive residual stresses were present throughout the CS coating as a result of the generated cold work during the CS processing, which were relieved to a greater extent with residual stresses in the tensile and low compressive magnitude range to be present at the surface and near sub-surface of LACS 304L SS coatings and with their magnitudes increasing towards the tensile region with an increase in the depth of the LACS coating.

The average grain sizes (GS) of SA, S5, S24, CS, LACS, AFS – top edge, and AFS – center area were also determined from their EBSD analysis and the co-relation between their grain sizes and their obtained hardness values satisfying the Hall-Petch relationship which states that hardness increases as grain size decreases and vice versa, is established here. The GS and hardness values of all the distinct 304L SS specimens studied here, are presented in the following table (4.6) and figure (4.29), in the decreasing order of grain size, which shows that as GS decreases hardness increases.

Specimen	**S5**	**S24**	**SA**	**AFS (center area)**	**LACS**	**AFS (top edge)**	**CS**
Grain Size (µm)	7.2	3.8	3.7	2.4	1	0.55	0.24
Hardness (Hv)	238	264	297	322	378	533	594

Table 4.6: Grain Size and Hardness values of distinct 304L SS specimens studied in this research.

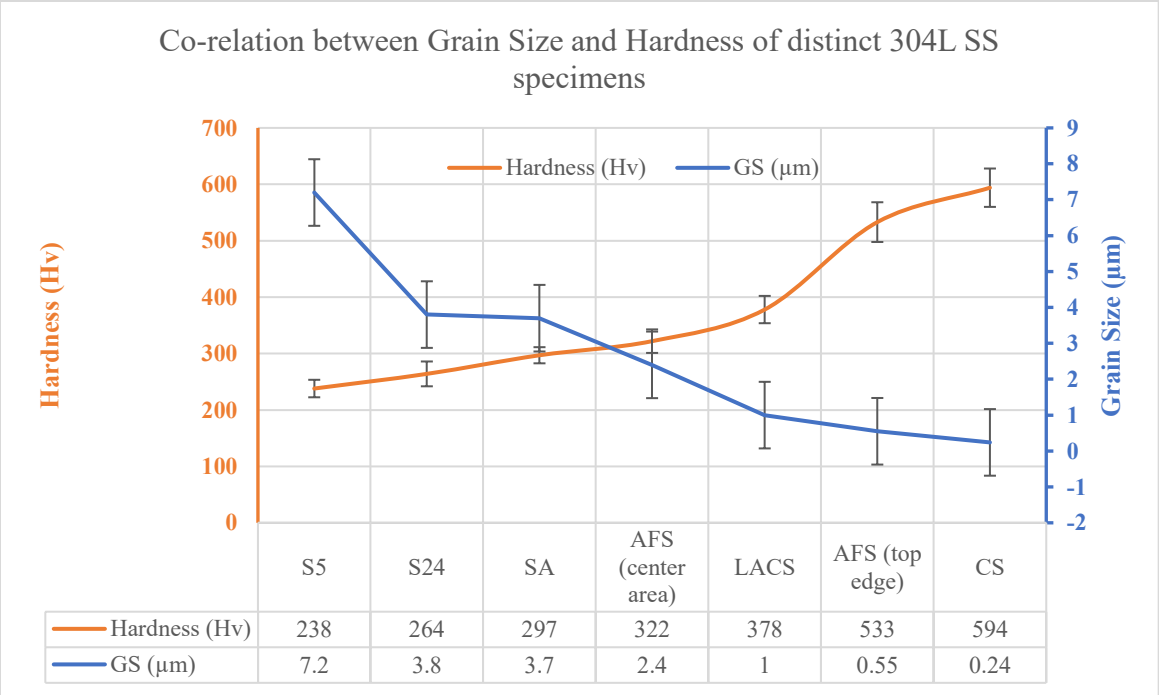

Figure 4.29: Line chart showing the co-relation between grain size and hardness of distinct 304L SS specimens studied in this research work.

Corrosion Behavior Analysis of Distinct 304L SS Specimens

The data obtained with respect to the corrosion behavior of distinct 304L SS specimens studied in this research work, such as the degree of sensitization / susceptibility (DOS), corrosion rate (CR), and pitting potentials (PP) of as-SA, SA + P, S5 + P, S24 + P, as-CS, CS + P, as-LACS, LACS + P, as-AFS, and AFS + P 304L SS specimens are presented in tables 4.7 and 4.8. The corrosion rate and pitting potential data of these specimens in their untreated (i.e., before their UNSM treatment) surface state have been pulled from section 5.2.7 of chapter 5 in this dissertation, where this data has been used to determine the impact of UNSM treatment on the CR and PP of these distinct 304L SS specimens.

Analysis with respect to Sensitization / Corrosion Susceptibility Behavior

The extremely low DOS ratio of solution annealed (SA) 304L SS specimen, in either of it's as-is or polished surface condition clearly represents that of an unsensitized material that will

greatly resist corrosion by the formation of a strong passive oxide film on its surface. Also, there is not much difference between the DOS ratios of as-SA and polished SA (SA + P) 304L SS specimens.

The 304L SS specimens sensitized at 650°C for 5h (S5) and 24h (S24) exhibited very high DOS ratios of 2.95 % and 14.1 % respectively, giving a quantitative representation of the degree of chromium depleted zones formed in these specimens, as a result of their aging or sensitization treatment.

The cold sprayed 304L SS coatings have very tiny grains possessing porosity and inherently weak interparticle bonding, due to which the CS specimen in both of its as sprayed (as-CS) and polished (CS + P) surface conditions experienced heavy metal dissolution during their DLEPR tests consequently resulting in higher DOS ratios which are on par with that of the S24 specimen's DOS ratio.

Specimen	**As-SA**	**SA + P**	**S5 + P**	**S24 + P**	**As - CS**	**CS + P**	**As - LACS**	**LACS + P**	**As - AFS**	**AFS + P**
DOS (%)	0.002	0.003	2.95	14.1	12.1	13.8	19.7	3.2	107.8	0.009

Table 4.7: Degree of Sensitization / Susceptibility ratios of distinct 304L SS specimens studied in this research work.

The as sprayed LACS (as-LACS) coating exhibited an even worse DOS ratio than the as-CS coating which is attributed to the combined effect of the surface oxide film formed on the as-LACS surface due to the application of high temperature laser during its processing, persistent presence of porosity in the coating and its high surface roughness. With the porosity levels and the surface roughness of as-CS and as-LACS coatings being approximately the same, the significant difference between their DOS ratios is attributed to the presence of surface oxide film on the latter specimen.

Whereas the polished LACS coating (LACS + P) yielded a much-improved DOS ratio exhibiting a value of ~ 6X times less than the DOS ratio of as-LACS specimen and its DOS ratio is close to the DOS ratio of S5 304L SS specimen. This significant improvement in the sensitization behavior of LACS + P coating is attributed to the removal of the deleterious surface oxide film and the significant decrease in surface roughness of as-LACS coating by polishing. The removal of deleterious surface oxide film and the decrease in surface roughness by polishing reduces / limits the number of localized concentration sites present in the LACS + P coating, to its lone porosity sites. This significant reduction in the number of localized concentration sites by polishing will in turn result in the improvement of the passive film characteristics of LACS + P coating reducing the corrosion experienced by it compared to the as-LACS coating. Also, the DOS ratio obtained for the LACS + P coating can be regarded as the true DOS ratio of LACS processed 304L SS material and with the porosity levels of CS and LACS 304L SS coatings being approximately the same, the huge improvement in the DOS ratio of LACS + P coating from that of the CS + P coating can be attributed to the improvement in the interparticle bonding of LACS coatings, that is occurring by the simultaneous application of laser to CS technique resulting in in-situ annealing or recrystallization of LACS deposited 304L SS coating.

The thick oxide film present on the surface of as deposited AFS (as-AFS) 304L SS cladding resulted in it exhibiting an abnormally high DOS ratio. And the true DOS ratio of the 304L SS material deposited by AFS is obtained from the oxide free polished surface of AFS cladding (AFS + P), whose value is extremely close to the DOS ratio of the conventionally hot-rolled and solution annealed 304L SS plate specimen, indicating that the 304L SS deposited by AFS is free of porosity or is close to being 100 % dense, resulting in the formation of a strong passive film on its surface that is greatly resisting corrosion like the CH-R & SA 304L SS material. However, the AFS + P

304L SS cladding's DOS ratio is slightly higher than the DOS ratio of the as-SA or SA + P specimens, indicating the presence of greater number of inclusions and/or impurities on the surface of the polished AFS cladding material.

Analysis with respect to Pitting Corrosion Behavior

The corrosion rate of a material is largely dependent on the amount of exposed surface area or surface roughness of the material and the number of inclusions or impurities present on its surface that can act as localized corrosion sites which can be preferentially attacked by the corrosive environment leading to the occurrence of localized corrosion phenomenon such as pitting or crevice corrosion.

The corrosion rate of as-SA 304L SS specimen decreased along with an increase in its pitting potential to a more noble value upon polishing it, indicating that the as-SA specimen surface had some inclusions or impurities on its surface that were reduced or removed by polishing.

The CR of S24 + P 304L SS specimen is approximately the same as that of the SA + P 304L SS specimen, as the sensitization treatment would not introduce any new inclusions or impurities into the specimen and since the oxide film formed on the surface of sensitized specimen is removed by polishing, sensitization treatment will not impact the corrosion rate results. However, due to the formation of chromium depleted zones during the sensitization treatment in S24 304L SS specimen, S24 + P specimen exhibits a pitting potential that is far inferior to the pitting potential of SA + P specimen. And this inferior pitting potential of S24 + P specimen is attributed to the chromium depleted zones in the sensitized 304L SS specimen acting as localized concentration sites where segregation of chloride ions occurs during the CPP tests, leading to earlier stable pit formation due to the relatively easy breakdown of passive film on its surface at the chromium depleted zones than when compared to the unsensitized SA + P 304L SS specimen.

Specimen	As-SA	SA + P	S24 + P	As - CS	CS + P	As - LACS	LACS + P	As - AFS	AFS + P
CR (mpy)	0.016	0.012	0.014	0.235	0.05	0.325	0.036	0.36	0.07
PP (mV)	164	489	257	-	-78.2	-	-141	-	245

Table 4.8: Corrosion rates and pitting potentials of distinct 304L SS specimens studied in this current research work that are obtained from the CPP corrosion tests performed in 3.5 Wt.% NaCl solution.

The extremely high unevenness or high surface roughness seen on the surfaces of as-CS, as-LACS, and as-AFS 304L SS specimens, provides numerous localized corrosion sites where the corrosive chloride ions in the test solution can accumulate, leading to enhanced localized corrosive attack at these sites by the setup of higher degree of concentration cells, resulting in these specimens to exhibit extremely high corrosion rates. In the case of as-LACS and as-AFS 304L SS specimens, the additional presence of non-homogenous oxide film on their surface contributes to a much greater number of localized corrosive sites to be present, tending these materials to exhibit far worse corrosion rates than that of the as-CS 304L SS coating.

Because of the high corrosion rates of as-CS, as-LACS, and as-AFS 304L SS specimens, they could not exhibit any pitting potential or resistance to pitting, indicating that a stable passive film that could resist pitting was not able to form on them at any point during their CPP tests. That is due to the higher degree of concentration cells of chloride ions being setup on the surfaces of as-CS, as-LACS, and as-AFS specimens, because of the higher variations in their surface unevenness, led to their inability of being able to show any re-passivation ability of the initial pits formed on their surface thereby, resulting in the continuous growth of the initial pits formed on their surface throughout their CPP tests without yielding any sign of resistance to pitting. In short, the kinetics of chloride ions attack at the pits or chloride ion accumulation regions is much greater than the kinetics of passive film regeneration at these regions or pits.

Polishing of as-CS, as- LACS, and as-AFS 304L SS specimens, resulted in them exhibiting a significant decrease in their CRs, which is attributed to the significant decrease in the unevenness of their surfaces and the removal of oxide film as well in the case of LACS + P and AFS + P specimens by the polishing action, which in turn resulted in a decrease in the degree of concentration cells that can be setup on their surfaces by the corrosive chloride ions in the test solution thereby, decreasing their CRs significantly. The CRs of CS + P, LACS + P, and AFS + P specimens are extremely close to each other but are higher than the CR of SA + P 304L SS specimen, indicating that there are factors at play which are responsible for the higher CR of the former specimens than that of SA + P specimen. In the case of CS + P and LACS + P coatings, smaller degree of concentration cells could be set up at the porosity sites on their surfaces, leading them to exhibit slightly higher CRs than that of SA + P specimen's CR. But in the case of AFS + P cladding, even though it is 100 % dense like the SA + P specimen, its CR is slightly higher than that of CS + P and LACS + P coatings, leading to or asserting the hypothesis that the AFS cladding has many inclusions and/or impurities on its surface where the corrosive chloride ions are attacking, leading it to exhibit higher CR than the CRs of SA + P, CS + P, and LACS + P specimens.

Additionally, polishing of as-CS, as- LACS, and as-AFS 304L SS specimens, led them to exhibit a pitting potential showing some resistance to the pitting phenomenon occurring in these specimens during their CPP tests. This exhibition of pitting potential by CS + P, LACS + P, and AFS + P 304L SS specimens, is attributed to the polishing action reducing the localized corrosion sites on their surfaces to the lone porosity sites in the case of CS + P and LACS + P specimens and to the inclusions or impurities in the case of AFS + P specimen, thereby significantly slowing down the accumulation of chloride ions on their surfaces during CPP tests than when compared to the extremely rougher and/or oxidized surfaces of as-CS, as-LACS, and as-AFS specimens that are

having numerous accumulation sites, ultimately resulting in a significant delay in the formation of stable pits on the surface of polished CS, LACS, and AFS specimens i.e., allowing the initial pits formed on their surface to re-passivate (unstable pits) during their CPP tests and allowing them to exhibit a pitting potential. That is, the kinetics of passive film regeneration at the initial pits formed on the CS + P, LACS + P, and AFS + P specimen surfaces during their CPP tests is greater than the kinetics of chloride ions attack at these areas.

However, the pitting potentials exhibited by these polished CS, LACS, and AFS 304L SS specimens are still significantly lower than the pitting potential of SA + P 304L SS specimen, which can be attributed to the presence of defects like porosity sites in the case of polished CS and LACS coatings and to the presence of inclusions in the case of AFS + P cladding. Nevertheless, the pitting potential exhibited by the AFS + P cladding is the closest to the SA + P specimen's pitting potential among the three specimens and is extremely closer to the pitting potential of S24 + P specimen, ascertaining the fact that AFS cladding is indeed 100 % dense, unlike the CS + P and LACS + P coatings. Even, in between the CS + P and LACS + P coatings that have approximately the same levels of porosity and despite the better interparticle bonding of LACS coating, it exhibits inferior pitting potential than that of CS + P coating, which is attributed to the presence of compressive residual stresses in the CS 304L SS coating aiding it to exhibit better pitting potential than the LACS 304L SS coating having tensile or very low magnitude compressive residual stress state. Also, despite the CS + P coating having greater magnitudes of compressive residual stresses than that of AFS + P, SA + P, and S24 + P specimens, it exhibits inferior pitting potential than the latter specimens, which is attributed to the presence of porosity in the CS coating deteriorating its pitting potential or deeming the benefit of compressive residual stresses generated during the CS processing to be of no significance when porosity is present.

4.4 Motivation for Further Research Carried Out in the Next Chapter

From the research work presented in this chapter, a few drawbacks or shortcomings have been observed with respect to the Sensitized, CS, LACS, and AFS 304L SS specimens, which provided the motivation for carrying out the research work presented in the next chapter, which involves the application of UNSM surface treatment on these specimens to improve their properties i.e., address the drawbacks observed in this chapter through UNSM, the drawbacks are as follows:

(i) The surface residual stress state of all the distinct 304L SS specimens studied in this research work have been found to be in the tensile or low compressive residual stress state except for the CS 304L SS coating, which are deemed to be insufficient in effectively tackling the SCC susceptibility of sensitized 304L SS specimen and insufficient in providing a complete hermetic seal to the canisters repaired through LACS and AFS processing techniques, as the tensile or low magnitude of compressive residual stresses would not be able to prevent the propagation of any un-arrested pre-existing cracks or even arrested cracks which can propagate in the future by the presence of external forces. Therefore, presence of greater magnitudes of compressive residual stresses at the surface and sub-surface of sensitized, LACS, and AFS 304L SS specimens will be desired for the canister applications, which can be provided by a cost-effective mitigation technique like UNSM.

(ii) The degree of sensitization of polished sensitized 304L SS specimens and the degree of susceptibility of as-CS, as-LACS, and as-AFS 304L SS specimens, needs to be improved. Even though polishing of as-LACS and as-AFS specimens led to a significant improvement in their degree of susceptibility by the removal of their deleterious surface oxide film due to polishing, the DOS ratio of LACS + P

specimen is on par with that of the 304L SS specimen sensitized at 650°C for 5h, necessitating the requirement of looking for means to improve its DOS ratio further. Whereas polishing did not impact the DOS of CS 304L SS specimen at all. It is to be seen if UNSM can impact the DOS of CS specimen in either of its as-is or polished surface state. Also, if UNSM can improve the DOS of LACS + P specimen and that of as-LACS and as-AFS specimens directly without requiring the need for polishing them is to be seen i.e., to find out if UNSM can directly impact the surface oxide film on these specimens. Nevertheless, the residual stress state of LACS + P, AFS + P, as-LACS, and as-AFS needs to be improved by UNSM, and it is to be observed how this impacts their DOS, especially that of AFS + P specimen's, as its DOS ratio is exceptionally close to that of as-is or polished SA specimen's, i.e., it is to be seen if UNSM improves the residual stress state of AFS + P specimen and also its DOS ratio or what would be the case.

(iii) The corrosion rates of as-CS, as-LACS, and as-AFS 304L SS specimens have been extremely high due to their extremely high surface roughness or unevenness and need to be improved. Although polishing improved their corrosion rates by the reduction in surface unevenness and/or removal of deleterious surface oxide film, the corrosion rates of CS + P, LACS + P, and AFS + P specimens were still slightly higher than the CR of SA 304L SS specimen due to the presence of porosity and/or inclusions on the surfaces of the former specimens. As UNSM is a direct material contact dynamic impact process, it is to be seen if it can further improve the corrosion rate of polished CS, LACS, and AFS specimens by decreasing their porosity levels and/or removal of inclusions on the surface of these specimens.

Also, as UNSM would be able to impact the as-CS, as-LACS, and as-AFS specimen surfaces through direct material contact, it is to be seen if UNSM would be able to affect these specimen's corrosion rates directly without requiring the polishing action, by decreasing their surface unevenness through the WC tool tip impact during UNSM.

(iv) The high corrosion rates of as-CS, as-LACS, and as-AFS 304L SS specimens prevented these specimens to exhibit a pitting potential, and if UNSM improves their corrosion rates, it is to be seen if it would be able to instill a pitting potential or positively impact the pitting corrosion behavior of these specimens. Although polishing of as-CS, as-LACS, and as-AFS specimens resulted in them exhibiting a pitting potential by the decrease in their corrosion rates i.e., by the removal of factors responsible for their high corrosion rates by polishing, their pitting potentials are still below that of the SA and sensitized 304L SS specimens. Also, the pitting potential of sensitized 304L SS specimen is below that of SA specimen's pitting potential. Therefore, the pitting potential or pitting corrosion behavior of polished sensitized, CS, LACS, and AFS 304L SS specimens needs to be improved as well and it is anticipated that this can be achieved to some degree by the induction of greater magnitudes of compressive residual stresses into these materials by UNSM.

Despite the differences in the microstructural characteristics of Sensitized, CS, LACS, and AFS 304L SS specimens, we hypothesize that UNSM surface treatment performed on these specimens will be able to impact them in a similar manner resulting in the improvement of their properties of residual stress state, hardness, surface topography, and most importantly enhancing

the corrosion behavior of the distinct 304L SS specimens studied in this research work through the induction of high magnitudes of compressive residual stresses, near-surface hardening, and near-surface nano crystallization which have been deemed to be responsible for improving the SCC resistance of a material. Therefore, the motivation for the research work performed in the next chapter is to find out if this hypothesis holds true or false or partially false, and in case if it is deemed to be false or partially false, the goal would be to determine the factors responsible for it.

Chapter 5. Impact of Ultrasonic Nanocrystal Surface Modification on the Microstructure, Hardness, Residual Stress and Corrosion Properties of Sensitized, CS, LACS & AFS 304L SS

In this chapter, with the intent of improving the properties, especially the corrosion properties of Sensitized, CS, LACS, and AFS 304L SS, the Ultrasonic Nanocrystal Surface Modification (UNSM) treatment was applied on the aforementioned 304L SS materials / coatings / cladding and the UNSM treatment's impact with respect to the properties that have an immense influence on the SCC resistance of a material like the microstructure, phases, hardness, surface roughness, residual stress, degree of sensitization/susceptibility and pitting corrosion behavior have been studied and the underlying mechanisms or factors that influenced the material's behavior to behave in one way or the other upon the application of UNSM treatment have been discussed extensively.

5.1 UNSM Parametric Study of 304L SS Alloy

In order to surface treat the Sensitized, CS, LACS, and AFS 304L SS with UNSM surface treatment technique, firstly, a UNSM parametric study was done to determine the most beneficial UNSM parameters that can be used for surface treating the 304L SS alloy in general, as UNSM processing involves several parameters like Static Load (SL), Dynamic Load or Amplitude (A), Peening Speed (PS), and Interval Feed Rate (IFR) whose degree of impact changes with different parameter combinations yielding different results for different materials. The combination of UNSM parameters studied in the current research work are given in table 3.3 and the specimen's surface preparation prior to UNSM treatment and the procedure followed for the UNSM surface treatment itself are outlined in sections 3.1.4 and 3.2 of Chapter 3 in this thesis, respectively. The surface roughness, hardness, surface and in-depth residual stress are the material properties, based on which the most beneficial UNSM parameters for surface treating the 304L SS alloy have been

chosen from the several parameter combinations studied in this research. These properties were considered because of their beneficial impact on a material's SCC resistance, with the ultimate goal of choosing a UNSM parameter combination that yields the best or desired combination of low surface roughness, high surface compressive residual stress (CRS), greater depth of CRS induction, high near-surface hardness and deeper hardness penetration depth. The results obtained during this UNSM parametric study, and the analysis performed for choosing the most beneficial UNSM parameter combination are discussed in the next few sections.

5.1.1 Surface Topography Analysis

Surface roughness average (Ra) values of 304L SS specimens UNSM treated with different combinations of parameters as shown in table 3.3 are presented in figure 5.1. The average Ra values of all the specimens were measured to be ≤ 1 µm except for peens 3, 4, and 7.

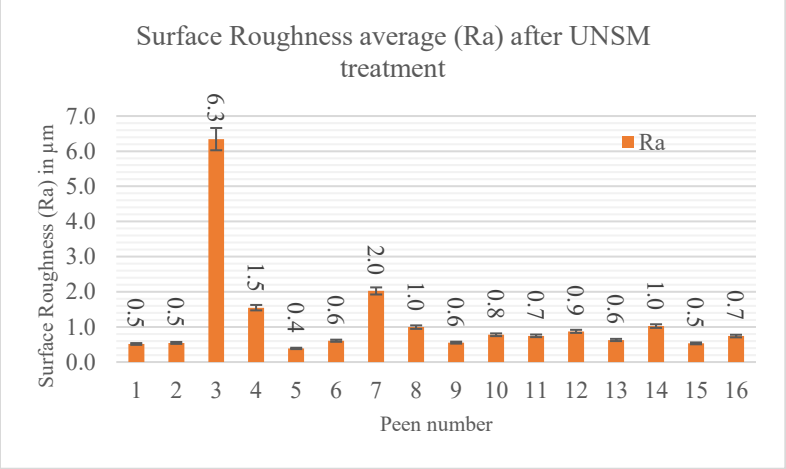

Figure 5.1: Surface Roughness average values of 304L SS specimens UNSM treated with different UNSM parameter combinations.

The UNSM parameters common between peens 3, 4, and 7 are the high peening speed (PS) of 3000 mm/min and low static load (SL) of 20N. Observing the peens 1-8 that were applied at 20N SL, it was found that the peens performed with 3000 mm/min PS (3, 4, 7 and 8) have considerably higher Ra values than the peens performed with 2000 mm/min PS (1, 2, 5 and 6). This increase in Ra can be attributed to a lack of sufficient SL and less overlap between peening

shots in the TD, forcing the material to form a wavy structure with taller peaks as seen in figure 5.2 (SD – step direction and TD – transverse direction of UNSM). Also, from peens 3, 4, 7 & 8 i.e., low SL + high PS, it was found that the Ra values increased significantly with a decrease in interval feed rate (IFR) from 70 µm (4&8) to 30 µm (3 & 7). This is because, when the IFR was decreased, the overlap between the parallel TD UNSM tracks increases, nudging the material peaks formed at low SL + high PS further taller, resulting in further higher Ra values. However, all these factors affecting the Ra of UNSM treated 304L SS specimens with low SL were minimized when the SL was increased to 40N (peens 9-16), which have much lower deviation in their measured Ra values. Hence, it can be said that the high SL alone has significant impact on the surface roughness of UNSM treated 304L SS specimens independent of other UNSM parameters.

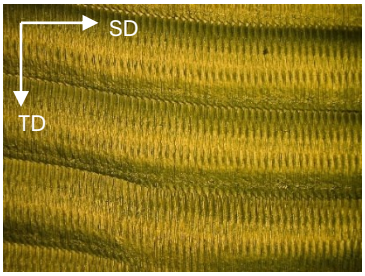

Figure 5.2: Optical microscopy image of peen 7 showing the wavy structure formed due to UNSM performed at low SL with high PS.

5.1.2 Residual Stress Analysis

Surface residual stress (SRS) values along both the orthogonal directions (step direction (SD) - 0° and transverse direction (TD) - 90°) of UNSM treated 304L SS specimens peened with different parameter combinations are presented in figure 5.3. All the UNSM peens made with different parameter combinations resulted in very high magnitude of surface compressive residual stresses (CRSs) along both the orthogonal directions of UNSM treated 304L SS specimens. The SRS values when compared with respect to SL keeping the other three parameters (amplitude (A), PS, IFR) constant i.e., comparing peens 1&9, 2&10 etc., it was observed that most of the peens

made with 40N SL have slightly higher SRS along both the orthogonal directions than the peens made with 20N SL.

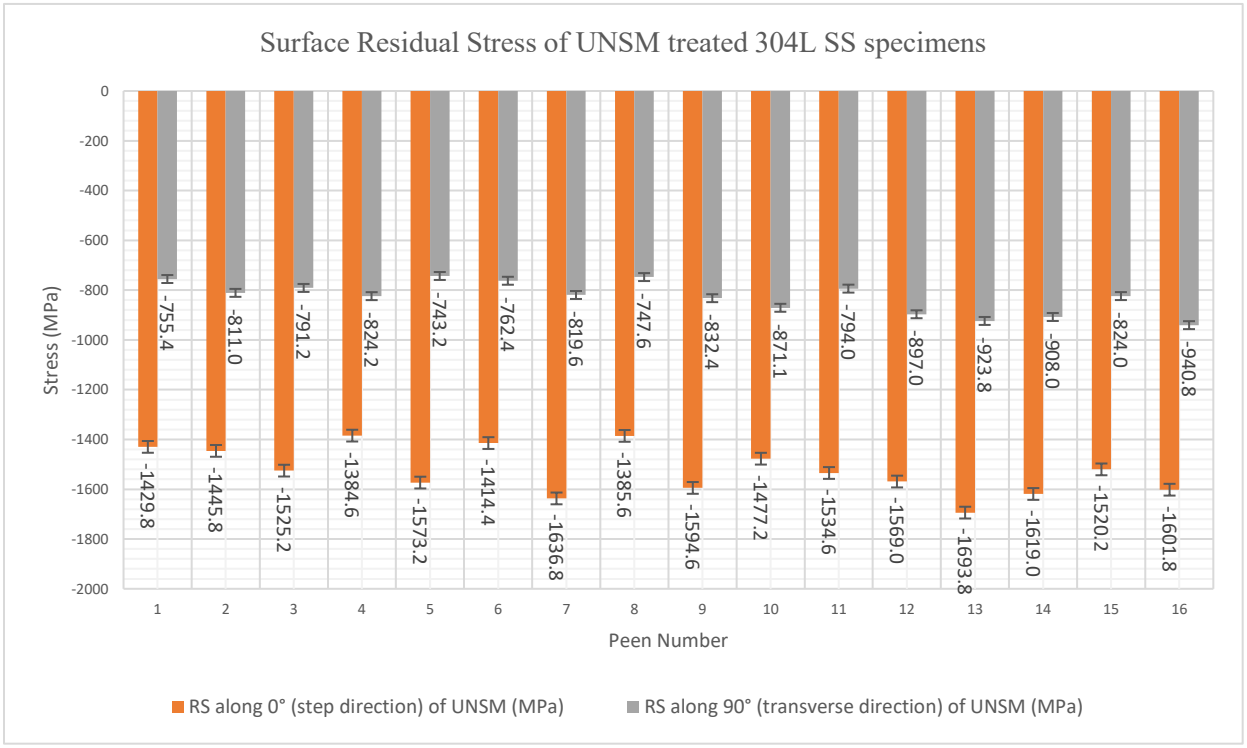

Figure 5.3: Surface Residual Stress values of UNSM treated 304L SS specimens along both the step and transverse direction of UNSM peens made with varying UNSM parameters.

Figures 5.4 and 5.5 represent through-the-depth residual stress profiles corresponding to martensite phase and austenite phase of all the 16 different UNSM treated 304L SS specimens respectively. In both the figures, (a) corresponds to RS depth profile along the SD of UNSM, (b) corresponds to RS depth profile along the TD of UNSM and (c) corresponds to the full width half maximum (FWHM) values representing the plasticity / plastic strain present in the respective specimen. UNSM treatment is performed in a zigzag manner resulting in dissimilar stress distribution along the orthogonal directions and hence residual stress depth profiles were performed along both the orthogonal directions of UNSM. Also, UNSM induces severe plastic deformation (SPD) in the material due to which 304L SS specimens undergo a complete martensitic transformation at the surface whose percentage gradually decreases along the depth of

the specimens with a subsequent increase in the percentage of austenite phase. Depending on the impact of UNSM parameters, the martensite is induced only up to a certain depth in the material. Therefore, the RS measurements after the removal of each layer by electropolishing were performed with both Mn and Cr X-ray tubes to determine the RSs due to both austenite and martensite phases respectively until the martensite peak weakens or completely disappears. Beyond which the RS due to austenite phase was only measured until at least two values were obtained in the tensile stress region (i.e., > 0 MPa or positive stress values).

Depending on the UNSM parameters, the depth of martensite (DOM) presence was observed to be in the range of 80 µm to 180 µm. The depth of compression (DOC) i.e., the depth up to which the CRSs were induced in the 304L SS specimens due to UNSM treatment was

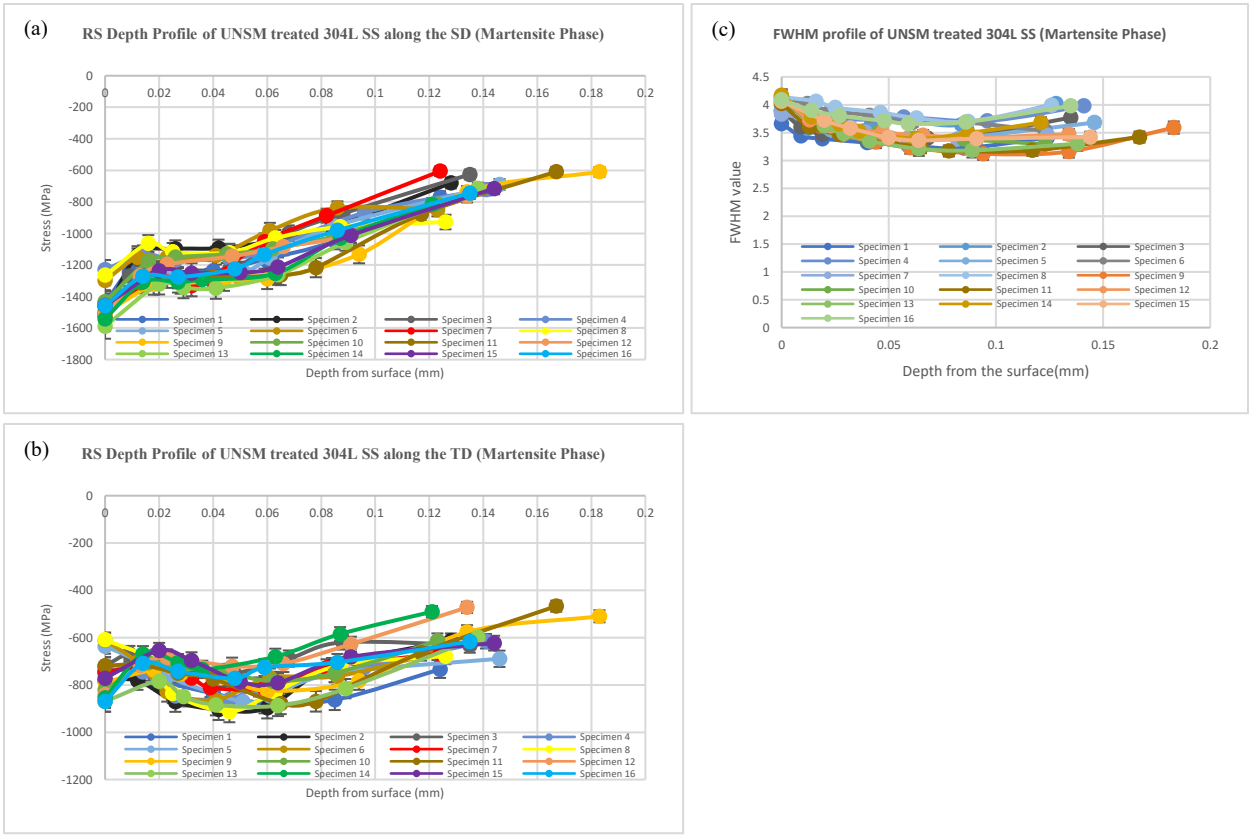

Figure 5.4: Residual stress depth profiles with respect to martensite phase of UNSM treated 304L SS specimens peened with different UNSM parameter combinations along the (a) step direction (SD), (b) transverse direction (TD) of UNSM treatment and their corresponding (c) full width half maximum (FWHM) values representing the plasticity in the material.

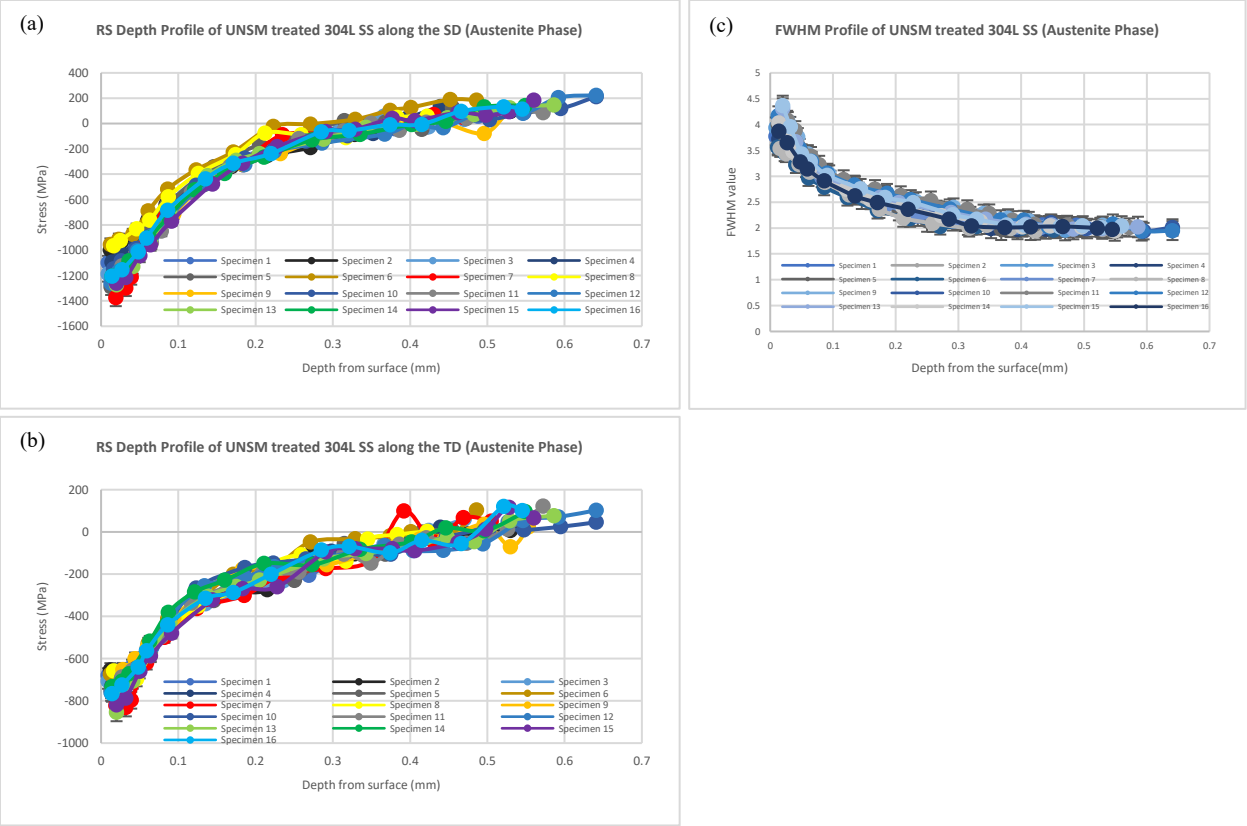

Figure 5.5: Residual stress depth profiles with respect to austenite phase of UNSM treated 304L SS specimens peened with different UNSM parameter combinations along the (a) step direction (SD), (b) transverse direction (TD) of UNSM treatment and their corresponding (c) full width half maximum (FWHM) values representing the plasticity in the material.

determined from the depth profile plots made with respect to the austenite phase (figure 5.5). The DOC along SD and TD of UNSM and the DOM presence obtained from the RS depth profile plots in figures 5.4 and 5.5 for all the 16 different 304L SS specimens are consolidated graphically in figure 5.6. It was observed that DOC along SD, TD, and DOM were slightly higher for specimens peened with high SL than the specimens peened with low SL. Also, in all the 8 specimens peened with high SL (peens 9 - 16), the results of DOC along SD, TD and DOM were consistent independent of the other three UNSM parameters whereas in the 8 specimens peened with low SL (peens 1 – 8) significant differences in the DOC along SD, TD and DOM were observed with a variance in the other three UNSM parameters. For example, among low SL peened specimens, those peened with low A have lowest DOC along SD when a PS of 2000 mm/min was used and

have lowest DOC along TD when a PS of 3000 mm/min was used. However, for most of the specimens treated with 40N SL, the DOC was found to be ~ 410 µm along SD and ~ 500 µm along TD of UNSM. Also, for all the specimens irrespective of UNSM parameters, it was found that the DOC along TD was higher than along SD. The FWHM depth profiles of all the specimens seen in figure 5.5 (c) showed that significant amount of plastic strain was induced in the 304L SS specimens through UNSM treatment up to a depth of ~ 200 µm from their surfaces, beyond which the plasticity remains low and constant.

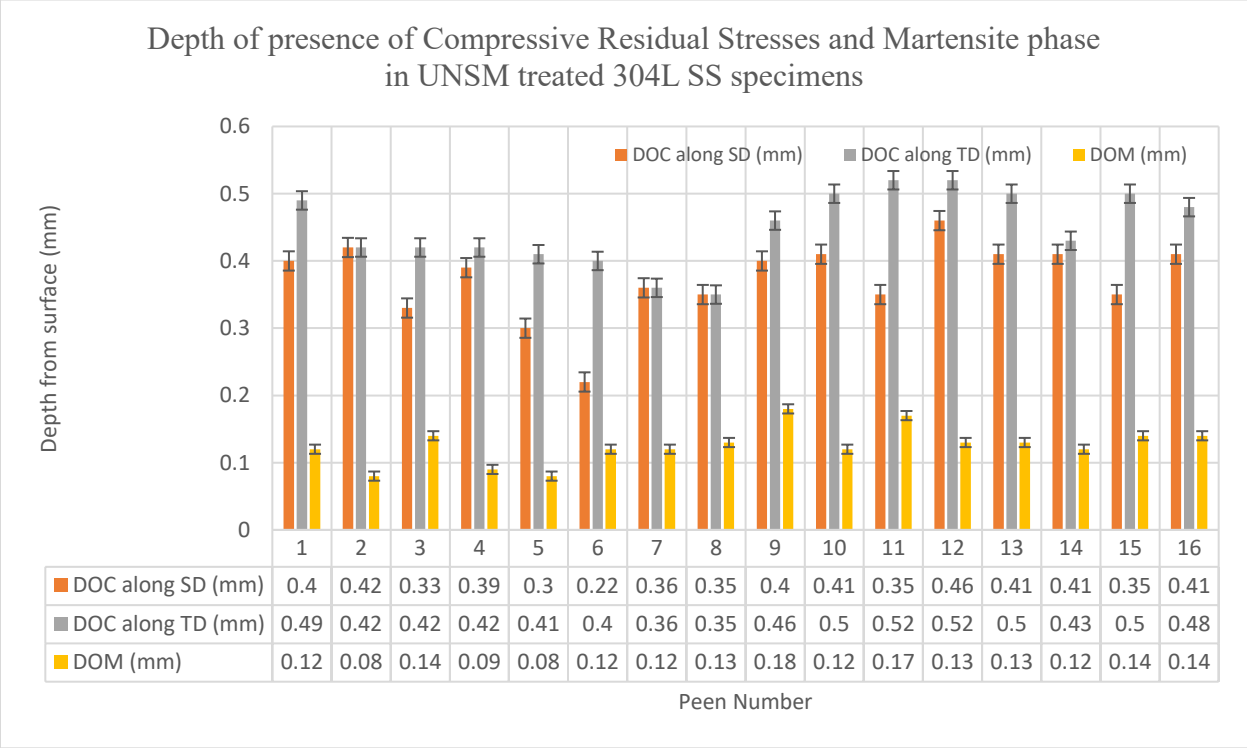

	1	2	3	4	5	6	7	8	9	10	11	12	13	14	15	16
DOC along SD (mm)	0.4	0.42	0.33	0.39	0.3	0.22	0.36	0.35	0.4	0.41	0.35	0.46	0.41	0.41	0.35	0.41
DOC along TD (mm)	0.49	0.42	0.42	0.42	0.41	0.4	0.36	0.35	0.46	0.5	0.52	0.52	0.5	0.43	0.5	0.48
DOM (mm)	0.12	0.08	0.14	0.09	0.08	0.12	0.12	0.13	0.18	0.12	0.17	0.13	0.13	0.12	0.14	0.14

Figure 5.6: Depth of compressive residual stresses along both the orthogonal directions of UNSM and depth of martensite phase presence in 304L SS specimens UNSM treated with different parameter combinations.

5.1.3 Nano Hardness Analysis

Nano hardness measurements along the depth of all 16 UNSM treated 304L SS specimens are compared against the baseline / solution annealed 304L SS specimen in figure 5.7. The average hardness value of SA specimen was found to be 297 Hv which was measured by averaging all the through-the-depth hardness values obtained for its hardness depth profile.

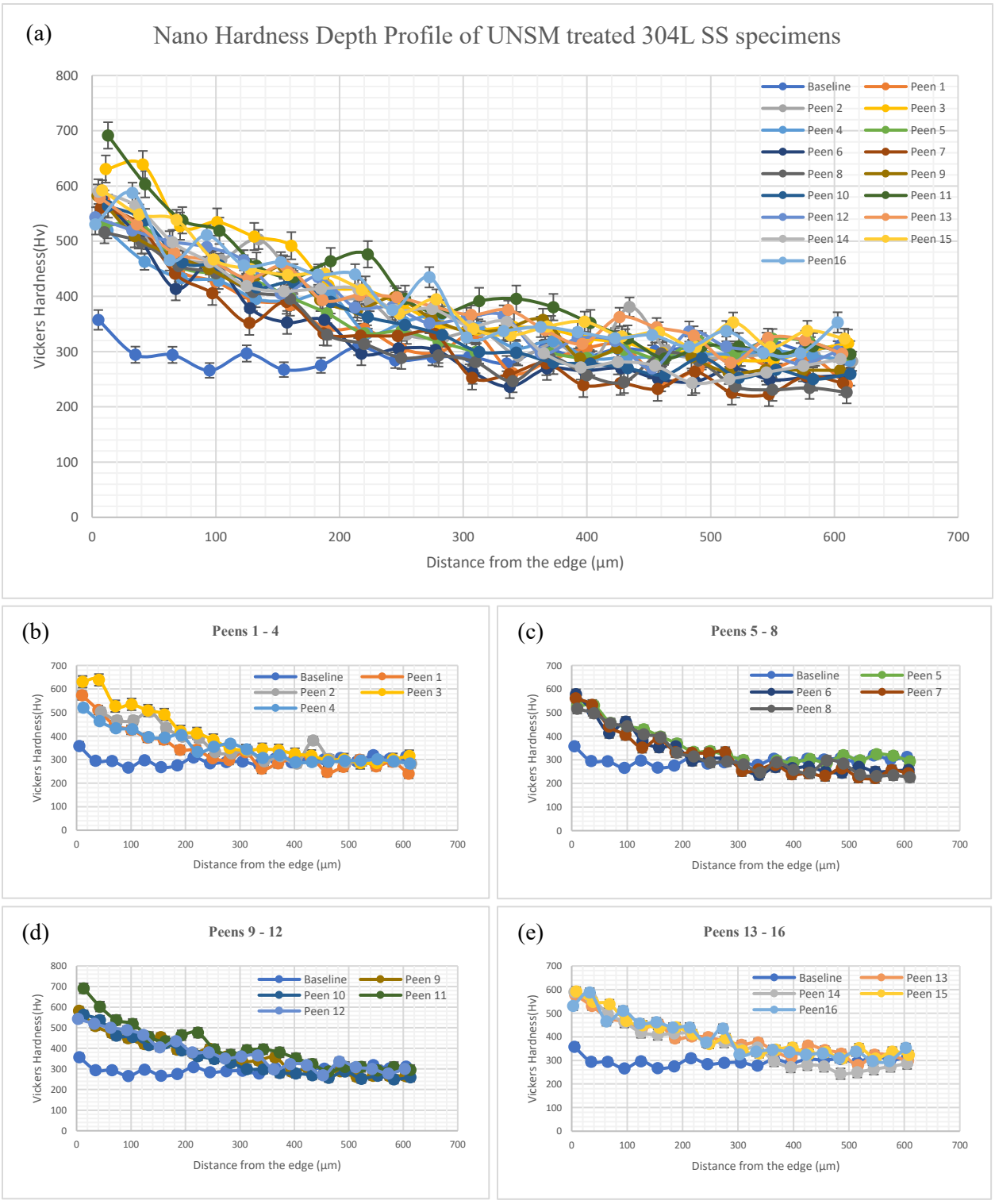

Figure 5.7: Vickers nano hardness depth profiles of all the 16 UNSM treated 304L SS specimens are compared against the baseline/solution annealed 304L SS specimen's nano hardness depth profile in (a) whereas (b), (c), (d), & (e) represent the same Vickers nano hardness depth profiles of all the 16 UNSM treated 304L SS specimens, but for better visual clarity, Vickers nano hardness depth profiles of peens 1-4, 5-8, 9-12, & 13-16 are compared against the baseline/solution annealed 304L SS specimen's nano hardness profile in small batches of four specimens in each line graph respectively.

From figure 5.7, it can be observed clearly that the near-surface hardness values of all the UNSM treated specimens increased to a range of 600 ± 100 Hv and decreased gradually along their depth before eventually reaching the SA / baseline specimen's nano hardness values. The significant increase in hardness values can be attributed to the hardening effect caused by the severe plastic deformation in the 304L SS specimens during their UNSM surface treatment inducing greater dislocation density, extreme grain refinement and martensitic transformation. The depth of hardening (DOH) effect i.e., the depth up to which the significant increase in hardness values could be observed in a UNSM treated specimen from figure 5.7, varied with varying UNSM parameter combinations and the obtained results are presented graphically in figure 5.8.

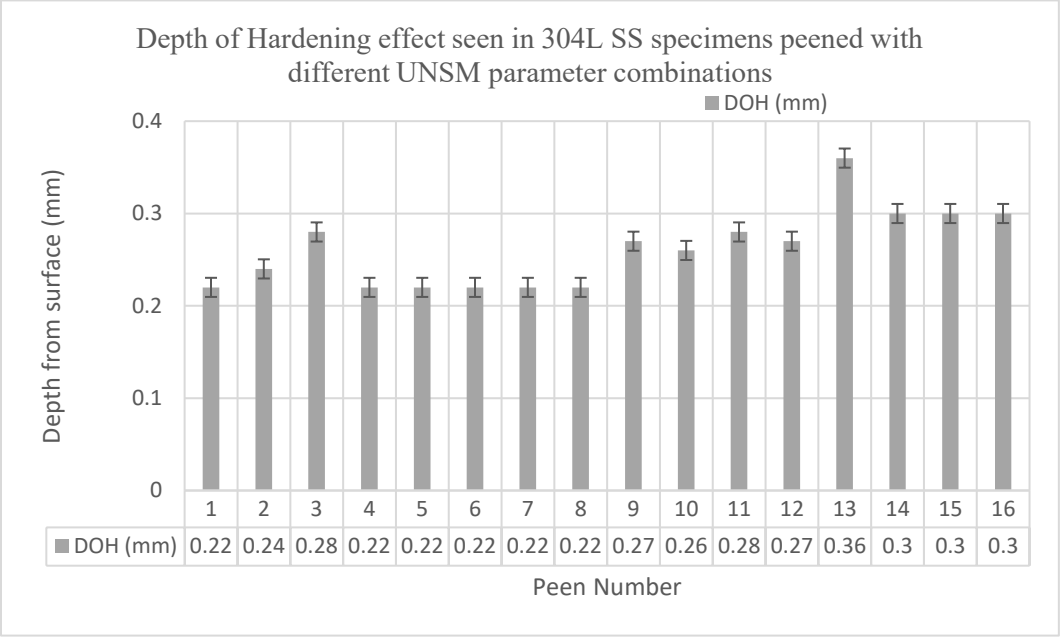

Figure 5.8: Depth of Hardening effect seen in the 304L SS specimens UNSM treated with different parameter combinations.

One clear observation from figure 5.8 is that the DOH effect increased and stayed consistent in the 304L SS specimens when the SL was increased from 20 N to 40 N for UNSM treating the 304L SS specimens. Also, among the specimens peened with 40N SL, independent of PS and IFR, the specimens peened with a low amplitude of 8 µm (i.e., peens 13 - 16) resulted in a

maximum DOH effect than all the other 12 specimens, exhibiting a DOH value of approximately ≥ 300 µm. Therefore, it can be concluded that the high SL + low A combination independent of PS and IFR resulted in the maximum DOH effect to be seen in the conventionally rolled 304L SS alloy. Furthermore, it must be noted that the 304L SS specimen peened with the parameter combination of peen 13 yielded the highest DOH effect among all the 16 differently peened specimens exhibiting a DOH value of up to ~ 360 µm.

Finally, all the UNSM parametric study results of 304L SS specimens with respect to their surface roughness (Ra), surface residual stress (SRS), depth of compression (DOC) along step direction (SD) and transverse direction (TD), depth of martensite (DOM) presence, and depth of hardening (DOH) effect are consolidated in table 5.1.

Peen number	SL (N)	A (µm)	PS (mm/min)	IFR (mm)	Ra (µm)	SRS along SD (MPa)	SRS along TD (MPa)	DOC along SD (mm)	DOC along TD (mm)	DOM (mm)	DOH (mm)
1	20	20	2000	0.03	0.5	-1429.8	-755.4	0.4	0.49	0.12	0.22
2	20	20	2000	0.07	0.5	-1445.8	-811.0	0.42	0.42	0.08	0.24
3	20	20	3000	0.03	6.3	-1525.2	-791.2	0.33	0.42	0.14	0.28
4	20	20	3000	0.07	1.5	-1384.6	-824.2	0.39	0.42	0.09	0.22
5	20	8	2000	0.03	0.4	-1573.2	-743.2	0.3	0.41	0.08	0.22
6	20	8	2000	0.07	0.6	-1414.4	-762.4	0.22	0.4	0.12	0.22
7	20	8	3000	0.03	2.0	-1636.8	-819.6	0.36	0.36	0.12	0.22
8	20	8	3000	0.07	1.0	-1385.6	-747.6	0.35	0.35	0.13	0.22
9	40	20	2000	0.03	0.6	-1594.6	-832.4	0.4	0.46	0.18	0.27
10	40	20	2000	0.07	0.8	-1477.2	-871.1	0.41	0.5	0.12	0.26
11	40	20	3000	0.03	0.7	-1534.6	-794.0	0.35	0.52	0.17	0.28
12	40	20	3000	0.07	0.9	-1569.0	-897.0	0.46	0.52	0.13	0.27
13	40	8	2000	0.03	0.6	-1693.8	-923.8	0.41	0.5	0.13	0.36
14	40	8	2000	0.07	1.0	-1619.0	-908.0	0.41	0.43	0.12	0.3
15	40	8	3000	0.03	0.5	-1520.2	-824.0	0.35	0.5	0.14	0.3
16	40	8	3000	0.07	0.7	-1601.8	-940.8	0.41	0.48	0.14	0.3

SL-Static Load; A-Amplitude; PS-Peening speed; IFR-Interval feed rate; Ra-Surface roughness; SRS-Surface residual stress; SD-Step direction, TD-Transverse direction of UNSM; DOC-Depth of compressive residual stress presence; DOM-Depth of martensite presence; DOH-Depth of hardening effect.

Table 5.1: Consolidated results of UNSM parametric study.

5.1.4 Discussion on Determining the Most Optimal UNSM Parameters

Static Load:

Analyzing the consolidated results presented in table 5.1 belonging to the UNSM parametric study performed on the 16 different 304L SS specimens, it was found that among all the four variable UNSM parameters (SL, A, PS, and IFR), the SL had the most significant impact on all the various results obtained for the purpose of UNSM parametric study. So, to determine or to show the effect of SL on the 304L SS specimens in a simple manner, the obtained results of Ra, SRS, DOC, DOM and DOH for all the 16 UNSM peens are averaged with respect to the two variable SLs used in this study i.e., results of peens 1-8 are averaged under low SL (20N) and peens 9-16 under high SL (40N). The average of the results is presented in table 5.2, from which it can be clearly seen that by increasing the SL from 20 N to 40 N, a significant amount of positive impact has occurred on all the properties. And the most significant impact being observed in the surface roughness values which depict a lower value by more than 2X times when the SL has been increased to 40 N. Therefore, it can be said that for UNSM treating the 304L SS alloy, using a static load of 40 N (over 20 N) is ideal to obtain optimal results.

SL (N)	Ra (µm)	SRS along SD (MPa)	SRS along TD (MPa)	DOC along SD (mm)	DOC along TD (mm)	DOM (mm)	DOH (mm)
20	1.60	-1474.43	-781.825	0.35	0.41	0.11	0.23
40	0.72	-1576.28	-873.883	0.40	0.49	0.14	0.29

Table 5.2: Results of UNSM parametric study averaged with respect to the static loads used in this study.

Amplitude:

Similar to static load, the effect of amplitude on the 304L SS specimens peened with 40 N SL was determined by averaging the obtained results of all the properties with respect to the two amplitudes employed in this study. The average of these results is presented in table 5.3 and it must be noted that the 304L SS specimens UNSM peened with 40 N SL were only considered here as we determined earlier that 40 N SL (over 20 N) is the ideal choice for obtaining optimal results on

304L SS alloy. Therefore, from table 5.3, it can be observed that the effect of amplitude in specimens peened with 40N SL with respect to their obtained SRS along both SD and TD of UNSM and DOH are slightly better when peened with 8 µm A than with 20 µm A. However, the difference in surface roughness (Ra), DOC along SD & TD and the DOM presence were observed to be negligible with respect to the amplitude used in specimens peened with 40 N SL. Therefore, it can be concluded that to get slightly better results while UNSM treating the 304L SS alloy, an amplitude of 8 µm must be used (over 20 µm) in conjunction with 40 N static load.

SL (N)	A (µm)	Ra (µm)	SRS along SD (MPa)	SRS along TD (MPa)	DOC along SD (mm)	DOC along TD (mm)	DOM (mm)	DOH (mm)
40	20	0.74	-1543.9	-848.6	0.41	0.50	0.15	0.27
	8	0.71	-1608.7	-899.2	0.40	0.48	0.13	0.32

Table 5.3: UNSM parametric study results of 304L SS specimens peened with 40 N static load, averaged with respect to the amplitudes employed in this study.

Peening Speed and Interval Feed Rate:

To determine the best combination of PS and IFR that yielded the best results when 304L SS alloy was peened with 40 N SL and 8 µm A, the UNSM parametric study results obtained for the last 4 peens i.e., peens 13 – 16 were compared with each other. The data obtained with respect to peens 13 – 16 are presented again here-below in table 5.4 for convenience. The major difference that was observed with respect to PS in peens 13 – 16 is that the obtained SRS is generally slightly higher when 304L SS alloy was peened with 2000 mm/min PS than with 3000 mm/min PS. Whereas with respect to the IFR, the major trend that was observed is that the surface roughness increases with an increase in the IFR from 30 µm to 70 µm irrespective of the peening speed used in specimens peened with 40 N SL and 8 µm A. The same trend between Ra and IFR was also observed in specimens peened with 40 N SL and 20 µm A as well i.e., in peens 9 – 12. However, the effect of IFR on SRS in peens 13 – 16 was found to be irregular. Therefore, in conclusion, to obtain a specimen surface with lower surface roughness, an IFR of 30 µm and to obtain a specimen

with higher SRS, a PS of 2000 mm/min must be used along with a SL of 40 N and A of 8 µm. The finalized four parameter combination that yielded the most optimal results in the UNSM treated 304L SS alloy belongs to peen 13. Additionally, the DOH obtained for peen 13 was also recorded to be the highest among all the 16 different 304L SS specimens UNSM treated with different parameter combinations.

PN	SL(N)	A (µm)	PS (mm/min)	IFR (mm)	Ra (µm)	SRS along SD (MPa)	SRS along TD (MPa)	DOC along SD (mm)	DOC along TD (mm)	DOM (mm)	DOH (mm)
13	40	8	2000	0.03	0.6	-1693.8	-923.8	0.41	0.5	0.13	0.36
14	40	8	2000	0.07	1.0	-1619.0	-908.0	0.41	0.43	0.12	0.3
15	40	8	3000	0.03	0.5	-1520.2	-824.0	0.35	0.5	0.14	0.3
16	40	8	3000	0.07	0.7	-1601.8	-940.8	0.41	0.48	0.14	0.3

Table 5.4: UNSM parametric study results of peens 13 – 16 used to determine the optimal PS and IFR to be used with 40 N SL and 8 µm A.

Hence, it can be concluded finally that the most optimal results by UNSM treating the 304L SS alloy were obtained with a parameter combination of 40 N - SL, 8 µm - A, 2000 mm/min – PS, and 30 µm - IFR (Peen 13). Therefore, to study the impact of UNSM treatment on the microstructure, hardness, surface roughness, residual stress, and corrosion properties of sensitized, CS, LACS, and AFS 304L SS specimens, the parameter combination of peen 13 will be applied on all the aforementioned 304L SS specimens possessing distinct microstructural characteristics.

5.2 Investigating the Impact of UNSM on the Microstructure, Hardness, Residual Stress and Corrosion Properties of Sensitized, CS, LACS & AFS 304L SS Materials Having Distinct Prior Microstructural Characteristics

The major goal of this study is to improve the corrosion behavior of Sensitized, CS, LACS, and AFS 304L SS materials through the application of UNSM treatment on their surface and also, to determine the underlying mechanisms or factors that are caused by the application of the mitigating UNSM surface treatment technique, that are responsible for either improving, or not having any effect, or deteriorating the corrosion behavior of these 304L SS materials possessing

distinct prior microstructural characteristics (i.e., sensitized 304L SS – possessing chromium carbide precipitates at the grain boundaries, CS 304L SS - structure with porosity having weak interparticle bonding and cold work, LACS 304L SS - structure with porosity but improved interparticle bonding, and AFS 304L SS – fully dense structure with nano-grains at surface or possessing gradient microstructure). For this purpose, the impact of UNSM on the microstructure, phases, hardness, residual stress, surface topography, degree of sensitization / susceptibility, and pitting corrosion behavior of Sensitized, CS, LACS, and AFS 304L SS materials has been studied extensively and the results obtained from this research, as well as the conclusions drawn from the analysis are presented and discussed thoroughly in the following sections of this chapter.

5.2.1 Microstructural Analysis using Electron Back Scattered Diffraction (EBSD) Technique

The parameters used to obtain the EBSD images and some of the key aspects of the EBSD analysis presented in the following paragraphs of this section related to the Sensitized, CS, LACS, and AFS 304L SS specimens subjected to UNSM surface treatment are the same as used for the untreated 304L SS specimens which are presented in detail in the first two paragraphs of section 4.2.1 of Chapter 4 in this dissertation. For maintaining consistency in EBSD measurements, the EBSD parameters like the magnifications and step sizes at which the images were taken and how the EBSD analysis was performed has been kept the same for the UNSM treated Sensitized, CS, LACS, and AFS 304L SS specimens as that of the untreated 304L SS specimens, allowing for determining the impact of UNSM surface treatment on the microstructures of these different 304L SS materials without the interference of any other factors arising from any difference in the EBSD measurements. Therefore, the information given in the text of the first two paragraphs of section 4.2.1 applies here as well i.e., to section 5.2.1 and has not been repeated here to avoid redundancy.

Sensitized 304L SS:

The near-surface area of UNSM treated SA, S5, and S24 304L SS specimens can be seen from their IPF maps presented in figure 5.9 (a-c) and (d-f) that are taken at 250X and 1000X magnifications respectively.

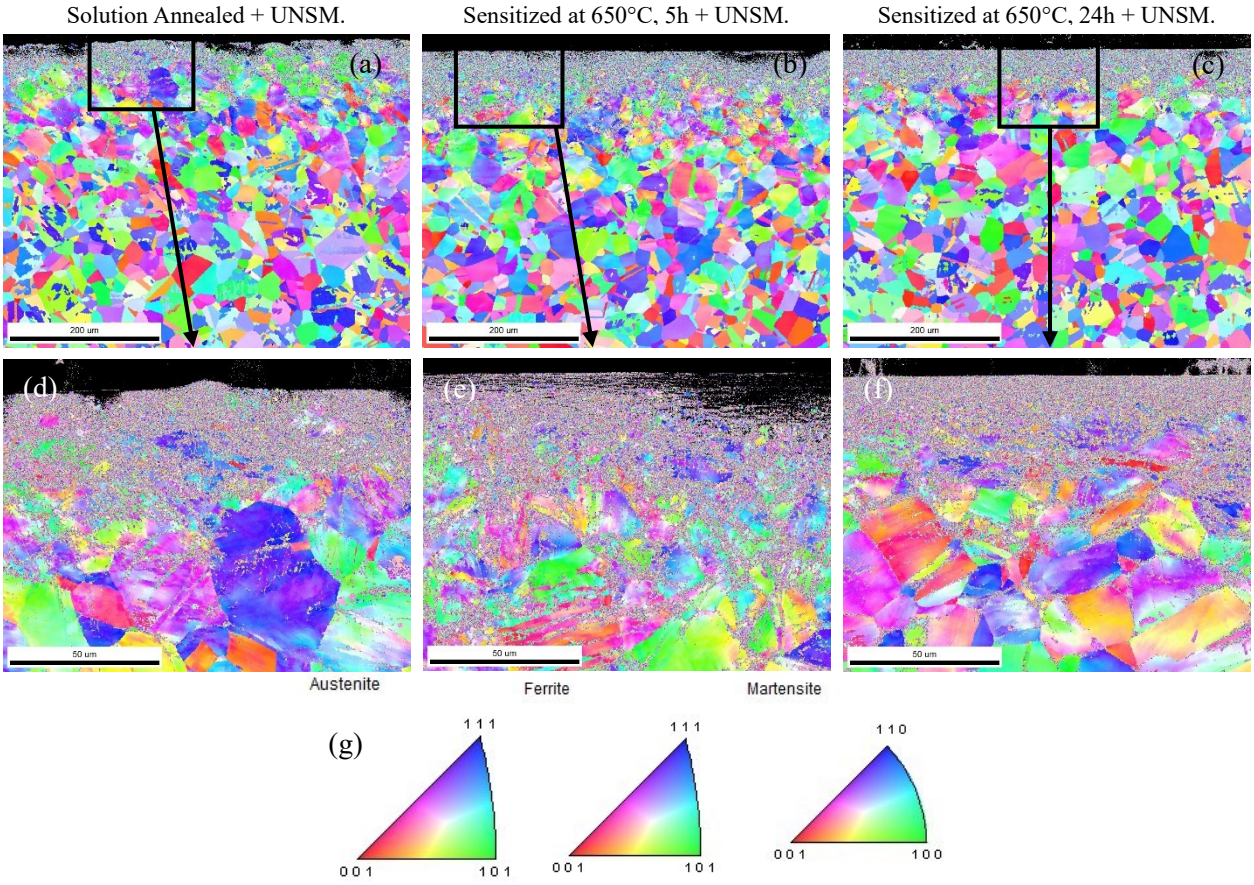

Figure 5.9: Maps obtained from EBSD analysis with (a), (b) & (c) representing the Inverse Pole Figure (IPF) maps at 250X magnification and, (d), (e) & (f) representing the IPF maps at 1000X magnification of the areas shown in boxes of (a-c) belonging to the cross-sectioned 304L SS specimens of SA, aged at 650°C for 5h & 24h respectively that are subjected to UNSM treatment, (g) legend of IPF maps in (a-f). The top black edge of all the images in (a-f) is the specimen's surface.

The UNSM treatment of SA, S5, and S24 specimens induced a gradient microstructure in all of them with nanosized grains observed to a depth of ~ 15 - 20 µm from their surface. These nanosized grains are a result of severe plastic deformation, dislocation activity, grain boundary sliding, and dynamic recrystallization induced by UNSM treatment in the 304L SS specimens during which stress concentration occurs at the grain boundaries favoring the phase transformation

of austenite to martensite which in turn leads to grain refinement. At subsurface level, these refined grains are primarily found at the GBs and extensive lattice distortion can be seen within the grains as discerned by the fading color of grain's orientation observed in the IPF maps of figure 5.9.

The GBM maps of UNSM treated SA, S5, and S24 304L SS specimens are presented in figure 5.10 (a-c) respectively and their corresponding average GS and average MA distribution charts are presented in figure 5.10 (d-f) and (g-i) respectively. On comparing the GBM maps of SA, S5, and S24 specimens before and after UNSM treatment that are shown in figures 4.4 and 5.10 respectively, it can be observed that the number of GBs (both LAGBs and HAGBs) increased tremendously in all the UNSM treated 304L SS specimens thereby, increasing their total GB area, which indicates the occurrence of extreme grain refinement and dynamic recrystallization in these specimens due to SPD during their UNSM treatment. Furthermore, despite the differences existing in the number of LAGBs and HAGBS among the SA, S5, and S24 specimens prior to surface treatment, these differences have become negligible after their UNSM treatment indicating that the surface treatment has affected all the three 304L SS specimens in a similar manner eradicating their prior surface treatment microstructural differences with respect to their number of GBs.

Additionally, due to UNSM surface treatment, the near-surface average GS of all the surface treated specimens reduced vastly from 3.7 μm in untreated SA specimen to 0.57 μm, 7.2 μm in untreated S5 to 0.55 μm, and 3.8 μm in untreated S24 to 0.57 μm showing a decline of ~ 6.5 X, 13 X and 6.6 X times respectively. It is noteworthy that even though the S5 specimen had coarser grains than SA and S24 specimens prior to surface treatment, the grain refinement occurring in all the three specimens due to UNSM appears to be uniform as per the obtained average GS values of all the three UNSM treated specimens being approximately of the same

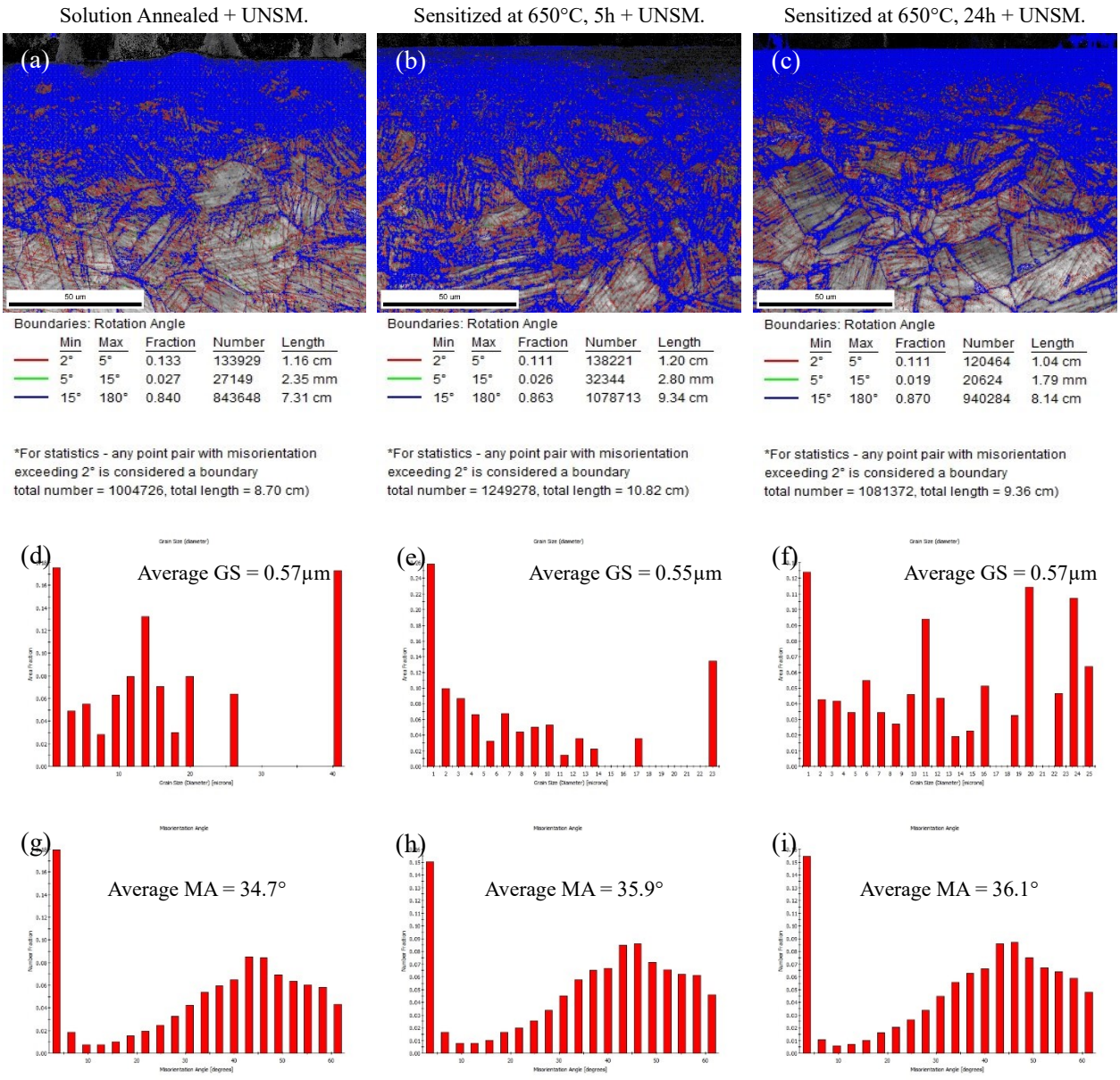

Figure 5.10: Maps obtained from EBSD analysis with (a), (b) & (c) representing the Grain Boundary Misorientation (GBM) maps, (d), (e) & (f) representing the grain size diameter vs area fraction charts, and (g), (h) & (i) representing the misorientation angle vs number fraction charts of cross-sectioned UNSM treated SA, aged at 650°C for 5h & 24h 304L SS specimens respectively. The top black edge in images (a-c) represents the specimen's surface.

value. However, the GS distribution of UNSM treated SA, S5, and S24 specimens appears to be different as seen in figure 5.10 (d-f), which could be attributed to the differences in their hardness characteristics that are presented later in section 5.2.3. Coming to the average MA, a decline in their values for all the surface treated specimens has been observed from those of the untreated

specimens' average MA values, which indicates an increase in the GB strength of the surface treated 304L SS specimens which can impede dislocation motion thereby, enhancing the material's mechanical strength and hardness. Also, the average MA values for all the UNSM treated specimens were found to be within 1° of each other, eliminating the differences existing in their values prior to surface treatment, and their MA distribution curves shown in figure 5.10 (g-i) also being very similar to each other with very minute differences. Therefore, this can be hypothesized as a demonstration of the uniform mechanical application of UNSM treatment with respect to both the SA & Sensitized 304L SS specimen surfaces.

The KAM maps of UNSM treated SA, S5, and S24 304L SS specimens and their corresponding KAM distribution charts are presented in figure 5.11 (a-c) and (d-f) respectively. On comparing the KAM maps of SA, S5, and S24 specimens before and after UNSM treatment that are given in figures 4.5 and 5.11 respectively, it can be clearly observed that the KAM maps of surface treated specimens exhibit the presence of higher degree of plastic strain / lattice distortion at their surface than the untreated specimens, which gradually decreased along the depth of the surface treated specimens whereas it remained constant and low in the untreated specimens. The transition area of mixed yellow, red region to that of mixed green, blue region in the KAM maps of UNSM treated 304L SS specimens represents the depth up to which the significant amount of plastic strain was induced into the respective specimen by UNSM treatment. So, from figure 5.11 (a) & (b), the significant amount of plastic strain induced into the SA and S5 specimens by UNSM can be observed up to a depth of ~ 200 – 220 μm, with the induced plastic strain appearing slightly deeper in the S5 specimen than that of SA specimen. Whereas in S24 specimen the induced plastic strain appears to be confined to a relatively lesser depth than the SA and S5 specimens, with it being observed only up to a depth of ~ 150 – 180 μm from the surface.

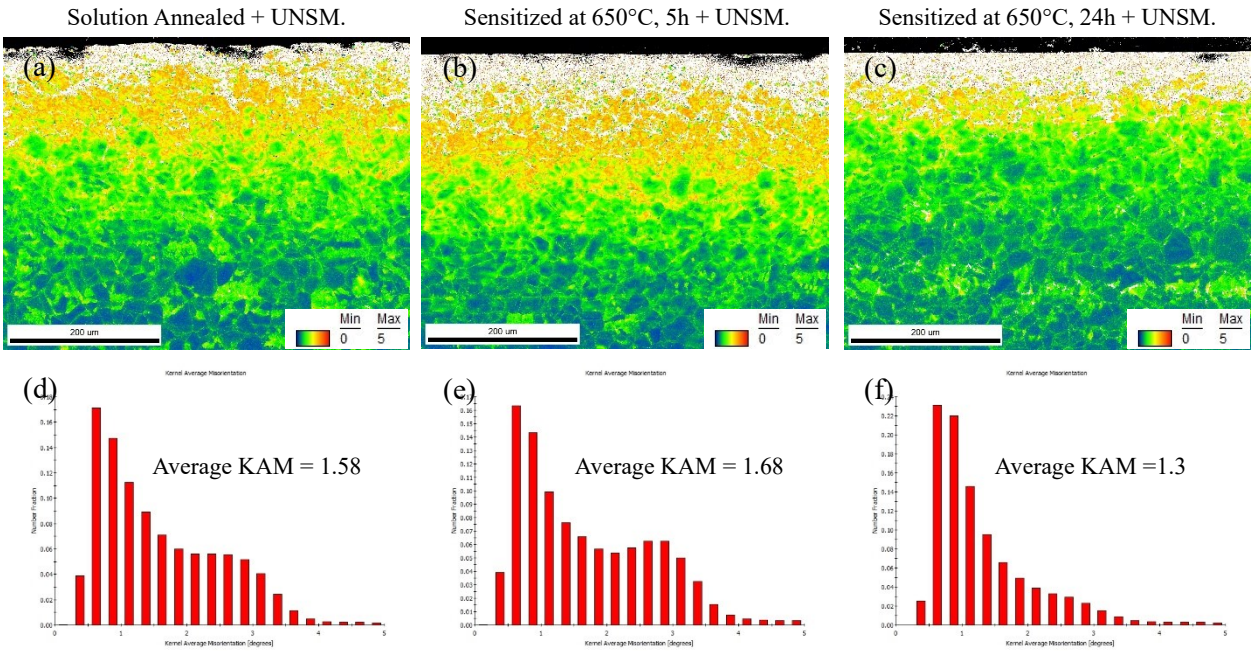

Figure 5.11: Maps obtained from EBSD analysis with (a), (b) & (c) representing the Kernel Average Misorientation (KAM) maps of cross-sectioned UNSM treated SA, aged at 650°C for 5h & 24h 304L SS specimens respectively and (d), (e) & (f) representing their respective KAM distribution charts showing the kernels misorientation in degrees vs number fraction. The top black edge in images (a-c) represents the specimen's surface.

The obtained average KAM values of all the three UNSM treated 304L SS specimens follow the same trend as well, with S5 specimen exhibiting the highest KAM value of 1.68, followed by SA specimen with 1.58, followed by S24 specimen with 1.3. Therefore, it can be expressed that UNSM treatment introduced a significant amount of plasticity into all the 304L SS specimens studied here, with S5 specimen experiencing the highest impact of all the three, which could be due to its overall lower hardness value than the others (i.e., SA and S24 specimens), led by the grain growth phenomenon during its aging/sensitization treatment resulting in the decrease of its hardness (S5 specimen). Finally, the higher KAM values of UNSM treated SA, S5, and S24 specimens than their untreated versions signify the presence of greater local distortions in the surface treated materials, indicating the introduction of higher dislocation densities and greater localized plastic deformation in the SA and sensitized 304L SS specimens by UNSM treatment.

CS & LACS 304L SS:

Figures 5.12 and 5.13 represent the EBSD microstructures and data pertaining to the near-surface cross-sectional areas of UNSM treated CS and LACS 304L SS coatings respectively.

Comparing the IPF maps (a) and GS distribution charts (f) of untreated and UNSM treated CS specimens given in figures 4.6 and 5.12 respectively, it can be observed that certain degree of grain refinement of the few large sized deformed grains seen in the untreated CS specimen has occurred due to UNSM treatment. This view is supported by their KAM distribution charts given in (c) as well with increased number fraction of 4° and 5° misorientations combined with a simultaneous decrease in 2° and 3° misorientations upon subjecting the CS specimen to UNSM

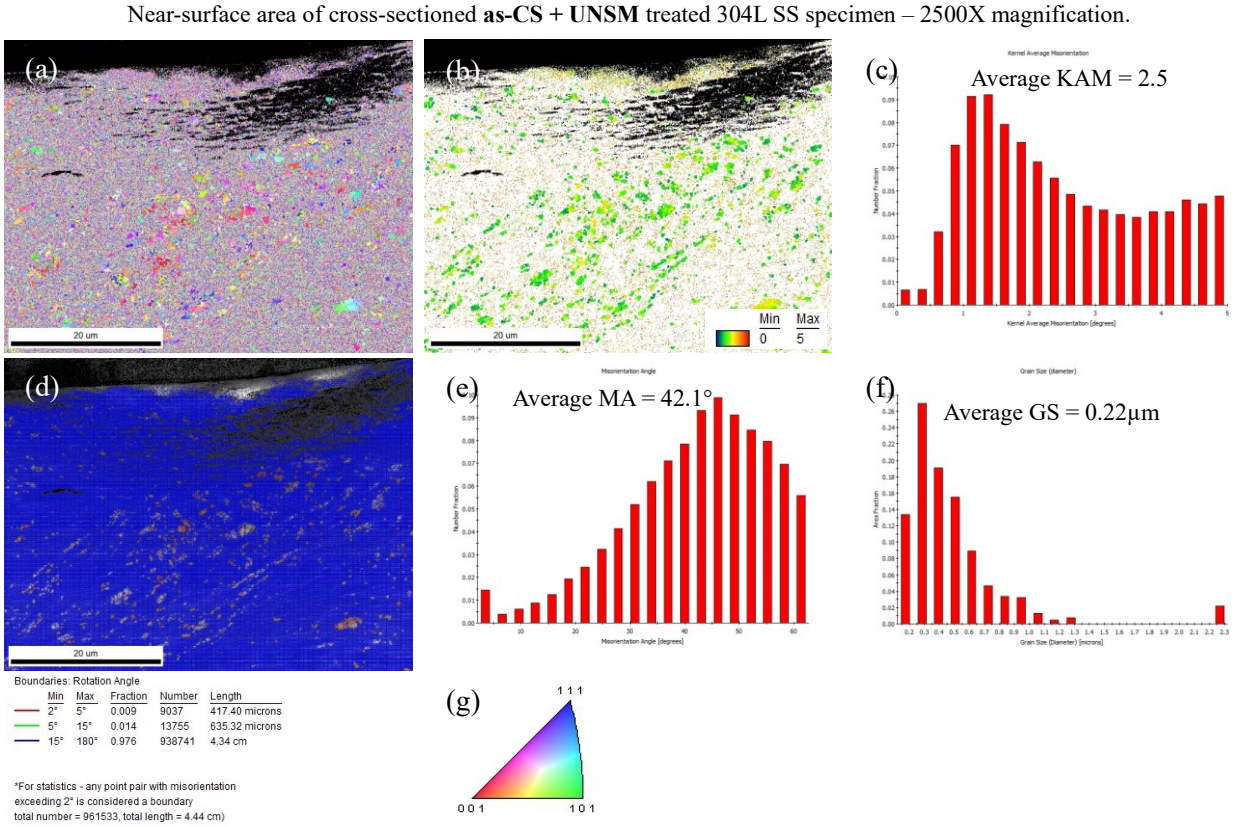

Figure 5.12: Maps obtained by EBSD analysis performed on the near-surface area of cross-sectioned as-CS + UNSM treated 304L SS specimen representing its (a) Inverse Pole Figure (IPF) map, (b) Kernel Average Misorientation (KAM) map, (c) KAM distribution chart (d) Grain Boundary Misorientation (GBM) map, (e) Misorientation Angle (MA) distribution chart, (f) Grain Size (GS) distribution chart, and (g) legend of IPF map in (a).

treatment asserting that some grain refinement had occurred due to UNSM. However, no notable difference in the average KAM values of untreated and UNSM treated CS specimens could be found because the untreated CS specimen had already undergone a significant amount of plastic deformation due to cold working during its CS deposition process, it was unaffected by UNSM treatment as the material's ability to implant anymore plasticity is saturated. Also, due to the very small degree of grain refinement occurring in the CS specimen by its UNSM treatment, a few negligible changes have been observed in the average GS and MA values of UNSM treated CS specimen from that of the untreated CS specimen, which are as follows: a slight decrease in average GS from 0.24 μm to 0.22 μm, an increase in average MA value from 38.3° to 42.1° upon UNSM treatment of CS specimen.

Now, upon comparing the near-surface EBSD analysis of untreated and UNSM treated LACS specimens given in figures 4.7 and 5.13 respectively, the IPF maps in (a) of both the figures show that the LACS coating has undergone considerable amount of severe plastic deformation (SPD) during the UNSM surface treatment due to the severe pounding of WC tool tip on its surface and that it led to near surface nano crystallization in the coating, a phenomenon typically observed in UNSM treated specimens. Moreover, due to the UNSM treatment performed on LACS specimen, the total length of LAGBs and HAGBs increased tremendously from 0.49 mm and 3.54 mm to 2.72 mm and 51.4 mm respectively along with a significant decrease in average GS from 1 μm to 0.23 μm indicating the occurrence of extreme grain refinement in the LACS deposited 304L SS coating by its UNSM surface treatment. Additionally, the average KAM value of surface treated LACS coating has increased enormously by ~ 4X times from 0.6 to 2.3 signifying that UNSM has induced a significant amount of plastic strain into the LACS specimen and immensely increased its dislocation density. In general, deformation caused in a material increases the average MA value

of the grains but, after UNSM surface treatment of LACS coating, the average MA value decreased from 44.7° to 40.5° which could be indicative of dynamic recrystallization occurring in the LACS coating as a result of the extreme SPD induced into the LACS specimen by UNSM.

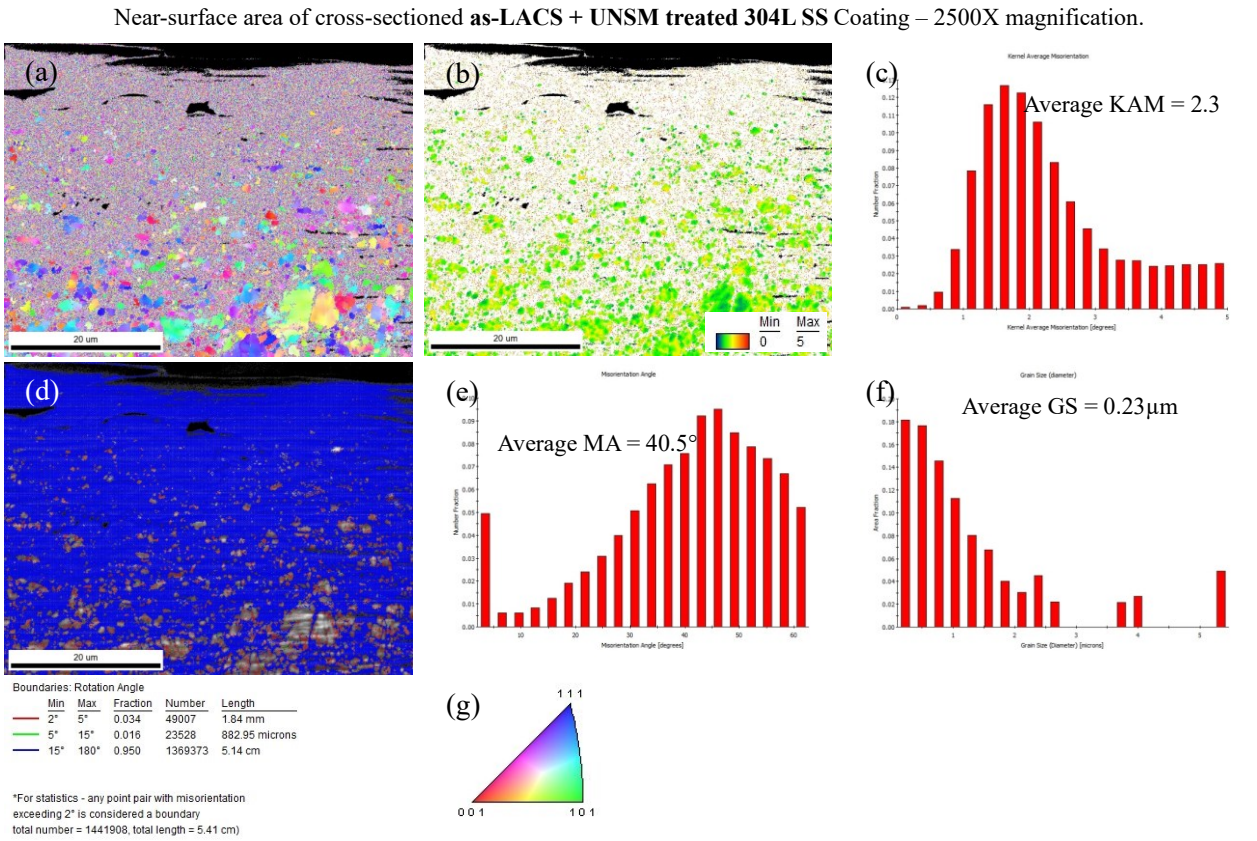

Figure 5.13: Maps obtained by EBSD analysis performed on the near-surface area of cross-sectioned as-LACS + UNSM treated 304L SS specimen representing its (a) Inverse Pole Figure (IPF) map, (b) Kernel Average Misorientation (KAM) map, (c) KAM distribution chart (d) Grain Boundary Misorientation (GBM) map, (e) Misorientation Angle (MA) distribution chart, (f) Grain Size (GS) distribution chart, and (g) legend of IPF map in (a).

The EBSD data obtained from the cross-sectioned areas of polished CS and LACS coatings subjected to UNSM treatment is compared with the EBSD data of UNSM treated as sprayed CS and LACS coatings in table 5.5. As per this EBSD analysis, it can be said that no differences were observed microstructurally when the CS and LACS coatings have been UNSM treated in either their as sprayed or polished conditions i.e., no differences microstructurally between as-CS + UNSM vs CS + P + UNSM specimens and as-LACS + UNSM vs LACS + P + UNSM specimens.

Therefore, it can be concluded that UNSM treatment is affecting the near-surface microstructure of CS and LACS coatings in a consistent manner irrespective of their prior surface condition.

	As-CS + UNSM	CS + P + UNSM	As-LACS + UNSM	LACS + P + UNSM
Number of LAGBs (2°-15°)	22792	22137	72535	72908
Number of HAGBs (15°-180°)	938741	1068158	1369373	1340071
Total number of boundaries	961533	1090295	1441908	1412979
Average GS	0.22	0.21	0.23	0.22
Average KAM	2.5	2.6	2.3	2.3
Average MA	42.1	42.3	40.5	40.4

Table 5.5: EDSD data of as-CS + UNSM compared with CS + P + UNSM and as-LACS + UNSM compared with LACS + P + UNSM.

However, it must be noted that even though the LACS coating had undergone extreme SPD during its UNSM treatment, the porosity within the LACS coating has not been eliminated by the surface treatment. But from the corrosion results presented in sections 5.2.6 and 5.2.7, it was observed that the UNSM treatment of polished LACS specimen led to a partial closure of the porous sites present on the surface of LACS coating consequently resulting in a significant improvement in their corrosion properties due to the surface treatment.

Finally, from the EBSD results presented on CS & LACS 304L SS coatings in this section, it can be concluded that the UNSM treatment of CS coating had a very negligible impact on it, whereas the UNSM treatment performed on the LACS coating resulted in a gradient microstructure with extreme grain refinement, near surface nano crystallization, dynamic recrystallization, and a significant increase in the plastic strain / dislocation density in the LACS 304L SS coating.

AFS 304L SS:

The EBSD analysis performed at the top edge of cross sectioned as-AFS + UNSM and AFS + P + UNSM specimens is given in figures 5.14 and 5.15 respectively. To determine the effect of UNSM on the as-AFS deposit, the EBSD analysis in figures 4.8 and 5.14 will be compared with

each other. To obtain a polished AFS surface a considerable amount of material had to be removed because of the grooves embedded by the rotating tool shoulder on the surface of as-AFS deposit during its processing which can be observed in figure 3.2. Therefore, after a considerable amount of material removal the very fine recrystallized nano grains and the fine grains at the top will be removed leaving relatively coarser grains at the top of the polished specimen which closely resembles the grains seen in figure 4.9 but not as coarse. So, to determine the effect of UNSM on the polished AFS deposit the EBSD analysis presented in figures 4.9 and 5.15 will be compared with each other.

The UNSM treatment performed on as-AFS specimen impacted its EBSD results in the following manner: the GS decreased from 0.55 µm to 0.13 µm showing significant grain

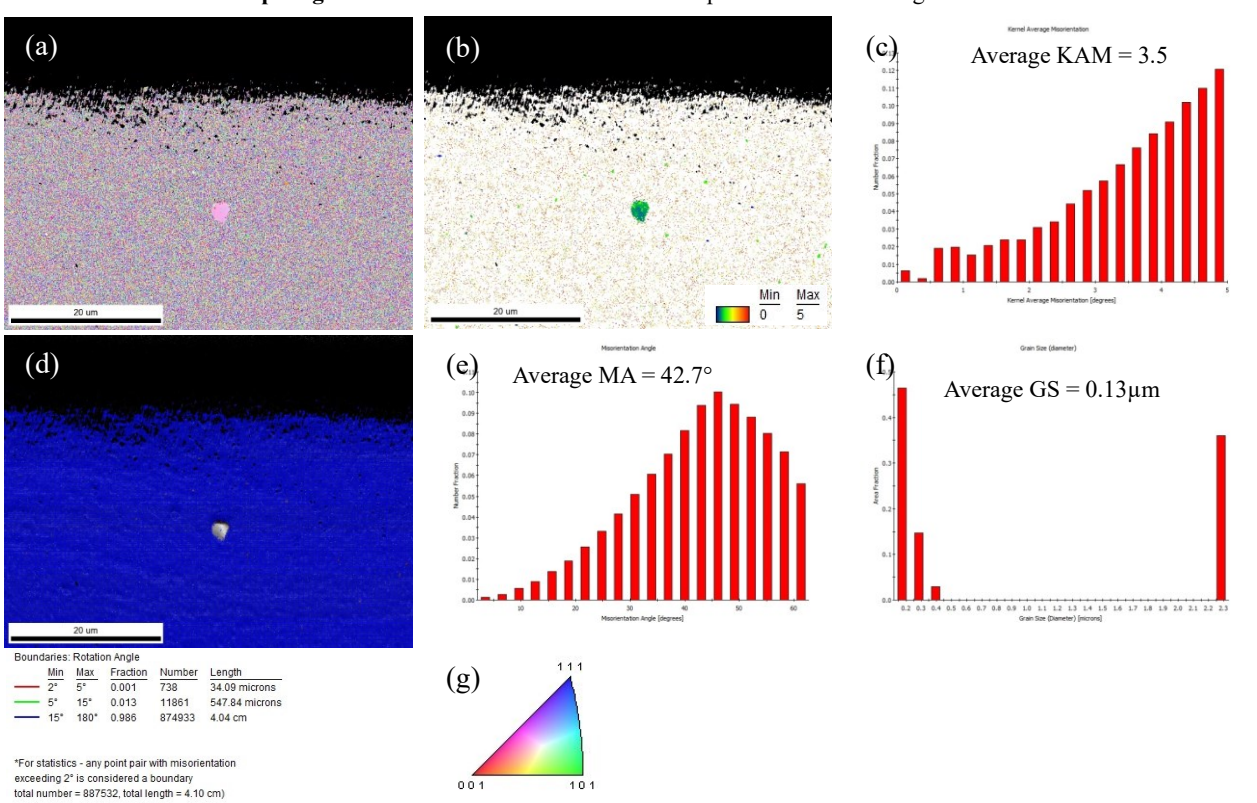

Figure 5.14: Maps obtained by EBSD analysis from the top-edge of cross-sectioned 304L SS as-AFS + UNSM treated specimen representing its (a) Inverse Pole Figure (IPF) map, (b) Kernel Average Misorientation (KAM) map, (c) KAM distribution chart (d) Grain Boundary Misorientation (GBM) map, (e) Misorientation Angle (MA) distribution chart, (f) Grain Size (GS) distribution chart, and (g) legend of IPF map in (a).

Top-Edge of cross-sectioned **AFS + P + UNSM** specimen – 2500X magnification.

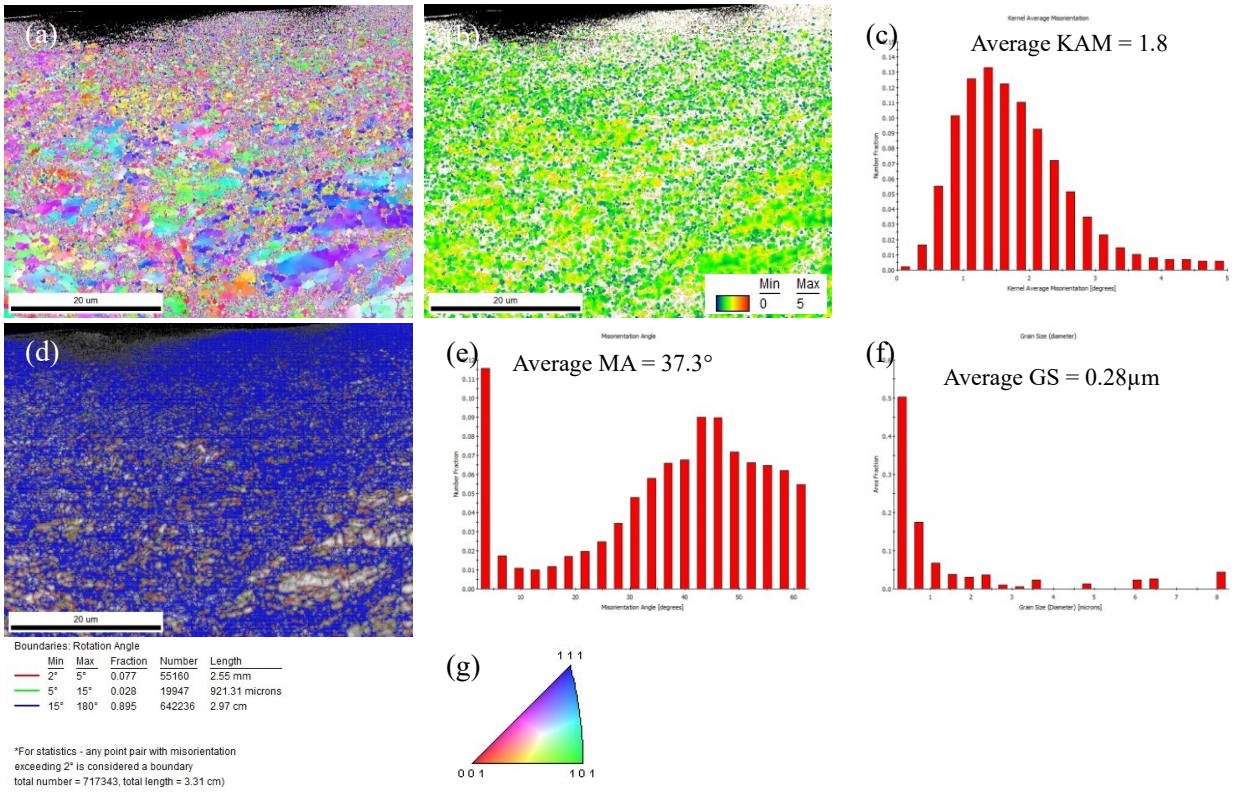

Figure 5.15: Maps obtained by EBSD analysis from the top-edge of cross-sectioned 304L SS AFS + P + UNSM treated specimen representing its (a) Inverse Pole Figure (IPF) map, (b) Kernel Average Misorientation (KAM) map, (c) KAM distribution chart (d) Grain Boundary Misorientation (GBM) map, (e) Misorientation Angle (MA) distribution chart, (f) Grain Size (GS) distribution chart, and (g) legend of IPF map in (a).

refinement; the LAGBs decreased which could be indicative of a small degree of dynamic recrystallization occurring in the very fine grains at the top AFS layer and the HAGBs increased due to severe plastic deformation (SPD); the MA increased significantly from 33° to 42.7° due to SPD; and the average KAM value increased enormously from 1.2 to 3.5 showing that significantly higher degree of plastic strain was introduced in the as-AFS deposit by UNSM. Also, the UNSM treatment performed on the polished AFS specimen impacted the EBSD results in a similar manner as that of the as-AFS + UNSM specimen showing a decrease in grain size due to grain refinement with an average GS of 0.28 µm; increase in both LAGBs and HAGBs with a significant change in misorientation angle distribution due to SPD; and an increase in the average KAM value to 1.8 due to an increase in the plastic strain by UNSM treatment.

One key observation that can be made between the two UNSM treated AFS specimens is that the as-AFS + UNSM specimen exhibits considerably higher plastic strain and lower average GS than AFS + P + UNSM specimen. Looking at the respective GS and KAM values prior to UNSM treatment of the top and center area of AFS layers (figure 4.8 and 4.9) and their after-surface treatment values (figure 5.14 and 5.15) it can be viewed that the impact of UNSM treatment is building proportionally on the prior surface characteristics. Finally, it can be said that UNSM treatment can induce significant degree of grain refinement with near-surface nano crystallization and embedment of appreciable amount of dislocation density (plastic strain) in the 304L SS AFS cladding in either of its surface conditions (i.e., in its as-deposited or polished surface condition).

5.2.2 X-Ray Diffraction Phase Analysis

Sensitized 304L SS:

Figure 5.16 shows the XRD scans of UNSM treated solution annealed and sensitized 304L SS specimens. They reveal that the surfaces of both the UNSM treated SA and sensitized 304L SS specimens have undergone a 100% austenitic to martensitic phase transformation, which can be attributed to the extreme grain refinement and dynamic recrystallization occurring in them due to the severe pounding of WC tool tip against their surface during UNSM treatment.

CS & LACS 304L SS:

Figure 5.17 represents the XRD scans of SA, CS, and LACS 304L SS specimens showing the phase changes associated with the UNSM treatment performed on them in their (a) as-is surface condition and (b) after polishing to 1200 grit surface condition. The UNSM treatment performed on the as-SA and SA + P 304L SS specimens resulted in a 100% near-surface martensitic phase transformation as expected because of the SPD induced onto the material during UNSM. However, the UNSM treatment performed on both the as sprayed and polished surfaces of CS and LACS

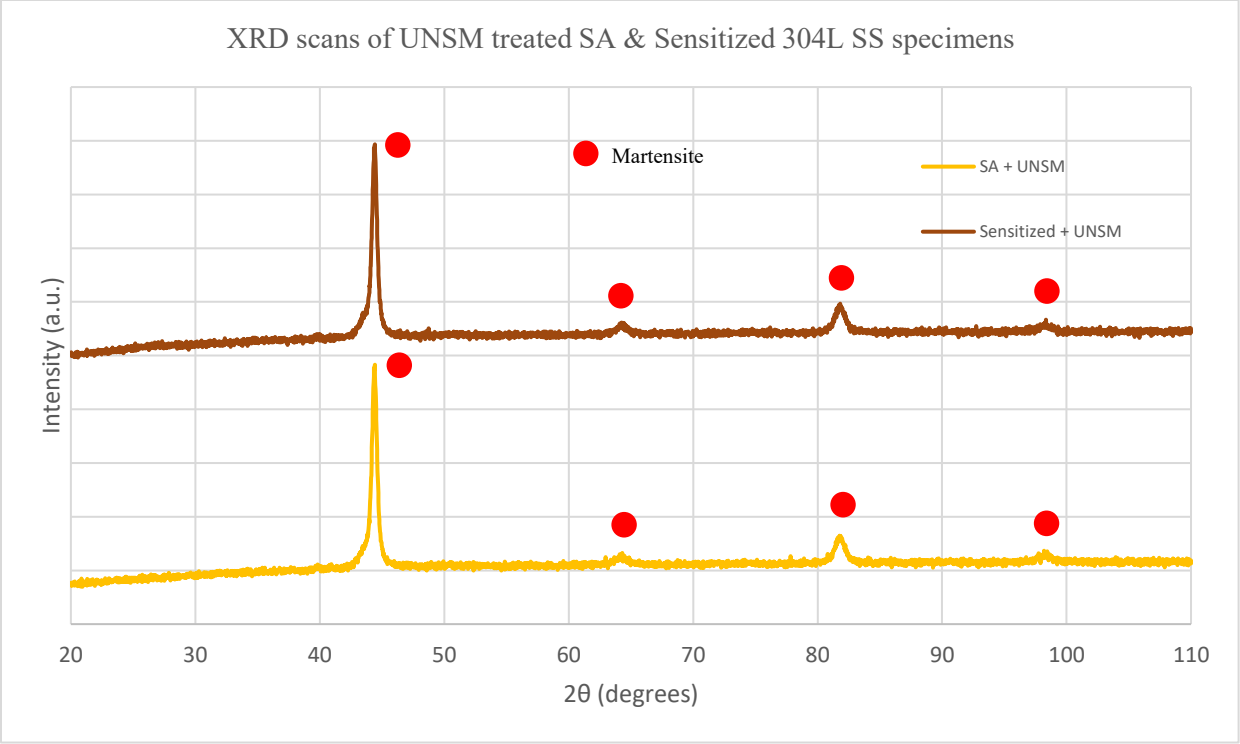

Figure 5.16: XRD surface scans of SA and Sensitized 304L SS specimens subjected to UNSM treatment.

coatings resulted in a martensitic phase transformation, but with a mixed presence of austenite and martensite phases at their surface unlike the 100% martensitic transformation observed in the UNSM treated SA specimens. The austenite phase peak in the XRD scans of UNSM treated CS and LACS coatings can be clearly seen at a 2θ of 43.5° in both the (a) and (b) of figure 5.17.

The reason for the partial transformation of austenite to martensite phase detected at the surface of the UNSM treated CS and LACS coatings can be explained from the BSE micrographs of untreated CS and LACS coatings shown in figure 5.18 that are taken from their top and cross-sectioned surface areas which are showing a persistent presence of porosity throughout the coatings. Typically, during UNSM surface treatment, the WC tool tip dynamically scans over the specimen's surface through direct contact, inducing SPD into the material that results in a 100% near-surface phase transformation from FCC austenite to BCT martensite, whose content gradually decreases through the depth of the specimen with a simultaneous increase in the percentage of

austenite before ultimately diminishing to 0% martensite (i.e., detection of 100% austenite). But while UNSM surface treating the CS and LACS coatings, because of the presence of large number

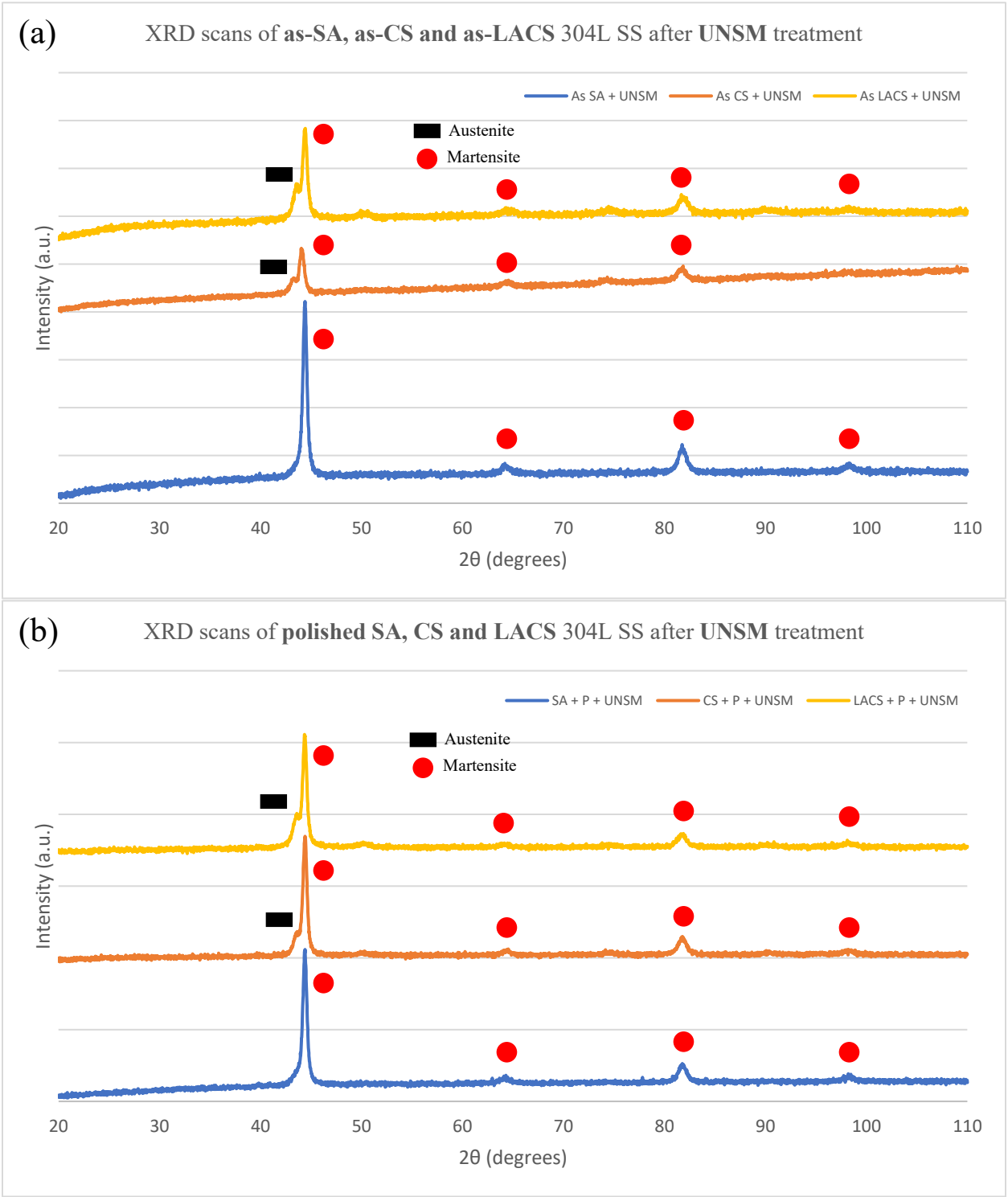

Figure 5.17: Comparing the XRD scans of SA, CS, and LACS 304L SS coatings after performing UNSM surface treatment on them in their (a) as-is surface condition and (b) polished to 1200 grit surface condition.

of porosity sites in the coatings, the WC tool tip will have restricted access to the material underneath the porous area i.e., depending on the depth of the porous sites the tool tip may have none to only limited contact with the underneath metal resulting in only a proportional degree of martensitic transformation. Therefore, unlike in the case of conventionally hot-rolled & SA 304L SS specimen, UNSM surface treatment does not induce a 100% near-surface martensitic transformation in the CS and LACS 304L SS coatings. However, it must also be noted that the surface of the UNSM treated CS and LACS coatings has predominantly transformed to martensite phase with only a small fraction of austenite phase remaining as seen from their XRD scans in figure 5.17.

CS – Top surface area

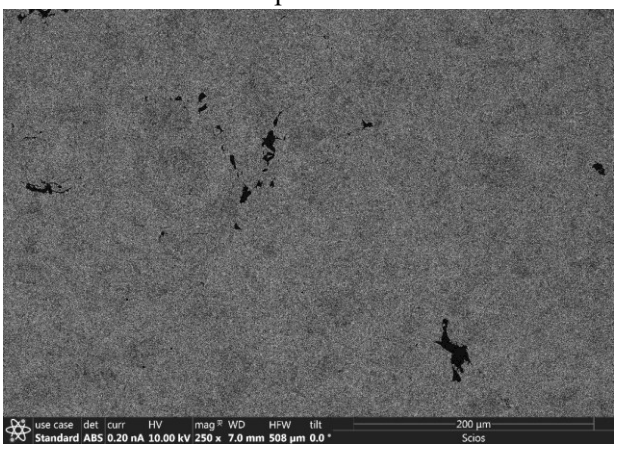

LACS – Top surface area

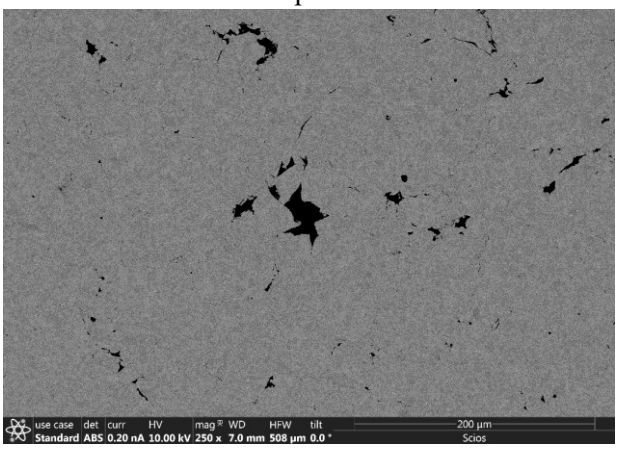

CS – Cross-sectional surface area

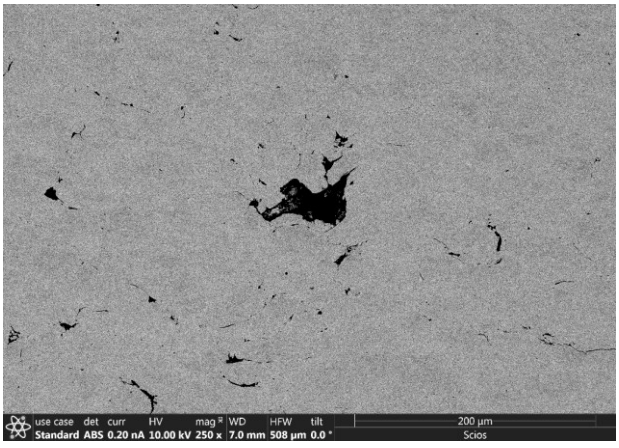

LACS – Cross-sectional surface area

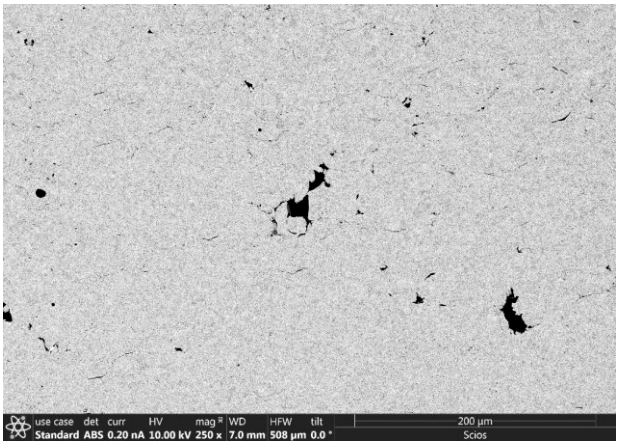

Figure 5.18: BSE micrographs showing the persistent presence of porosity in the untreated CS & LACS 304L SS coatings.

AFS 304L SS:

Figure 5.19 represents the XRD patterns obtained for the UNSM treated AFS 304L SS specimens showing the phase changes associated with the surface treatment performed on the AFS 304L SS cladding with respect to both of its surface conditions (i.e., UNSM treatment performed on its as-is surface condition and polished surface condition), along with the XRD pattern of UNSM treated SA specimen. The XRD patterns of both as-AFS + UNSM and AFS + P + UNSM specimen surfaces show that UNSM treatment resulted in a 100% martensitic phase transformation at their surface like that of the SA + UNSM treated 304L SS specimen. And it can also be observed from the XRD pattern of as-AFS + UNSM specimen not showing any oxide peaks indicating that the oxide film present on the as-AFS specimen was broken down by the surface treatment. However, EDS analysis was performed on the specimen surface to confirm if the oxide film has been completely removed by UNSM or not whose results are presented later in this chapter.

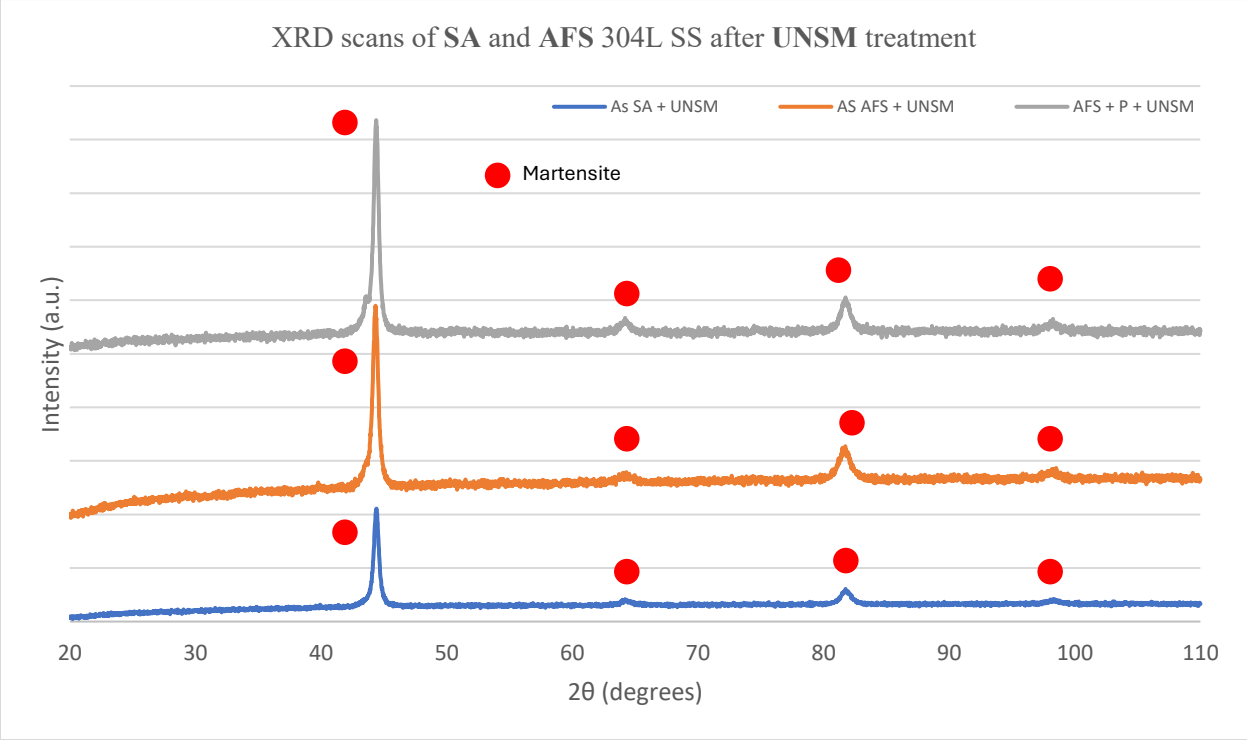

Figure 5.19: XRD patterns of UNSM treated as-AFS, polished AFS, and SA 304L SS specimens.

5.2.3 Nano Hardness Analysis

Sensitized 304L SS:

Figure 5.20 (a), (b), & (c) show the effect of UNSM treatment on the nano hardness depth profiles of SA, S5, and S24 specimens respectively. In all the three specimens, the near-surface nano hardness value after their UNSM treatment has increased tremendously to ~ 600 Hv increasing by more than 2X times. Furthermore, this tremendously high near-surface nano hardness value decreases gradually through the depth of all the three specimens eventually reaching their prior surface treatment hardness values due to the gradient nature of the microstructures obtained by UNSM treatment. The depths up to which the impact of UNSM treatment could be seen on the hardness values of SA, S5, and S24 specimens were determined to be 0.36 mm, 0.4 mm, and 0.28 mm respectively, which align proportionally well with the determinations made from their respective KAM maps (figure 5.11 (a-c)) regarding the depth up to which the induced plastic strain could be observed in these specimens, with the maximum depth impact seen in these specimens following the relationship S5 ≥ SA > S24.

The tremendous increase in near-surface and sub-surface hardness of UNSM treated SA, S5, and S24 304L SS specimens can be attributed to the combined effect of the following factors: (1) intense strain hardening caused by UNSM promoting the multiplication and entanglement of dislocations thereby, increasing the dislocation density and their accumulation at the grain boundaries within the material, (2) extreme grain refinement resulting in tiny grains increases the density of grain boundaries impeding dislocation motion, and (3) austenite to martensite phase transformation, since martensite phase generally possesses higher hardness than the austenite phase. Therefore, all these three factors combined are simultaneously contributing to the tremendous increase in hardness of the SA and sensitized 304L SS specimens by UNSM treatment.

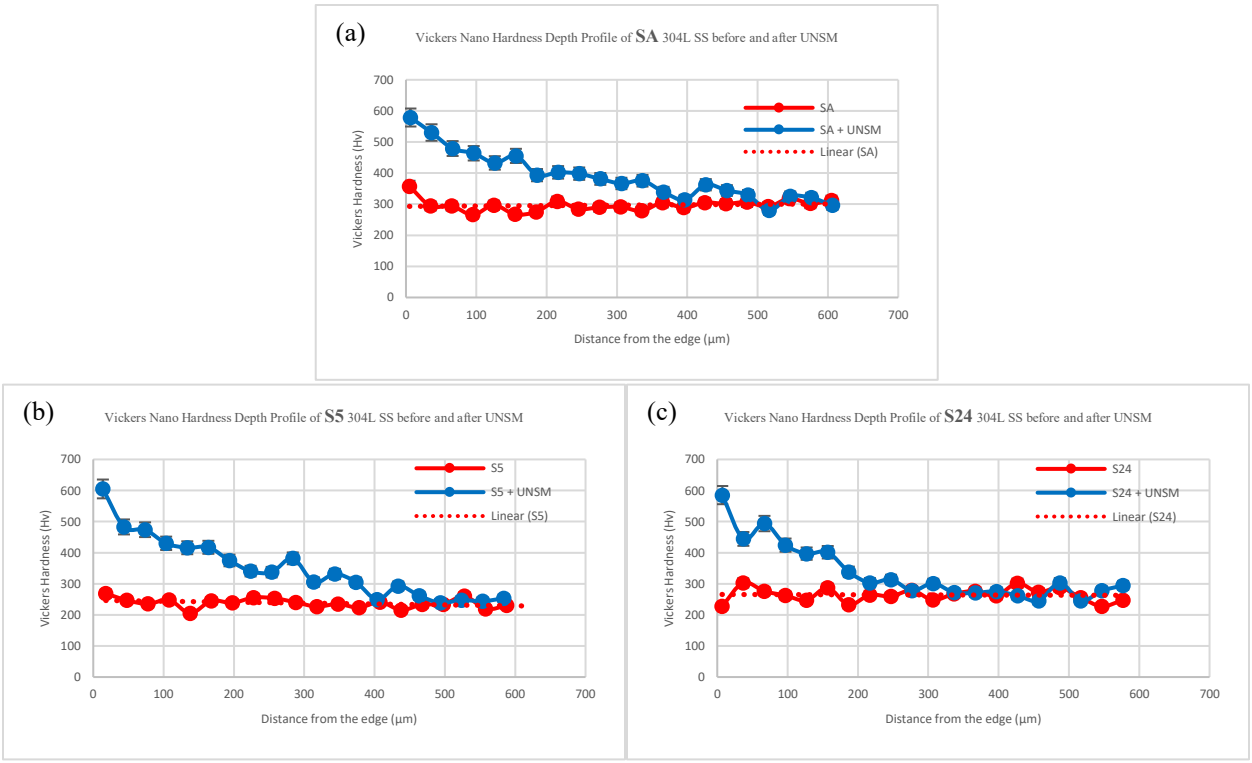

Figure 5.20: Nano Hardness Depth Profile comparison of (a) SA, Sensitized at 650°C for (b) 5h and (c) 24h 304L SS specimens before and after UNSM treatment.

CS & LACS 304L SS:

Figure 5.21 depicts the effect of UNSM treatment on as-CS and CS + P 304L SS specimens with respect to the variations in their through-the-depth nano hardness values. The near-surface hardness of as-CS and CS + P specimens increased slightly after their UNSM treatment from 594 Hv to ~ 700 Hv and 800 Hv respectively. The slight increase in the near-surface hardness of CS coatings after their UNSM treatment can be attributed to the martensitic phase transformation and the small degree of grain refinement occurring in the few larger sized deformed grains that were present in the untreated CS specimens by UNSM as can be observed by comparing figures 4.6 and 5.12. Also, the higher near-surface hardness of CS + P + UNSM specimen than that of the as-CS + UNSM specimen could be due to the increased efficiency of dynamic load transfer through the WC tool tip onto the smoother surface of polished CS specimen during its UNSM treatment than that of the rougher as-CS specimen surface. However, the depth hardening impact of UNSM on

both the as-CS and CS + P specimens was confined to < 40 µm from their surface.

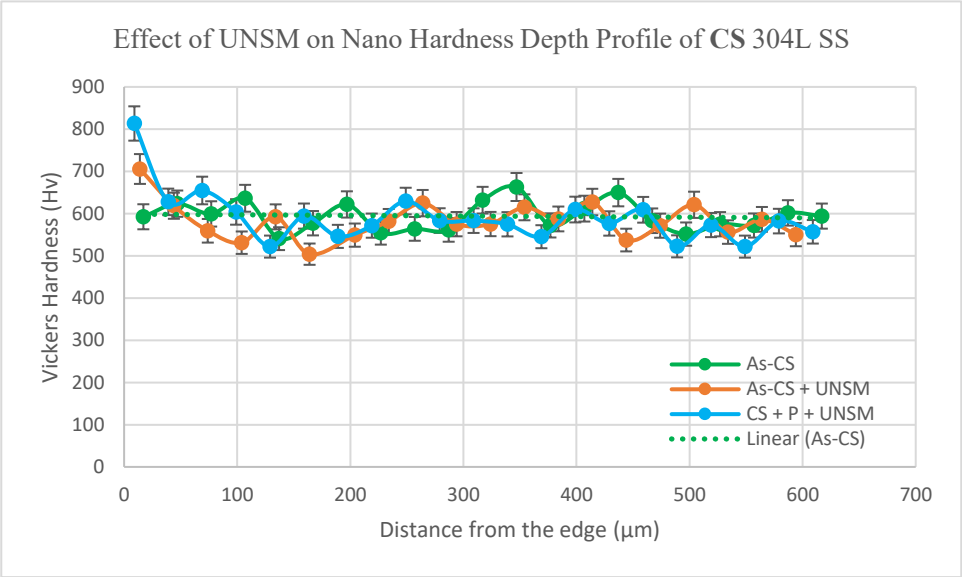

Figure 5.21: Nano Hardness depth profiles of CS 304L SS before and after UNSM treatment.

Figure 5.22 depicts the effect of UNSM treatment on the as-LACS and LACS + P 304L SS specimens with respect to the alterations in their through-the-depth nano hardness values. Upon UNSM treating the LACS coatings their near-surface hardness values have increased tremendously from 378 Hv to > 700 Hv in both the as-LACS + UNSM and LACS + P + UNSM specimens which could be attributed to the SPD induced into the specimens during their UNSM treatment resulting in nano crystallization and increased dislocation density at the surface as can be seen from figure 5.13. Additionally, martensitic phase transformation by UNSM treatment is also a contributing factor to the significant increase in near-surface hardness of UNSM treated LACS 304L SS specimens, as martensite phase generally has higher hardness than austenite phase. Like CS specimens, the LACS + P + UNSM specimen exhibits slightly higher near-surface hardness than the as-LACS + UNSM specimen for the same reason that the efficiency of the dynamic load transfer through the WC tool tip would have improved when UNSM peening was done on the smoother surface of LACS + P specimen than on the rougher surface of as-LACS specimen. The sub surface hardness of surface treated LACS coatings decreased gradually along

the depth of the specimens because of the gradient nature of the microstructure attained by the LACS coatings after their UNSM treatment (i.e., an increase in grain size, decrease in dislocation density and martensite phase with an increase in depth from the specimen surface tending to a decrease in the hardness values of UNSM treated LACS specimens along their depth). The relatively significant increase in hardness through the depth of both as-LACS + UNSM and LACS + P + UNSM specimens could be observed up to a depth of ~ 160 µm from their surfaces.

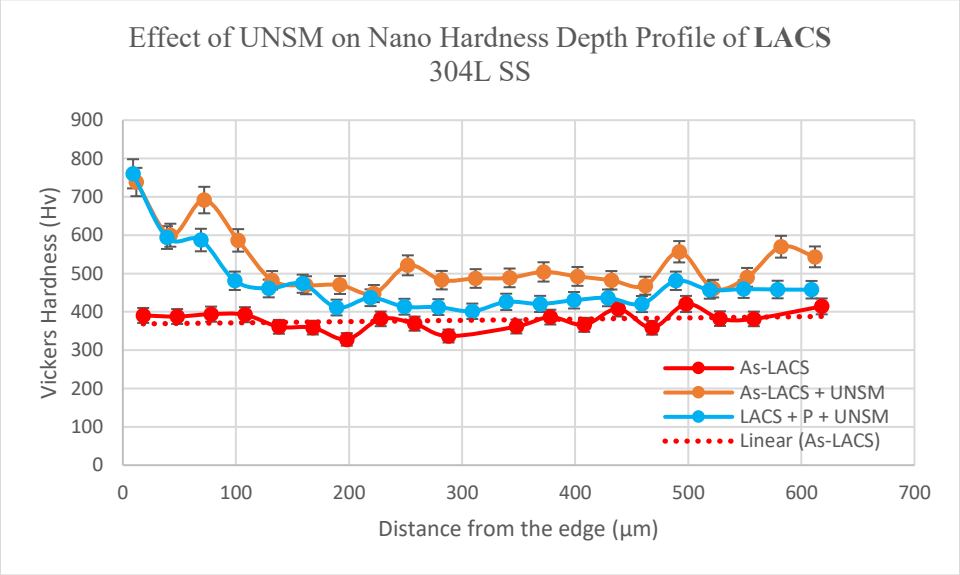

Figure 5.22: Nano Hardness depth profiles of LACS 304L SS before and after UNSM treatment.

AFS 304L SS:

Figure 5.23 shows the effect of UNSM on the as-AFS and AFS + P 304L SS specimens with respect to the variations in their through-the-depth nano hardness values. The near-surface hardness of both as-AFS and AFS + P specimens more than doubled from 533 Hv and 369 Hv to 1236 Hv and 789 Hv respectively after their UNSM treatment. From the variable increase in hardness values, it can be said that the UNSM treatment is enhancing the prior surface hardness of as-AFS and AFS + P specimens proportionally rather than elevating them to the same level. A similar observation was made with respect to their KAM values as well during their EBSD analysis. The tremendous increase in near-surface hardness of both as-AFS and AFS + P specimens

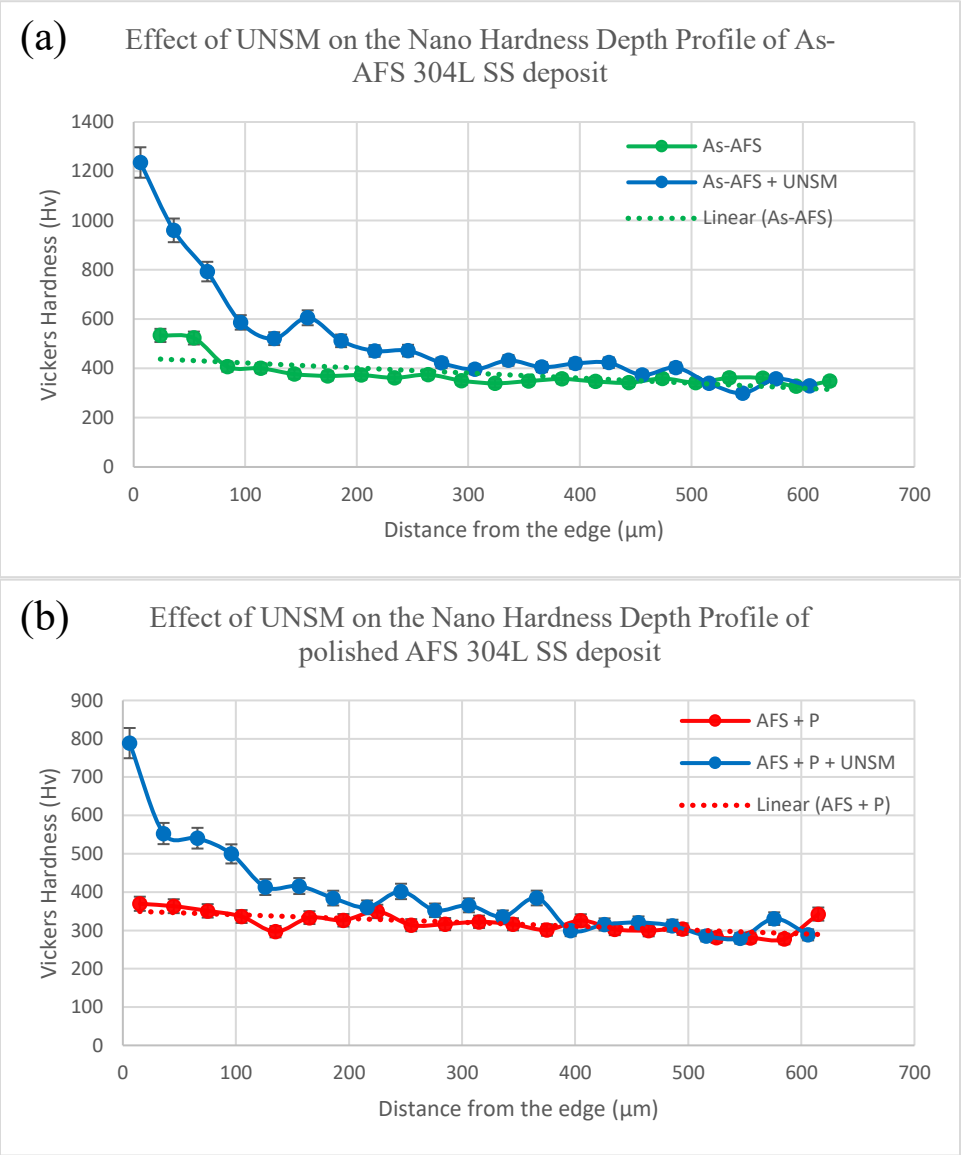

Figure 5.23: Effect of UNSM on the Nano Hardness depth profiles of (a) as-AFS and (b) polished to 1200 grit AFS 304L SS deposit surface.

can be attributed to a combination of factors like martensitic phase transformation, significant grain refinement and increased dislocation density resulting from the SPD induced by UNSM. However, the depth up to which the increased hardness values can be observed varies only slightly in as-AFS + UNSM and AFS + P + UNSM specimens, with it being observed up to a depth of ~ 100 µm and 130 µm from the surface of these specimens respectively. Therefore, it can be said in conclusion that UNSM is resulting in an enormous and proportional increase in the near surface

hardness of the AFS specimens whether the surface treatment is performed on the as-is or polished AFS cladding, & its impact is lasting up to a depth of at least ~ 100 µm from the specimen surface.

5.2.4 Surface Topography Analysis

Sensitized 304L SS:

Figure 5.24 represents the SE micrographs showing the surfaces of UNSM treated SA, S5, and S24 304L SS specimens. All the three specimen surfaces show UNSM tracks consisting of peaks and valleys that were made by the WC tool tip during their surface treatment. No substantial differences between their surface topography can be observed visually from their micrographs. However, when their surfaces were analyzed using Bruker contour GT optical profilometer, the obtained surface roughness (Ra) values of the three UNSM treated 304L SS specimens had minor differences exhibiting values of 0.63 ± 0.06 µm, 0.89 ± 0.06 µm, and 0.55 ± 0.18 µm by the UNSM treated SA, S5, and S24 specimens respectively. The UNSM treated SA and S24 specimens exhibit slightly lower Ra values than the S5 specimen indicating that the former two specimens have slightly smoother surface finish than the latter specimen after their surface treatment. The higher surface roughness value of UNSM treated S5 specimen can be attributed to its lower hardness (figure 4.13) allowing the WC tool tip to make slightly deeper valleys on its surface during UNSM treatment than when compared to the relatively harder SA and S24 specimens.

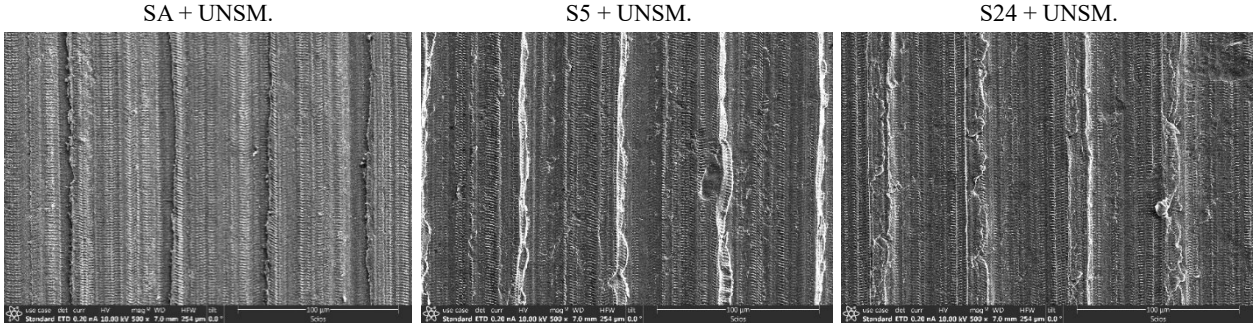

Figure 5.24: SE micrographs showing the surface of UNSM treated SA and sensitized at 650°C for 5h and 24h 304L SS specimens.

CS & LACS 304L SS:

The average Ra values of as-CS + UNSM, as-LACS + UNSM, CS + P + UNSM, and LACS + P + UNSM 304L SS specimens that are obtained using Bruker contour GT profilometer are depicted graphically with the help of bar charts in figure 5.25 (a) & (b) and their surface profile scans that visually depict their surface topography are given in figure 5.25 (c), (d), (e), & (f) respectively.

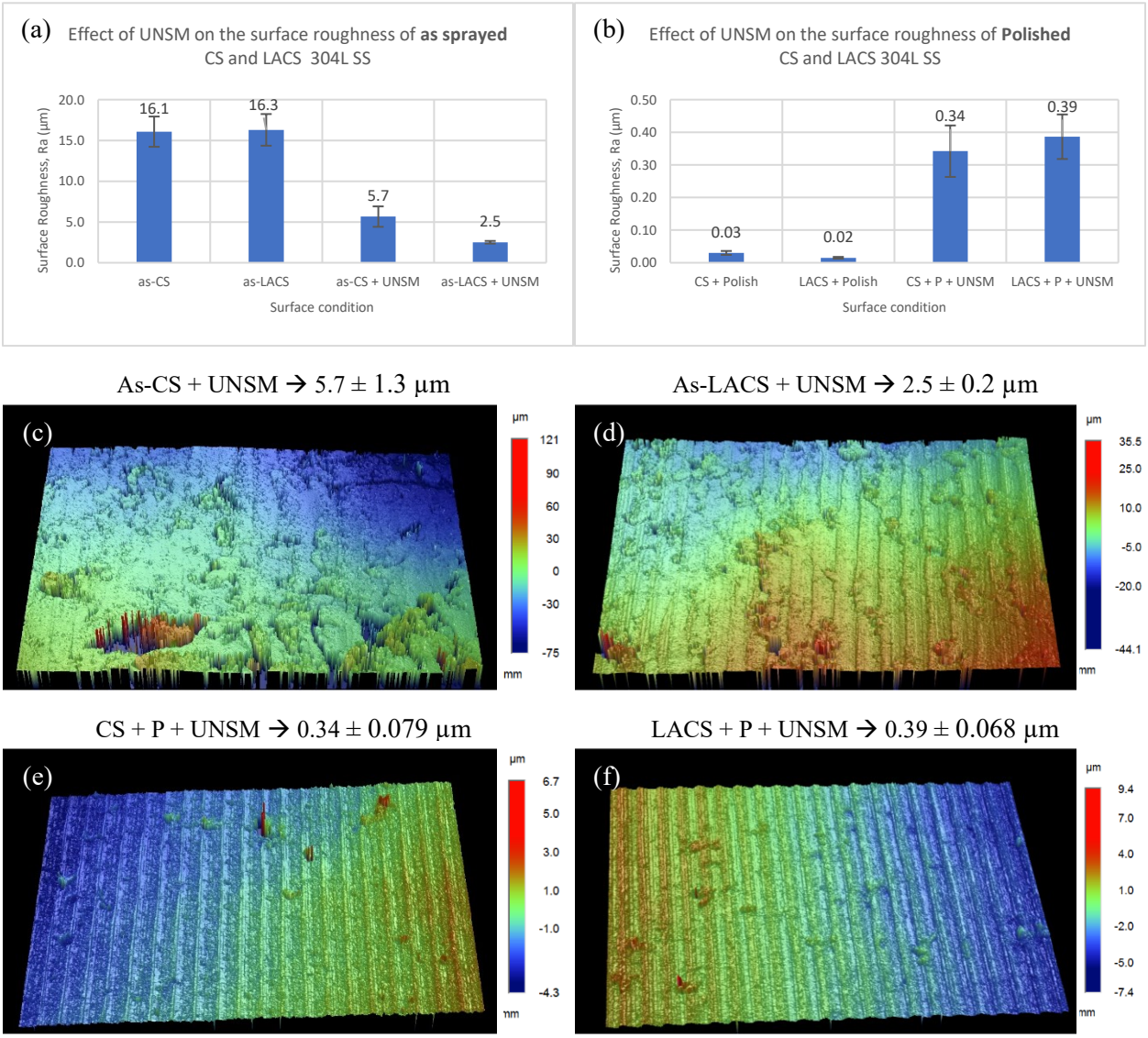

Figure 5.25: Surface topography analysis showing the effect of UNSM treatment on the surface roughness (Ra) values of (a) as sprayed and (b) polished to 1200 grit surface finish CS and LACS 304L SS coatings and (c), (d), (e), & (f) represent the surface profile scans of as-CS + UNSM, as-LACS + UNSM, CS + P + UNSM, and LACS + P + UNSM 304L SS specimens respectively.

Upon UNSM treating the as-sprayed CS and LACS coatings, their Ra values declined from ~ 16 ± 1.9 μm to 5.7 ± 1.3 μm and 2.5 ± 0.2 μm decreasing by ~ 3X and 6X times respectively. This decrease in the Ra of as-sprayed CS and LACS coatings by UNSM occurred due to the severe pounding of WC tool tip with significant impact density on the coating's surface. Also, the decrease in Ra value due to UNSM treatment is far greater in the as-LACS coating than in as-CS coating because of the lower hardness value of LACS coating allowing the WC tool tip to dynamically penetrate deeper into the material than it could into the heavily deformed CS specimen.

Whereas the UNSM treatment performed on the polished CS and LACS coatings increased their surface roughness marginally from that of their polished state because of the peaks and valleys created by WC tool tip on their surface during their UNSM treatment. However, the obtained Ra values of CS + P + UNSM (0.34 ± 0.079 μm) and LACS + P + UNSM (0.39 ± 0.068 μm) specimens can be considered as insignificant when compared to the Ra values of as-sprayed coatings (~ 16 ± 1.9 μm) or to that of the as-sprayed + UNSM treated coatings.

The surface scans of UNSM treated as-CS, as-LACS, CS + P, and LACS + P coatings depict a uniform surface area, characteristic of a typical UNSM treated specimen surface, showcasing clearly visible rows of vertical lines that represent the sequential impact of WC tool tip on the specimen surface. From the surface scans it appears that medium degree of concentration cells could be setup on the as-CS + UNSM and as-LACS + UNSM specimens whereas it would be extremely difficult for the corrosive chloride ions in the corrosion test solutions or during real time applications to settle or setup concentration cells on the CS + P + UNSM and LACS + P + UNSM specimen surfaces similar to that of the CS + P and LACS + P specimen surfaces.

Finally, it can be concluded that UNSM surface treatment performed on both the as-sprayed

CS and LACS 304L SS coatings was extremely effective in reducing their surface roughness or surface unevenness, with the most impact being seen on the surface of the as-LACS coating than on the as-CS coating surface owing to the huge difference observed in their hardness characteristics and that UNSM does not significantly impact the surface roughness of polished CS and LACS coatings in a negative manner.

AFS 304L SS:

The attained average Ra values for as-AFS + UNSM and AFS + P + UNSM 304L SS specimens are presented graphically using a bar chart in figure 5.26 (a), along with their surface profile scans in figure 5.26 (b) & (c) respectively. The UNSM treatment on as-AFS cladding was performed on the rightmost section of the as-AFS cladding shown in figure 3.2 or figure 4.17 (a).

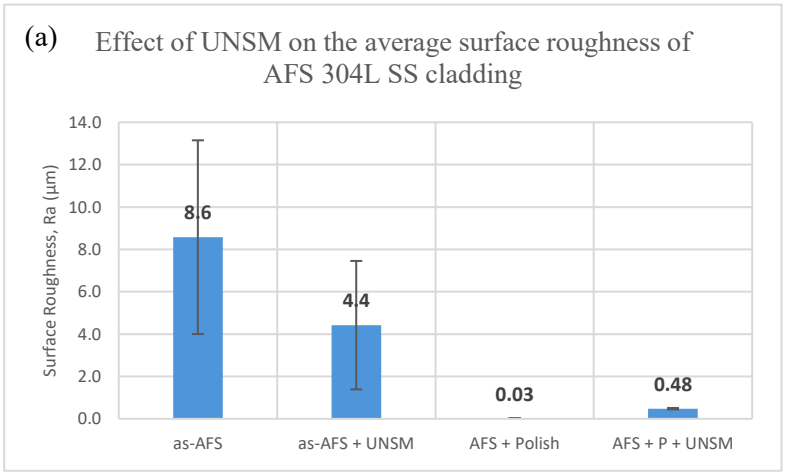

As-AFS + UNSM → 4.4 ± 3.0 µm

AFS + P + UNSM → 0.48 ± 0.034 µm

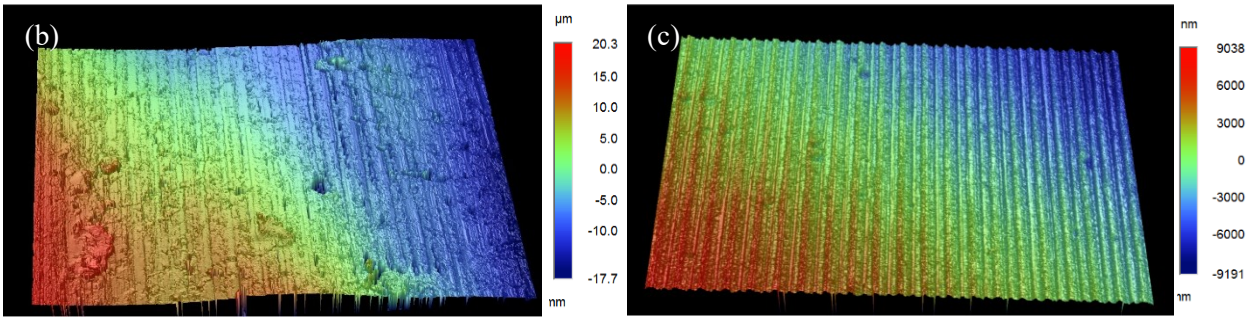

Figure 5.26: Surface topography analysis showing the effect of UNSM treatment on the surface roughness (Ra) values of (a) as sprayed and polished to 1200 grit surface finish AFS 304L SS coatings, and (b) & (c) represent the surface profile scans of as-AFS + UNSM and AFS + P + UNSM 304L SS specimens respectively.

Therefore, to determine the effect of UNSM on the surface roughness of as-AFS specimen, only the Ra value pertaining to the rightmost section was considered and compared with the Ra value of as-AFS + UNSM treated specimen surface. And from figure 5.26, it can be seen that UNSM treating the as-AFS specimen resulted in nearly 2X decrease in its Ra value from 8.6 ± 4.6 μm to 4.4 ± 3.0 μm due to the severe pounding of WC tool tip on its surface during the surface treatment. Whereas upon UNSM treating the polished AFS specimen, its surface roughness increased slightly as expected, from a value of 0.03 ± 0.012 μm to 0.48 ± 0.034 μm, because of the peaks and valleys created by the dynamic action of WC tool tip on the polished AFS specimen surface. Nevertheless, it can be said that UNSM can effectively reduce the surface roughness of the as-AFS 304L SS cladding and does not negatively impact the Ra of polished AFS much.

5.2.5 Residual Stress Analysis

Sensitized 304L SS:

Upon UNSM treating the polished SA, S5, and S24 specimens, their surface residual stress (SRS) increased enormously in the compressive stress state to greater than -1600 MPa and -900 MPa along their step direction (SD) and transverse direction (TD) of UNSM respectively and their exact magnitudes are presented in figure 5.27. The CRSs are generated in a material by the creation of stress concentration and strain accumulation regions in it through rearrangement of atomic positions, dislocation pile-up and development of strain incompatibility between neighboring grains caused by the SPD and grain fragmentation in the material during UNSM.

Through-the-depth RS profiles of UNSM treated SA and sensitized 304L SS specimens were determined because they can have an impact on the SCC resistance of a material. At every depth interval, the RSs due to both austenite and martensite phases were measured until martensite phase disappeared. Beyond it, only RS pertaining to austenite phase was measured until at least

two RS values were obtained in the tensile region, so as to determine the depth up to which the impact of UNSM was felt in the induction of CRSs in the SA, S5, and S24 304L SS specimens.

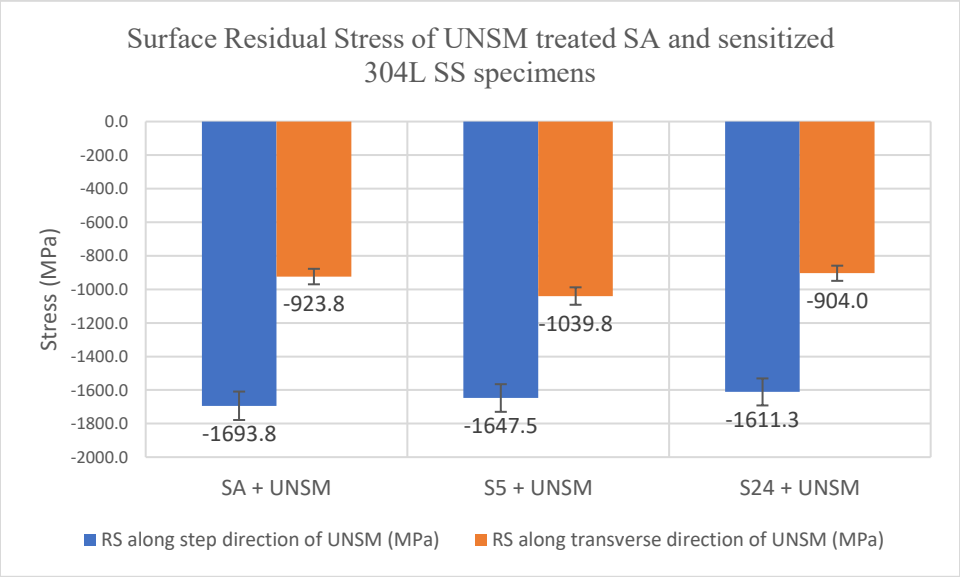

Figure 5.27: Surface residual stress comparison along both the orthogonal directions of UNSM treated Polished SA and sensitized 304L SS specimens.

The RS depth profiles related to both the martensite and austenite phases and their corresponding full width half maximum (FWHM) profiles of UNSM treated SA, S5, and S24 304L SS specimens are presented in figures 5.28 (martensite) and 5.29 (austenite) respectively. In both the figures, (a) represents the SA + UNSM treated, (b) represents the S5 + UNSM treated, (c) represents the S24 + UNSM treated 304L SS specimens RS depth profiles along both the orthogonal directions of UNSM and (d) represents the FWHM depth profiles of all the three specimens. The RS depth profiles of all the three specimens with respect to both the austenite and martensite phases show stress distribution curves that are typically observed in specimens processed by common surface processing techniques, with the highest CRS being observed at the surface of the specimen that gradually decreases along its depth.

The near-surface CRSs with respect to both the austenite and martensite phases of UNSM treated SA, S5, and S24 specimens along their SD were observed to be significantly greater in

magnitude than the CRSs along their TD of UNSM. The induction of CRSs pertaining to the martensite phase of all the three specimens was seen up to a depth of ~ 140 – 150 µm below their surface along both the orthogonal directions of UNSM. Whereas the CRSs pertaining to the austenite phase of all the three specimens could be observed up to a depth of ~ 400 µm and 500 µm along the SD and TD of UNSM respectively.

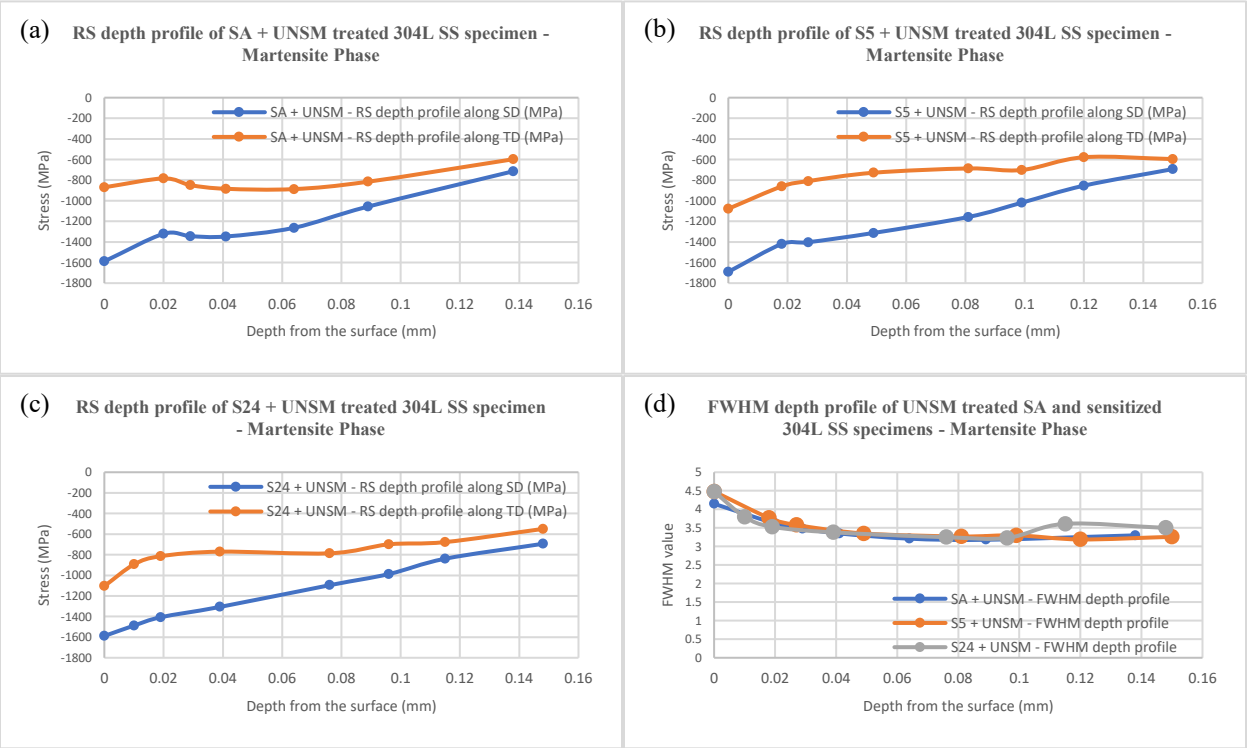

Figure 5.28: Residual stress depth profiles along both the orthogonal directions of UNSM treated (a) SA, (b) S5, and (c) S24 304L SS specimens w.r.t their martensite phase and (d) their corresponding FWHM profiles depicting the plasticity present in the material along their depth.

Despite the near-surface CRS values along the TD of all the three UNSM treated specimens being of a lower magnitude than their CRS values along their SD of UNSM, the induction of CRSs up to a certain depth of the specimens has been highest along their TD of UNSM than along their SD of UNSM. Another observation made from the CRS values of UNSM treated SA, S5, and S24 specimens is that the CRS values pertaining to the martensite phase at every depth interval along both the orthogonal directions of the UNSM treated specimens is exceptionally higher than the

CRS values pertaining to the austenite phase. Also, as the CRS values due to both the austenite and martensite phases are not the same, it indicates that the RS due to both these phases are not equi-biaxial. Lastly, despite the differences in the GS and hardness characteristics of untreated SA, S5, and S24 specimens, the depth up to which the CRSs and martensite phase were induced in all the three specimens by UNSM treatment along both their SD and TD of UNSM are extremely close to each other with their exact values being presented in figure 5.30.

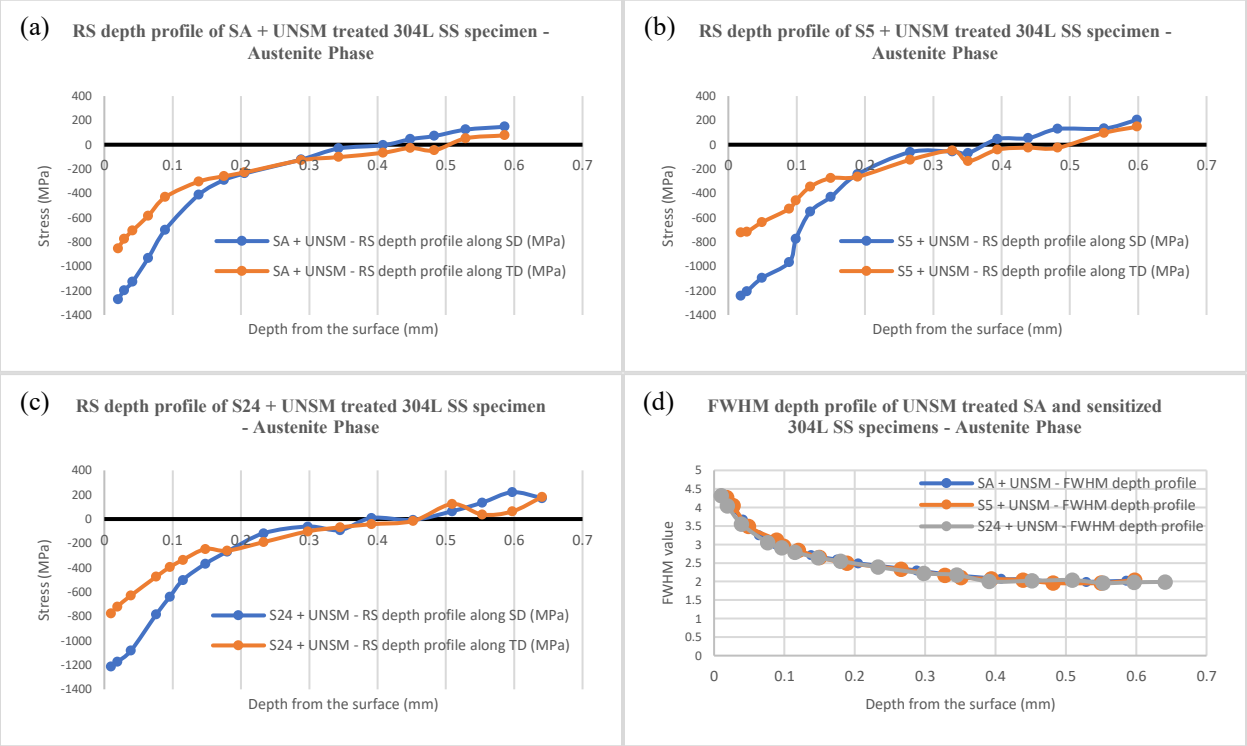

Figure 5.29: Residual stress depth profiles along both the orthogonal directions of UNSM treated (a) SA, (b) S5, and (c) S24 304L SS specimens w.r.t their austenite phase and (d) their corresponding FWHM profiles depicting the plasticity present in the material along their depth.

The FWHM values presented in figures 5.28 and 5.29 that are obtained along the depth of the SA and sensitized 304L SS specimens depict the plasticity or strain present in the respective specimen's material. As martensite phase exists only up to a certain limited amount of depth, the FWHM profile pertaining to austenite phase is considered to demonstrate the plasticity embedded by UNSM treatment throughout the entire depth of the 304L SS specimens studied here. Therefore,

from figure 5.29 (d), it can be observed that the UNSM treatment has embedded a significant and similar degree of plasticity or strain at the surface of all the three specimens which decreased gradually along their depth. The notably higher plastic strain deduced from the FWHM profiles of the UNSM treated SA and sensitized 304L SS specimens is determined to exist up to a depth of ~ 200 – 230 µm which coordinates well with the observations made from the KAM maps in figure 5.11 (a-c) where the extensive plastic strain introduced into the specimens by UNSM could be seen visually.

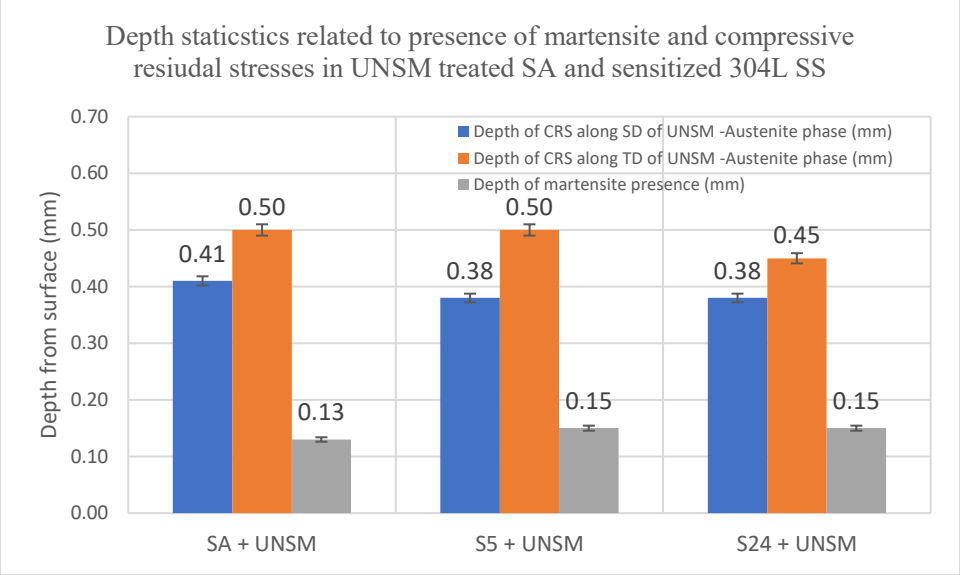

Figure 5.30: Depth of presence of martensite phase and induction of compressive residual stresses in the UNSM treated SA and sensitized 304L SS specimens.

<u>CS & LACS 304L SS</u>:

The effect of UNSM surface treatment on the residual stress state of as sprayed and polished CS and LACS 304L SS coatings has been studied along both the orthogonal directions of the specimens (step direction -SD and transverse direction - TD) i.e., every residual stress measurement taken on the surface of UNSM treated CS and LACS coatings has been determined with respect to both the SD and TD of the specimens. Also, to maintain constant directionality, the UNSM surface treatment was performed on the CS and LACS coatings by aligning the step and

transverse directions of UNSM processing with those of the CS and LACS processed coatings. Moreover, the XRD phase analysis seen in figure 5.17 shows that the UNSM treated CS and LACS coating surfaces consisted, both the austenite and martensite phases because of the partial phase transformation occurring in the CS and LACS coatings by SPD during their UNSM treatment. Therefore, the RS measurements of surface treated CS and LACS coatings were measured with respect to both the austenite and martensite phases.

The SRS measurements obtained for the UNSM treated as sprayed and polished to 1200 grit surface finish CS and LACS coatings are presented graphically in figure 5.31 with (a) and (b) representing the SRS due to their austenite and martensite phases respectively. The SRSs of as-CS and as-LACS specimens after their UNSM treatment with respect to both the austenite and martensite phases have increased vastly in the compressive stress region exhibiting magnitudes greater than -1250 MPa and -730 MPa along their SD and TD respectively. Whereas the SRSs of polished CS and LACS specimens after their UNSM treatment with respect to both the austenite and martensite phases have increased further in the compressive state than the as sprayed + UNSM treated CS and LACS coatings to an even higher magnitudes of greater than -1570 MPa and -980 MPa along their SD and TD respectively.

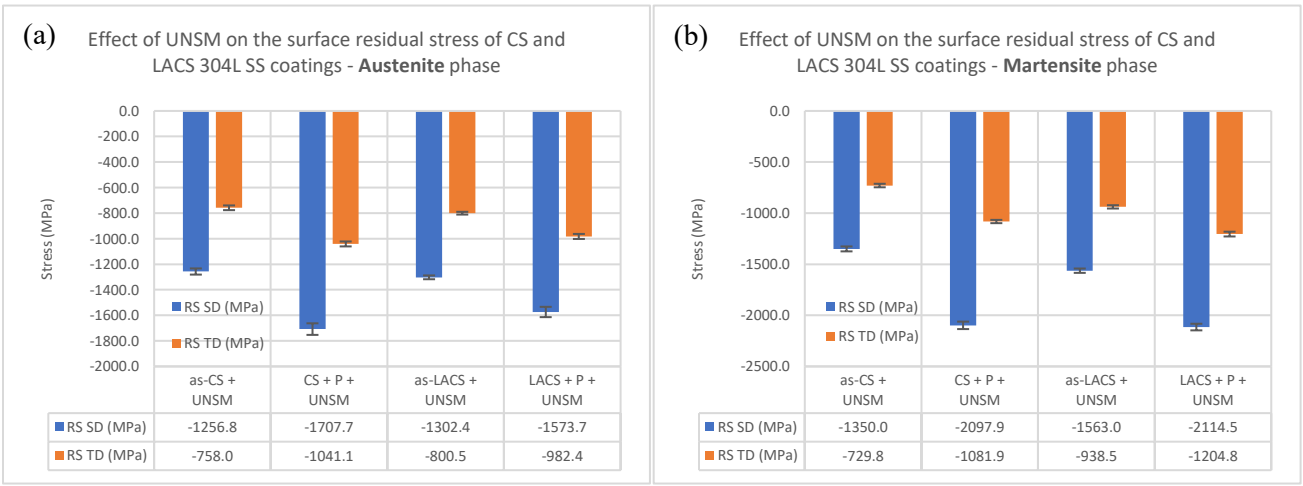

Figure 5.31: Effect of UNSM treatment on the surface residual stress measurements of as sprayed and polished CS and LACS 304L SS coatings pertaining to (a) austenite phase and (b) martensite phase.

It was established earlier in section 4.2.5, that polishing the CS and LACS 304L SS coatings resulted in higher SRSs than that were present on the surface of the as sprayed CS and LACS coatings. Now, it can be observed that the SRSs related to both austenite and martensite phases of CS + P + UNSM & LACS + P + UNSM specimens are higher than the SRSs of as-CS + UNSM and as-LACS + UNSM specimens indicating that the higher SRSs present in the polished coatings than those of the SRSs in the as sprayed coatings are heightening proportionately to higher magnitudes upon subjecting the as sprayed and polished CS and LACS coatings to UNSM surface treatment. That is the magnitude of SRS present on the respective specimen's surface prior to its surface treatment is having an influence on the magnitude of SRS obtained on the specimen's surface after its UNSM surface treatment. Also, the residual stresses due to austenite and martensite phases are not equi-biaxial.

Through-the-depth residual stress profiles of **UNSM treated** CS and LACS 304L SS coatings: Effect of UNSM on the RS depth profile of **CS** specimens: The residual stress depth profiles performed on both the as-CS + UNSM and CS + P + UNSM specimens with respect to both the austenite and martensite phases along both of their orthogonal directions are presented in figure 5.32. The RS depth profiles of UNSM treated CS specimens pertaining to their martensite phase shown in figure 5.32 (c) could be attained only up to a depth of ~ 90 μm, beyond which strong martensite peaks were not present. Whereas the RS depth profiles of UNSM treated as-CS and CS + P coatings pertaining to their austenite phase are presented in figure 5.32 with (a) and (b) representing the depth profiles along their SD and TD respectively. The impact of UNSM on through the depth RS of CS coatings was determined by comparing the heightened CRSs due to UNSM with the already present CRSs in the CS coating prior to surface treatment. The vast increase in CRSs in the CS coatings due to UNSM treatment could be observed along their SD and

TD up to a depth of ~ 350 µm and 260 µm in the as-CS + UNSM specimen and up to a depth of ~330 µm and 310 µm in the CS + P + UNSM specimen respectively from their respective surfaces.

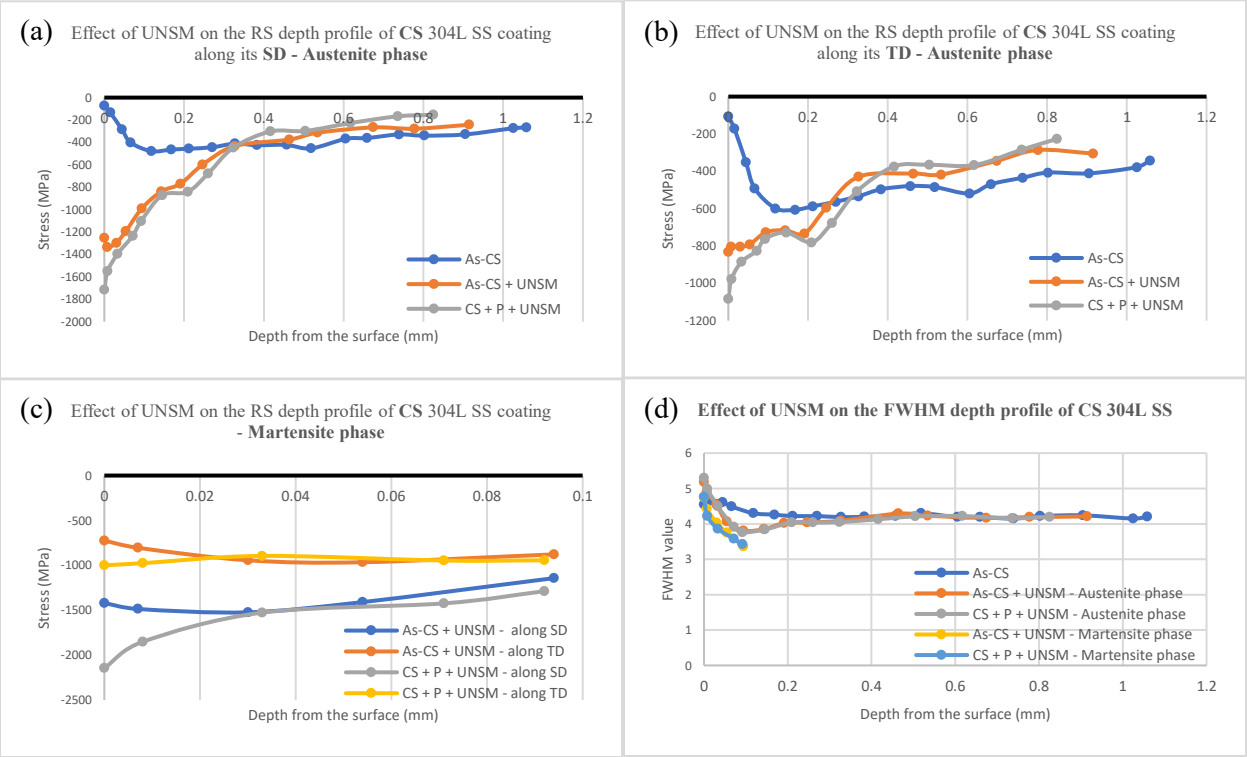

Figure 5.32: Residual stress depth profiles of as-CS + UNSM and CS + P + UNSM specimens pertaining to their austenite phase along their (a) step direction, and (b) transverse direction, (c) pertaining to their martensite phase along both the orthogonal directions, and (d) all their corresponding FWHM depth profiles.

The FWHM depth profiles of UNSM treated CS specimens with respect to both austenite and martensite phases are compared against the FWHM depth profile of as-CS specimen in figure 5.32 (d). The FWHM profiles pertaining to martensite phase of UNSM treated CS specimens show that the plasticity due to martensite phase increases only at the top surface of the coating and decreases drastically along its depth. The FWHM profiles pertaining to the austenite phase of UNSM treated CS specimens show a notable increase in their near-surface plastic strain due to UNSM but is confined to a mere 20 µm depth from their surface. At their sub-surface between 20 and 200 µm, there is a marginal decrease in plastic strain in both the as-CS + UNSM and CS + P + UNSM specimens before retreating to the levels of strain already present in the as-CS specimen.

This decrease in plastic strain at the sub surface after UNSM of the CS coating can be attributed to dynamic recovery and dynamic recrystallization occurring through SPD during UNSM. Dynamic recrystallization occurring in an already heavily deformed material can help redistribute the plastic strain to the newly formed grains resulting in a decrease of the strain concentration that was present in the former heavily deformed areas. Therefore, it can be concluded that UNSM is resulting in sub-surface strain relief of the heavily deformed CS coating up to a small depth.

Effect of UNSM on the RS depth profile of **LACS** specimens: The RS depth profiles performed on both the as-LACS + UNSM and LACS + P + UNSM specimens with respect to both the austenite and martensite phases along both their SD and TD are presented in figure 5.33. The RS due to martensite phase in both the UNSM treated LACS specimens could be obtained only up to a depth of 60 µm – 70 µm and the respective depth profiles are given in figure 5.33 (c). Beyond 60 µm - 70µm depth of UNSM treated LACS specimens, strong enough martensite peaks were not present in either of the orthogonal directions of the specimen representing the disappearance of martensite phase. Whereas the RS depth profiles pertaining to the austenite phase of UNSM treated LACS specimens along their SD and TD are given in figure 5.33 (a) and (b) respectively which were carried out until the CRSs seen at their surface transformed to TRS state along their depth in both of their orthogonal directions. The CRSs in both as-LACS + UNSM and LACS + P + UNSM specimens were present up to a depth of ~ 390 µm and 420 µm from their surface along the SD and TD of UNSM respectively.

The FWHM depth profiles of UNSM treated LACS specimens with respect to both the austenite and martensite phases are compared against the FWHM depth profile of as-LACS specimen in figure 5.33 (d). The FWHM profiles related to both the austenite and martensite phases after UNSM show substantial increase in plastic strain at the surface of the coatings which

gradually decreased along their depth. The significantly high degree of plasticity induced by the surface treatment into both the LACS coatings can be seen up to a depth of ~ 200 µm from their surface, as can be observed from the FWHM profiles pertaining to the austenite phase of the UNSM treated LACS specimens. Beyond 200µm depth, the plastic strain appears to have reverted to the levels present in the untreated LACS coating. This increase in plastic strain observed from the surface treated LACS specimens FWHM profiles corelates well with the observation made from the increase in average KAM value signifying the increase in plastic strain / dislocation density in UNSM treated LACS coating while comparing the EBSD analysis in figures 4.7 & 5.13.

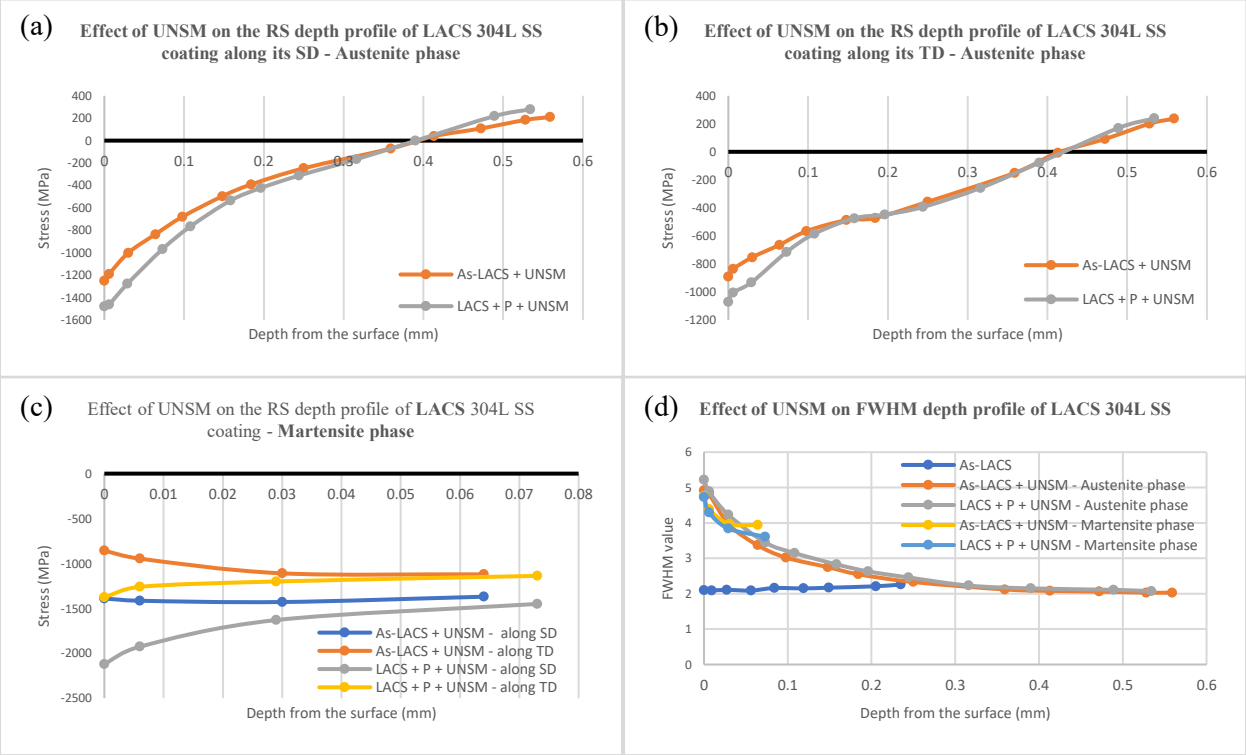

Figure 5.33: Residual stress depth profiles of as-LACS + UNSM and LACS + P + UNSM specimens pertaining to their austenite phase along their (a) step direction, and (b) transverse direction, (c) pertaining to their martensite phase along both the orthogonal directions, and (d) all their corresponding FWHM depth profiles.

The depth of presence of martensite and the depth of induction of CRSs data obtained for all the UNSM treated CS and LACS coatings are consolidated into table 5.6. In both CS and LACS coatings subjected to UNSM treatment no notable differences in the depth of induction of CRSs

or the depth of presence of martensite could be seen between them i.e., between as sprayed + UNSM vs polished + UNSM treated CS and LACS coatings. Therefore, the difference in the impact of UNSM with respect to the surface condition (as sprayed or polished) of the CS and LACS coatings was majorly confined to the near-surface compressive residual stresses only.

	Depth of CRS along SD of UNSM - Austenite phase (mm)	Depth of CRS along TD of UNSM - Austenite phase (mm)	Depth of martensite presence (mm)
As-CS + UNSM	0.35	0.26	0.09
CS + P + UNSM	0.33	0.31	0.09
As-LACS + UNSM	0.39	0.42	0.06
LACS + P + UNSM	0.39	0.42	0.07

Table 5.6: Depth of presence of martensite and depth of induction of CRSs by UNSM on CS and LACS coatings.

Finally, it can be concluded that the UNSM surface treatment of the CS and LACS coatings enormously increased their SRS magnitudes in the compressive region lasting up to an appreciable depth from the specimen's surfaces which can be extremely beneficial in improving the SCC resistance of the CS and LACS 304L SS coatings.

AFS 304L SS:

The UNSM treatment was performed on the AFS specimens by aligning the SD and TD of UNSM process with that of the AFS specimens. The XRD phase analysis performed on the UNSM treated AFS specimens revealed that both as-AFS + UNSM and AFS + P + UNSM have undergone a 100% martensitic phase transformation at their surface (figure 5.19). Therefore, the SRS measurements of UNSM treated AFS specimens given in figure 5.34 are pertaining to martensite phase measured by Cr X-ray tube whereas the SRS of untreated AFS specimens are pertaining to austenite phase measured by Mn X-ray tube using Proto LXRD system. The SRSs of AFS specimens have increased enormously in the compressive region due to UNSM treatment in both as-AFS and AFS + P specimens to magnitudes of - 2370 MPa and - 1990 MPa along the SD and -

1434 MPa and -1040 MPa along the TD respectively. The high magnitude of compressive residual stresses (CRSs) introduced into the specimens by UNSM is due to the severe plastic deformation and extreme grain refinement leading to dislocation pile up near the surface creating a stress field that induces compressive stresses in the material. Moreover, like the EBSD and hardness analysis, the SRS after UNSM of as-AFS cladding was measured to be higher than that of the UNSM treated AFS + P specimen due to the assistance of nano grains present at the as-AFS specimen's surface.

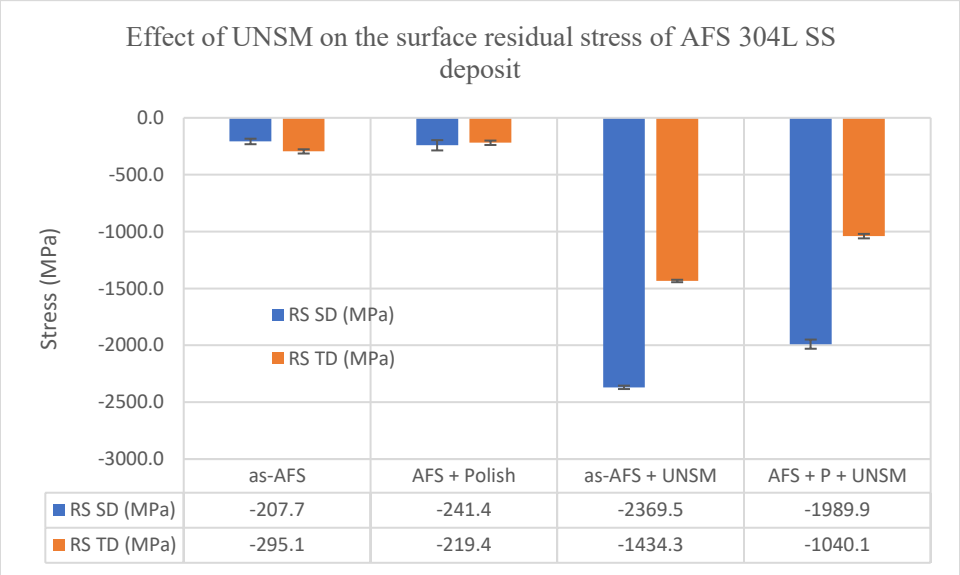

	as-AFS	AFS + Polish	as-AFS + UNSM	AFS + P + UNSM
RS SD (MPa)	-207.7	-241.4	-2369.5	-1989.9
RS TD (MPa)	-295.1	-219.4	-1434.3	-1040.1

Figure 5.34: Surface residual stress measurements of as deposited and polished AFS 304L SS before and after UNSM treatment.

Through-the-depth residual stress (SRS) analysis of UNSM treated AFS specimens: The surface of AFS specimens was found to have been transformed from austenite to 100 % martensite upon UNSM treatment due to the SPD. However, the amount of martensite content will decrease through the depth with a subsequent increase in austenite phase because of the gradient microstructure created by UNSM treatment. Therefore, the residual stress depth profile of UNSM treated AFS specimens was performed at every depth interval with respect to both austenite and martensite phases until the martensite phase disappears completely. The residual stress depth profile with respect to austenite phase was performed until the compressive residual stresses induced by UNSM transform to tensile residual stresses (TRSs) which helps in determining the

depth impact of UNSM in inducing CRSs.

The RS depth profiles performed on both as-AFS + UNSM and AFS+ P + UNSM specimens with respect to austenite and martensite phases along both SD and TD of UNSM are presented in figure 5.35. The RS depth profiles due to martensite phase are given in figure 5.35 (c) which shows that the depth up to which martensite phase could be found in as-AFS + USNM and AFS + P + UNSM was limited to ~ 60 μm and 100 μm respectively. The RS depth profiles related to the austenite phase in UNSM treated AFS specimens along their SD and TD are given in figure 5.35 (a) and (b) respectively. Comparing the RS depth profiles pertaining to austenite phase with that of martensite phase, it can be noticed that until the little while martensite existed, the RS due to it has always been higher than RS due to austenite phase showing that the stress due to them is not equi-biaxial. The CRSs in as-AFS + UNSM specimen measured with respect to austenite phase could be observed up to a depth of 500 μm and 520 μm along SD and TD of UNSM respectively. Whereas the CRSs in AFS + P + UNSM specimen could be found up to 560 μm and 470 μm from the surface along the SD and TD of UNSM respectively.

The FWHM depth profiles of UNSM treated AFS specimens related to both austenite and martensite phases are displayed in figure 5.35 (d). FWHM values represent the degree of plastic strain present in a material. The FWHM profiles of UNSM treated AFS specimens related to both austenite and martensite phases show significantly higher plastic strain near-surface which gradually decreased through their depth. The near-surface plastic strain of as-AFS + UNSM specimen is considerably higher than AFS + P + UNSM specimen due to both austenite and martensite phases. Therefore, the correlation of near-surface plastic strain observed from these FWHM values aligns exceptionally well with the plastic strain determined from the KAM maps during EBSD analysis (figures 5.14 and 5.15). Also, the plastic strain induced by UNSM through

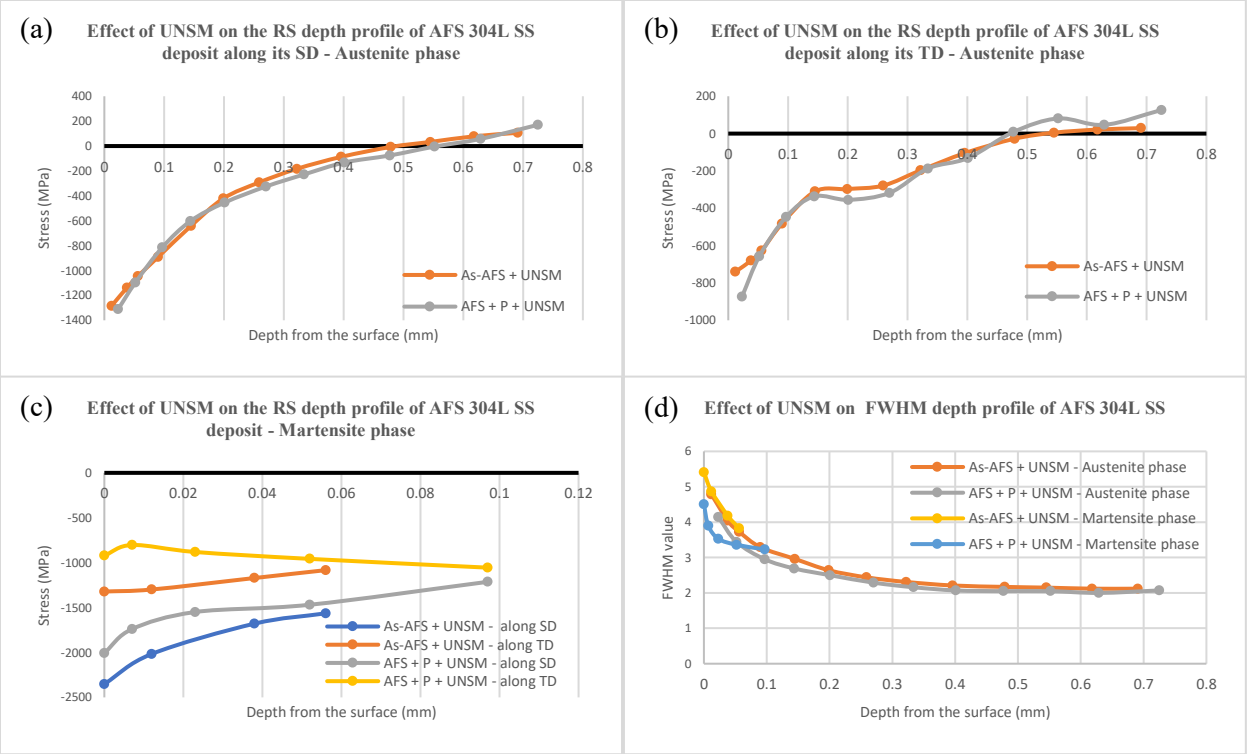

Figure 5.35: Residual stress depth profiles of as-AFS + UNSM and AFS + P + UNSM specimens pertaining to their austenite phase along their (a) step direction, and (b) transverse direction, (c) pertaining to their martensite phase along both orthogonal directions, and (d) all their corresponding FWHM depth profiles.

the depth of AFS specimens could be seen from the austenite phase FWHM profiles. The induction of plastic strain by UNSM in as-AFS specimen appears to be higher than AFS + P + UNSM throughout their depth up to 200 µm beyond which not much difference exists between them. Also, the increase in plastic strain due to UNSM in both AFS specimens could be seen up to a depth of ~ 300 µm from their surface before becoming constant beyond it.

5.2.6 Corrosion Analysis – Sensitization / Susceptibility Behavior

<u>Sensitized 304L SS</u>:

The DLEPR test curves of SA, S5, and S24 304L SS specimens before and after their UNSM treatment are compared in figure 5.36 (a), (b), and (c) respectively. Whereas the relevant data pertaining to these specimens showing the effect of UNSM treatment on their degree of sensitization (DOS) ratios is presented in table 5.7.

Specimen condition	Peak Activation Current Density, Ia (A/cm^2)	Peak Re-Activation Current Density, Ir (A/cm^2)	Degree of Sensitization, %DOS = ((Ir/Ia) *100)	Corrosion potential, Ecorr (mV)	Passivation potential, Epp (mV)	Epp - Ecorr
SA	5.60E-02	1.80E-06	0.003	-430	159	589
SA + UNSM	4.85E-02	1.90E-05	0.039	-427	53	480
S5	5.14E-02	1.52E-03	2.95	-426	153	580
S5 + UNSM	5.52E-02	1.60E-04	0.29	-443	62	505
S24	5.99E-02	8.44E-03	14.1	-420	184	604
S24 + UNSM	6.42E-02	9.81E-03	15.3	-445	130	575

Table 5.7: Degree of sensitization ratios and the relevant corrosion data, showing the impact of UNSM treatment on the SA, S5, and S24 304L SS specimens.

Figure 5.36 (a) compares the DLEPR curves of SA specimen before and after UNSM treatment. The Epp-Ecorr value of SA specimen decreased considerably by 109 mV after UNSM treatment showing that its passivation behavior improved by the surface treatment. The improvement in the passivation behavior of SA specimen by UNSM can be attributed to the extreme grain refinement caused by the surface treatment in the SA specimen resulting in smaller sized grains that can accelerate the formation of passive film on its surface. However, the DOS ratio obtained for the UNSM treated SA specimen was 0.039 % which increased considerably from that of the untreated SA specimen's DOS ratio (0.003 %) but in hindsight it's value is still considerably lower than the DOS ratio of S5 specimen (2.95 %). The increase in the DOS ratio of SA specimen after its UNSM treatment can be attributed to the severe pounding of WC tool tip on its surface leading to the formation of peaks and valleys at its surface as seen in figure 5.24. These minor peaks and valleys present on the surface of UNSM treated SA specimen can act as crevices/initiation sites for the breakdown of passive film during the reverse scan of the DLEPR test leading to slightly higher amount of uniform corrosion occurring on its surface than when compared to the untreated SA specimen's surface during their respective DLEPR corrosion tests. These observations are affirmed by the BSE micrographs of untreated SA and SA + UNSM treated

specimens seen in figure 5.37 which clearly show that the UNSM treated SA specimen is undergoing slightly more uniform corrosion than that of the untreated SA specimen. Also, unlike the sensitized specimens S5 and/or S24, the UNSM treated SA specimen's micrograph does not show the formation of any deeper ditches on its surface, confirming that there is no localized corrosion occurring anywhere on its surface due to the preferential attack of the corrosive solution.

Figure 5.36 (b) compares the DLEPR curves of S5 specimen before and after UNSM treatment. They show that UNSM treatment had a huge positive impact on the DOS ratio of S5 specimen, with it's value decreasing immensely by 10X times from 2.95 % prior to surface treatment to 0.29 % after surface treatment. Visually as well, from the BSE micrographs showing the surface of untreated and surface treated S5 specimens after their DLEPR test in figure 5.37, a clear distinction in their micrographs could be observed with only a very few shallow ditches seen on the UNSM treated S5 specimen surface as opposed to a lot of them seen on the untreated S5 specimen surfaced indicating an improvement in the sensitiation behavior of S5 specimen by

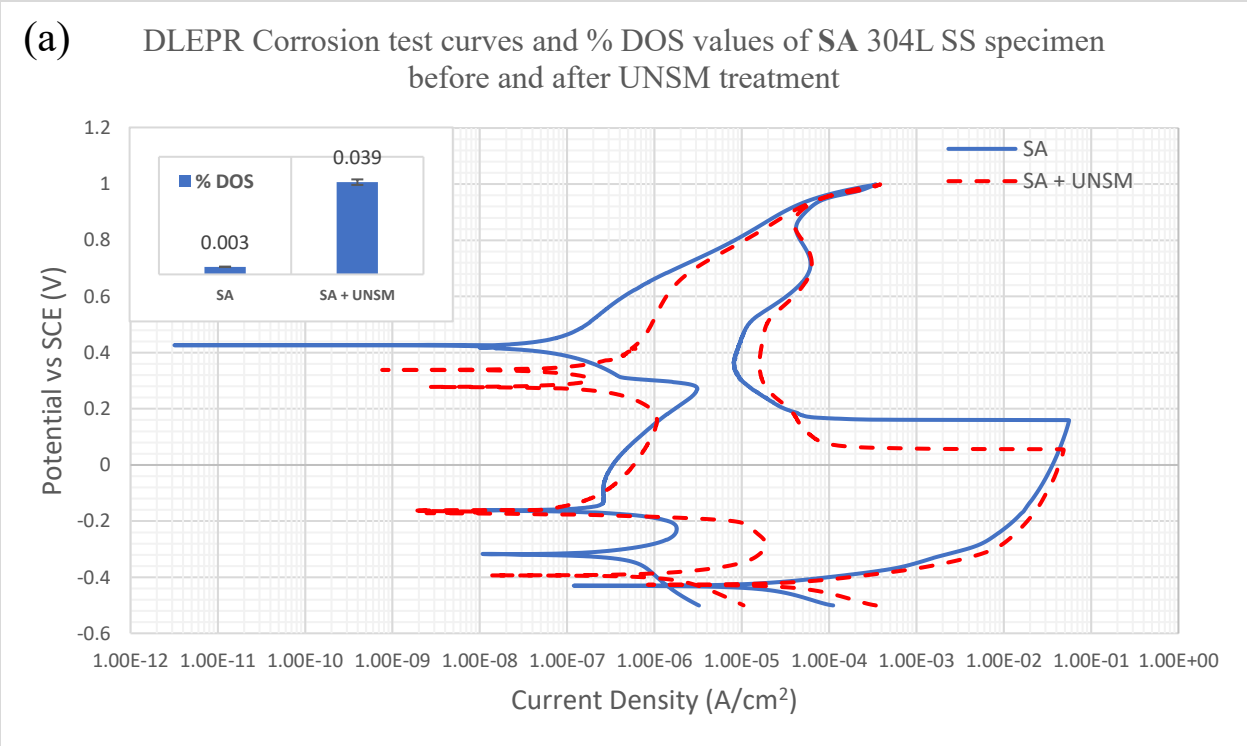

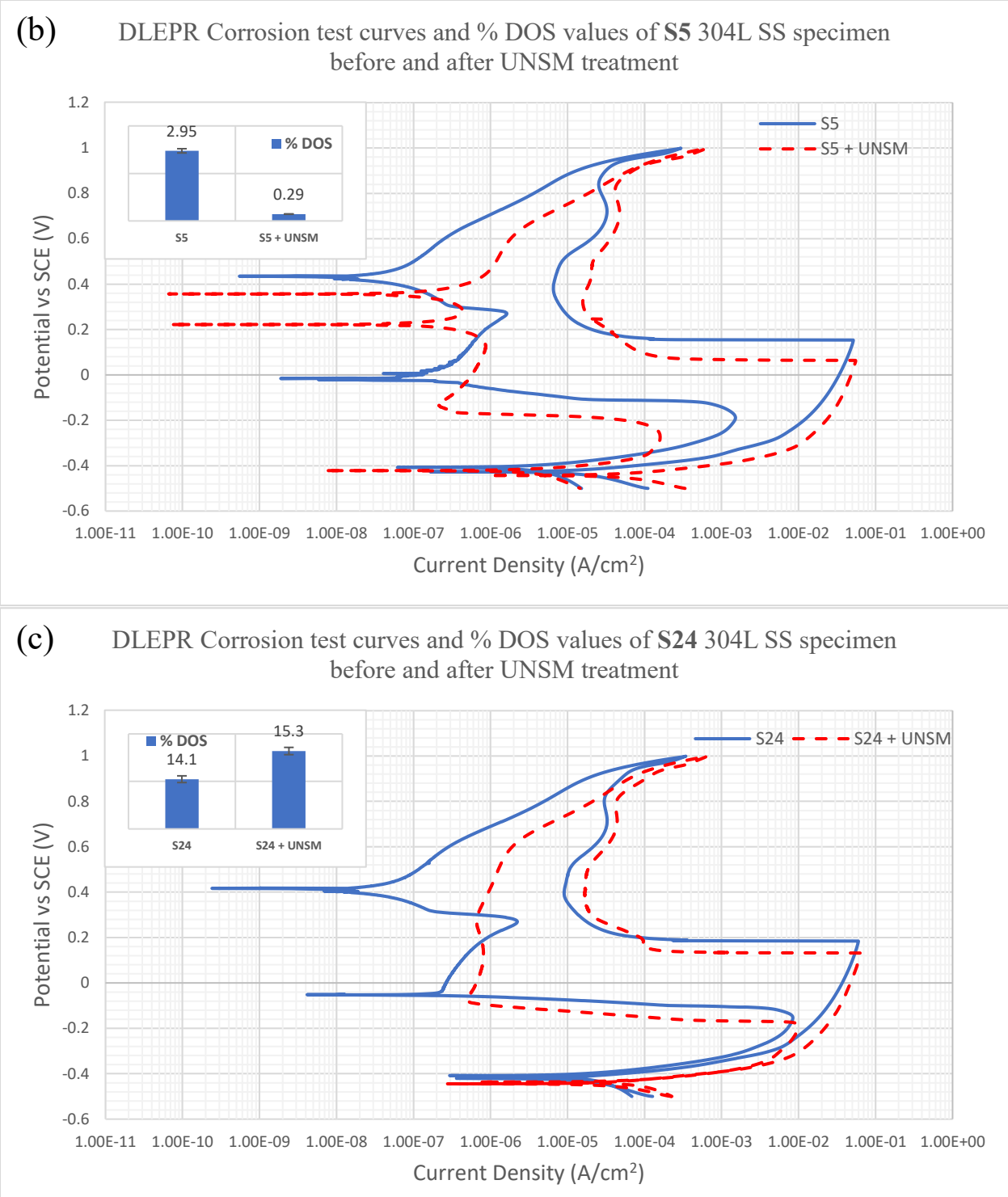

Figure 5.36: DLEPR Corrosion test curves and the corresponding % degree of sensitization values, showing the effect of UNSM treatment on the sensitization behavior of (a) SA, (b) S5, and (c) S24 304L SS specimens.

UNSM treatment. The improvement in the sensitization behavior of S5 specimen by UNSM treatment can be attributed to Cr redistribution occurring in the S5 specimen as a result of the

extreme grain refinement casued by the SPD in the specimen during its UNSM treatment. Due to the Cr redistribution occurring in the UNSM treated S5 specimen, the overall surface area of the small and isolated CDZs that were present in the untreated S5 specimen would decrease in the UNSM treated S5 specimen leading to the formation of a stronger chromium oxide film on the latter specimen surface that would greatly resist localized corrosion during the reverse scan of its DLEPR test yeilding a much improved DOS ratio for it. Additionally, the Epp-Ecorr value of S5 specimen also decreased after its UNSM treatment by 75 mV indicating a betterment of its passivation behavior due to the extreme grain refinement occurring in it by the surface treatment. However, the improvement seen in the passivation behavior of UNSM treated S5 specimen was not as prominent as it was seen in the UNSM treated SA specimen because of the few remaining CDZs that were still present on the UNSM treated S5 specimen surface as can be stated by observing its after DLEPR test surface shown in the BSE micrograph of figure 5.37 which is showing a few shallow ditches being formed on its surface during its DLEPR test.

Figure 5.36 (c) compares the attained DLEPR curves of S24 specimen before and after UNSM treatment. The DOS ratios obtained for the untreated and UNSM treated S24 specimens are 14.1 % and 15.3 % respectively, showing no positive impact due to UNSM treatment on it. The BSE micrographs in figure 5.37 showing the after DLEPR test surfaces of S24 specimens without and with UNSM treatment also show similar surfaces with almost the same number of well-connected or merged ditches being formed. The only minor difference that was observed between them is that the ditches formed on the untreated S24 specimen surface have sharper edges whereas the ditches formed on the UNSM treated S24 specimen surface have rounder or hazy edges which could be due to smudging of the CDZ edges by WC tool tip during UNSM. Unlike S5 specimen which had small and isolated CDZs, the S24 specimen has large interconnected CDZs which could

Solution Annealed + DLEPR tested.

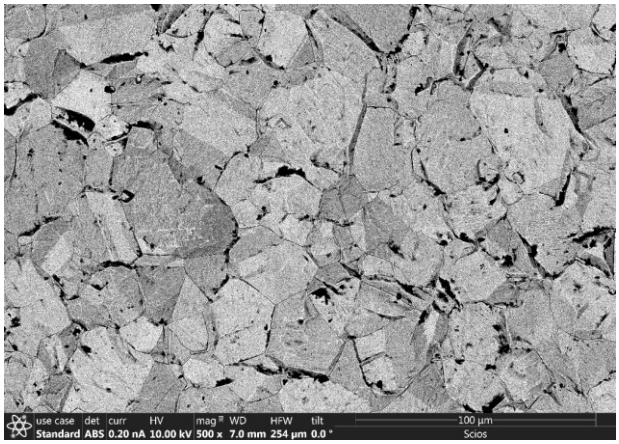

Solution Annealed + UNSM + DLEPR.

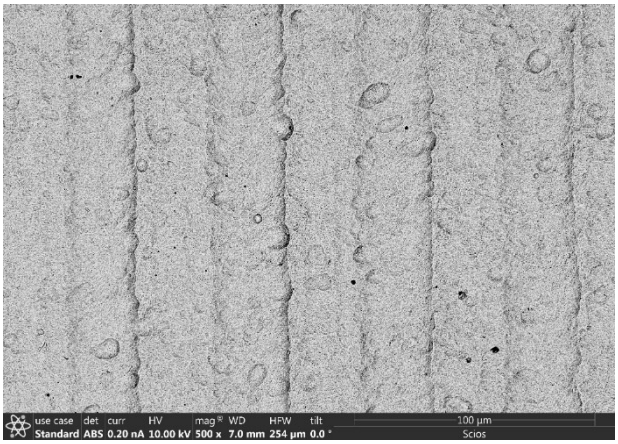

Sensitized at 650°C, 5h + DLEPR.

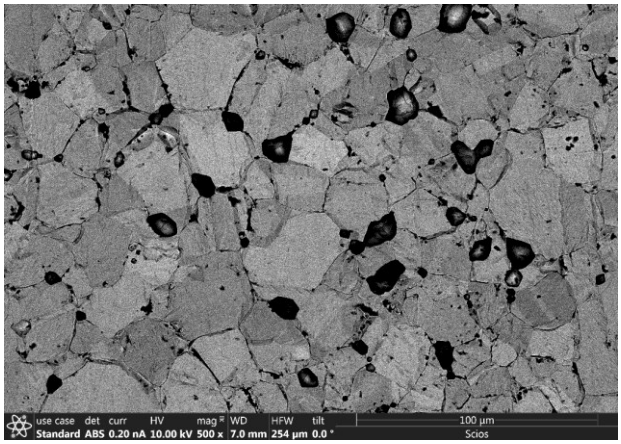

Sensitized at 650°C, 5h + UNSM + DLEPR.

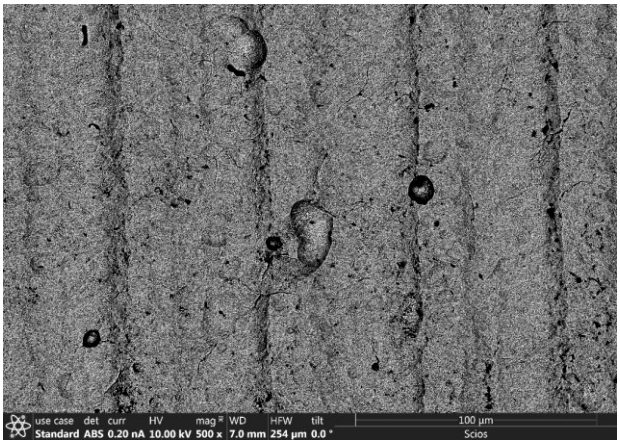

Sensitized at 650°C, 24h + DLEPR.

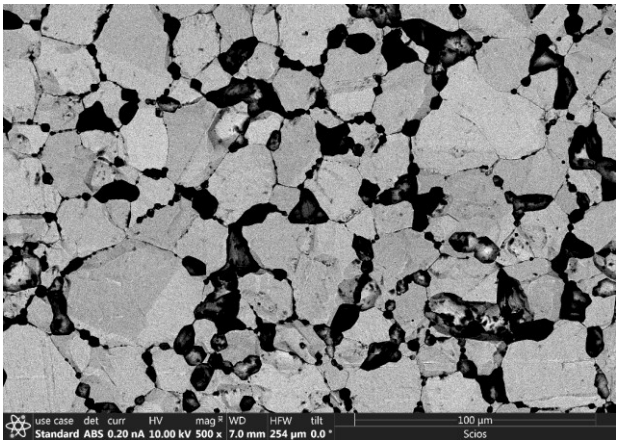

Sensitized at 650°C, 24h + UNSM + DLPER.

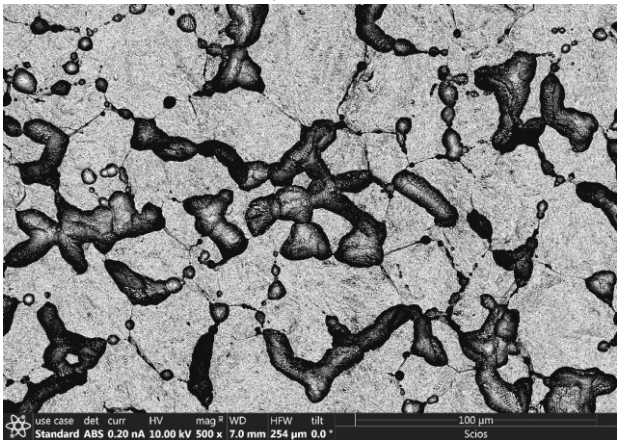

Figure 5.37: BSE micrographs showing the surface after DLEPR testing of SA and sensitized for 5h and 24h at 650°C 304L SS specimens on the left side and the surface after DLEPR testing of their UNSM treated counterpart specimens on the right side.

not be impacted or reduced by UNSM treatment because of their larger and wider sizes, as well as their interconnectedness. Moreover, despite the significant grain refinement caused in the S24

specimen by UNSM, its Epp-Ecorr value exhibited a decrement of only 29 mV upon its UNSM treatment from that of its untreated specimen's value, showing only a minor improvement in its passivation behavior by UNSM which could be because of the large unaffected CDZs being still present on its surface even after the surface treatment.

So, in conclusion, it can be expressed that UNSM treatment was not able to redistribute Cr to the larger well-interconnected CDZs present in S24 specimen, leading to the hypothesis that the positive impact of UNSM treatment on the sensitization behavior of sensitized 304L SS speicmens has a limitation and that it depends on the critical size and distribution characteristics of CDZs present in the material. More research would have to be done to ascertain the critical size of CDZs up to which the UNSM treatment can positively influence in redistributing Cr content to i.e., leading to a reduction in the total area of CDZs present in the material thereby, resulting in an overall decrease in the DOS ratio of a sensitized 304L SS material by UNSM treatment. However, it can be concluded that UNSM treatment could be effective in reducing the DOS of welded 304L SS material since a welded material undergoes sensitization phenomenon for only a few minutes to less than an hour depending on the welding technique being employed. Also, even though UNSM treatment cannot effectively improve the sensitization behavior of 304L SS alloy that has undergone sensitization phenomenon for a longer time period, its residual stress state and mechanical properties can be improved drastically by UNSM treatment which could be extremely benefical in improving its SCC resistance characteristics.

CS & LACS 304L SS:

The DLEPR curves of untreated and surface treated as sprayed and polished CS and LACS 304L SS specimens are compared in figures 5.38 (CS) and 5.40 (LACS). The corrosion data such as Ecorr, Epp, Ia, Ir acquired from the DLEPR curves and the calculated Epp - Ecorr &

DOS ratios of the UNSM treated CS and LACS 304L SS coatings are consolidated in table 5.8.

Specimen designation	Peak Activation Current Density Ia (A/cm2)	Peak Re-Activation Current Density I_r (A/cm^2)	Degree of Susceptibility, %DOS = ((I_r/I_a) *100)	Corrosion potential, Ecorr (mV)	Passivation potential, Epp (mV)	Epp - Ecorr
As-CS + UNSM	9.87E-02	1.38E-02	**13.9**	-433	318	751
CS + P + UNSM	8.72E-02	1.33E-02	**15.2**	-449	258	706
As-LACS + UNSM	7.78E-02	1.55E-02	**20.0**	-426	207	633
LACS + P + UNSM	8.68E-02	1.26E-03	**1.4**	-444	294	737

Table 5.8: Degree of susceptibility and corrosion data of UNSM treated CS and LACS 304L SS coatings obtained from their DLEPR curves in figures 5.38 and 5.39.

Passivation behavior of UNSM treated CS and LACS 304L SS coatings: The Epp – Ecorr values of all the UNSM treated CS and LACS specimens decreased from their respective untreated specimen's Epp – Ecorr values, suggesting that the surface treatment is improving the passivation behavior of both CS and LACS 304L SS coatings irrespective of their prior surface condition (i.e., UNSM performed on as sprayed or polished CS and LACS). UNSM treatment generally results in a uniform redistribution of alloy composition in the surface treated specimens which improves the passivation behavior of a specimen. Additionally, in case of the CS and LACS coatings, due to the severe pounding of WC tool tip on their surface, partial closure of their surface porosity sites occurs reducing their total surface pore area thereby, improving their passivation characteristics in this manner as well. Therefore, the combined effect of these two factors i.e., uniform redistribution of alloy composition and the reduction in the total surface pore area by UNSM would be the reason for the improvement seen in the passivation behavior of all the UNSM treated CS and LACS coatings from that of their untreated counterparts.

Sensitization behavior of **As-CS + UNSM and CS + P + UNSM** 304L SS coatings: The UNSM treatment performed on the as-CS and CS + P specimens resulted in a slight worsening of their DOS ratios from 12.1 % and 13.8 % to 13.9 % and 15.2 % respectively. Firstly, UNSM treatment process which does not involve the application of any significant amount of heat input

into the specimen being surface treated, will not be able to do anything to improve the inherently weak interparticle bonding existing in the CS coating. Therefore, UNSM treatment could not improve the sensitization behavior of the CS 304L SS coatings.

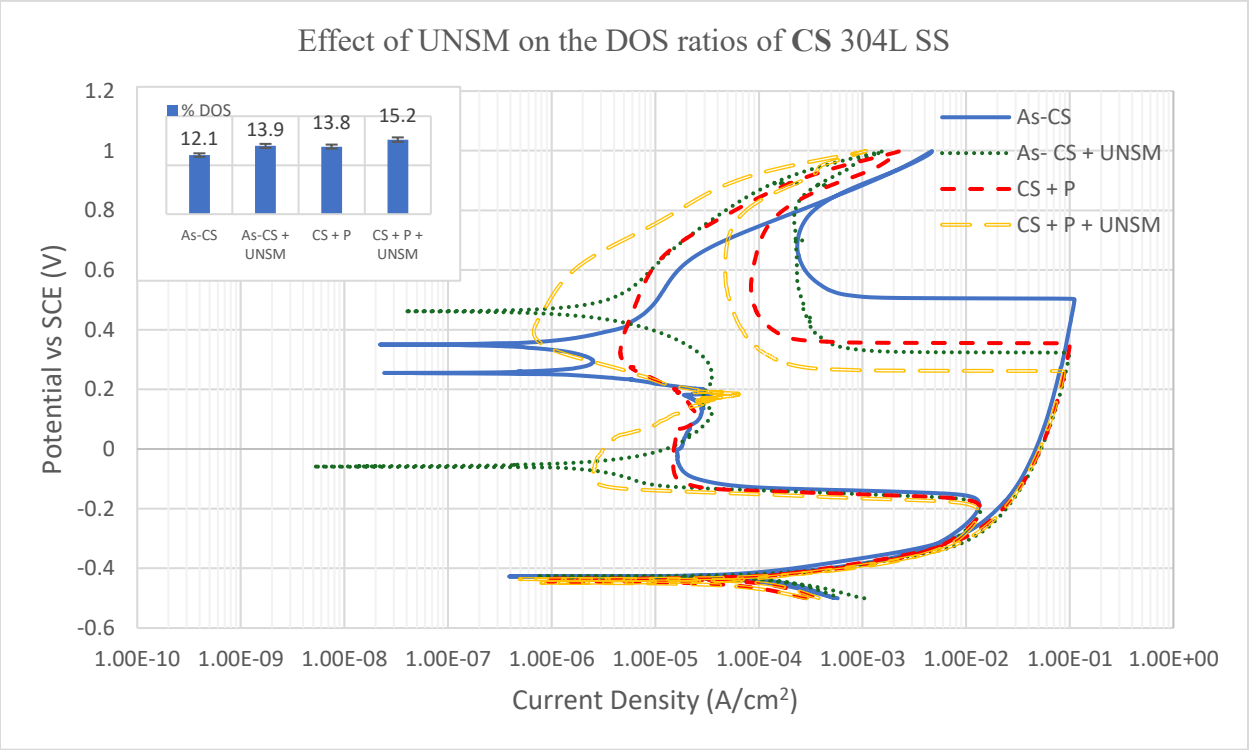

Figure 5.38: Effect of UNSM on the DLEPR corrosion test curves and % degree of susceptibility values of as sprayed and polished CS 304L SS coatings.

Moreover, the slight worsening seen in the DOS ratios of as-CS and CS + P specimens upon their UNSM surface treatment can be explained by observing their UNSM treated surfaces shown in figure 5.39 which show that the surface treatment has created many smudges on their surfaces along the UNSM tracks some of which are indicated by arrows in their SE micrographs in figure 5.39. These numerous sharp-edged smudges formed on the UNSM treated CS coatings surface can act as crevices or initiation sites where DLEPR test solution can attack preferentially leading to the breakdown of passive film and exposing the underneath metal to corrosion.

These smudges are formed on the surface of as-CS and CS + P specimens upon their UNSM treatment because of the higher hardness or the heavy plastic deformation already present in the

CS coatings prior to their surface treatment, would resist the WC tool tip penetration into the coatings, causing the material at the surface of the CS coatings to be smudged by the dynamic action of the WC tool tip during their UNSM treatment. The statement made in the prior sentence is also supported evidently by comparing the EBSD & hardness analysis performed on the untreated and surface treated CS coatings whose results are presented in figures 4.6, 5.12, and 5.21 which show that due to the extensive plastic deformation already present in the CS coatings, the impact of UNSM treatment on them was limited to only their utmost top surface of < 20 μm.

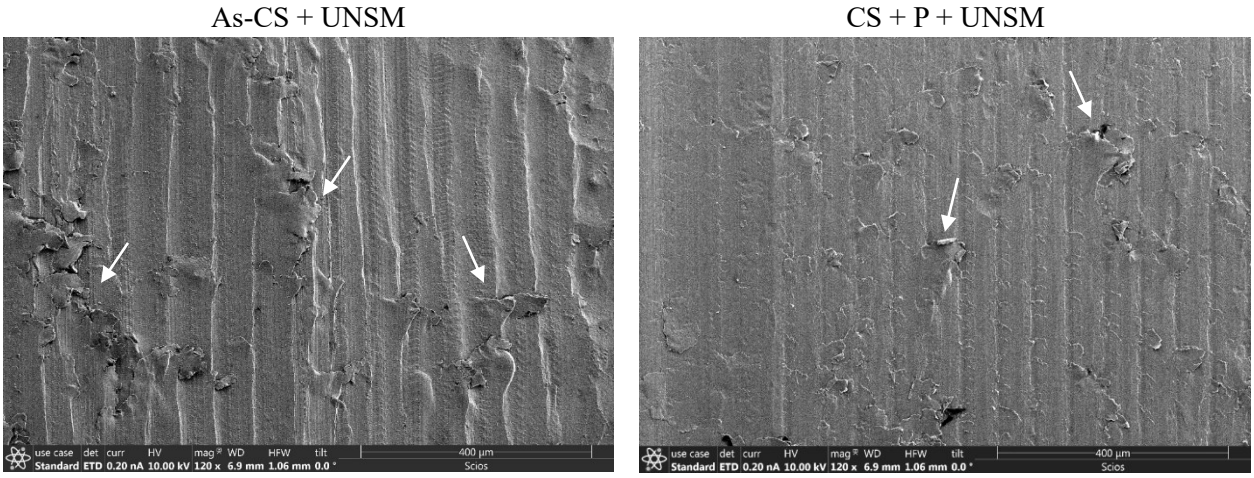

Figure 5.39: SE micrographs of as-CS and polished CS coatings showing the smudges formed on their surface due to UNSM treatment.

Although the following observation does not lead to any relevant consequences or conclusions, it is simply stated here, which is that the smudges formed on the surface of the as-CS + UNSM specimen appear thicker than the ones formed on the CS + P + UNSM specimen surface. The smudges formed on the former specimen appear thicker than those formed on the latter specimen because of an additional contributing factor apart from the higher hardness and/or prior plastic deformation present in the CS coatings which is the extremely high surface roughness of as-CS specimen from that of the CS + P specimen. The bubbled like rougher surface of as-CS specimen seen in figure 4.24, upon impact of WC tool tip on its surface tends to the creation of

thicker smudges than those formed by the WC tool tip's impact on the smoother surface of CS + P specimen.

Finally, it can be said that due to the prior heavy plastic deformation already present in the CS coatings, resisting the penetration of WC tool tip into the coatings during their UNSM treatment, tends to the formation of numerous smudges on the UNSM treated CS coating surfaces which act as crevice or initiation sites, where preferential attack of the corrosive test solution occurs during their DLEPR tests, contributing to the slight worsening in the DOS of UNSM treated CS coatings from that of their untreated counterpart specimens.

Sensitization behavior of **As-LACS + UNSM** 304L SS coating: The DOS ratios of untreated and surface treated as-LACS specimens determined from their respective DLEPR curves are 19.7 % and 20 % respectively indicating that UNSM surface treatment had no impact on improving the sensitization behavior of as-LACS coating. It was stated earlier that the untreated as-LACS coating had oxidized surface which contributed to its significantly high DOS ratio. Therefore, with both the as-LACS and as-LACS + UNSM specimens yielding almost the same DOS ratios indicates that UNSM treatment must not have had any impact on the oxide film of the as-LACS specimen.

To clearly determine the impact or non-impact of the UNSM treatment on the oxide film of the as-LACS specimen, EDS analysis was performed on the as-LACS + UNSM specimen whose results are presented in figure 5.41. The EDS analysis results show that the oxide layer on the as-LACS coating surface was broken down by UNSM as indicated by the absence of oxygen element in the EDS results obtained from the areas 1 and 2 in figure 5.41. However, some of the particles from the broken-down oxide film got embedded and/or finely dispersed on the surface of UNSM treated as-LACS specimen as indicated by the presence of oxygen element in the elemental

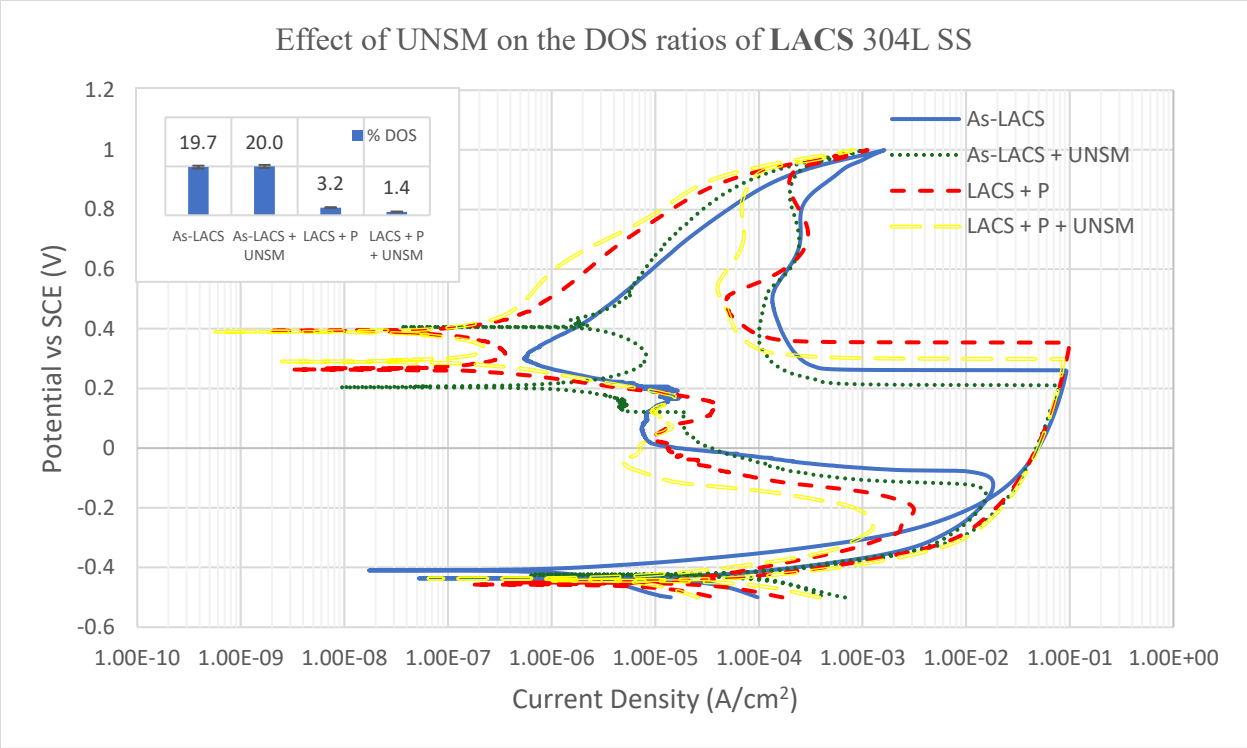

Figure 5.40: Effect of UNSM treatment on the DLEPR corrosion test curves and % degree of susceptibility values of as sprayed and polished LACS 304L SS coatings.

composition obtained from the EDS analysis performed at spots 1 and 2 in figure 5.41.

Moreover, similar to the CS coatings, the UNSM treatment of as-LACS coating led to the formation of smudges on its surface, some of which are shown by arrows in figure 5.41 (a). As reasoned with the CS coatings, the smudges on the as-LACS + UNSM specimen surface formed because of its bubbled like extremely high rougher surface (exhibiting an Ra value of ~ 16 µm) seen in figure 4.24.

As-LACS + UNSM surface

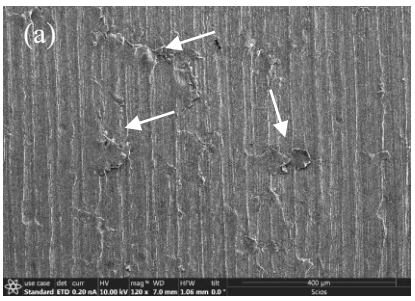

EDS analysis area

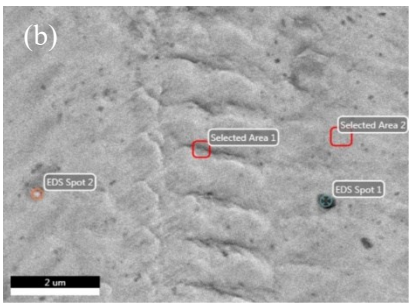

Element (Wt.%)	Area 1	Area 2	Spot 1	Spot 2
C K	5.51	4.42	3.14	14.39
FeL	55.36	39.66	10.32	26.3
CrK	39.12	55.92	64.52	29.5
O K			13	6.64
SiK			9.01	
CuL				17.9
S K				5.27

Figure 5.41: SE image of (a) as-LACS + UNSM treated specimen surface and (b) showing the area and spots where EDS analysis was performed on it along with the corresponding EDS analysis results.

Therefore, even though UNSM breaks down majority of the deleterious oxide film on the as-LACS specimen surface, the other consequences of UNSM treatment on its surface like the creation of smudged areas and the dispersion of broken-down oxide particles on the coating's surface led to the as-LACS + UNSM specimen obtaining an equally worse DOS ratio as that of the as-LACS specimen. That is the smudged areas and the dispersed oxide particles in the as-LACS + UNSM specimen act as localized corrosion sites for preferential attack of DLEPR test solution where passive film breaks down with relative ease which onsets the accelerated corrosion phenomenon in the surface treated as-LACS specimen similar to the untreated as-LACS specimen thereby, both the specimens yielding worse DOS ratios.

Sensitization behavior of **LACS + P + UNSM** 304L SS coating: The DOS ratio of LACS + P + UNSM treated specimen was measured to be 1.4 % showing an improvement of more than 2X times from that of the untreated LACS + P coating DOS ratio of 3.2 % even though the surface roughness of LACS + P coating increased slightly by UNSM surface treatment. The average surface roughness (Ra) value of LACS + P specimen increased from 0.02 ± 0.003 μm to 0.39 ± 0.068 μm after its UNSM surface treatment which can be considered as negligible when compared to the average Ra value of 16.3 ± 1.9 μm measured for the as-LACS coating.

Also, the UNSM surface treatment performed on the LACS + P coating did not create any smudges on the surface of LACS + P + UNSM specimen whose smudge free surface can be observed from its SE micrograph shown in figure 5.42. Since the surface of LACS coating was smoothened by polishing prior to its surface treatment, the bubbled surface of the as-LACS coating was eliminated which in turn avoided the formation of smudges due to the impact of WC tool tip on the LACS +P coating surface during UNSM. Also, the hardness and plastic strain present in the LACS coating were lower than the CS coating which allows a dynamically efficient penetration

of WC tool tip onto the surface of LACS coating thereby, resulting in a smudge free surface after its UNSM surface treatment unlike the CS + UNSM treated specimens.

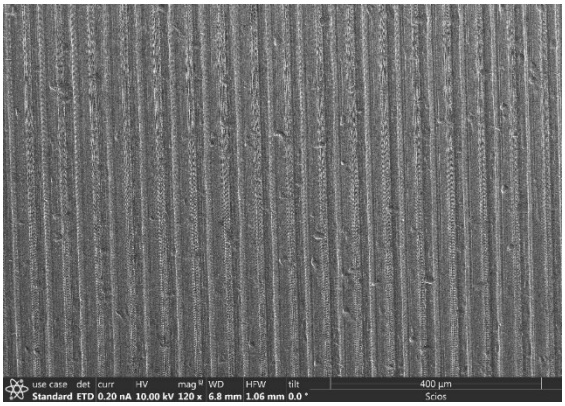

Figure 5.42: SE micrograph of LACS + P + UNSM treated 304L SS specimen surface.

Moreover, polishing of LACS coating removed the deleterious oxide film formed on the surface of as-LACS coating thereby eliminating the possibility of embedment of oxide particles onto the surface of LACS + P coating by its UNSM treatment. Furthermore, UNSM treatment on the LACS + P coating surface would result in the partial closure of porous sites at the absolute surface of the coating due to the severe pounding of WC tool tip on the coating's surface which reduces the total surface porous area that can be attacked preferentially by the corrosive test solution. Therefore, with the absence of both the sharp-edged smudges & embedded oxide particles that can act as localized corrosion sites combined with the partial closure of porosity sites by UNSM treatment without causing any notable increase in the surface roughness of LACS + P specimen led to the formation of a stronger passive oxide film on the surface of LACS + P + UNSM specimen, consequently resulting in a decrease in the corrosion during the reverse scan of its DLEPR test yielding a better DOS ratio than both the as-LACS + UNSM and untreated LACS + P specimens.

SE Micrography showing the after DLEPR test surfaces of as sprayed and polished CS and LACS coatings with and without UNSM treatment: The SE micrographs showing the corrosion

attack incurred on the as sprayed and polished CS and LACS coatings with and without UNSM treatment during their respective DLEPR corrosion tests are presented in figures 5.43 and 5.44 respectively. The corrosion attack on all the CS coatings appears to be more pronounced at their grain boundaries whereas on LACS coatings the corrosion attack seems to be affecting the material surface in a uniform manner. Within the CS coatings i.e., as sprayed and polished with and without UNSM treatment, no notable differences in their degree of corrosion can be observed from their after-DLEPR test micrographs shown in figure 5.43 which bodes well with the very close quantitative DOS ratios obtained for all the CS coatings.

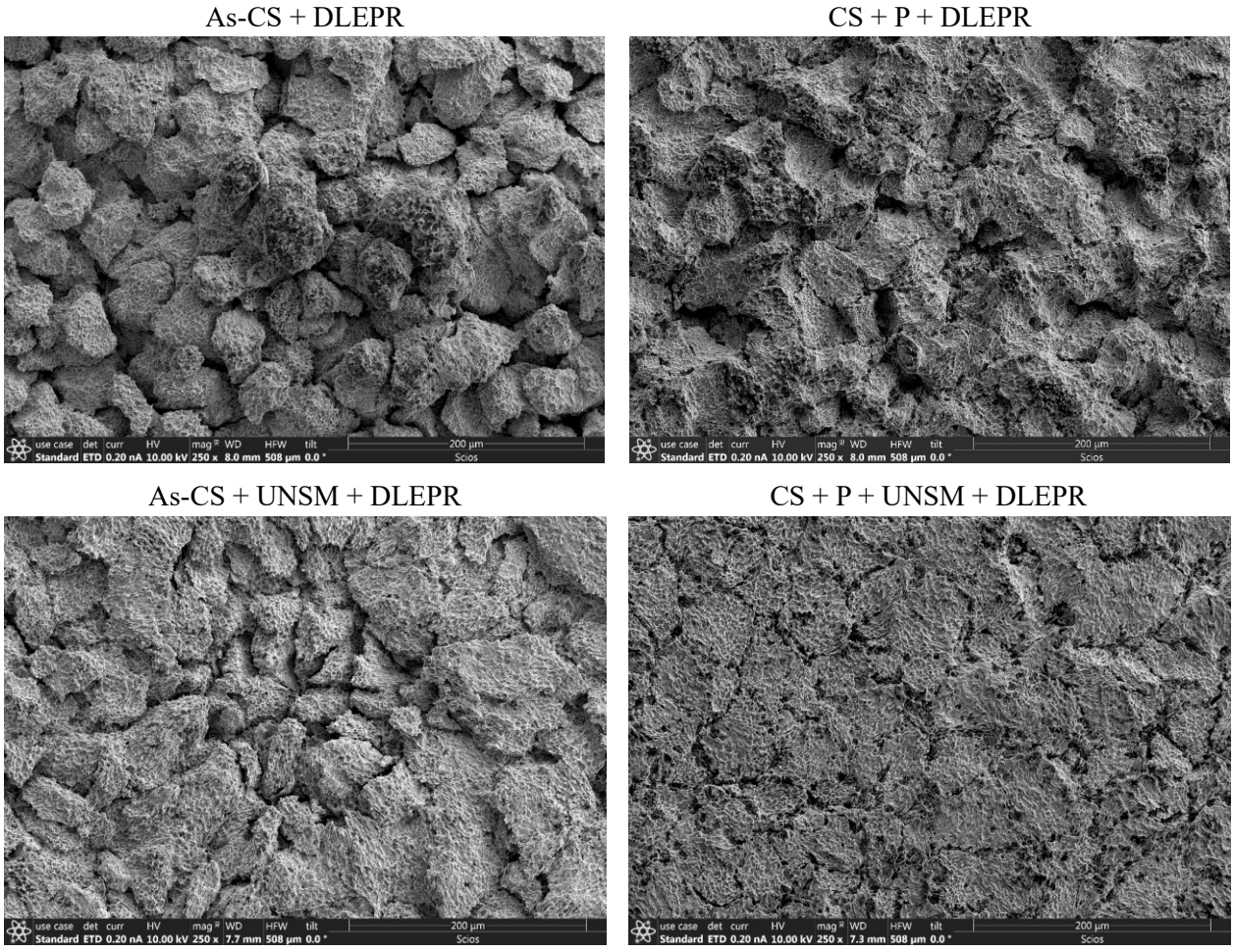

Figure 5.43: SE micrographs showing the surface after DLEPR testing of as sprayed and polished CS coatings with and without UNSM treatment.

Upon observing the after-DLEPR test micrographs of LACS coatings shown in figure 5.44, a clear distinction in the degree of corrosion can be seen between the as-LACS vs LACS + P specimen and their respective UNSM treated specimens as well. The corrosion dimples formed on the as-LACS specimen appear deep whereas the dimples formed on the LACS + P specimen appear shallow indicating the formation of a stronger passive film on the polished specimen surface resulting in it showing better corrosion resistance than the as-LACS specimen during their respective DLEPR tests as indicated by their respective DOS ratios.

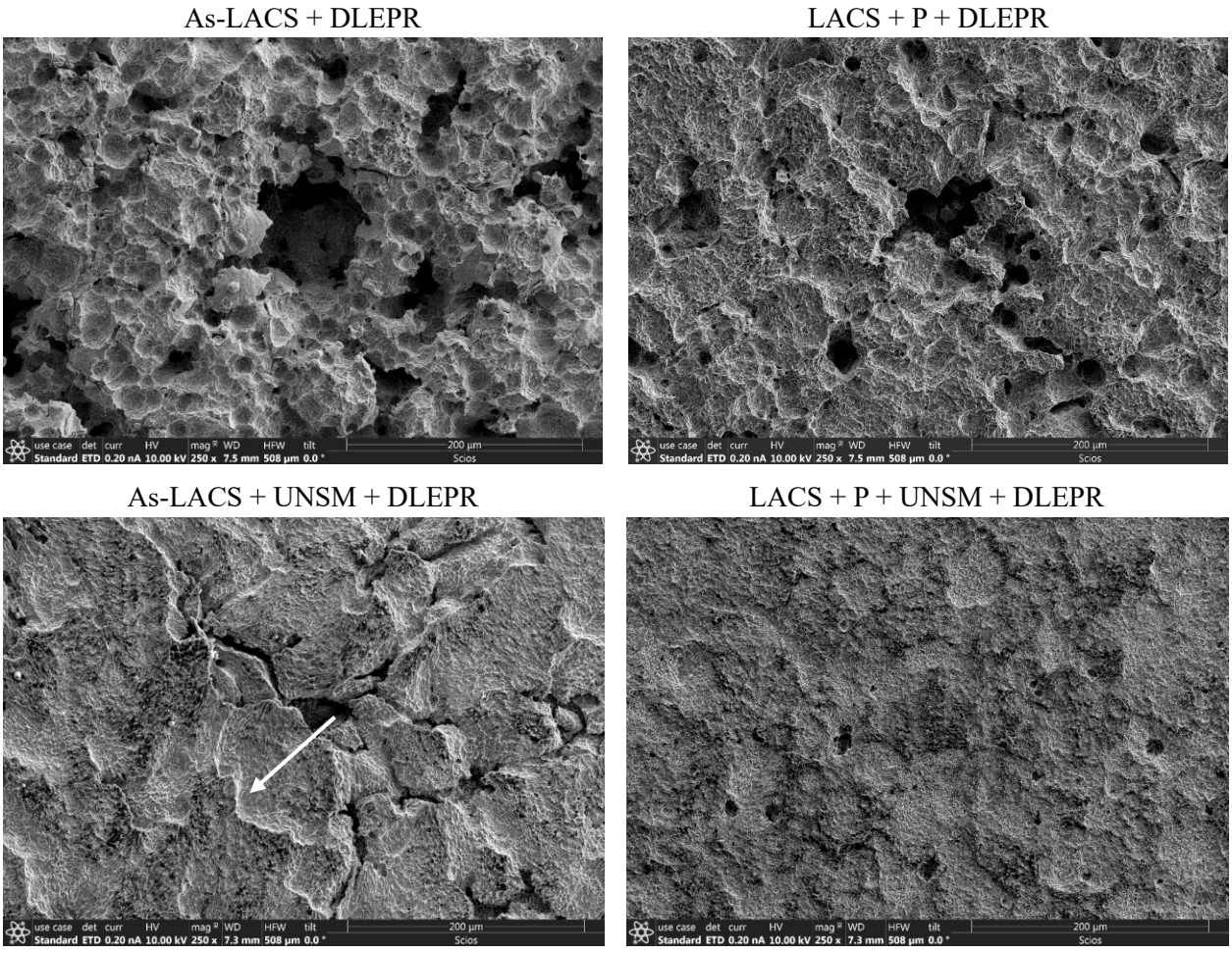

Figure 5.44: SE micrographs showing the after DLEPR test surface of as sprayed and polished LACS coatings without and with UNSM treatment.

The SE micrograph of as-LACS + UNSM + DLEPR tested specimen in figure 5.44 shows that the sharp-edged smudges observed in its prior to DLEPR testing micrograph in figure 5.41 (a)

have been corroded during its corrosion test, leaving trough shaped areas on the after DLEPR tested surface. Also, it seems like the corrosion during its DLEPR test might have initiated at or underneath those sharp-edged smudges with the corrosive test solution flowing inwards into them as shown by the arrow in figure 5.44 indicating the occurrence of a crevice type corrosion at the smudged areas on the as-LACS + UNSM surface.

The SE micrograph of LACS + P + UNSM + DLEPR tested specimen in figure 5.44 shows very few and smaller sized porous sites on its after-corrosion surface when compared to the untreated as-LACS or LACS + P specimens, pointing out that UNSM is leading to partial closure of porous sites at the surface of LACS + P coating that results in the strengthening of passive film formed on its surface thereby further improving the corrosion resistance / DOS ratio of LACS + P coating by UNSM.

AFS 304L SS:

The DLEPR test curves of as-AFS and polished AFS specimens before and after UNSM treatment are compared with as hot-rolled & SA 304L SS specimen in figure 5.45 and the data corresponding to UNSM treated as-AFS and AFS + P specimens is given in table 5.9.

Specimen designation	Peak Activation Current Density Ia (A/cm2)	Peak Re-Activation Current Density I_r (A/cm^2)	Degree of susceptibility, %DOS = ((I_r/I_a) *100)	Corrosion potential, Ecorr (mV)	Passivation potential, Epp (mV)	Epp - Ecorr
As-AFS + UNSM	4.67E-02	2.30E-02	**49.3**	-412	46.3	458
AFS + P + UNSM	5.32E-02	2.00E-05	**0.038**	-435	57.5	492

Table 5.9: Degree of susceptibility and other corrosion data pertaining to the UNSM treated as-AFS and AFS + P 304L SS specimens.

As-AFS + UNSM: The Epp – Ecorr and DOS ratio of as-AFS + UNSM treated specimen are measured to be 458 mV and 49.3% respectively. The SE micrographs of as-AFS + UNSM specimen before and after DLEPR test are shown in figure 5.46. The increase in Epp – Ecorr of

as-AFS specimen after UNSM treatment points that the oxide film on the as deposited AFS surface was affected by the surface treatment. Also, the XRD phase analysis performed on as-AFS + UNSM specimen did not show any presence of oxides (figure 5.19) leading to the conclusion that UNSM treatment was able to successfully remove the oxide film from the as-AFS surface. But the DOS ratio obtained for as-AFS + UNSM specimen is still considerably higher. So, EDS analysis was performed on the as-AFS + UNSM specimen surface and the obtained results are presented in figure 5.46. They reveal the presence of oxide film on its surface even after UNSM treatment.

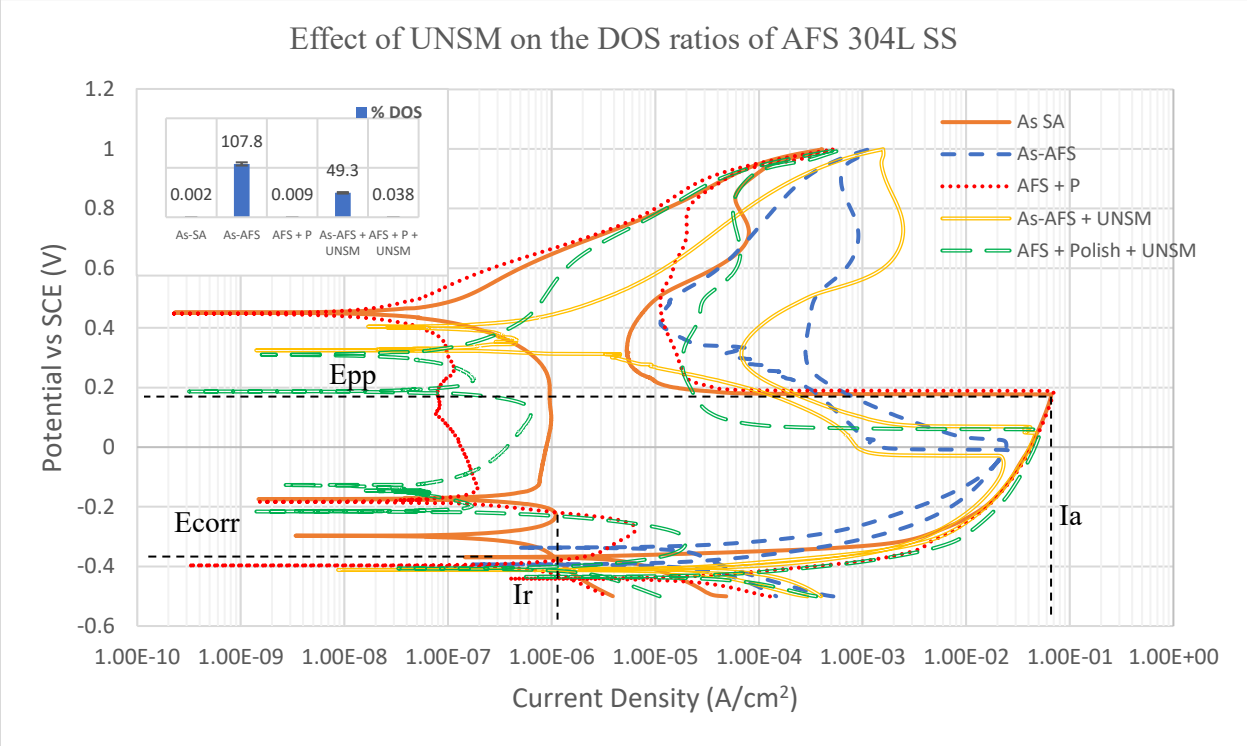

Figure 5.45: DLEPR Corrosion test curves and their corresponding % degree of susceptibility values of as deposited and polished AFS 304L SS before and after UNSM treatment compared with SA 304L SS specimen.

Therefore, from the results of EDS analysis it can be established that the oxide layer was not eliminated completely by UNSM treatment and the high DOS of as-AFS + UNSM specimen is again related to the oxide film on its surface and is not the true representation of the effect of UNSM on the AFS 304L SS alloy. On another note, since the XRD phase analysis did not show any oxide presence in its pattern it could be assumed that the thickness of the oxide film has been

reduced allowing the X-rays to penetrate deeper into the material retrieving the data of martensitic transformation due to UNSM of as-AFS specimen. So, it must be noted that despite the presence of an oxide layer on the AFS surface, UNSM treatment was able to induce 100% martensitic transformation on the underneath AFS 304L SS.

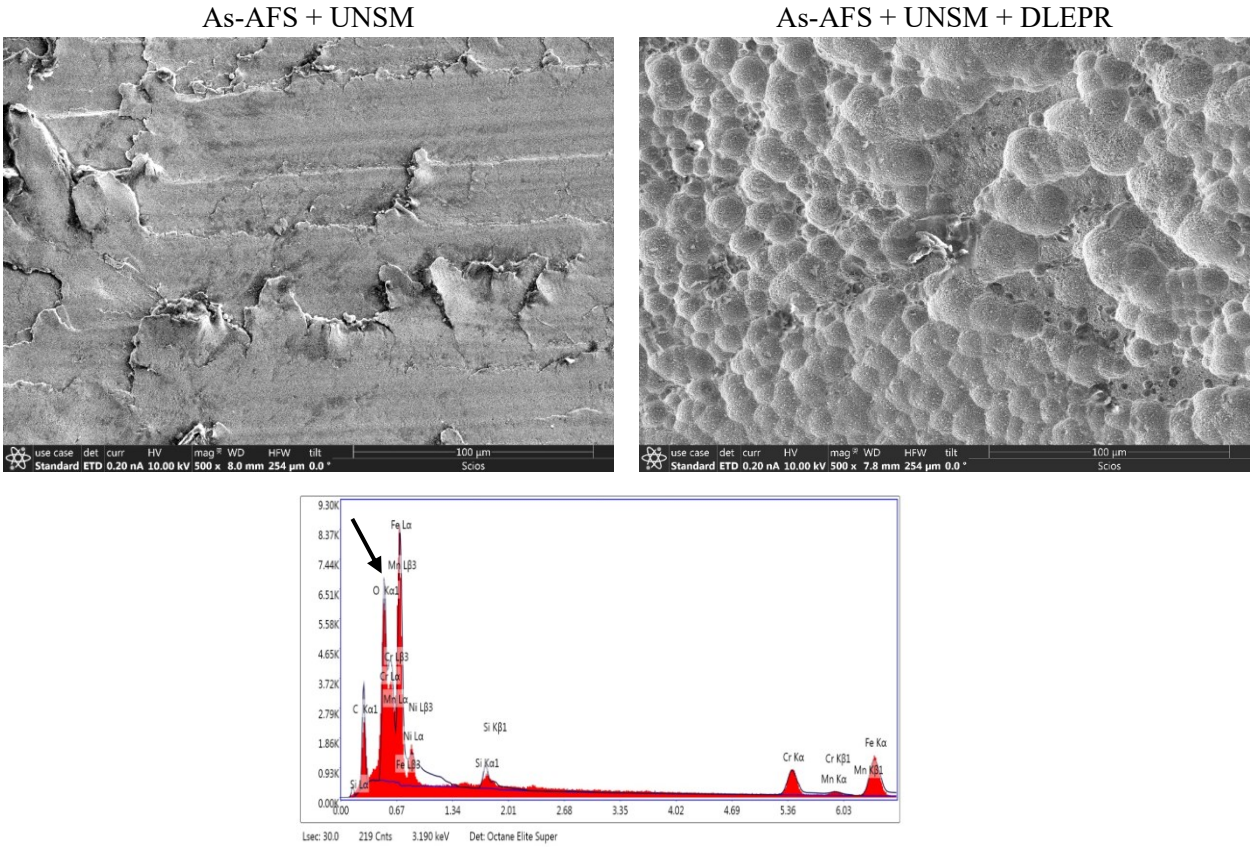

Figure 5.46: SE micrographs of as-AFS + UNSM treated surface before and after DLEPR test and the results of the EDS analysis performed on as-AFS + UNSM specimen surface.

AFS + P + UNSM: The obtained Epp – Ecorr and the DOS ratio of AFS + P + UNSM specimen are 492 mV and 0.038 % respectively. The SE micrographs of AFS + P + UNSM specimen before and after DLEPR test are shown in figure 5.47. The Epp – Ecorr value of polished AFS specimen decreases from 628 mV to 492 mV after UNSM treatment indicating that the passivation behavior is immensely improved by the surface treatment. This could be attributed to the grain refinement and increased dislocation density by UNSM treatment providing more

nucleation sites for the initiation of passive film formation thereby leading to a quicker formation of a stable and stronger passive film on the material surface.

The DOS ratio of polished AFS specimen was 0.009 % which increased to 0.038 % after UNSM treatment. The small increase in DOS ratio after UNSM treatment of polished AFS specimen can be attributed to the formation of peaks and valleys by WC tool tip during UNSM, that can act as localized crevice sites for corrosion during the reverse scan of its DLEPR test. From an earlier study it was found that the DOS ratio of a 304L SS specimen sensitized at 650°C for only 5h was 2.95% and for a specimen sensitized for 24h was 14.09 %.

So, comparing the DOS ratios of these sensitized specimens to the DOS ratio of AFS + P + UNSM specimen it can be said that the DOS ratio of the later specimen is still representative of an unsensitized material. Therefore, it can be expressed that with a small sacrifice in the DOS of AFS specimen other good factors like grain refinement, high magnitude of compressive residual stresses, greater near-surface hardening that are beneficial for improving the overall SCC resistance of a material can be introduced into the polished oxide-free AFS 304L SS cladding by its UNSM surface treatment.

Polished AFS + UNSM

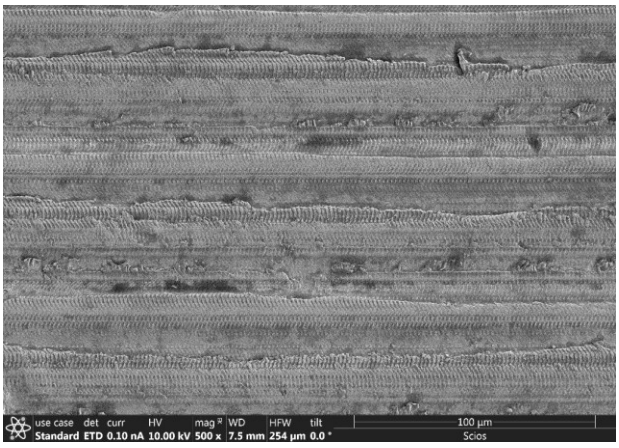

Polished AFS + UNSM + DLEPR

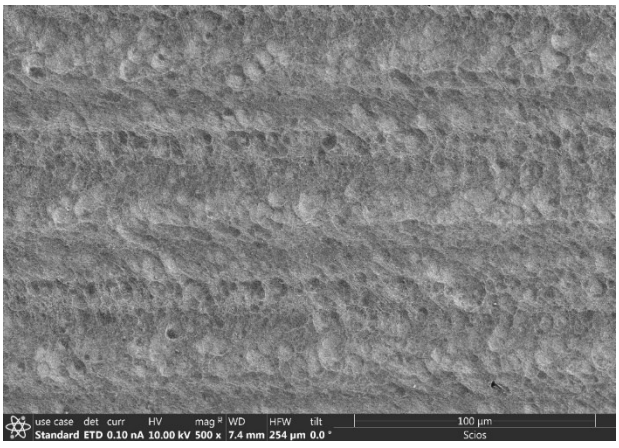

Figure 5.47: SE micrographs of AFS + P + UNSM specimen surface before and after DLEPR test.

5.2.7 Corrosion Analysis – Pitting Corrosion Behavior

The cyclic potentiodynamic polarization (CPP) tests carried out in 3.5 Wt.% NaCl solution were performed to determine the impact of UNSM treatment on the corrosion rate (CR) and pitting corrosion behavior (i.e., pitting potential (PP)) of Sensitized, CS, LACS, and AFS 304L SS specimens in chloride containing environment. For this purpose, the CPP tests were performed on these different 304L SS specimens before and after their UNSM surface treatment, and the pits formed on all the specimen surfaces due to the CPP corrosion tests were examined with SE/BSE micrography and some of the visualized pits are presented in the following sections.

Sensitized 304L SS:

The CPP test curves obtained from the corrosion tests performed in 3.5 Wt.% NaCl solution on SA and S24 304L SS specimens with and without UNSM treatment are presented in figure 5.48. Note that, since the DLEPR corrosion tests showed that the DOS of S24 specimen did not improve with UNSM, the effect of UNSM on the CR and PP of sensitized 304L SS specimen in 3.5 Wt.% NaCl solution using CPP tests was studied with respect to only the S24 specimen here. The obtained values of corrosion potential (Ecorr), pitting potential (Epit), & corrosion current density (Icorr), and the calculated values of corrosion rate (CR) for the untreated and UNSM treated SA and S24 specimens are presented in table 5.10.

Specimen condition	Corrosion potential, Ecorr (mV)	Pitting potential, Epit (mV)	Icorr (µA/cm2)	Corrosion Rate (mpy)
SA	-117	372	0.027	0.012
SA + UNSM	-198	421	0.072	0.033
S24	-140	257	0.031	0.014
S24 + UNSM	-179	347	0.045	0.020

Table 5.10: Effect of UNSM on the pitting potential and corrosion rate of SA and Sensitized at 650°C for 24h 304L SS specimens.

Figure 5.48 (a) represents the CPP curves of untreated SA and S24 304L SS specimens. The Ecorr value of S24 specimen decreased from that of the SA specimen showing that the sensitized specimen has slightly more tendency to corrode in 3.5 Wt.% NaCl test solution than the SA specimen. However, the corrosion rates calculated for the untreated SA and S24 specimens were determined to have values that are very close to each other with magnitudes of 0.012 mpy and 0.014 mpy respectively. As expected, the corrosion rate of S24 specimen was obtained to be higher than the SA specimen but considering that the aged specimen has undergone significant sensitization at 650°C for 24h the difference between their corrosion rates would have been anticipated to be much higher. But this was not the case with the SA and S24 specimens, with their corrosion rates which signify the localized corrosion behavior of a specimen prior to the formation of stable pits exhibiting almost similar behavior. This is not an anomaly and it can be explained as follows, the localized corrosion phenomenon involving crevice corosion or initiation of unstable pits (that signifies as corrosion rate) occurs at inclusions, impurities, or at rougher surfaces with discontinuities on the material surface and therefore, the effect of sensitization on the corrosion rate of 304L SS alloy was very minimal as sensitization involves compositional changes and not physical surface changes.

However, the pitting potential obtained for the S24 specimen is notably worse than the pitting potential of SA speicmen establishing that the formation of stable pits was much more faster in the sensitized 304L SS specimen. This phenomenon can be explained as follows, once the unstable pits initiate or the passive film breaks down due to discontinuities present on the material surface, the CDZs possessing less amount of Cr get preferentially attacked by the chloride ions in the test solution leading to the formation of pits relatively much quicker in the sensitized specimen than when compared to the CDZ-free SA speicmen. In figure 5.49, the BSE micrographs taken at

higher magnifications that are showing the inside area of pits formed in SA and S24 304L SS specimens subjected to CPP tests in 3.5 Wt.% NaCl solution are presented on the left hand side. And from these micrographs it is evidently noticed that the pitting corrosion behavior of SA & S24

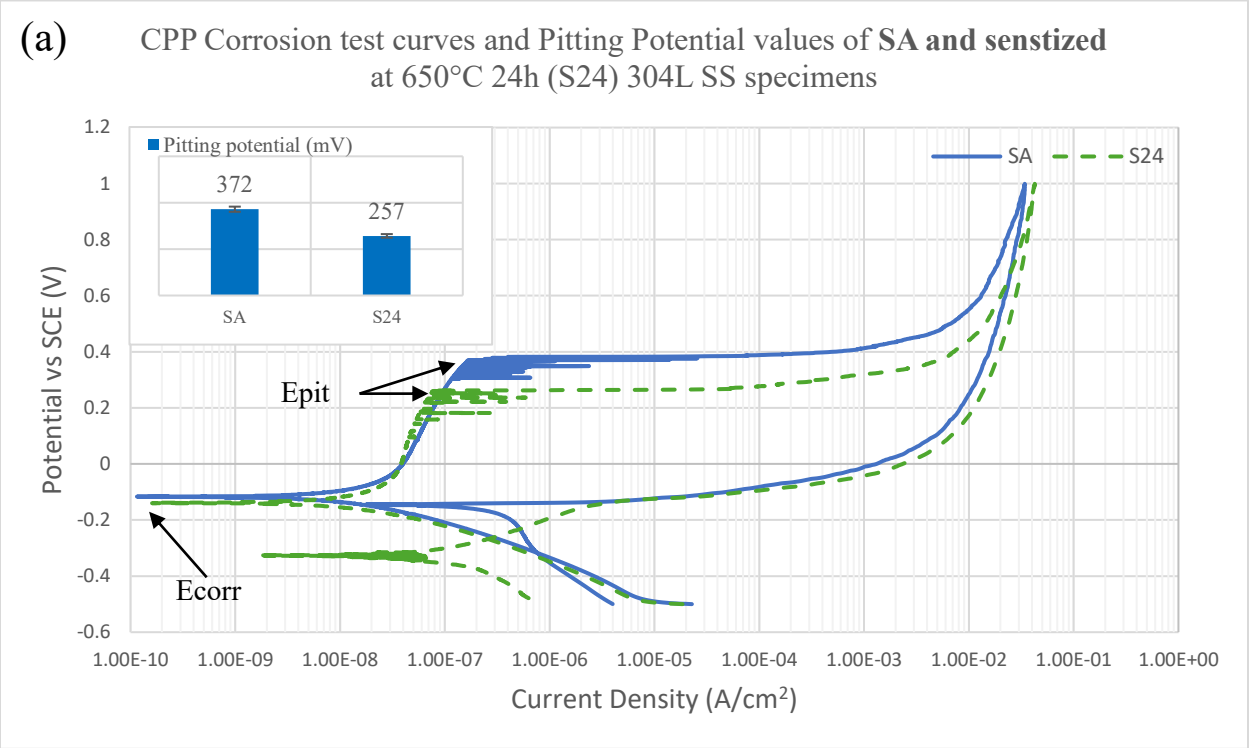

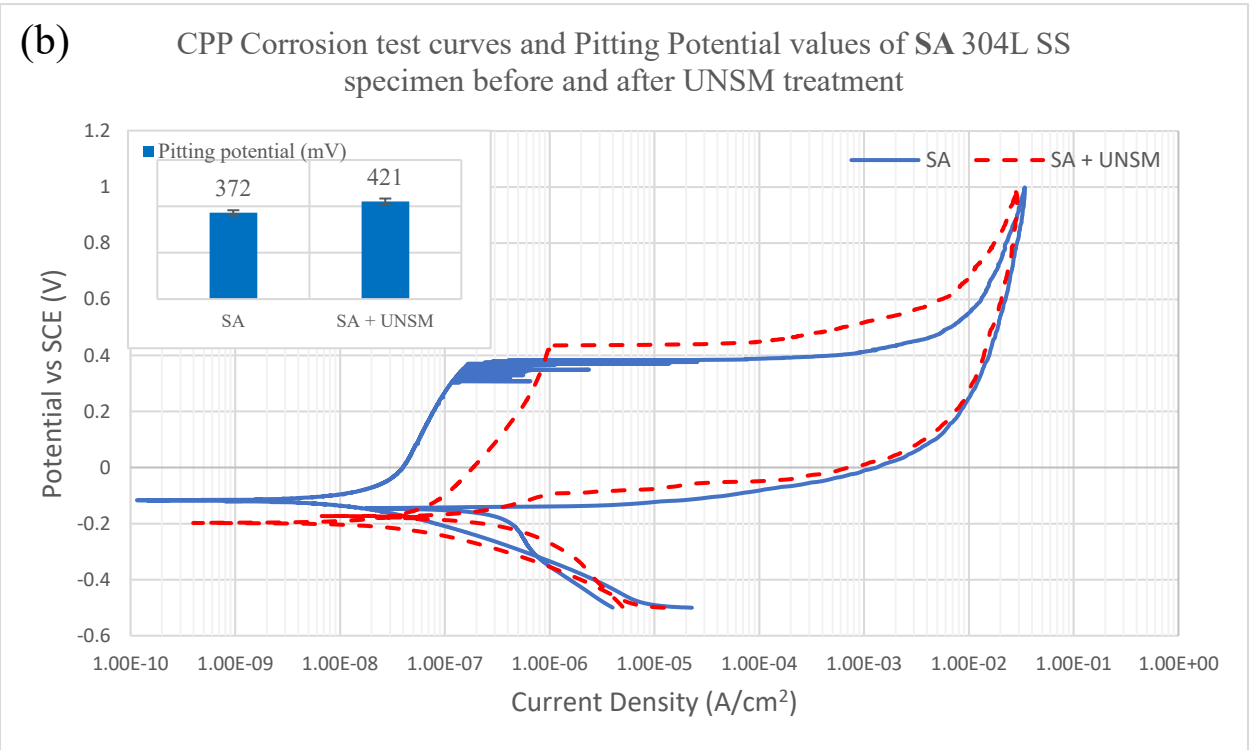

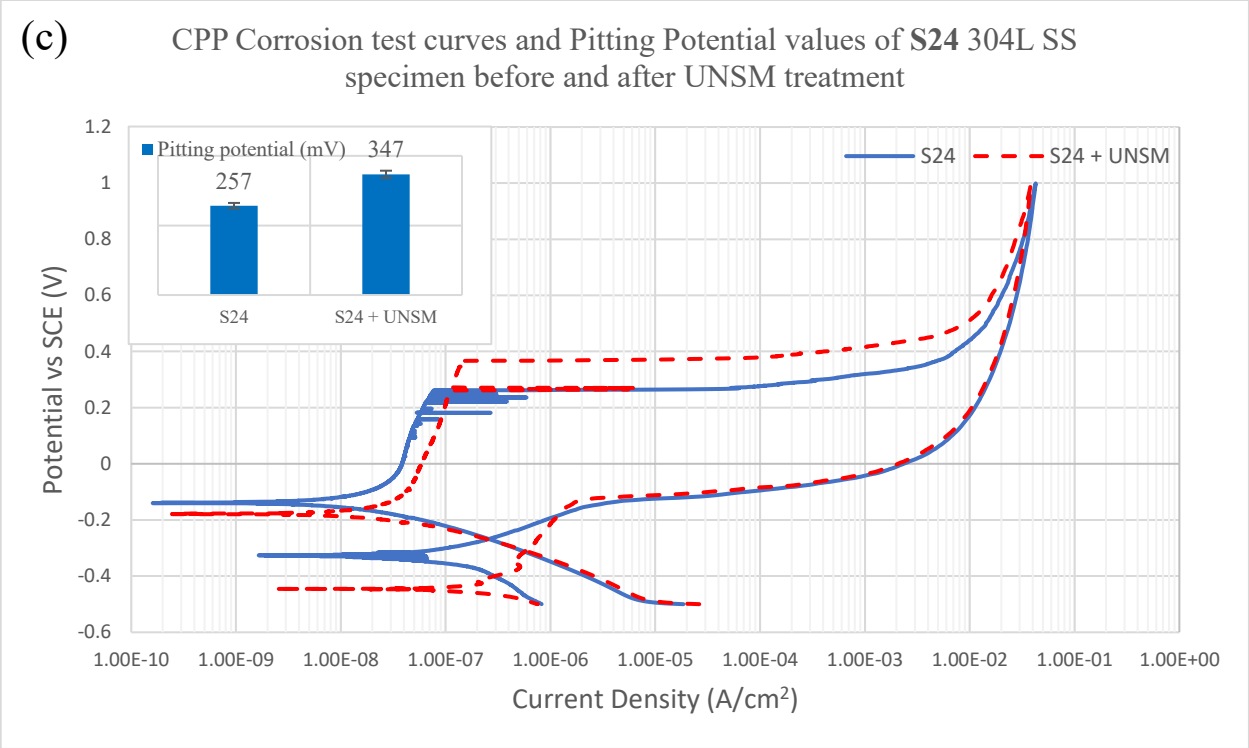

Figure 5.48: CPP Corrosion test curves and their corresponding pitting potential values of (a) SA and sensitized at 650°C for 24h 304L SS specimens and comparing them with their UNSM treated counterpart specimens in (b) SA + UNSM and (c) S24 + UNSM.

specimens is very different. In SA specimen, the pitting corrosion appears to be attacking the grains inside the pits uniformly whereas in sensitized specimen, the corrosion attack is much more pronounced at the grain boundaries with CDZs, indicated by the deep valleys created in between the grains. The difference observed in the corrosion attack mechanism of chloride ions on SA and S24 specimens seems to be the main implication for the huge difference observed in their pitting potentials, with CDZs favoring or accelerating the kinetics of pitting corrosion in the sensitized specimen. Therefore, the quantitative assessment of the pitting characteristics of SA and S24 304L SS specimens is supported visually by the BSE micrographs presented in figure 5.49.

Figure 5.48 (b) and (c) represent the CPP test curves demostrating the effect of UNSM treatment on the pitting potential and corrosion rate of SA and S24 304L SS specimens respectively. Upon UNSM treatment, the Ecorr value of SA and S24 specimens decreased from -

Solution Annealed + CPP.

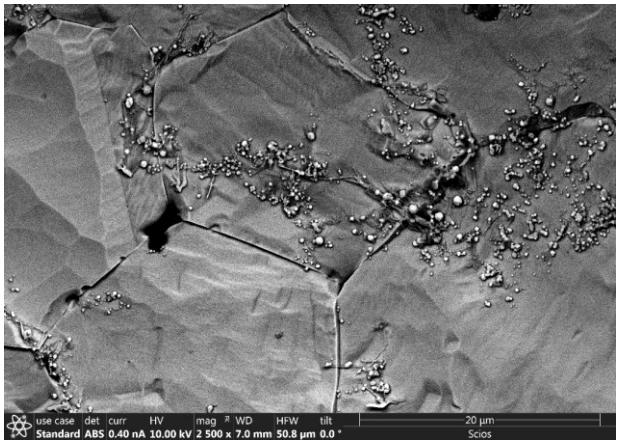

Solution Annealed + UNSM + CPP.

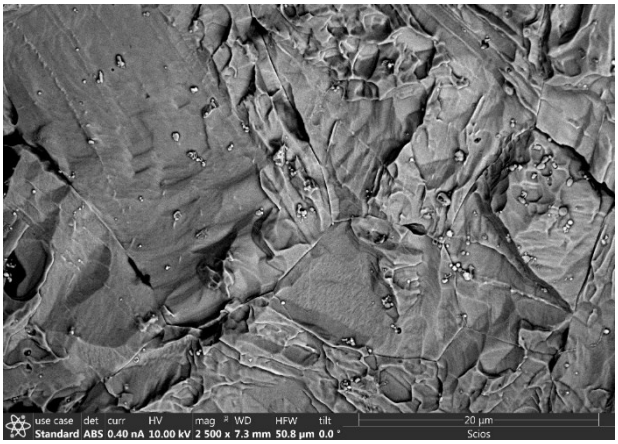

Sensitized at 650°C, 24h + CPP.

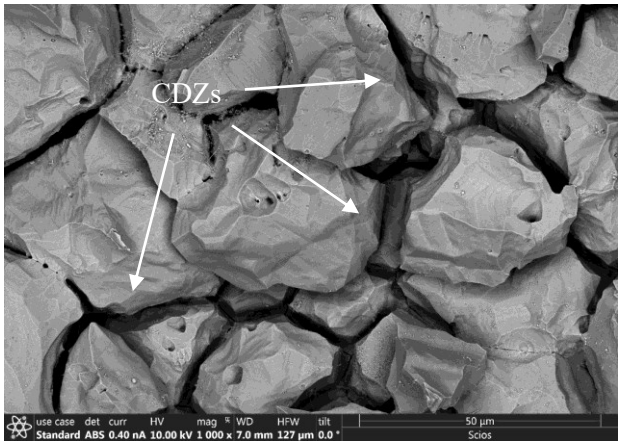

Sensitized at 650°C, 24h + UNSM + CPP.

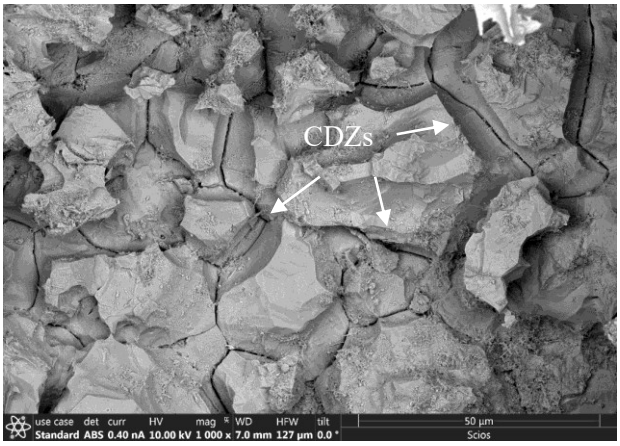

Figure 5.49: BSE images showing the pitting corrosion mechanism in SA and sensitized at 650°C for 24h 304L SS specimens with and without UNSM treatment upon exposing to 3.5 Wt.% NaCl solution through CPP corrosion tests.

117 mV and -140 mV to -198 mV and -179 mV respectively and the corrosion rate worsened from 0.012 and 0.014 mpy to 0.033 and 0.020 mpy respectively. The decrease in the Ecorr value of SA and S24 specimens by UNSM treatment indicates that the surface treatment increased the 304L SS specimens tendency to corrode in the 3.5 Wt.% NaCl solution. Whereas the increase in the corrosion rate of UNSM treated SA and S24 specimens from that of their untreated CR values indicates that the localized corrosion phenomenon occuring at the surface of the UNSM treated specimens prior to the formation of stable pits aggravated due to their surface treatment. The negative impact of UNSM treatment on both the Ecorr and the corrosion rate values of both the

SA and S24 304L SS specimens can be attributed to the formation of peaks, valleys, and smudged edges on their surface by the impact of WC tool tip during their surface treatment as shown by arrows in figure 5.50, along with the breakdown and dispersion of inclusions as seen in figure 5.51, all of which can act as additional crevices or initiation sites for localized corrosion to occur thereby, worsening the Ecorr and CR of UNSM treated SA and S24 specimens.

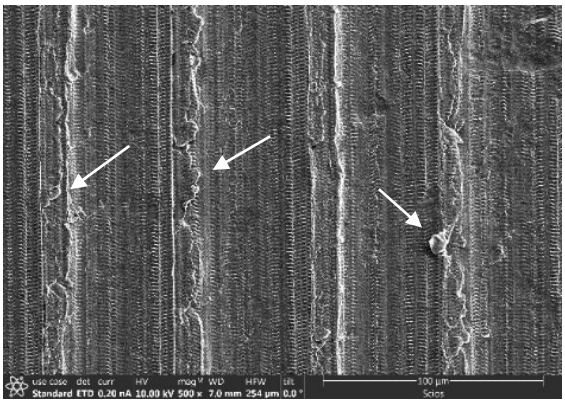

Figure 5.50: SE image showing the possible crevice sites where corrosion could occur preferentially on the surface of UNSM treated 304L SS specimen.

As mentioned in the previous paragraph, the inference indicating the presence of inclusions in the untreated 304L SS specimen that were brokendown and dispersed in the UNSM treated 304L SS specimen, was determined through EDS analysis performed on the untreated SA 304L SS specimen and on the UNSM + DLEPR tested SA specimen. The area / spots on which the EDS analysis was performed on both the untreated and UNSM + DLEPR tested SA 304L SS specimens is shown by the BSE micrographs in figure 5.51 (a) & (b) respectively, along with their corresponding compositional data presented to the right hand side of their respective BSE micrographs. The EDS analysis pertaining to the determination of inclusions in the UNSM treated 304L SS specimen was performed on the after DLEPR tested surface of UNSM treated SA 304L SS specimen because the surface of a specimen gets severely altered by UNSM treatment due to which it becomes extremely difficult to spot any inclusions present on the surface of a UNSM treated specimen. Therefore, EDS analysis was carried out on the after DLEPR tested surface of

UNSM treated SA 304L SS specimen, which should not be of any concern as it underwent only minimal uniform corrosion at its surface as observed from its very low DOS ratio of 0.039 % and also from its BSE micrograph in figure 5.51 (b) which shows that most of the UNSM tracks are still intact even after its DLEPR test.

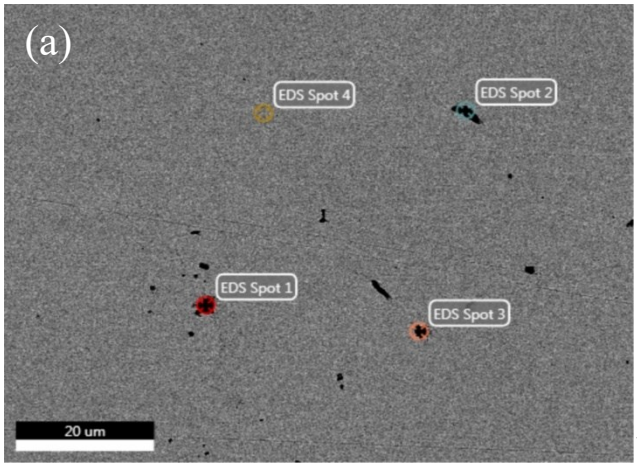

Element (Wt.%)	Spot 1	Spot 2	Spot 3	Spot 4
C K	1.91	12.31	8.15	3.92
O K	33.33	36.93	42.47	
MgK	8.86			
AlK	25.46			
TiK	4.15			
CrK	11.72	39.55	37.75	42.52
MnK	14.56			
S K		11.21	11.62	
FeL				53.56

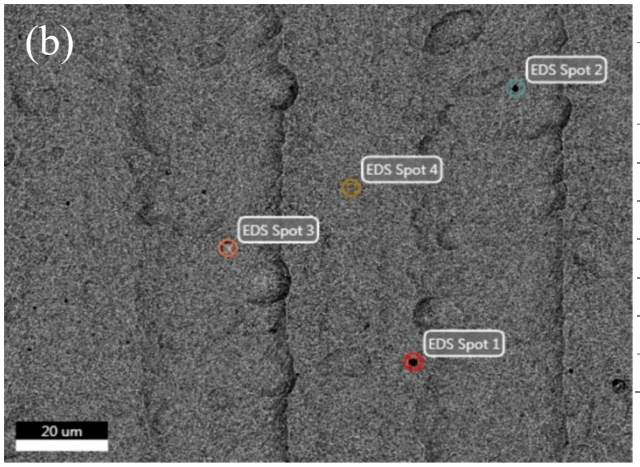

Element (Wt.%)	Spot 1	Spot 2	Spot 3	Spot 4
C K	4.54	5.45	3.01	4.71
O K	29.42	23.75		
AlK	1.71	2.34		
TiK	26.26	22.99		
CrK	15.18	21.72	58.11	40.17
MnK	22.89	23.76		
FeL			38.88	55.12

Figure 5.51: BSE micrographs of (a) untreated SA 304L SS specimen and (b) UNSM treated SA 304L SS specimen after its DLEPR test, showing the spots where the EDS analysis was performed on their respective surfaces along with the obtained corresponding compositional data that is presented to the right hand side of the respective specimen's BSE micrograph.

From figure 5.51 (a), small inclusions could be observed on the surface of untreated SA 304L SS specimen, which appear as black or dark spots on the surrounding gray colored matrix. The EDS spot analysis performed on some of these inclusions revealed that they are comprised of Mg, Al, Ti, Mn, O, and S elements. And the spot EDS analysis performed on the UNSM + DLEPR tested SA 304L SS specimen revealed that these inclusions were present even after the UNSM

treatment of SA specimen and are comprised of Ti, Mn, Al, and O elements, similar to the inclusions found on the untreated SA specimen but not of the same exact chemistry. Thus, it can be said that the UNSM treatment performed in this study on the SA 304L SS specimen was not able to eliminate the inclusions entirely from its surface but could have broken them down into pieces and dispersed them on their surface which can act as additional crevices or initiation sites for localized corrosion to occur thereby, contributing to the worsening of Ecorr and CR of UNSM treated SA and S24 specimens along with the other factors as mentioned earlier.

However, the pitting potential after UNSM treatment of both the SA and sensitized 304L SS specimens increased greatly from 372 mV and 257 mV to 421 mV and 347 mV respectivley, showing an improvement of 49 mV and 90 mV by SA and S24 speicmens respectively. The significant increase in the pitting potential of SA and S24 304L SS specimens by UNSM treatment can be attributed to the gradient microstructure and high magnitude of compressive residual stresses induced into them by UNSM treatment. Both these factors stated in the previous sentence are contributing to resisting the formation of stable pits for a longer time in the UNSM treated SA and S24 304L SS specimens than when compared to their untreated counterpart specimens.

From figure 5.49, it can be observed by comparing the BSE micrographs of CPP tested SA and S24 specimens with and without UNSM treatment, that the corrosion attack mechanism of chloride ions on the 304L SS specimens is the same even after their UNSM treatment with uniform corrosion occurring on the grains of both the SA specimens (i.e., with and without UNSM) and preferential attack occurring at the grain boundaries with CDZs in both the sensitized speicmens. Therefore, it can be confirmed that the improvement in the pitting potential of UNSM treated SA and S24 specimens from that of their untreated specimens is due to the gradient microstructure and high magnitude of CRSs induced into them by UNSM.

Hence, it can be concluded that even though UNSM treatment increases the localized corrosion rate of sensitized 304L SS alloy due to the increase in its surface roughness by the formation of peaks, valleys etc. by UNSM, the formation of stable pits is delayed significantly by the induction of gradient microstructure and high magnitude of CRSs into the sensitized material by UNSM which delays the formation and propogation of cracks i.e., it can greatly improve the SCC resistance of sensitized 304L SS alloy.

SE Micrography showing the pits formed on the after CPP test surfaces of SA and S24 304L SS specimens with and without UNSM treatment: The pits formed on the SA and S24 specimens with and without UNSM treatment that are subjected to CPP corrosion tests in 3.5 Wt.% NaCl solution were examined with SE/BSE micrography and some of them are presented in figure 5.52. The SEM analysis revealed that different sized pits formed in all the specimens, i.e., in untreated and UNSM treated SA and S24 specimens and that the pits have predominantly formed in two different shapes, oval and foot shaped. The smaller pits were all oval or circular shaped and the larger pits were all foot shaped. Whereas the pits that were of intermediate size formed in both shapes. Therefore, it can be assumed that the medium and larger sized pits that formed in the shape of foot could be branched pits i.e., the smaller pits that formed close to each other during the initial stages of CPP tests must have conglomerated together as the tests progressed, forming into larger pits with branches in between the initial smaller sized pits. Many of the branched pits formed on the surface of UNSM treated SA and S24 specimens have edges that appear to have undergone only shallow corrosion i.e., corrosion confined to only the topmost surface of the specimen. Some of these areas are marked by arrows in figure 5.52. Also, the pits formed on the surface of UNSM treated SA and S24 specimens appear to be wider / larger than the pits formed on the untreated SA and S24 specimens.

Pits formed in **Solution Annealed** specimen.

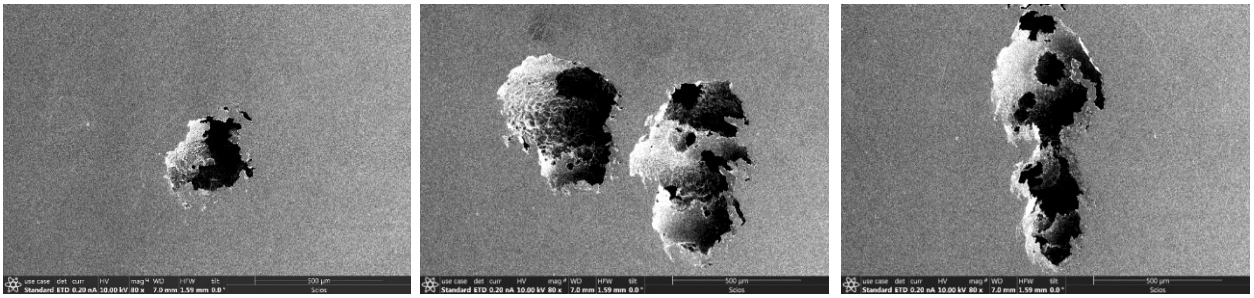

Pits formed in **Solution Annealed + UNSM treated** specimen.

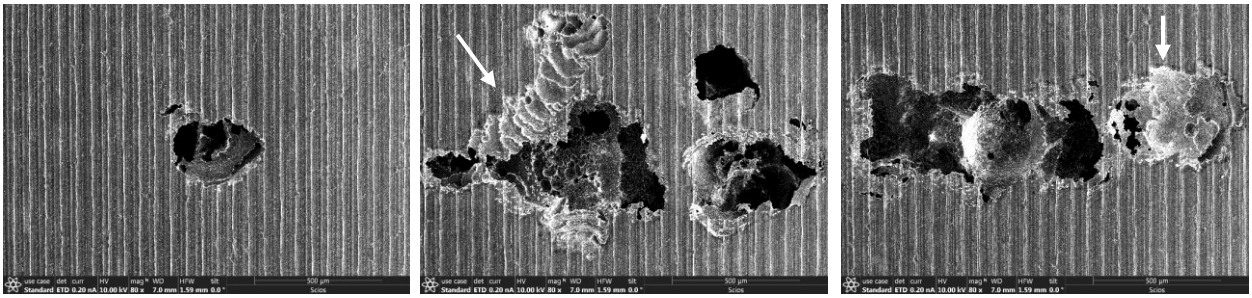

Pits formed in **Sensitized at 650°C for 24h** specimen.

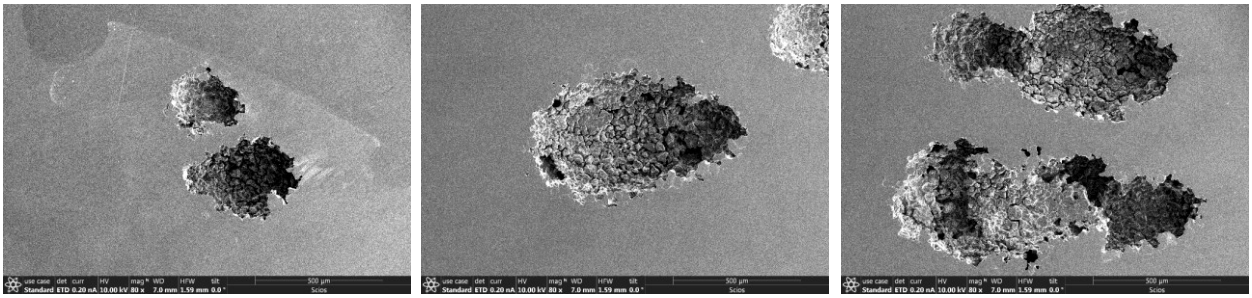

Pits formed in **Sensitized at 650°C for 24h + UNSM treated** specimen.

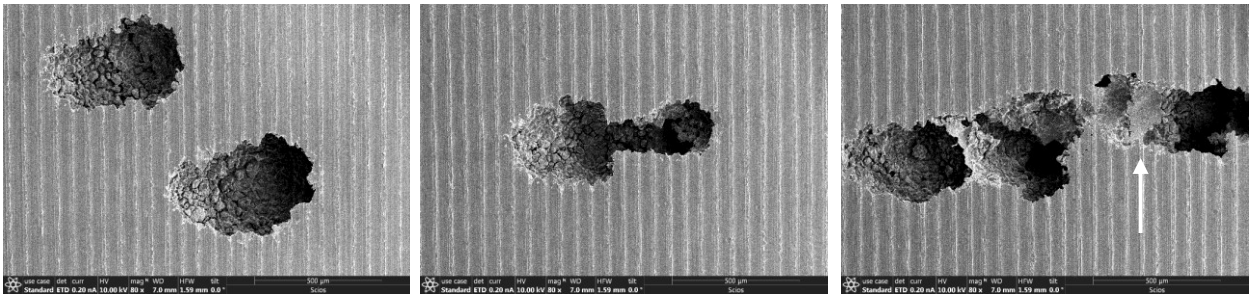

Figure 5.52: SE images showing the pits formed on the surface of SA and sensitized at 650°C for 24h 304L SS specimens with and without UNSM treatment upon exposing them to 3.5 Wt.% NaCl solution during their CPP corrosion tests.

Upon examining the inside areas of the pits at higher magnifications, three distinct areas could be observed that are common to all the specimens and these could be representative of the different stages occurring in the 304L SS specimens during corrosion i.e., during their CPP tests.

These areas are shown in figure 5.53 (a-c). The BSE micrographs showing the three distinct areas inside the pits of CPP tested 304L SS specimens that are presented in figure 5.53 hypothetically appear to be in the following order of stages: (a) initial stage of chloride attack on the grains conceived by the tiny pits in them, (b) metal yet to completely oxidize before freeing the loose material into the test solution, and (c) surface that is clear of pits and oxidized metal probably just before corrosion initiation or just after complete oxidation of prior metal layer.

Figure 5.53: BSE images showing different areas observed from the pits formed in SA and sensitized 304L SS specimens with and without UNSM treatment that are subjected to CPP corrosion tests in 3.5Wt.% NaCl test solution with (a) representing small pits formed in grains, (b) representing debris like oxidized metal that is stuck to the grains underneath and (c) representing clear surface with no small pits or debris.

CS & LACS 304L SS:

The CPP test curves obtained for the as sprayed and polished CS and LACS 304L SS coatings without and with UNSM treatment are presented in figure 5.54 (a) and (b) representing CS and LACS specimens respectively. Whereas the corrosion data deduced from these CPP test curves such as the corrosion potential (Ecorr), pitting potential (Epit), and corrosion current density (Icorr), along with the corrosion rate (CR) determined from the Icorr value using the formula CR (mpy) = (0.13*Icorr*EW)/(d*A), are all consolidated and presented in table 5.11 along with the corrosion data related to the as-SA and polished SA (SA + P) 304L SS specimens.

The CR of as-SA and SA + P 304L SS plate specimens were found to be 0.016 mpy and 0.012 mpy respectively whereas their pitting potentials were measured to be ~ 164 mV and 372 mV respectively.

Specimen designation	Corrosion potential, Ecorr (mV)	Pitting potential, Epit (mV)	Icorr (µA/cm2)	Corrosion Rate (mpy)
As-SA	-177	164	0.035	0.016
SA + P	-117	372	0.027	0.012
As-CS	-346	-	0.510	0.235
CS + P	-244	-78.2	0.110	0.050
As-CS + UNSM	-261	-	0.139	0.064
CS + P + UNSM	-297	-15.6	0.152	0.070
As-LACS	-368	-	0.705	0.325
LACS + P	-331	-141	0.077	0.036
As-LACS + UNSM	-251	-	0.085	0.039
LACS + P + UNSM	-254	-31.7	0.059	0.027

Table 5.11: Corrosion data obtained from the CPP tests performed in 3.5 Wt.% NaCl solution on CS and LACS coatings with different surface conditions along with as-SA and SA + P rolled solution annealed 304L SS specimens.

Corrosion rate and pitting characteristics of **as-CS** and **as-LACS** 304L SS coatings: The corrosion rates of as-CS and as-LACS coatings were found to be 0.235 mpy and 0.325 mpy respectively exhibiting significantly higher values than that of as-SA specimen's CR of 0.016 mpy suggesting that the as sprayed CS and LACS 304L SS coatings undergo extremely faster corrosion than the conventionally hot-rolled as-SA 304L SS specimen. The corrosion rate of a material is largely dependent on the amount of exposed surface area or surface roughness of the material and the number of inclusions or impurities present on its surface that can act as localized corrosion sites which can be preferentially attacked by the corrosive environment leading to the occurrence of localized corrosion phenomenon such as pitting or crevice corrosion.

The as-CS and as-LACS coatings having average surface roughness values of ~ 16 ± 1.9 µm, provide large surface areas for the NaCl solution to attack. Also, from figures 4.16 and 4.24 which are showing the surfaces of as-CS and as-LACS coatings, it can be observed that there are numerous pores and crevices on their surfaces which can act as localized corrosion sites where the corrosive chloride ions in the test solution can accumulate leading to enhanced corrosive attack at

these localized areas by the setup of concentration cells. These two factors combined are largely contributing to the high corrosion rates experienced by both the as sprayed CS and LACS 304L SS coatings in 3.5 Wt.% NaCl solution CPP tests.

Whereas in the case of as-LACS coating, there is an additional contributing factor which is propelling its corrosion rate to exhibit a further higher value than that of as-CS coating's CR, which is the non-homogenous deleterious oxide film present on the as-LACS coating surface that contributes to numerous additional localized concentration sites for the accumulation of chloride ions. Therefore, because of the availability to set up concentration cells at numerous sites on the surface of as sprayed CS and LACS coatings, the corrosion in both of these coatings occurs at an accelerated rate during their CPP tests performed in 3.5 Wt.% NaCl solution resulting in extremely high CR values.

Additionally, because of such high accelerated CRs exhibited by as-CS and as-LACS coatings, no pitting potential could be observed in their CPP curves indicating that a stable passive film that could resist pitting could not form on these coatings at any point of time during their CPP tests. The CRs of as-CS and as-LACS coatings align well with their DOS ratios obtained during their DLEPR corrosion tests, with a high DOS ratio seen for the as-CS coating and a far worse DOS ratio seen for the as-LACS coating due to the presence of non-homogenous prior oxide film on its surface.

Corrosion rate and pitting characteristics of **CS + P** and **LACS + P** 304L SS coatings: The CRs of CS + P and LACS + P coatings were measured to be 0.050 mpy and 0.036 mpy respectively decreasing immensely from their as-CS and as-LACS coatings CRs. One of the factors for the immense decrease in their CRs is the vast decrease in the coatings surface roughness by polishing i.e., reduction in the amount of surface area available for attack by the corrosive environment.

Moreover, because of polishing, the number of crevices present on the surface of these coatings decrease, and additionally, in the case of as-LACS coating, the deleterious surface oxide film on its surface will also be removed by polishing. Therefore, polishing of CS and LACS coatings results in a reduction of the number of localized concentration sites present on their surface that can be preferentially attacked by the corrosive species in the CPP test environment. As a result, the CRs of CS + P and LACS + P coatings improved significantly from that of the CRs of as-CS and as-LACS coatings.

However, the porosity in the CS and LACS coatings will not be impacted by polishing and the pore areas in them can act as localized concentration sites during their CPP tests, which is why the CRs obtained for the CS + P and LACS + P coatings are still higher than the CR of SA + P specimen. Nevertheless, the pores present in the CS + P and LACS + P coatings are small (figure 5.18) and can only act as pit initiation sites, unlike the higher degree of concentration cells (i.e., accumulation of chloride ions) that can be set up on the as-CS and as-LACS coatings due to the vast differences in their surface roughness. Hence the accumulation of chloride ions at these small porous areas on the CS + P and LACS + P coatings occur at a much slower pace than compared to their as sprayed coatings thereby, delaying the formation of stable pits, or allowing the pits to re-passivate i.e., the formation of unstable pits. Therefore, both the CS + P and LACS + P coatings exhibit a pitting potential unlike their as sprayed coatings and their PP values were measured to be ~ -78 mV and -141 mV respectively. It must be noted here that despite the better interparticle bonding of LACS coating due to recrystallization during its processing and despite both the coatings possessing similar levels of porosity, the pitting potential of CS + P coating is better than the LACS + P coating attributed to the presence of decent magnitudes of compressive residual stresses that are generated during processing due to cold work in the CS 304L SS coating.

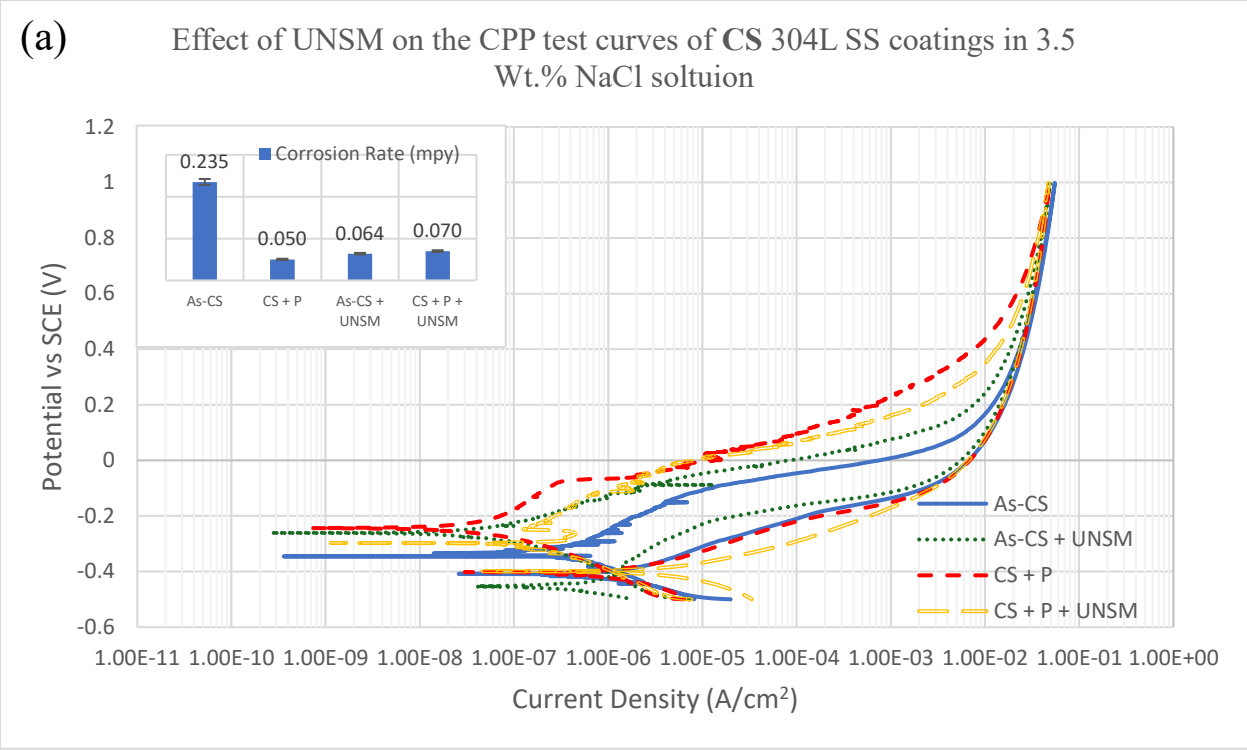

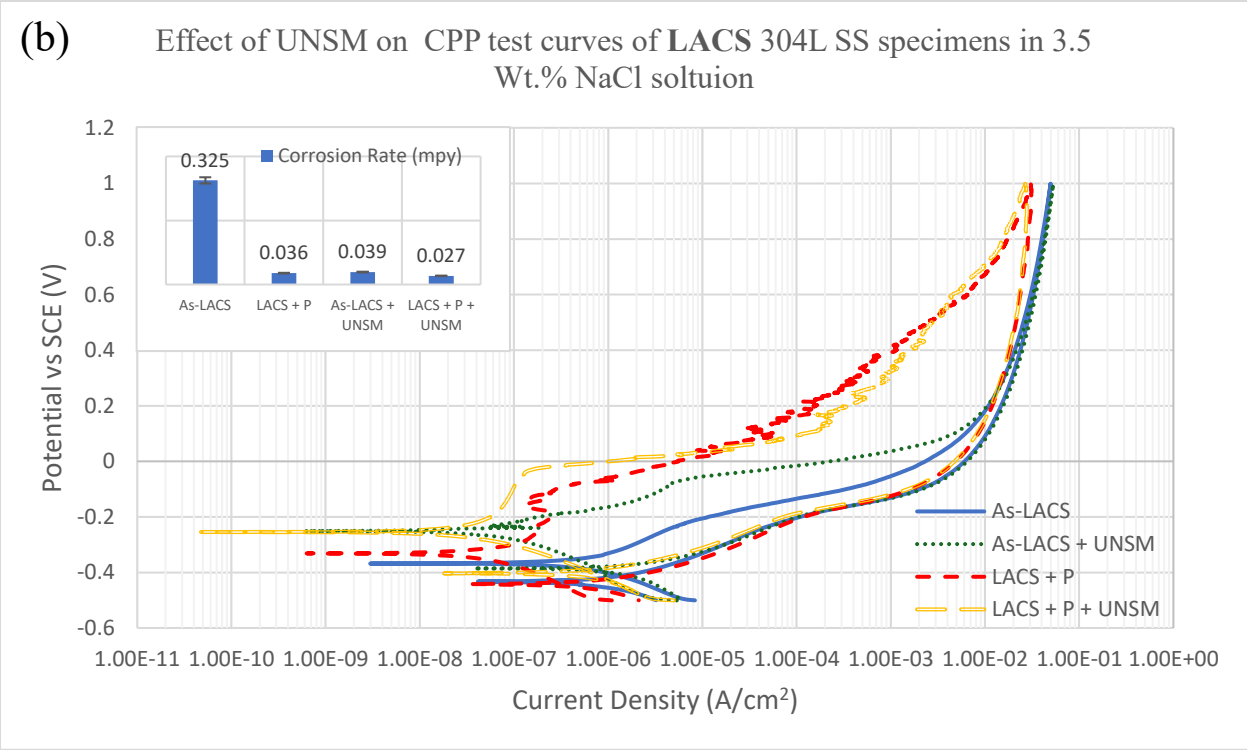

Figure 5.54: Effect of UNSM on the CPP Corrosion test curves and the corresponding corrosion rates of as sprayed and polished (a) CS and (b) LACS 304L SS coatings.

Corrosion rate and pitting characteristics of **as-CS + UNSM** and **as-LACS + UNSM** 304L SS coatings: The CRs of UNSM treated as-CS and as-LACS coatings were measured to be 0.064 mpy and 0.039 mpy respectively, decreasing prominently from that of their untreated as sprayed coatings CRs. Like polishing of as sprayed coatings, UNSM treatment of as-CS and as-LACS coatings resulted in a significant decrease in their surface roughness (Ra) values from ~ 16 ± 1.9 μm for both the as sprayed coatings to 5.7 ± 1.3 μm and 2.5 ± 0.2 μm for the as-CS + UNSM and as-LACS + UNSM specimens respectively. This decrease in Ra reduces the surface area exposed to the corrosive environment. Additionally, UNSM results in a uniform surface with not much variance in Ra from area to area on the specimen surface. As a result, the degree of concentration cells set up on the as-CS + UNSM and as-LACS + UNSM specimen surfaces during the initial phase of CPP tests would be lower in concentration than that of the untreated as-CS and as-LACS coatings. Moreover, it was seen from the DLEPR corrosion tests that UNSM treatment improves the passivation behavior of both the as sprayed and polished CS and LACS coatings. Therefore, due to the combined effect of all these factors the CR of as-CS and as-LACS coatings decreased prominently after their UNSM treatment with their CR values getting much closer to the CR values exhibited by CS + P and LACS + P coatings. It can also be seen from figure 5.54 (a) and (b) that the CPP curves of as-CS + UNSM and as-LACS + UNSM specimens, during the initial phase or forward scan of the CPP test curves, are shifting to the left and above of as-CS and as-LACS specimens CPP curves i.e., the curves are shifting towards a nobler side of potentials indicating an improvement in the CR of as-CS and as-LACS specimens due to their UNSM treatment.

However, even though UNSM treatment performed on the as-CS and as-LACS coating surfaces resulted in a decrease in the unevenness of their surfaces (i.e., increase in uniformity of surfaces), the Ra values of as-CS + UNSM and as-LACS + UNSM specimens are still much greater

than ideal conditions (such as in case of polished specimen's surface), which allows for a median degree of concentration cells to be setup on their surfaces by the chloride ions in the test solution. Due to the setup of these median degree of concentration cells on the surface of as-CS + UNSM and as-LACS + UNSM specimens, despite the improvement in their passivation behavior by UNSM, the kinetics of the passive film regeneration would still be lagging than the kinetics of the attack of chloride ions at the pitted areas due to the exponential increase in the chloride ions activity at these areas during the later phase of the forward scan of CPP tests, which aids in the continuous growth of the initially formed pits. Because of which the UNSM treatment of as-CS and as-LACS coatings could not induce any clear pitting potential in the as-CS + UNSM and as-LACS + UNSM treated specimens unlike how polishing was able to introduce a PP in the CS + P and LACS + P coatings. However, from figure 5.54 (a) and (b), it can be observed that the area under the hysteresis loops of as-CS + UNSM and as-LACS + UNSM treated specimens notably increased from that of the as-CS and as-LACS coatings hysteresis loop areas indicating that UNSM surface treatment is improving the pitting corrosion characteristics of as-CS and as-LACS coatings.

Corrosion rate and pitting characteristics of **CS + P + UNSM** and **LACS + P + UNSM** 304L SS coatings: The CRs of CS + P + UNSM and LACS + P + UNSM specimens were found to be 0.070 mpy and 0.027 mpy respectively. UNSM treatment on polished CS and LACS coatings increases their surface roughness slightly to approximately the same value in both the coatings. But the CR of CS + P + UNSM coating worsens whereas the CR of LACS + P + UNSM coating improves from that of their polished CS and LACS coatings CRs. This mixed behavior in the CRs with respect to the slight increase in the surface roughness of CS+ P and LACS + P by UNSM can be explained by observing the CS + P + UNSM and LACS + P + UNSM specimen surfaces shown in figures 5.39 and 5.42 respectively. The UNSM treatment performed on the CS + P coating

created smudges or sharp edges along the UNSM tracks because of the heavy plastic deformation already present in the CS coatings restricting the dynamic penetration of WC tool tip during UNSM. These sharp edges on the CS + P + UNSM coating surface can act as surface irregularities increasing the number of sites for attack by the corrosion solution thereby, worsening its corrosion rate from that of the CS + P coating.

Whereas the UNSM treatment performed on the LACS + P coating resulted in a smudge free surface because of the lower hardness of LACS coating allowing the WC tool tip to efficiently apply the dynamic load into the material. Also, UNSM treatment of LACS + P specimen results in the partial closure of the pores on its surface decreasing the area of localized sites available for the corrosive solution to attack. Therefore, the smudge free surface and the reduction in porous area of the LACS + P coating by UNSM treatment reduces the total number of preferential sites for the corrosive solution to attack thereby, decreasing the corrosion rate of LACS + P + UNSM treated coating.

It is to be noted that the surface roughness of polished CS and LACS coatings after their UNSM treatment is considerably lower than the surface roughness of as sprayed and as sprayed + UNSM treated coatings. Therefore, accumulation or setup of concentration cells by chloride ions will be more difficult on the polished + UNSM treated coatings than the as sprayed and as sprayed + UNSM treated coatings. So, the polished CS and LACS coatings treated with UNSM display the presence of a pitting potential like the untreated polished CS and LACS coatings. With the comparatively low Ra values of CS + P + UNSM and LACS + P + UNSM coatings not giving a chance for heavy accumulation of chloride ions at the defect sites on their surface, the high degree of CRSs embedded in them and the improvement in their passivation behavior (i.e., improvement in the kinetics of passive film formation or regeneration) through UNSM assist in further

improving the PP of the coatings from that of the PP exhibited by CS + P and LACS + P coatings.

SE Micrography showing the after CPP test surfaces of as sprayed and polished CS and LACS coatings with and without UNSM treatment: The SE micrographs showing the pitting behavior of CS and LACS coatings in 3.5 Wt.% NaCl test solution are shown in figure 5.55. The major difference observed in the pitting behavior of CS and LACS coatings is that the CS coating having very fine grains with inherently weak interparticle bonding forms deeper and wider pits due to the conglomeration of porous sites after pit initiation. Whereas the LACS coating having relatively larger grains with better interparticle bonding is exhibiting an initial shallow corrosion followed by a possible growth of pits through the depth of the material following the porous channels existing in it. With UNSM treatment on CS coatings, no notable changes in the pitting behavior can be observed from that of the untreated CS coating, as UNSM does not involve any significant heat input into the specimens it cannot influence the inherent weak interparticle bonding of CS coatings. But the pitting behavior of LACS coatings after UNSM treatment appears to have changed because of the grain refinement occurring during UNSM treatment might be leading to coagulation of the nearby pit initiation sites through the increased grain boundaries. However, the pits formed on the UNSM treated LACS coating are still considerably smaller than the pits formed on the CS coatings due to the better interparticle bonding of LACS coating.

Finally, it can be expressed that corrosion in 3.5 Wt.% NaCl solution is lower in all the LACS coatings (i.e., with and without UNSM treatment) when compared with the corresponding same surface condition of CS coatings, because of the former coatings enhanced interparticle bonding. Except for the as sprayed LACS coating whose oxidized surface is accelerating the CR and exhibiting a value higher than the as-CS coating's CR. Therefore, polishing of as sprayed LACS coatings is recommended and subsequent UNSM treatment enhances its corrosion

resistance characteristics by decreasing its corrosion rate through reduction in porosity and increasing its pitting potential through the induction of beneficial CRSs in the coating.

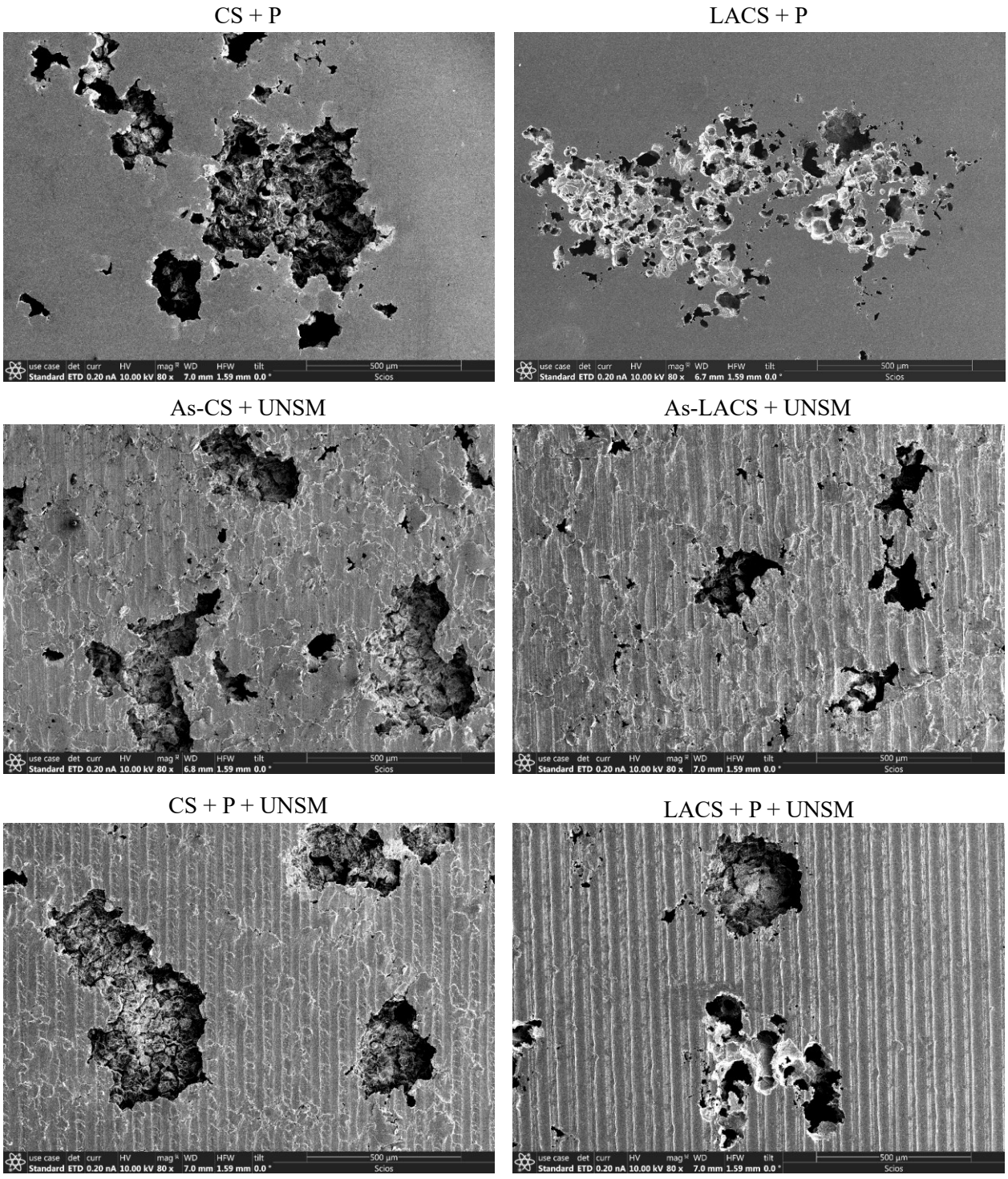

Figure 5.55: SE micrographs showing the pits formed on the surface of untreated and UNSM surface treated CS and LACS 304L SS coatings that are subjected to CPP tests in 3.5 Wt.% NaCl solution.

AFS 304L SS:

The CPP test curves of untreated and UNSM treated AFS 304L SS specimens are presented in figure 5.56 and the corrosion data obtained from the CPP curves is consolidated in table 5.12.

Specimen designation	Corrosion potential, Ecorr (mV)	Pitting potential, Epit (mV)	Icorr (µA/cm2)	Corrosion Rate (mpy)
As-AFS	-361.80	-	0.777	0.36
AFS + P	-269.00	245	0.150	0.07
As-AFS + UNSM	-422.80	-	1.650	0.76
AFS + P + UNSM	-166.00	294	0.090	0.04

Table 5.12: Corrosion data obtained from the CPP tests performed in 3.5 Wt.% NaCl solution on as-AFS and polished AFS with and without UNSM treatment.

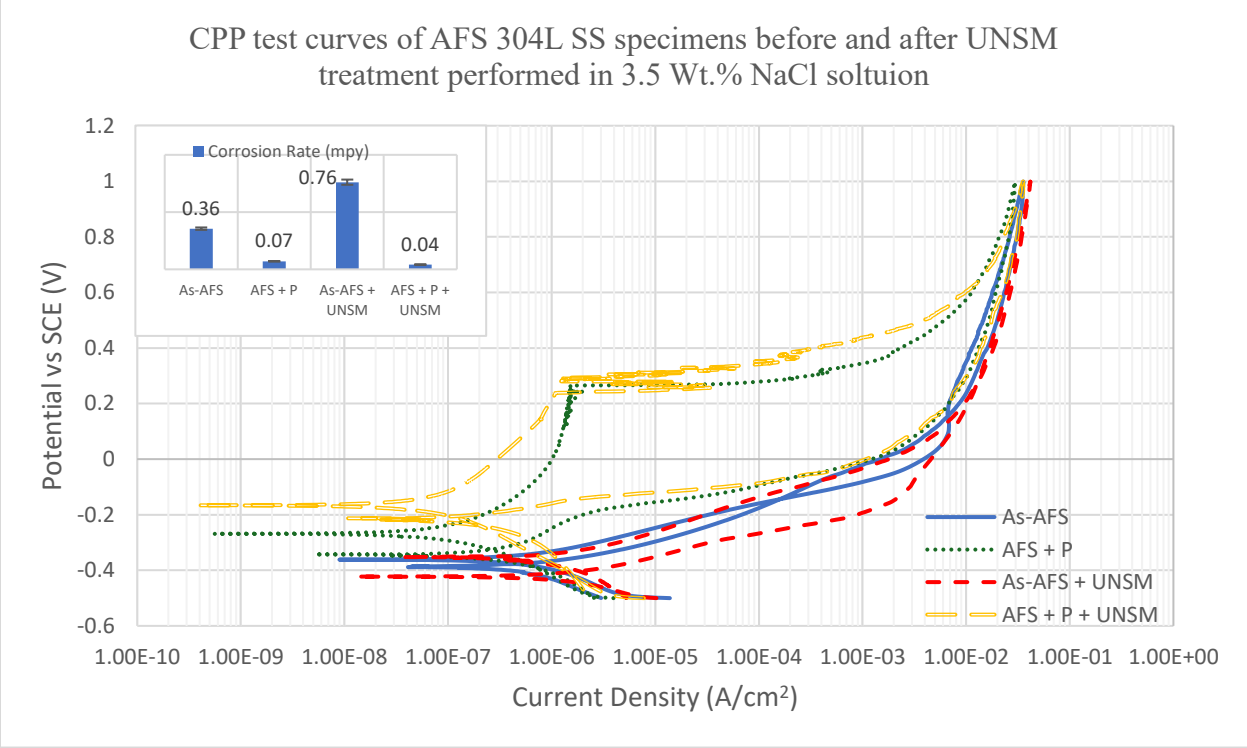

Figure 5.56: CPP Corrosion test curves and the corresponding corrosion rates of as-AFS and polished AFS specimens before and after UNSM treatment.

As-AFS and as-AFS + UNSM: Both the corrosion rates obtained for the as-AFS cladding before and after UNSM treatment exhibit very high values of 0.36 mpy and 0.76 mpy respectively. The SE micrographs showing the pitting corrosion occurring in both the as-AFS and as-AFS +

UNSM specimens due to CPP tests are presented in figure 5.57. The corrosion rate of a material is majorly influenced by the number of localized corrosion prone sites available for the corrosive test solution to attack. It was already established earlier that the oxide film on the as-AFS specimen is of mixed nature possessing irregularities/defects that can act as localized sites for corrosion. Therefore, the defects present in the oxide film are aggressively attacked by the chloride ions forming localized attack zones where they tend to accumulate and easily form pits resulting in its high CR. The left SE micrograph in figure 5.57 shows the pit formed on as-AFS specimen surface.

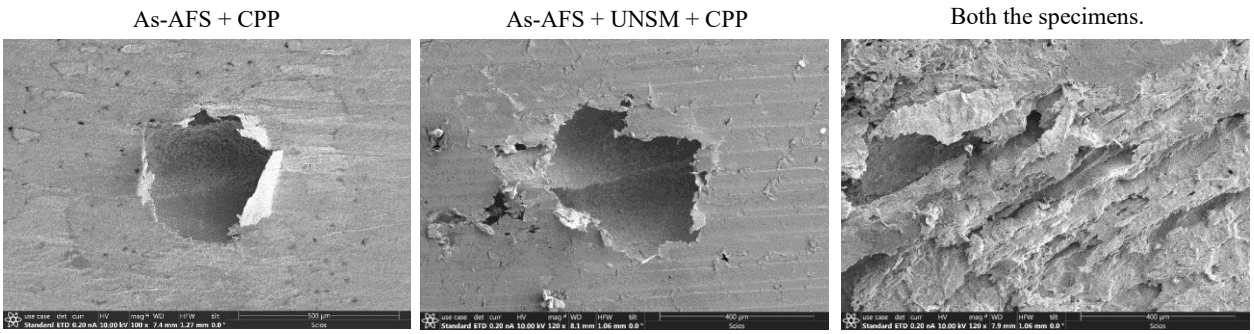

Figure 5.57: SE micrographs showing the corrosion occurring in as-AFS and as-AFS + UNSM specimens during their CPP corrosion tests.

It was also found that UNSM treatment did not eliminate the oxide film from the as-AFS specimen surface. Additionally, UNSM treatment forms peaks and valleys on the specimen surface by the severe pounding of WC tool tip, which further increases the number of attack sites for the Cl- ions, in addition to the already present defects in the oxide film. Hence, the CR of as-AFS + UNSM treated specimen deteriorated further than as-AFS specimen's CR. The SE micrograph in the middle of figure 5.57 shows the pit formed on the as-AFS + UNSM treated specimen surface which appears to be the same as that of the pit formed on the as-AFS specimen surface but slightly larger.

Whereas the micrograph on the right side of figure 5.57 shows the corrosion occurring in the oxide film of both as-AFS and as-AFS + UNSM treated specimens before converting into pits

by the flaking of off material. Thus, the high corrosion rates of both the as-AFS cladding before and after UNSM treatment can be attributed to the combined contribution of both the corrosion of oxide film and the subsequent pitting in 304L SS AFS deposit, with the major contribution to their CRs coming from the corrosion of oxide film. Therefore, the as-AFS and as-AFS + UNSM treated specimens CRs obviously do not represent the corrosion behavior of 304L SS AFS deposit or the impact of UNSM on it. Also, because of the very high corrosion rates of both as-AFS and as-AFS + UNSM treated specimens, stable pits readily form on their oxidized surfaces thereby showing no pitting potential at all by both these specimens.

AFS + P and AFS + P + UNSM: After polishing the AFS specimen and removing the surface oxide layer, the actual corrosion rate of AFS deposited 304L SS was found to be 0.07 mpy. In a fully dense material with a smooth oxide-free surface like the polished AFS specimen, the localized attack sites for the NaCl solution would be the inclusions present on the specimen's surface, which are contributing to the CR seen for the AFS + P specimen. Also, with the removal of oxide layer from the AFS specimen surface, it exhibits a pitting potential at 245 mV. Thus, it can be stated that an oxide free AFS specimen surface can indeed exhibit resistance to pitting. The SE micrograph on the left-hand side of figure 5.58 shows the pit formed on the surface of polished AFS specimen.

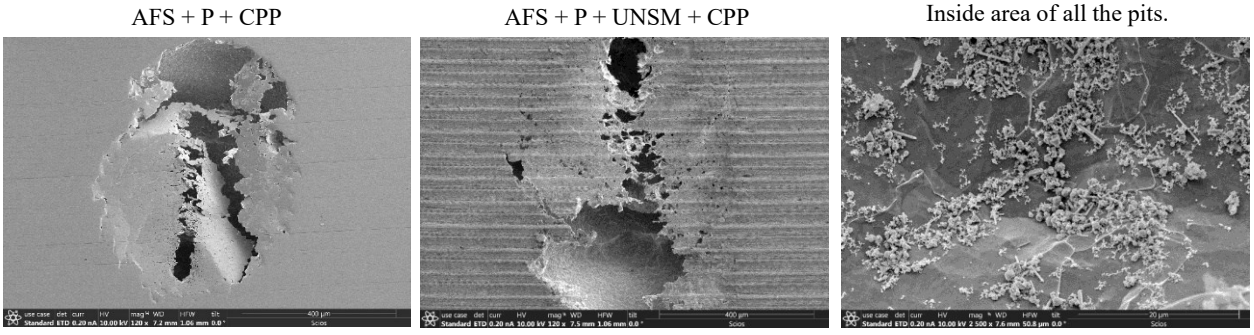

Figure 5.58: SE micrographs showing the corrosion occurring in AFS + P and AFS + P + UNSM specimens during their CPP corrosion tests.

Upon UNSM treating the polished AFS specimen its CR decreased slightly to 0.04 mpy and its pitting potential increased towards a nobler value, with it exhibiting a value of 294 mV. The SE micrograph in the middle of figure 5.58 shows the pit formed on the AFS + P + UNSM specimen which appears similar to the pit formed on AFS + P specimen. Also, the rightmost SE image in figure 5.58 shows the inside area of the pits formed on all the specimens i.e., as-AFS and polished AFS with and without UNSM treatment. And no changes were observed in the pitting mechanism of AFS 304L SS cladding with respect to its various surface conditions studied in this research work.

Coming back to the improvement seen in the pitting potential of AFS + P specimen after its UNSM treatment, it's improvement can be attributed to the grain refinement, increased dislocation density, and majorly to the high magnitude of compressive residual stresses induced into the specimen by the surface treatment. As for the corrosion rate, generally, the peaks and valleys formed by UNSM will act as localized crevice sites resulting in a small increase in the specimen's corrosion rate. But the opposite effect is observed in the polished AFS specimen after UNSM treatment i.e., the corrosion rate slightly declined due to UNSM. Hypothetically, this can be attributed to the removal of inclusions from its surface, which was reported to be possible by UNSM surface treatment of 304 SS (i.e., removal of inclusions) by Shengxi Li [45]. However, more research needs to be done on the inclusions present in AFS deposited 304L SS and to emphatically determine if UNSM treatment is indeed removing the inclusions from its surface leading to a slight decrease in its CR. Nevertheless, it can be concluded with certainty that UNSM treatment is improving the microstructure, surface, mechanical, and corrosion properties of an AFS/MELD deposited 304L SS alloy provided that the oxide layer formed on its surface is removed or prevented from forming by taking measures during MELD processing.

5.3 Discussion

In this chapter, the impact of UNSM surface treatment on the Sensitized, CS, LACS, and AFS 304L SS specimens has been studied extensively, with the intent of enhancing the hardness, residual stress, and corrosion properties of these different 304L SS materials with distinct prior microstructural characteristics through the application of UNSM technique, for the purpose of presenting UNSM as a cost-effective mitigation technique that can effectively deal with the SCC susceptibility of sensitized 304L SS alloy and provide a hermetic seal and restore the load carrying capacity of nuclear canisters repaired through CS or LACS or AFS processing techniques. For this purpose, the impact of UNSM treatment on the microstructures, phase changes, hardness, residual stress, surface topography, sensitization behavior, and pitting corrosion behavior of Sensitized, CS, LACS, and AFS 304L SS specimens has been studied, analyzed, and compared with the prior to UNSM properties of these specimens.

The EBSD analysis performed on the cross-sectional areas of UNSM treated sensitized, CS, LACS, and AFS 304L SS specimens, revealed that the UNSM surface treatment performed on them induced significant amount of severe plastic deformation (SPD) into the specimens resulting in gradient microstructures with extreme near and sub-surface grain refinement as evidenced by the significant increase in number of grain boundaries and decrease in grain size that led to near-surface nano crystallization, dynamic recrystallization, and an enormous increase in dislocation density or embedment of plastic strain into the distinct 304L SS materials studied in this research by their UNSM treatment. The near-surface nano crystallization by UNSM surface treatment in the sensitized, LACS, and AFS 304L SS specimens was induced up to a depth of ~ 10 μm – 20 μm from their surface. The degree of plastic strain present in a material determined by the kernel average misorientation (KAM) value for the sensitized, LACS, and AFS 304L SS specimens increased enormously by ~ 2X, 4X, and 3X times respectively after their UNSM surface treatment.

The SPD induced by UNSM surface treatment also resulted in a 100 % near-surface austenite to martensite phase transformation in the sensitized and AFS deposited 304L SS material. The high strain rates and localized stresses resulting from the SPD caused by UNSM surface treatment generating the high dislocation densities and significant lattice distortions in the material favors the strain-induced transformation of the face-centered cubic (FCC) austenite phase to body-centered tetragonal (BCT) martensite phase, with increased dislocations and grain boundaries acting as nucleation sites for the martensite phase. In contrast, UNSM treated CS and LACS 304L SS coatings exhibited predominantly martensite phase transformation at their surfaces, with a minor presence of residual austenite phase. This residual austenite is attributed to the persistent presence of porosity in these coatings, which creates unevenness on their surface and limits the dynamic penetration of the WC tool tip into the underlying material at the porous sites.

The martensite phase transformation which generally has higher hardness than austenite phase along with the near-surface nano crystallization and immense increase in dislocation density by UNSM led to an enormous increase in the near-surface hardness of sensitized, LACS, and AFS 304L SS by ~ 2X times in all of them. The gradient nature of the microstructures produced by UNSM treatment led to a gradual decrease in the enormously high near-surface hardness values of all the UNSM treated 304L SS specimens along their depth, with the notably higher hardness induced by UNSM lasting up to a depth of ~ 300 μm – 400 μm, 160 μm, and 100 μm in the sensitized, LACS, and AFS 304L SS specimens respectively.

The severe pounding of tungsten carbide (WC) tool tip with its high impact density on the surface of as sprayed CS, as sprayed LACS, and as deposited AFS 304L SS during their UNSM surface treatment resulted in a tremendous decrease in their surface roughness by ~ 3X, 6X, and 2X times respectively which also resulted in improving the uniformity of their surfaces i.e.,

reducing the unevenness on their surfaces to a greater extent by UNSM.

X-Ray Diffraction (XRD) using the conventional $Sin^2\psi$ technique was employed to determine the residual stress state of all the differently processed 304L SS materials studied in this research work which established that the UNSM surface treatment induced monumental magnitudes of beneficial CRSs at the surfaces of sensitized, CS, LACS, and AFS 304L SS specimens along both of their orthogonal directions that lasted in the compressive stress state (having negative magnitude) up to depths of ~ 400 μm, 500 μm (sensitized); 350 μm, 300 μm (CS); 400 μm, 420 μm (LACS); and 500 μm, 470 μm (AFS) from their surface along the step and transverse directions of the respective specimen's UNSM treatment respectively before transitioning to a TRS state (having positive magnitude of residual stress). The CRSs are generated in a material by the creation of stress concentration and strain accumulation regions in it through rearrangement of atomic positions, dislocation pile-up and development of strain incompatibility between neighboring grains caused by the SPD and grain fragmentation in the material during UNSM. The residual stress state due to both the austenite and martensite phases of all the differently processed 304L SS specimens treated with UNSM have been measured at their surface and through-their-depth which revealed that the residual stresses due to austenite and martensite phases are not equi-biaxial. Also, the martensite phase was induced in the sensitized, CS, LACS, and AFS 304L SS specimens up to a depth of ~ 140 μm – 150 μm, 90 μm, 60 μm - 70 μm, and 60 μm – 100 μm respectively along both of their orthogonal directions by the UNSM surface treatment.

The full width half maximum (FWHM) profiles determine the extent of plasticity present in a material along the depth of the respective specimen which revealed that UNSM induced a significantly higher degree of plastic strain at the near-surface of sensitized, LACS, and AFS 304L SS specimens that gradually decreased along their depth before reverting to the plasticity levels present in their respective untreated 304L SS specimens. The significantly higher degree of plastic

strain induced by UNSM in the sensitized, LACS and AFS 304L SS specimens lasted up to a depth of ~ 200 µm – 230 µm, 200 µm, and 300 µm respectively which aligned well with the observations made from their respective KAM maps which also give an indication of the plastic strain present in a material. Whereas in the CS specimen which already has a significant degree of plastic strain in it prior to surface treatment due to the cold work generated by the bombardment of powder particles during CS processing, the UNSM surface treatment of CS 304L SS specimen resulted in a slight strain relief at its sub surface in between 20 µm and 200 µm due to the dynamic recovery and dynamic recrystallization occurring in it by UNSM as observed from its FWHM depth profiles. The dynamic recovery and dynamic recrystallization occurring by UNSM in an already heavily deformed material can help redistribute the plastic strain to the newly formed grains resulting in a decrease of the strain concentration that was present in the former heavily deformed areas.

Impact of UNSM on the Corrosion Behavior of Sensitized 304L SS

Sensitization Behavior - Double loop electrochemical potentiodynamic reactivation (DLEPR) tests performed in 0.5M H_2SO_4 + 0.05M KSCN solution: The UNSM surface treatment performed on the 304L SS specimens sensitized at 650°C for 5h (S5) and 24h (S24) resulted in an improvement in the degree of sensitization (DOS) of only the S5 specimen by ~ 10 X times which was attributed to the chromium redistribution occurring in it because of the extreme grain refinement caused by the SPD during UNSM. The Cr redistribution in S5 specimen by UNSM reduces the overall surface area of the small sized and isolated chromium depleted zones (CDZs) present in it prior to surface treatment leading to the formation of a stronger chromium oxide film on the UNSM treated S5 specimen surface that would greatly resist corrosion yielding a much-improved DOS than the untreated S5 specimen.

Unlike S5 specimen which had small and isolated CDZs, the S24 specimen had large and

very well-interconnected CDZs due to which UNSM had no impact on the DOS of S24 specimen i.e., redistribution of Cr to these large well-interconnected CDZs was not possible through the UNSM surface treatment. This led to the hypothesis that UNSM surface treatment's positive influence on improving the DOS of sensitized 304L SS has a limitation which depends on the size and distribution characteristics of CDZs present in the sensitized material. Further research is required to determine the critical size of CDZs which can be affected or reduced in size through Cr redistribution at the specimen surface by UNSM surface treatment thereby, consequently resulting in the improvement of the sensitized 304L SS specimens DOS or sensitization behavior. However, it can be expressed here that UNSM treatment could be effective in reducing the DOS of welded 304L SS material since a welded material undergoes sensitization phenomenon for only a few minutes to less than an hour depending on the welding technique being employed.

Pitting Corrosion Behavior - Cyclic potentiodynamic polarization (CPP) tests performed in 3.5 Wt.% NaCl solution: Nevertheless, even though UNSM surface treatment could not improve the sensitization behavior of S24 specimen, its pitting potential in 3.5 Wt.% NaCl solution improved significantly by UNSM, with UNSM treatment bringing its value extremely close to the pitting potential of solution annealed (SA) specimen. This improvement in the pitting potential of surface treated S24 specimen is attributed to the very high magnitude of compressive residual stresses induced into the S24 specimen by UNSM which are contributing in resisting the formation of stable pits for a longer time in the UNSM treated S24 specimen than when compared to the untreated S24 specimen. In addition to the significant improvements seen in the sensitzation behavior of S5 specimen and pitting corrosion behavior of S24 specimen, both their residual stress state and hardness characteristics improved tremendously by UNSM which are all extremely beneficial in improving the SCC resistance characteristics of sensitized 304L SS alloy.

Impact of UNSM treatment on the Sensitization Behavior of CS, LACS, and AFS 304L SS

CS 304L SS: The cold sprayed 304L SS coatings have very tiny grains possessing inherently weak interparticle bonding, due to which the CS specimen in both of its as sprayed (as-CS) and polished (CS + P) surface conditions experiences heavy metal dissolution during their DLEPR tests consequently resulting in higher DOS ratios.

The application of UNSM surface treatment on the surfaces of as sprayed (as-CS + UNSM) and polished CS (CS + P + UNSM) specimens does not yield in any improvement in the sensitization behavior of CS 304L SS because the UNSM treatment process does not involve the application of any significant amount of heat input into the specimen being surface treated and therefore, will not be able to improve the inherently weak interparticle bonding existing in the CS 304L SS coating. Thus, UNSM treatment could not improve the sensitization behavior of the CS 304L SS coatings.

LACS 304L SS: The as sprayed LACS (as-LACS) coating exhibited an even worse DOS ratio than the as-CS coating which is attributed to the combined effect of the surface oxide film formed on the as-LACS surface due to the application of high temperature laser during its processing, persistent presence of porosity in the coating and its high surface roughness. With the porosity and the surface roughness of as-CS and as-LACS coatings being approximately the same, the significant difference between their DOS ratios is attributed to the presence of surface oxide film on the latter specimen.

The UNSM treatment of as-LACS coating (as-LACS + UNSM) resulted in a breakdown of the majority of the deleterious oxide film on its surface, reduction in its surface roughness, and possible partial closure of porosity sites as well but the DOS ratio of as-LACS + UNSM specimen was equally worse as that of the as-LACS specimen. This is attributed to the other consequences

of UNSM treatment of as-LACS specimen seen on its surface like the creation of sharp-edged smudges due to the severe pounding of WC tool tip on the bubbled like surface of as-LACS coating and the dispersion of broken-down oxide particles on its surface by UNSM, both of which act as localized corrosion sites where passive film breaks down with relative ease and onsets the accelerated corrosion phenomenon in the surface treated as-LACS specimen similar to the untreated as-LACS specimen thereby, both the specimens yielding worse DOS ratios.

The polished LACS coating (LACS + P) yielded a much-improved DOS ratio exhibiting a value of ~ 6X times less than the DOS ratios of as-LACS and as-LACS + UNSM specimens. This significant improvement in the sensitization behavior of LACS + P coating is attributed to the removal of the deleterious surface oxide film and the significant decrease in surface roughness of as-LACS coating by polishing. The removal of deleterious surface oxide film and the decrease in surface roughness by polishing reduces / limits the number of localized concentration sites present in the LACS + P coating, to its lone porosity sites. This significant reduction in the number of localized concentration sites by polishing will in turn result in the improvement of the passive film characteristics of LACS + P coating reducing the corrosion experienced by it compared to the as-LACS and as-LACS + UNSM coatings. Also, the DOS ratio obtained for the LACS + P coating can be regarded as the true DOS ratio of LACS processed 304L SS material.

The UNSM treatment of LACS + P coating (LACS + P + UNSM) further improved the DOS ratio of LACS + P coating by slightly more than 2X times. This improvement in the sensitization behavior of LACS + P specimen by surface treatment is attributed to the partial closure of porosity sites by UNSM leading to the formation of a stronger passive oxide film on the surface of LACS + P + UNSM specimen consequently resulting in a decrease in its corrosion or improvement in the DOS ratio. Unlike UNSM of as-LACS specimen, LACS + P + UNSM

specimen surface was free of sharp-edged smudges and embedded oxide particles because of the removal of bubbled rougher surface and oxide film present on the as-LACS specimen surface by polishing prior to surface treatment. This was also a crucial contributing factor in the improvement seen in the DOS of LACS + P coating by UNSM.

AFS 304L SS: The thick oxide film present on the surface of as deposited AFS (as-AFS) and the inability to completely remove the oxide film by UNSM surface treatment led to the extremely high DOS ratios obtained by the as-AFS and as-AFS + UNSM specimens.

The true DOS ratio of the 304L SS material deposited by AFS processing technique is obtained from the oxide free polished surface of AFS coating (AFS + P) whose value is extremely close to the DOS ratio obtained by the conventionally hot-rolled and solution annealed 304L SS plate specimen indicating that the 304L SS deposited by AFS is free of porosity or close to 100 % dense.

Upon UNSM treating the polished AFS specimen (AFS + P + UNSM) its DOS ratio slightly worsened due to the formation of peaks and valleys on its surface by the impact of WC tool tip on its surface during UNSM. These peaks and valleys can act as localized concentration sites for corrosion during the reverse scan of its DLEPR test.

However, the DOS ratio of AFS + P + UNSM specimen is still ~ 70 X times lower than the DOS ratio of 304L SS specimen sensitized at 650°C for 5h and ~ 370 X times lower than the DOS ratio of 304L SS specimen sensitized at 650°C for 24h indicating that the AFS + P + UNSM specimen still represents that of an unsensitized material with the added beneficial components of near-surface nano crystallization, near-surface hardening and high magnitude of compressive residual stresses induced into the AFS + P cladding by UNSM, which can lead to an enhancement in its SCC resistance.

Impact of UNSM treatment on Pitting Corrosion Behavior of CS, LACS, & AFS 304L SS

Corrosion rate

The corrosion rate of a material is largely dependent on the amount of exposed surface area or surface roughness of the material and the number of inclusions or impurities present on its surface that can act as localized corrosion sites which can be preferentially attacked by the corrosive environment leading to the occurrence of localized corrosion phenomenon such as pitting or crevice corrosion.

CS and LACS 304L SS: The extremely high unevenness on the surfaces of as-CS and as-LACS 304L SS coatings provides numerous localized corrosion sites where the corrosive chloride ions in the test solution can accumulate leading to enhanced localized corrosive attack at these sites by the setup of concentration cells which resulted in an extremely high corrosion rates (CRs) to be obtained for the as-CS and as-LACS 304L SS coatings.

Both polishing (CS +P & LACS + P) and UNSM treatment (as-CS + UNSM & as-LACS + UNSM) of as-CS and as-LACS 304L SS coatings resulted in a significant decrease in their CRs which is attributed to the significant decrease in the unevenness of their surfaces by these actions which in turn results in a decrease in the degree of concentration cells that can be setup on its surface by the corrosive chloride ions in the test solution thereby, decreasing their CRs significantly. Smaller degree of concentration cells can be setup on the polished CS and LACS coatings at their porosity sites and in the UNSM treated as-CS and as-LACS coatings, even though their surface roughness decreased considerably by UNSM, the surface roughness of as-CS + UNSM and as-LACS + UNSM specimens is still notably higher than the polished CS and LACS specimens therefore, allowing a median degree of concentration cells to be setup on their surface that are lower in degree than the as sprayed coatings but higher in degree than the polished

coatings. This is why the CR of as-CS + UNSM and as-LACS + UNSM are slightly higher or worse than the CS + P and LACS + P coatings respectively.

The UNSM treatment performed on the CS + P coating created sharp-edged smudges along the UNSM tracks because of the heavy plastic deformation already present in the CS coatings restricting the dynamic penetration of WC tool tip into the CS material during UNSM. These smudged areas on the surface of CS + P + UNSM coating can act as localized crevice sites where the chlorides in the test solution can accumulate and attack preferentially thereby, slightly worsening its corrosion rate from that of the CS + P coating. Whereas the UNSM treatment performed on the LACS + P coating results in a smudge free surface because of the lower hardness of LACS coating allowing the WC tool tip to efficiently apply the dynamic load into the material. Also, UNSM treatment of LACS + P specimen results in the partial closure of the pores on its surface decreasing the area of localized corrosion sites available for the corrosive solution to attack. Therefore, the smudge free surface and the reduction in pore area of the LACS + P coating by UNSM treatment reduces the total number of preferential sites for the corrosive solution to attack thereby, decreasing the corrosion rate of LACS + P + UNSM treated coating from that of the LACS + P coating.

AFS 304L SS: The high surface roughness and the thick non-homogenous oxide film on the surface of as-AFS cladding and the inability of UNSM surface treatment to remove this thick oxide film from its surface contributed to the presence of numerous localized corrosion sites on the surface of as-AFS and as-AFS + UNSM specimens where the chloride ions accumulate and preferentially attack eventually leading to these two specimens exhibiting extremely high CRs.

Polishing the as-AFS specimen removes the deleterious oxide film on its surface and reduces its surface roughness as well thereby reducing the presence of localized corrosion sites on

its surface because of which the CR of AFS + P specimen improved tremendously from that of as-AFS specimen's CR. But it's CR is still slightly higher than the SA + P specimen's CR and also slightly higher than the CS + P and LACS + P 304L SS specimen's CRs which have porosity, thereby leading to the hypothesis that AFS 304L SS cladding has inclusion and/or impurities on its surface (i.e., on AFS + P specimen surface) which are contributing to its slightly higher CR than that of the other specimens mentioned before.

UNSM treatment performed on the AFS + P specimen resulted in a further improvement in its CR to a smaller degree, bringing its value closer to that of LACS + P specimen and better than that of CS + P specimen, which is attributed to the removal of some inclusions present on the surface of AFS + P specimen by UNSM.

Pitting Behavior

CS and LACS 304L SS: Because of the high corrosion rates of as-CS and as-LACS coatings, they could not exhibit any pitting potential indicating that a stable passive film that could resist pitting was not able to form on them at any point during their CPP tests. That is due to the higher degree of concentration cells of chloride ions being setup on the as-CS and as-LACS coatings because of the higher variations in their surface unevenness led to their inability of being able to show any re-passivation ability of the initial pits formed on their surface thereby, resulting in the continuous growth of the pits formed on their surface throughout their CPP tests without yielding any sign of resistance to pitting. In short, the kinetics of chloride ions attack at the pits or accumulation regions is much greater than the kinetics of passive film regeneration at these regions or pits.

UNSM treatment performed on as-CS and as-LACS coatings could not instill a pitting resistance in these coatings because even though the uniformity of these coatings' surfaces

improved by their UNSM i.e., reduction in their unevenness, their surface roughness is still slightly rougher than ideal conditions (like polished surface) allowing a median degree of concentration cells to be setup on the surfaces of as-CS + UNSM and as-LACS + UNSM specimens which undermines the possibility of them exhibiting a pitting potential or resistance to pitting. However, the increase in the area of hysteresis loops seen from the CPP test curves of UNSM treated as-CS and as-LACS specimens from that of their untreated specimens indicates that UNSM treatment is improving the corrosion behavior of as-CS and as-LACS coatings and confirms that only a median degree of concentration cells were setup on their surfaces. That is the kinetics of chloride ions attack at the accumulated regions or pits slowed down in the UNSM treated as-CS and as-LACS from that of the untreated as-CS and as-LACS specimens.

Polishing the as-CS and as-LACS coatings led to them exhibiting a pitting potential because polishing reduces the localized corrosion sites on their surface to the lone small porosity sites present in them where the accumulation of chloride ions occur at a much slower rate than on the rougher surfaces of as-CS and as-LACS coatings thereby, delaying the formation of stable pits i.e., allowing the pits to re-passivate (unstable pits). The kinetics of passive film regeneration at the initial pits formed on the CS + P and LACS + P specimens' surface during their CPP tests is greater than the kinetics of chloride ions attack at these areas.

UNSM treatment of the CS + P and LACS + P coatings further improved their pitting potentials to exhibit nobler values because of two contributing factors, of which one factor contributing in a minor capacity is the partial closure of porosity sites on their surfaces by UNSM. More importantly, the major factor contributing to the further improvement seen in the pitting potential of CS + P and LACS + P coatings by UNSM is the induction of very high magnitudes of CRSs into these specimens which assist in providing further resistance to the formation of stable

pits on their surfaces.

AFS 304L SS: Due to the very high corrosion rates of both as-AFS and as-AFS + UNSM specimens stable pits form readily on their surface thereby showing no pitting potential at all by these specimens. However, these pits were seen forming majorly on the thick oxide film present on their surface and hence, do not represent the pitting characteristics of the 304L SS material deposited by AFS processing technique or the impact of UNSM on it.

Polished AFS specimen reveals the actual surface of 304L SS material deposited by AFS which exhibits a pitting potential indicating that the material does have the ability to re-passivate any initially formed pits and that it does show a resistance to pitting by chloride ions.

The pitting potential of AFS + P + UNSM specimen improved further to a nobler value indicating an improvement in the pitting corrosion characteristics of AFS + P specimen by UNSM which is attributed to the extreme grain refinement, increased dislocation density and high magnitude of compressive residual stresses induced into the specimen by the surface treatment.

Finally, the hypothesis driven discoveries and the major conclusions drawn from this dissertation research work performed on the differently processed 304L SS materials with distinct prior microstructural characteristics are presented in detail in the next chapter.

Chapter 6. Summary of Impact to the Field, Conclusions, and Scope for Future Work

6.1 Summary of Impact to the Field

The research work presented in this dissertation makes many significant scientific and mechanistic advancements to the field of tackling Chloride-Induced Stress Corrosion Cracking (CISCC) Susceptibility of welded austenitic 304L SS Spent Nuclear Fuel Dry Storage Canisters (SNFDSCs), with respect to both the prevention or enhancement of resistance to Stress Corrosion Cracking (SCC) susceptibility of newly built canisters and to repair and mitigate the CISC-Cracks formed on the already existing canisters, by studying the material deposited through a variety of competent additive manufacturing repair methods such as Cold Spray (CS), Laser Assisted Cold Spray (LACS), and Additive Friction Stir (AFS), with mitigation to be provided by cost-effective Ultrasonic Nanocrystal Surface Modification (UNSM) technique. Some of the advancements fill the gap existing in the scientific literature, such as determining the underlying factors responsible for the improvement of SCC resistance of sensitized or welded 304 SS / 304L SS alloy by the application of UNSM treatment on their surface. Whereas others present new data and analysis that will be extremely useful, especially to the nuclear industry, in evaluating the solid-state AM manufacturing techniques that are being considered for the repair of CISC-Cracks in nuclear canisters, such as determining the corrosion behavior of 304L SS alloy deposited by CS, LACS, and AFS processing techniques, which has been attempted for the first time and demonstrating the need and potential of utilizing a cost-effective mitigation technique such as UNSM to substantially improve the SCC resistant properties of CS or LACS or AFS repaired / deposited 304L SS alloy.

The hypothesis driven discoveries made from this dissertation research work include, the discovery that the improvement seen in the SCC resistance of sensitized or welded 304 SS / 304L SS alloy by UNSM treatment involves dual impact, one with respect to improving its pitting

corrosion behavior by the induction of high magnitudes of compressive residual stresses into the material by UNSM and the other with respect to improving its sensitization behavior by the reduction in the area of chromium depleted zones through uniform redistribution of Cr in the alloy composition by UNSM treatment, making UNSM a unique mitigation technique that can have a dual impact on the corrosion behavior of 304 SS / 304L SS alloy, unlike other mitigation techniques like LSP which involve high temperatures deeming them incapable of positively influencing the sensitization behavior of the alloy. But it is also further hypothesized that there is a critical size limit on the chromium depleted zones that can be positively influenced by UNSM thereby leading to a reduction in their area or reduction in the sensitized alloy's degree of sensitization i.e., UNSM will be ineffective in improving the sensitization behavior of sensitized 304L SS alloy, when the chromium depleted zones present in it are beyond a critical size limit.

Also, it was discovered that UNSM treatment of 304 SS / 304L SS alloy resulting in the phase transformation of FCC austenite to BCT martensite, leaving the presence of either 100 % strain induced martensite as in UNSM treated SA, Sensitized, and AFS 304L SS materials, or a mixture of strain induced martensite and residual austenite as in UNSM treated CS and LACS 304L SS specimen surfaces, does not have a negative impact on either the alloy's pitting corrosion behavior in 3.5 Wt. % NaCl solution / simulated seawater containing environment or on its sensitization behavior i.e., the presence of strain induced martensite does not have a negative impact on the corrosion behavior of 304 SS / 304L SS alloy and also, the mixed presence of strain induced martensite and residual austenite on its surface does not lead to galvanic corrosion in the alloy.

Finally, it was also discovered that, despite the differences in the prior microstructural characteristics of 304L SS alloy (as in Sensitized, CS, LACS, and AFS 304L SS materials), UNSM

can effectively enhance the alloy's properties of residual stress and pitting corrosion behavior in a consistent manner but it's impact on the alloy's near and sub-surface hardness, phase transformation, dislocation density, grain refinement, surface topography, and sensitization behavior varies or depends on the prior microstructural characteristics including the presence of prior cold work, porosity levels, chromium depleted zones size, distribution etc. which are discussed extensively in Chapter 5 of this dissertation research work and the conclusions drawn are given below in section 6.2.

Overall, this thesis research study demonstrated that UNSM surface treatment of sensitized, LACS, and AFS 304L SS resulted in inducing severe plastic deformation into these specimens that led to near-surface nano crystallization, near-surface hardening, reduction in the surface unevenness of as processed LACS and AFS specimens, induction of high magnitudes of CRSs up to an appreciable depth, and improvements in the passivation, sensitization, corrosion rate, and pitting corrosion characteristics of these specimens which are all beneficial in improving the SCC resistance of 304L SS alloy. Hence, LACS and AFS repair methods in conjunction with UNSM mitigation technique can be a plausible avenue to seal the CISCC cracks on the welded austenitic SNFDSCs thereby restoring their hermetic seal and load carrying capacity. However, the 304L SS material deposited through CS repair method has been determined to possess inferior corrosion properties which could not even be improved by UNSM treatment deeming the use of CS or CS with UNSM to be ineffective for the purpose of dealing with CISCC problem in the SNFDSCs. Nevertheless, UNSM can be a cost-effective mitigating alternative method to LSP or an additional mitigating method to efficiently and effectively tackle the sensitization phenomenon or the SCC susceptibility of newly constructed welded austenitic 304L SS SNFDSCs.

6.2 Conclusions

The key conclusions drawn from this dissertation research work are presented below in detail but in no particular order:

1. The UNSM surface treatment performed on the different 304L SS materials studied in this research work possessing distinct prior microstructural characteristics, such as a material with chromium depleted zones – Sensitized, a material with porosity, weak interparticle bonding, and cold work – CS, a material with porosity and improved interparticle bonding – LACS, and a material fully dense, possessing gradient microstructure and near-surface nano crystalline grains – AFS, was able to induce a significant amount of severe plastic deformation (SPD) into all the specimens except the already cold worked and heavily deformed CS 304L SS coating material, resulting in gradient microstructures with extreme near and sub-surface grain refinement as evidenced by the significant increase in number of grain boundaries and decrease in grain size that led to near-surface nano crystallization, dynamic recrystallization, and an enormous increase in dislocation density or embedment of plastic strain into the UNSM treated Sensitized, LACS, and AFS 304L SS specimens. The near-surface nano crystallization by UNSM surface treatment in the sensitized, LACS, and AFS 304L SS specimens was induced up to a depth of ~ 10 μm – 20 μm from their surface. The degree of plastic strain present in a material determined by the kernel average misorientation (KAM) value for the sensitized, LACS, and AFS 304L SS specimens increased enormously by ~ 2X, 4X, and 3X times respectively after their UNSM surface treatment. This high degree of plastic strain introduced into the 304L SS specimens through UNSM treatment is attributed to the multiplication & entanglement of dislocations and grain fragmentation, that is caused by the severe pounding of WC tool tip on their surface during UNSM treatment resulting in an increase in their total grain boundary area and

dislocation density. Whereas in the UNSM treated CS 304L SS coating, a very small degree of grain refinement combined with a slight decrease in KAM value was observed from that of its untreated CS 304L SS coating, indicating the occurrence of only a very small degree of dynamic recrystallization in the CS 304L SS coating by UNSM, which is attributed to the presence of prior cold work, that is generated in the CS 304L SS coating during its processing, restricting the impact of UNSM surface treatment.

2. The microstructures of Sensitized, CS, LACS, and AFS 304L SS, having predominantly austenitic microstructures with the presences of a minor amount of delta ferrite in them, have undergone a strain induced phase transformation from face-centered cubic (FCC) austenite phase to body-centered tetragonal (BCT) martensite phase, due to their UNSM surface treatment. But due to the differences in their prior microstructural characteristics that were mentioned earlier in conclusion (1), the degree of austenitic to martensitic phase transformation by UNSM surface treatment has not been the same or consistent among the distinct 304L SS specimens studied in this research work. The SPD induced by UNSM surface treatment resulted in a 100 % near-surface austenite to martensite phase transformation in the sensitized and AFS deposited 304L SS material. In contrast, UNSM treated CS and LACS 304L SS coatings exhibited predominantly martensite phase transformation at their surfaces, with a minor presence of residual austenite phase. This residual austenite is attributed to the persistent presence of porosity in these coatings, which creates unevenness on their surface and limits the dynamic penetration of the WC tool tip into the underlying material at the porous sites. The SPD caused by UNSM results in high strain rates and localized stresses, generating high dislocation densities and significant lattice distortions in the material, which favor the strain-induced transformation of the FCC

austenite phase to BCT martensite phase, with the increased dislocations and grain boundaries acting as nucleation sites for the inception of martensite phase.

3. UNSM surface treatment resulting in martensitic phase transformation which generally has higher hardness than austenite phase, along with the extensive grain refinement resulting in near-surface nano crystallization, sub-surface deformation - leading to a reduction in grain size, and the immense increase in dislocation density, number of grain boundaries - impeding dislocation motion, together led to an enormous increase in the near-surface hardness of sensitized, LACS, and AFS 304L SS specimens consistently, by ~ 2X times, despite the differences existing in the prior microstructural characteristics of these three specimens. The gradient nature of the microstructures produced by UNSM treatment led to a gradual decrease in the enormously high near-surface hardness values of all the UNSM treated 304L SS specimens along their depth, with the notably higher hardness induced by UNSM lasting up to a depth of ~ 300 μm – 400 μm, 160 μm, and 100 μm in the sensitized, LACS, and AFS 304L SS specimens respectively. Whereas in the case of CS 304L SS coating, the impact of UNSM treatment on its near-surface hardness has been very minimal resulting in an increment of only ~ 1.1X – 1.3X times, that too confined to only the top 10 to 20 μm of its surface, which is again attributed to the presence of prior heavy deformation / cold work generated during the traditional CS processing, restricting the dynamic load transfer through the WC tool tip to its surface during UNSM.
4. The severe pounding of tungsten carbide (WC) tool tip with its high impact density on the surface of as sprayed CS, as sprayed LACS, and as deposited AFS 304L SS during their UNSM surface treatment resulted in a tremendous decrease in their surface roughness by ~ 3X, 6X, and 2X times respectively which also resulted in improving the uniformity of

their surfaces i.e., reducing the unevenness on their surfaces to a greater extent by UNSM.

5. The UNSM surface treatment induced monumental magnitudes of beneficial CRSs at the surfaces of sensitized (> -1600 MPa – SD; > -900 MPa – TD), CS (> -1200 MPa – SD; > -700 MPa – TD), LACS (> -1300 MPa – SD; > -800 MPa – TD), and AFS (> -1900 MPa – SD; > -1000 MPa – TD) 304L SS specimens along both of their orthogonal directions that lasted in the compressive stress state (having negative magnitude) up to depths of ~ 400 µm, 500 µm (sensitized); 350 µm, 300 µm (CS); 400 µm, 420 µm (LACS); and 500 µm, 470 µm (AFS) from their surface along the step and transverse directions of the respective specimen's UNSM treatment's directions respectively before transitioning to a TRS state (having positive magnitude of residual stress). The austenite to martensite phase transformation occurring due to the UNSM surface treatment in the distinct 304L SS materials studied in this research work, led to the induction of martensite phase in the sensitized, CS, LACS, and AFS 304L SS specimens up to a depth of ~ 140 µm – 150 µm, 90 µm, 60 µm - 70 µm, and 60 µm – 100 µm respectively along both the orthogonal directions of these distinct 304L SS specimens. The CRSs are generated in a material by UNSM surface treatment due to the creation of stress concentration and strain accumulation regions in it, through the rearrangement of atomic positions, dislocation pile-up and development of strain incompatibility between neighboring grains, that is caused by the SPD and grain fragmentation in the material during UNSM.

6. The full width half maximum (FWHM) profiles obtained during the residual stress depth profile analysis, which determine the extent of plasticity present in a material along the depth of the respective specimen, showed that UNSM treatment induced a significantly higher degree of plastic strain at the near-surface of sensitized, LACS, and AFS 304L SS specimens that gradually decreased along their depth before reverting to the plasticity

present in their respective untreated 304L SS specimens. The significantly higher degree of plastic strain induced by UNSM in the sensitized, LACS, and AFS 304L SS specimens lasted up to a depth of ~ 200 µm – 230 µm, 200 µm, and 300 µm respectively which aligns well with the observations made from their respective KAM maps which also give an indication of the plastic strain present in a material. Whereas in the case of CS 304L SS coating, which already has a significant degree of plastic strain present in it prior to surface treatment due to the cold work generated by the bombardment of powder particles during CS processing, the UNSM surface treatment of CS 304L SS coating resulted in a small degree of strain relief at its sub surface in between 20 µm and 200 µm due to the dynamic recovery and dynamic recrystallization occurring in it by UNSM as observed from its FWHM depth profiles. The dynamic recovery and dynamic recrystallization occurring by UNSM in an already heavily deformed material can help redistribute the plastic strain to the newly formed grains resulting in a decrease in the strain concentration that was present in the former heavily deformed areas as indicated from both the FWHM profiles and a slight decrease in KAM value of CS 304L SS coating after UNSM.

7. UNSM treatment led to an improvement in the degree of sensitization of 304L SS specimen sensitized at 650°C for 5h (S5) by ~ 10X times, which is attributed to the reduction in the overall area of chromium depleted zones (CDZs) in the sensitized material, that is occurring due to the severe hammering of WC tool tip on its surface causing Cr redistribution in the alloy composition thereby, restoring some of the strength of the naturally forming passive chromium oxide film on the surface of the sensitized specimen by UNSM treatment which in turn improves its ability to resist corrosion. However, when the size of the CDZs increased vastly and became well interconnected with each other due

to prolonged aging / sensitization treatment i.e., in the case of 304L SS specimen sensitized at 650°C for 24h (S24), UNSM treatment has proved to be ineffective in reducing the DOS of this heavily sensitized 304L SS specimen. Therefore, it is hypothesized that UNSM treatment is only effective in positively influencing the sensitization behavior of sensitized 304L SS alloy when the CDZS in it are up to a critical size.

8. Nevertheless, UNSM treatment performed on the 304L SS specimen sensitized at 650°C for 24h (S24), notably improved its pitting potential in 3.5 Wt.% NaCl solution or simulated seawater containing environment to a nobler value that is extremely close to the pitting potential of SA 304L SS specimen. This improvement in the pitting potential of surface treated heavily sensitized 304L SS specimen is attributed to the introduction of very high magnitudes of compressive residual stresses into the material through SPD by UNSM surface treatment, which are contributing in resisting the formation of stable pits for a longer time in the UNSM treated S24 specimen than when compared to the untreated S24 specimen. In totality, it can be said that UNSM treatment can remarkedly amend the sensitization behavior of lightly sensitized material (which is representative of typically welded material) and also enhance the resistance to pitting corrosion of heavily sensitized material, along with significantly improving the residual stress state and hardness characteristics of sensitized 304L SS specimens (irrespective of the degree of sensitization present in the specimen), all of which will be extremely beneficial in improving the SCC resistance of sensitized 304L SS alloy.
9. The degree of susceptibility (DOS) ratio of as-CS 304L SS coating was found to be high, with it being on par with that of the S24 304L SS specimen (i.e., sensitized at 650°C for 24h), which is attributed to the porosity and inherent weak interparticle bonding of CS

304L SS coating. Whereas the DOS ratios of as-LACS and as-AFS 304L SS specimens were found to be worse than the as-CS coating's DOS ratio, which were attributed to the presence of an inhomogeneous or deleterious oxide film on the surface of both the former specimens and additionally to the presence of porosity in the as-LACS 304L SS coating. This inhomogeneous or deleterious oxide film forms on the surfaces of as-LACS and as-AFS 304L SS coating / cladding during their processing, as both the processes are performed in open atmosphere involving semi-high to high temperatures in their processing techniques. Although polishing of as-LACS and as-AFS 304L SS specimens improved their DOS ratios due to the removal of oxide film on their surfaces by polishing, the DOS ratio of CS 304L SS coating has not been improved by its polishing, ascertaining the fact that its inherent weak interparticle bonding is indeed the factor contributing to its worse DOS ratio, especially with both the CS and LACS 304L SS coatings having approximately the same degree of porosity levels.

10. Similar to the DOS ratios, the corrosion rate (CR) of as-CS 304L SS coating was found to be extremely high which is attributed to the coating's extremely high surface roughness resulting in the formation of higher degree of corrosive chloride ion concentration cells to be setup on its surface. With the presence of deleterious oxide film on the surfaces of as-LACS and as-AFS 304L SS coatings contributing to the addition of more localized concentration sites where corrosive chloride ions can be setup, their CRs were found to be even worse than that of as-CS 304L SS coating's CR, and especially with the surface roughness of as-CS and as-LACS 304L SS coatings being approximately the same and with the surface roughness of as-AFS cladding being less than the former coatings, ascertains the fact that the presence of oxide film on the surfaces of as-LACS and as-AFS 304L SS

specimens is indeed the exact factor that is further affecting their CRs in a negative manner from that of the as-CS 304L SS coating's CR and also ascertains the fact that the oxide film formed on their surface is in fact detrimental to the corrosion behavior (both in terms of DOS and CR) of the as deposited LACS and AFS 304L SS coating / cladding materials. Again, like DOS ratios, polishing of as-LACS and as-AFS 304L SS specimens, resulted in an improvement of their CRs but this time, polishing of as-CS 304L SS coating also resulted in an improvement in its CR, which ascertains the fact that the extremely high surface roughness of as-CS, as-LACS, and as-AFS 304L SS specimens and the presence of oxide film on the latter two specimens are indeed contributing to their high CRs. So, the improvement in the CR of polished CS, LACS, and AFS 304L SS specimens from that of their as-deposited versions is attributed to the removal of oxide film and decrease in surface roughness by polishing action, which results in a reduction in the number of localized concentration sites on the surfaces of polished CS, LACS, and AFS specimens where setup of concentration cells by the corrosive chloride ions will decrease or be difficult thereby, resulting in the decrease of their CRs. Nevertheless, the CRs of even the polished CS and LACS 304L SS specimens were found to be slightly higher than those of polished SA 304L SS specimen and the CR of polished AFS cladding was found to be slightly further higher than that of the polished CS and LACS coatings CRs. This draws for a conclusion that the presence of porosity sites on the CS and LACS coating surfaces led to them exhibiting slightly higher CRs than that of polished SA specimen's CR, whereas with respect to the polished AFS cladding, even though it is 100 % dense, its CR being higher than that of polished CS and LACS coatings suggests the presence of inclusions and/or impurities on its surface that are contributing to its slightly higher CR than that of the latter specimens.

11. Any pitting potential or resistance to pitting could not be exhibited by the as-CS, as-LACS, and as-AFS 304L SS specimens, owing to their extremely high corrosion rates not allowing the formation of a stable passive film on their surface that could resist pitting. That is due to the higher degree of concentration cells being setup by the corrosive chloride ions on the surfaces of as-CS, as-LACS, and as-AFS specimens, because of the higher variations in their surface unevenness and presence of inhomogeneous deleterious oxide film on the latter two specimen surfaces, led to their inability of being able to show any re-passivation of the initial pits formed on their surface thereby, resulting in the continuous growth of the initial pits formed on their surface throughout their corrosion tests without yielding any sign of resistance to pitting. In short, the kinetics of chloride ions attack at the pits or chloride ion accumulation regions is much greater than the kinetics of passive film regeneration at these pits or regions in the as deposited CS, LACS, and AFS 304L SS specimens. Upon polishing the as-CS, as- LACS, and as-AFS 304L SS specimens, they exhibit a pitting potential showing resistance to the pitting phenomenon occurring in these specimens during their CPP tests. This exhibition of pitting potential by CS + P, LACS + P, and AFS + P 304L SS specimens, is attributed to the polishing action reducing the localized corrosion sites on their surfaces to the lone porosity sites in the case of CS + P and LACS + P specimens and to the lone inclusions or impurities in the case of AFS + P specimen, thereby significantly slowing down the accumulation of chloride ions on their surfaces during CPP tests than when compared to the extremely rougher and/or oxidized surfaces of as-CS, as-LACS, and as-AFS specimens that are having numerous corrosive chloride ion accumulation sites, ultimately resulting in a significant delay in the formation of stable pits on the surface of polished CS, LACS, and AFS specimens i.e., allowing the

initial pits formed on their surface to re-passivate (unstable pits) during their CPP tests and allowing them to exhibit a pitting potential. That is, the kinetics of passive film regeneration at the initial pits formed on the CS + P, LACS + P, and AFS + P specimen surfaces during their CPP tests is greater than the kinetics of chloride ions attack at these areas.

12. Despite the better interparticle bonding of LACS coating from that of the CS coating and despite both the coatings having approximately the same degree of porosity levels, the pitting potential of polished CS 304L SS coating was notably nobler than the pitting potential of polished LACS coating due to the presence of decent magnitudes of compressive residual stresses in the CS coating, which are assisting it to exhibit better resistance to the pitting phenomenon. But despite the polished AFS cladding having lower magnitudes of CRSs than polished CS coating, the pitting potential of polished AFS 304L SS cladding was significantly nobler than the pitting potential of polished CS 304L SS coating due to the latter specimen having some degree of porosity in it and the former specimen being completely dense. And despite both the polished SA and polished AFS 304L SS specimens being 100 % dense and having similar magnitudes of compressive residual stresses, the pitting potential of polished SA 304L SS specimen was significantly nobler than the pitting potential of AFS 304L SS cladding, which indicates the presence of greater number of inclusions in the latter specimen than that of the former specimen. These relationships established between these distinct 304L SS specimens demonstrate how prior microstructural characteristics, such as inclusions, porosity, and compressive residual stresses, can qualitatively and/or quantitatively in a relative manner impact the pitting corrosion characteristics of 304L SS alloy.

13. From the corrosion analysis of as-deposited and polished CS, LACS, and AFS 304L SS specimens with respect to both their degree of susceptibility and pitting corrosion behavior (involving CR and pitting potentials), it is concluded that polishing step is absolutely necessary for these specimens to exhibit a better corrosion behavior, by the decrease of the surface roughness of all the three specimens and by the removal of oxide film on the surface of the latter two specimens by polishing and/or measures must be taken to restrict the formation of oxide film on the latter two specimen surfaces. However, in the case of the latter two specimens i.e., for LACS and AFS 304L SS materials, it might be cost-effective to polish them after processing rather than taking measures for the prevention of the formation of the deleterious surface oxide film which may involve performing the processes in vacuum etc. Also, it must be noted here that in the case of CS coating, polishing improved only its corrosion rate and pitting corrosion behavior and did not have any impact on its degree of susceptibility due to the coating's inherent weak interparticle bonding.
14. UNSM surface treatment performed on either the as sprayed or polished CS 304L SS coatings did not result in any improvement in its sensitization behavior because of the UNSM treatment process not involving the application of any significant amount of heat input into the specimen that is being surface treated and therefore, was not able to improve or influence the inherently weak interparticle bonding existing in the CS 304L SS coating, consequently not being able to improve its sensitization behavior. In fact, the UNSM treatment performed on the as-CS and polished CS 304L SS coatings, resulted in a slight worsening of their DOS ratios, which is attributed to the creation of sharp edged smudges on these specimen surfaces by the impact of WC tool tip on their surface during UNSM

and these sharp edged smudges acting as additional localized sites where quicker breakdown of the passive film can occur during their DLEPR corrosion tests, ultimately resulting in the UNSM treated CS 304L SS coatings to exhibit slightly worsened DOS ratios than that of their untreated counterparts. However, the factors contributing to the formation of these sharp-edged smudges on the surface of UNSM treated as-CS and polished CS 304L SS coatings are slightly different, in the case of as-CS coating, these smudges are formed due to its extremely higher surface roughness i.e., the smudging of the bubbled like surface of as-CS coating occurs by UNSM creating the smudges on its surface. Whereas in the case of polished CS coating which does not have the bubbled surface like as-CS coating due to the removal of surface unevenness by polishing, its prior cold work generated during CS processing is responsible for the creation of smudges on its surface by UNSM treatment i.e., the prior cold work or the heavy plastic deformation present in the CS coating does not allow or it restricts the dynamic penetration of WC tool tip on its surface during UNSM, contributing to the creation of smudges on its surface.

15. Similar to UNSM treated as-CS coating, the UNSM treatment performed on the bubbled like surface of as-LACS coating resulted in the creation of sharp-edged smudges on its surface, which along with the embedment of oxide particles broken down from the thin oxide film present on its surface by UNSM resulted in the as-LACS + UNSM treated coating to not exhibit any improvement in its sensitization behavior due to UNSM treatment. However, when the UNSM treatment was performed on the recrystallized LACS 304L SS coating (i.e., with better interparticle bonding than CS coating) that is free of oxide film and free of bubbled like surface due to their removal by polishing action, led to greater than 50 % betterment in its degree of susceptibility by the reduction of total porous area

i.e., the dynamic hammering of the WC tool tip on the coating surface closing some of the surface pore area by pushing the adjacent material into the pores. This improvement in the sensitization behavior of LACS + P specimen by surface treatment is attributed to the partial closure of porosity sites by UNSM leading to the formation of a stronger passive oxide film on the surface of polished LACS + UNSM treated specimen consequently resulting in a decrease in its corrosion or enhancement in its DOS ratio.

16. The UNSM treatment performed on the as-AFS 304L SS cladding surface, was able to impact the thick deleterious oxide film on its surface but was not able to completely remove it, which is why even though UNSM of as-AFS cladding resulted in an improvement in its DOS ratio, the DOS value obtained for the as-AFS + UNSM treated specimen was still significantly higher, which upon comparison to the DOS ratio of 304L SS sensitized at 650°C for 24h is still 3X times greater / worse. Even when UNSM treatment was performed on the oxide free surface of polished AFS 304L SS cladding, the surface treatment resulted in the worsening of its DOS ratio, but to an extremely smaller degree which can be considered as negligible, and upon comparing the DOS ratio of polished AFS + UNSM treated specimen with that of 304L SS specimen sensitized at 650°C for 5h, it is still ~ 70 X times lower and when compared to the DOS ratio of 304L SS specimen sensitized at 650°C for 24h, it is ~ 370X times lower, indicating that the polished AFS + UNSM treated specimen represents that of an unsensitized material with the added beneficial components of near-surface nano crystallization, near-surface hardening and high magnitude of compressive residual stresses introduced into the AFS + P cladding by UNSM. This slight worsening of the DOS ratio of polished AFS + UNSM treated specimen is because of the formation of peaks and valleys on its surface which are typical of UNSM surface treatment,

acting as additional sites where passive film can break down during the corrosion tests.

17. The UNSM treatment performed on the as-CS and as-LACS 304L SS coatings resulted in a significant decrease in their CRs, which is attributed to the significant decrease in the unevenness of their surfaces by the severe pounding of WC tool tip on their surfaces during UNSM, which in turn resulted in a decrease in the degree of concentration cells that can be setup on their surfaces by the corrosive chloride ions in the test solution. However, the surface roughness values of as-CS + UNSM and as-LACS + UNSM specimens are still notably higher than the surface roughness values of polished CS and LACS specimens therefore, allowing a median degree of concentration cells to be setup on the former specimen surfaces by the corrosive chloride ions, whose degree is lower than that of the as sprayed coatings but higher than that of the polished coatings, which is why the CRs of as-CS + UNSM and as-LACS + UNSM treated specimens have improved from that of the as-CS and as-LACS specimens CRs but are still slightly higher or worse than the CS + P and LACS + P coatings CRs. Whereas in the case of as-AFS + UNSM treated specimen, its CR worsened significantly from that of the untreated as-AFS specimen, which is attributed to the inability of UNSM to completely remove the thick oxide film on the as-AFS specimen surface and in addition, resulting in the formation of peaks and valleys in the oxide film which act as additional sites for the localized attack of corrosive species i.e., setup of concentration cells by corrosive chloride ions, leading to higher CR for the as-AFS + UNSM treated specimen from that of the untreated as-AFS specimen's CR.

18. The UNSM treatment performed on the polished CS, LACS, and AFS 304L SS specimens also yielded mixed results, where in the UNSM treatment slightly improved the CR of polished LACS and AFS specimens but slightly worsened the CR of polished CS coating.

The slight worsening of the CR of polished CS coating by UNSM treatment is attributed to the presence of prior cold work in CS coating, which is restricting the efficient dynamic penetration of WC tool tip during its UNSM treatment, leading to the creation of sharp-edged smudges on the polished CS + UNSM treated specimen surface which are acting as additional localized concentration sites for the attack of corrosive chloride ions leading to it exhibiting higher CR than that of untreated polished CS 304L SS coating. Whereas the slight enhancement of the CR of polished LACS 304L SS specimen by UNSM surface treatment is attributed to the partial closure of porosity sites on its surface by UNSM and the absence of sharp edged smudges and the absence of embedment of oxide particles on the surface of polished LACS + UNSM treated specimen, due to the recrystallized / free of cold work and oxide free surface of polished LACS coating allowing the efficient dynamic penetration of WC tool tip on its surface during UNSM treatment. And the slight enhancement in the CR of polished AFS + UNSM treated 304L SS cladding is attributed to the removal of inclusion and/or impurities from the surface of polished AFS cladding by UNSM surface treatment. Both the closure of porosity sites in the case of polished LACS + UNSM treated specimen and the removal of inclusions in the case of polished AFS + UNSM treated specimen, results in a decrease in the number of localized corrosion sites where the corrosive chloride ions can attack on their surface, which in turn results in a decrease in their CRs from that of their untreated polished counterpart specimens.

19. The pitting corrosion characteristics of as-deposited and polished CS, LACS, and AFS 304L SS specimens have all been enhanced by the application of UNSM treatment on their surfaces and this enhancement is attributed to the introduction of high magnitudes of compressive residual stresses into these materials by UNSM surface treatment. The

enhancement in the pitting corrosion behavior of polished CS, LACS, and AFS 304L SS specimens by their UNSM treatment could be seen more clearly in a quantitative manner from the shifting of their pitting potentials to more noble values after their UNSM surface treatment. Whereas the enhancement in the pitting corrosion behavior of as-deposited CS, LACS and AFS 304L SS specimens by UNSM treatment must be observed qualitatively from their CPP corrosion test curves, since the as-deposited + UNSM treated specimens do not exhibit a clear pitting potential as well similar to the untreated as-deposited specimens but the area under the hysteresis loops of as-deposited + UNSM treated specimens increased significantly from that of their untreated as-deposited specimens hysteresis loops area, indicating that the UNSM surface treatment is impacting the pitting corrosion behavior of as-deposited CS, LACS, and AFS 304L SS specimens in a positive manner by the induction of high magnitudes of compressive residual stresses into them through SPD.

20. For convenience, the impact of UNSM treatment on the corrosion behavior – degree of susceptibility, corrosion rate, and pitting potential of as-deposited and polished CS, LACS, and AFS 304L SS specimens is collectively presented in a qualitative manner in the table below and the factors that influenced the corrosion behavior of these distinct 304L SS specimens with varying surface conditions upon their UNSM treatment are discussed in detail in the conclusions 14 – 19 and the quantitative results from which these assessments are drawn are presented in sections 5.2.6 and 5.2.7 of Chapter 5 of this dissertation research work. In the table below X denotes – No significant change, Pos denotes – positive impact of UNSM and Neg – denotes negative impact of UNSM on the particular corrosion property. By observing the table below and from conclusions 7 & 8, it could be seen clearly that UNSM surface treatment is able to impact the pitting corrosion behavior of all the

different 304L SS materials possessing distinct prior microstructural characteristics consistently in a positive manner by the induction of high magnitudes of compressive residual stresses into these different 304L SS materials. However, the impact of UNSM surface treatment on the degree of sensitization or susceptibility of 304L SS alloy is found to be strongly dependent on its prior microstructural characteristics, with UNSM only being able to significantly impact the DOS in a positive manner either when the material has smaller sized chromium depleted zones (lightly sensitized) or when the material is possessing porosity with better interparticle bonding (LACS), but could not influence either when the material was porous having weak interparticle bonding and possessing cold work (CS) or when the material possesses large well-interconnected chromium depleted zones (heavily sensitized), and had negative but negligible impact when the material was 100 % dense with no chromium depleted zones (SA & AFS). Also, when the 304L SS material surface was oxidized, UNSM was not able to improve its degree of susceptibility directly at all or to the levels desired, as UNSM technique alone was found to be inefficient in eliminating the oxide film completely from the oxidized specimen's surface.

	Impact of UNSM on the respective specimen's		
Specimen	**Degree of Susceptibility**	**Corrosion rate**	**Pitting Potential**
As-CS	Neg (but small change)	Pos (significant)	Pos
As-LACS	Neg (but negligible impact)	Pos (significant)	Pos
As-AFS	Pos (improvement but irrelevant)	Neg (significant)	Pos
Polished CS	Neg (but small change)	Neg (slight change)	Pos
Polished LACS	Pos (Improvement by 50 %)	Pos (slight change)	Pos
Polished AFS	Neg (but negligible impact)	Pos (slight change)	Pos

21. Despite the 100 % austenite to martensite phase transformation seen at the surfaces of SA, Sensitized, and AFS 304L SS specimens due to their UNSM surface treatment, the improvements in the degree of sensitization of the sensitized specimen, the negligible impact on the degree of susceptibility of SA and AFS specimens, and the improvements in the pitting potential / pitting corrosion characteristics of SA, sensitized, and AFS 304L SS specimens - suggests that the strain induced martensite formed at the surfaces of these UNSM treated specimens does not have any negative impact on the corrosion behavior of 304L SS alloy. Similarly, despite the presence of both the strain induced martensite and residual austenite phases on the surfaces of UNSM treated CS and LACS 304L SS coatings, the negligible worsening of the degree of susceptibility of as-CS + UNSM, as-LACS + UNSM, and polished CS + UNSM specimens, and the 50 % improvement in the degree of susceptibility of polished LACS specimen by UNSM, and the significant improvements in the pitting potential / pitting corrosion behavior of both the CS and LACS coatings after their UNSM treatment - suggests that the mixed presence of strain induced martensite and austenite phases on the surface of 304L SS alloy does not impact its corrosion behavior in a negative manner or that they do not contribute to the formation of a galvanic couple on these 304L SS specimen surfaces. Therefore, it is concluded here that the presence of 100 % strain induced martensite or the mixed presence of strain induced martensite and residual austenite phases on the surface of 304L SS alloy does not impact its corrosion behavior in a negative manner.

6.3 Scope for Future Work

- Slow Strain Rate Tests (SSRT) of UNSM treated sensitized, CS, LACS, and AFS 304L SS materials will be useful in determining the impact of UNSM treatment on the SCC resistance characteristics of these materials and the associated fractography using advanced

microscopy techniques will be helpful in further understanding the impact of UNSM treatment on these different 304L SS materials possessing distinct microstructural characteristics.

- Studies on the inclusions present in the AFS 304L SS cladding and their removal mechanism by UNSM and the densification impact of UNSM treatment on the LACS 304L SS coatings would be very useful in further understating the impact of UNSM on the corrosion behavior and other properties of LACS and AFS 304L SS materials.
- Studying the high temperature UNSM surface treatment processing of CS 304L SS coatings would be extremely interesting to find out if it can simultaneously improve the corrosion behavior of CS 304L SS coatings along with retaining or improving its mechanical and residual stress properties with the high temperature application resulting in recrystallization of the coating and the induction of severe plastic deformation resulting in the enhancement of corrosion properties and the retention or improvement of its mechanical and residual stress properties.
- The critical size of chromium depleted zones that can be affected positively by UNSM surface treatment thereby reducing the sensitization behavior of sensitized 304L SS alloy can be studied by conducting a series of experiments on 304L SS specimens sensitized at 650°C for different periods of time in the range of 5h to 24h.
- More corrosion analysis can be performed by halting the corrosion tests at different time intervals to determine the precise pitting mechanism in the differently processed 304L SS materials studied in this research work.
- A thorough analysis on the pitted specimens along their cross section will be useful in determining the impact of UNSM surface treatment on the depth of the pits being formed.

References

[1] G. Shit and S. Ningshen, “The Effect of Severe Plastic Deformation on the Corrosion Resistance of AISI Type 304L Stainless Steel,” *J. Mater. Eng. Perform.*, vol. 29, no. 9, pp. 5696–5709, 2020.

[2] L. Ji, J. Lu, C. Liu, C. Jing, H. Fan, and S. Ma, “Microstructure and mechanical properties of 304L steel fabricated by arc additive manufacturing,” in *MATEC Web of Conferences*, 2017, vol. 128.

[3] C. Doerr, J. Y. Kim, P. Singh, J. J. Wall, and L. J. Jacobs, “Evaluation of sensitization in stainless steel 304 and 304L using nonlinear Rayleigh waves,” *NDT E Int.*, vol. 88, pp. 17–23, Jun. 2017.

[4] S. Uns and S. W. Nr, “Specification Sheet : Alloy 304 / 304H,” no. 1, pp. 9–11, 2013.

[5] X. He, T. S. Mintz, R. Pabalan, L. Miller, and G. Oberson, “Assessment of Stress Corrosion Cracking Susceptibility for Austenitic Stainless Steels Exposed to Atmospheric Chloride and Non-Chloride Salts,” *United States Nucl. Regul. Commision, Washington, DC, Rep. No. NUREG/CR-7170*, p. 173, 2014.

[6] T. M. Mekonen Bayssie, Darrell Dunn, Aladar Csontos, Leonardo Caseres, “EVALUATION OF AUSTENITIC STAINLESS STEEL DRY STORAGE CASK STRESS CORROSION CRACKING SUSCEPTIBILITY.” [Online]. Available: https://www.nrc.gov/docs/ML0923/ML092330013.pdf.

[7] A. Rustandi, Nuradityatama, M. F. Rendi, and S. Setiawan, “The use of cyclic polarization method for corrosion resistance evaluation of austenitic stainless steel 304L and 316L in aqueous sodium chloride solution,” *Int. J. Mech. Eng. Robot. Res.*, vol. 6, no. 6, pp. 512–518, 2017.

[8] S. Holzleitner, G. Mori, H. Falk, and S. Eglsaeer, “Electrochemical And Scc Behavior Of Highly Alloyed Austenitic Stainless Steels In Different Chloride Containing Media,” *CORROSION 2007*. p. NACE-07477, 11-Mar-2007.

[9] H. Jung, “Evaluation of Atmospheric Chloride-Induced Stress Corrosion Cracking of Austenitic Stainless Steel Canister,” *CORROSION 2015*. p. NACE-2015-6132, 15-Mar-2015.

[10] H. J. Qu and J. P. Wharry, “Crystallographic orientation data from chloride-induced stress corrosion crack (CISCC) paths in gas tungsten arc welded (GTAW) austenitic stainless steel 304L,” *Data Br.*, vol. 42, p. 108059, 2022.

[11] M. O. Speidel, “STRESS CORROSION CRACKING OF STAINLESS STEELS IN NaCl SOLUTIONS.,” *Metall. Trans. A, Phys. Metall. Mater. Sci.*, vol. 12 A, no. 5, pp. 779–789, 1981.

[12] S. Kim, G. Kim, C. K. Kim, and S. W. Song, “Effects of environmental parameters on chloride-induced stress corrosion cracking behavior of austenitic stainless steel welds for dry storage canister application,” *Nucl. Eng. Technol.*, vol. 56, no. 1, pp. 317–327, 2024.

[13] S. Kim, K. Ahn, G. Kim, and S. W. Song, “Synchrotron X-ray fluorescence imaging study on chloride-induced stress corrosion cracking behavior of austenitic stainless steel welds via selective corrosion of δ-ferrite,” *Corros. Sci.*, vol. 218, no. January, p. 111176, 2023.

[14] D. Enos and C. Bryan, “Final Report: Characterization of Canister Mockup Weld Residual Stresses,” *Sandia Natl. Lab. Rep.*, vol. SAND2016-1, pp. SAND2016-12375R, 2016.

[15] E. A. Trillo *et al.*, “Combined effects of deformation (strain and strain state), grain size, and carbon content on carbide precipitation and corrosion sensitization in 304 stainless steel,” *Mater. Charact.*, vol. 35, no. 2, pp. 99–112, 1995.

[16] A. S. Lima, A. M. Nascimento, H. F. G. Abreu, and P. De Lima-Neto, “Sensitization evaluation of the austenitic stainless steel AISI 304L, 316L, 321 and 347,” *J. Mater. Sci.*, vol. 40, no. 1, pp. 139–144, 2005.

[17] A. P. Majidi and M. A. Streicher, “Double Loop Reactivation Method for Detecting Sensitization in Aisi 304 Stainless Steels.,” *Corrosion*, vol. 40, no. 11, pp. 584–593, 1984.

[18] A. V. Bansod, A. P. Patil, A. P. Moon, and N. N. Khobragade, “Intergranular Corrosion

Behavior of Low-Nickel and 304 Austenitic Stainless Steels," *J. Mater. Eng. Perform.*, vol. 25, no. 9, pp. 3615–3626, 2016.

[19] W. Zhou, W. Ma, Y. Li, and Y. Sun, "Effect of Sensitizing Treatment on the Microstructure and Susceptibility to Intergranular Corrosion of High-Nitrogen Austenitic Stainless Steel," *Metallogr. Microstruct. Anal.*, vol. 10, no. 1, pp. 25–35, 2021.

[20] C. R. Bryan and D. G. Enos, "Analysis of Dust Samples Collected from Spent Nuclear Fuel Interim Storage Containers at Hope Creek , Delaware , and Diablo Canyon , California," *SANDIA Rep. SAND2014-16383*, no. July, 2014.

[21] J. Kusnick, M. Benson, and S. Lyons, "Finite Element Analysis of Weld Residual Stresses in Austenitic Stainless Steel Canisters in Dry Storage of Spent Fuel," *NRC Tech. Lett. Rep.*, no. December, pp. 1–13, 2013.

[22] Y. Toshima, Y. Ikeno, Y. Fujiwara, and Y. Nakao, "Long-Term Exposure Test for External Stress Corrosion Cracking on Austenitic Stainless Steels in Coastal Areas," *CORROSION 2000*. p. NACE-00456, 26-Mar-2000.

[23] L. Wen, Y. Wang, Y. Zhou, L. Guo, and J. Ouyang, "Microstructure and corrosion resistance of modified 2024 Al alloy using surface mechanical attrition treatment combined with microarc oxidation process," *Corros. Sci.*, vol. 53, no. 1, pp. 473–480, 2011.

[24] H. L. Chan, H. H. Ruan, A. Y. Chen, and J. Lu, "Optimization of the strain rate to achieve exceptional mechanical properties of 304 stainless steel using high speed ultrasonic surface mechanical attrition treatment," *Acta Mater.*, vol. 58, pp. 5086–5096, 2010.

[25] K. Lu and J. Lu, "Nanostructured surface layer on metallic materials induced by surface mechanical attrition treatment," *Mater. Sci. Eng. A*, vol. 375–377, pp. 38–45, 2004.

[26] H. W. Zhang, Z. K. Hei, G. Liu, J. Lu, and K. Lu, "Formation of nanostructured surface layer on AISI 304 stainless steel by means of surface mechanical attrition treatment," *Acta Mater.*, vol. 51, pp. 1871–1881, 2003.

[27] L. Tan, X. Ren, K. Sridharan, and T. R. Allen, "Effect of shot-peening on the oxidation of

alloy 800H exposed to supercritical water and cyclic oxidation," *Corros. Sci.*, vol. 50, pp. 2040–2046, 2008.

[28] D. J. Child, G. D. West, and R. C. Thomson, "Assessment of surface hardening effects from shot peening on a Ni-based alloy using electron backscatter diffraction techniques," *Acta Mater.*, vol. 59, no. 12, pp. 4825–4834, 2011.

[29] G. Liu, S. C. Wang, X. F. Lou, J. Lu, and K. Lu, "LOW CARBON STEEL WITH NANOSTRUCTURED SURFACE LAYER INDUCED BY HIGH-ENERGY SHOT PEENING," *Scr. Mater.*, vol. 44, pp. 1791–1795, 2001.

[30] V. Azar, B. Hashemi, and M. Rezaee Yazdi, "The effect of shot peening on fatigue and corrosion behavior of 316L stainless steel in Ringer's solution," *Surf. Coatings Technol.*, vol. 204, no. 21–22, pp. 3546–3551, 2010.

[31] P. S. Preve and J. T. Cammett, "The influence of surface enhancement by low plasticity burnishing on the corrosion fatigue performance of AA7075-T6," *Int. J. Fatigue*, vol. 26, pp. 975–982, 2004.

[32] J. Z. Lu *et al.*, "Effects of laser peening on stress corrosion cracking (SCC) of ANSI 304 austenitic stainless steel," *Corros. Sci.*, vol. 60, pp. 145–152, 2012.

[33] K. Y. Luo, J. Z. Lu, Q. W. Wang, M. Luo, H. Qi, and J. Z. Zhou, "Residual stress distribution of Ti-6Al-4V alloy under different ns-LSP processing parameters," *Appl. Surf. Sci.*, vol. 285P, pp. 607–615, 2013.

[34] J. Z. Lu, H. Qi, K. Y. Luo, M. Luo, and X. N. Cheng, "Corrosion behaviour of AISI 304 stainless steel subjected to massive laser shock peening impacts with different pulse energies," *Corros. Sci.*, vol. 80, pp. 53–59, 2014.

[35] A. Gill *et al.*, "Comparison of mechanisms of advanced mechanical surface treatments in nickel-based superalloy," *Mater. Sci. Eng. A*, vol. 576, pp. 346–355, 2013.

[36] C. Ye, S. Suslov, B. Joong, E. A. Stach, and G. J. Cheng, "Fatigue performance improvement in AISI 4140 steel by dynamic strain aging and dynamic precipitation during

warm laser shock peening," *Acta Mater.*, vol. 59, pp. 1014–1025, 2011.

[37] J. Z. Lu *et al.*, "Grain refinement mechanism of multiple laser shock processing impacts on ANSI 304 stainless steel," *Acta Mater.*, vol. 58, pp. 5354–5362, 2010.

[38] Q. Xue, I. J. Beyerlein, D. J. Alexander, and G. T. Gray III, "Mechanisms for initial grain refinement in OFHC copper during equal channel angular pressing," *Acta Mater.*, vol. 55, pp. 655–668, 2007.

[39] D. Song, A. B. Ma, J. H. Jiang, P. H. Lin, D. H. Yang, and J. F. Fan, "Corrosion behaviour of bulk ultra-fine grained AZ91D magnesium alloy fabricated by equal-channel angular pressing," *Corros. Sci.*, vol. 53, pp. 362–373, 2011.

[40] M. Kattoura, A. Telang, S. R. Mannava, D. Qian, and V. K. Vasudevan, "Effect of Ultrasonic Nanocrystal Surface Modification on residual stress, microstructure and fatigue behavior of ATI 718Plus alloy," *Mater. Sci. Eng. A*, vol. 711, pp. 364–377, Jan. 2018.

[41] C. Ye *et al.*, "Effects of Ultrasonic Nanocrystal Surface Modification on the Residual Stress, Microstructure, and Corrosion Resistance of 304 Stainless Steel Welds," *Metall. Mater. Trans. A Phys. Metall. Mater. Sci.*, vol. 49, no. 3, pp. 972–978, 2018.

[42] H. Zhang *et al.*, "The effects of ultrasonic nanocrystal surface modification on the fatigue performance of 3D-printed Ti64," *Int. J. Fatigue*, 2017.

[43] A. Amanov, O. V Penkov, Y. Pyun, and D. Kim, "Effects of ultrasonic nanocrystalline surface modification on the tribological properties of AZ91D magnesium alloy," *Tribiology Int.*, vol. 54, pp. 106–113, 2012.

[44] C. Ye *et al.*, "Gradient nanostructure and residual stresses induced by Ultrasonic Nano-crystal Surface Modification in 304 austenitic stainless steel for high strength and high ductility," *Mater. Sci. Eng. A*, vol. 613, pp. 274–288, 2014.

[45] S. Li, Z. Ren, Y. Dong, C. Ye, G. Cheng, and H. Cong, "Enhanced Pitting Corrosion Resistance of 304 SS in 3.5 wt% NaCl by Ultrasonic Nanocrystal Surface Modification," *J. Electrochem. Soc.*, vol. 164, no. 12, pp. C682–C689, 2017.

[46] U. Martin, J. Ress, and D. M. Bastidas, “Intergranular SCC mechanism of ultrasonic nanocrystalline surface modified AISI 304 SS in H2SO4 solution containing chloride,” *Electrochim. Acta*, vol. 405, 2022.

[47] C.-H. Han, Y. S. Phyoun, and C. S. Kim, “Ultrasonic micro-burnishing in view of eco-materials processing,” *Adv. Technol. Mater. Mater. Process. J.*, vol. 4, no. 1, pp. 25–28, 2002.

[48] I. H. Cho *et al.*, “Nano Structured Surface Modification of Tool Steel and its Beneficial Effects in Mechanical Properties,” *J. Mech. Sci. Technol.*, vol. 19, no. 11, pp. 2151–2156, 2005.

[49] A. Amanov, I. S. Cho, Y. S. Pyoun, C. S. Lee, and I. G. Park, “Micro-dimpled surface by ultrasonic nanocrystal surface modification and its tribological effects,” *Wear*, vol. 286–287, pp. 136–144, 2012.

[50] M. S. Kim, S. H. Park, Y. S. Pyun, and D. S. Shim, “Optimization of ultrasonic nanocrystal surface modification for surface quality improvement of directed energy deposited stainless steel 316L,” *J. Mater. Res. Technol.*, vol. 9, no. 6, pp. 15102–15122, 2020.

[51] M. K. Khan, M. E. Fitzpatrick, Q. Y. Wang, Y. S. Pyoun, and A. Amanov, “Effect of ultrasonic nanocrystal surface modification on residual stress and fatigue cracking in engineering alloys,” *Fatigue Fract. Eng. Mater. Struct.*, vol. 41, no. 4, pp. 844–855, Apr. 2018.

[52] X. Hou *et al.*, “A systematic study of mechanical properties , corrosion behavior and biocompatibility of AZ31B Mg alloy after ultrasonic nanocrystal surface modification,” *Mater. Sci. Eng. C*, vol. 78, pp. 1061–1071, 2017.

[53] R. K. Gupta *et al.*, “A Hybrid Laser Surface Treatment for Refurbishment of Stress Corrosion Cracking Damaged 304L Stainless Steel,” *J. Mater. Eng. Perform.*, vol. 24, no. 6, pp. 2569–2576, 2015.

[54] S. Gencalp Irizalp, B. K. Koroglu, and D. Sokol, “Influence of Laser Peening With and Without Coating on the Surface Properties and Stress Corrosion Cracking Behavior of

Laser-Welded 304 Stainless Steel," *Metall. Mater. Trans. A Phys. Metall. Mater. Sci.*, vol. 52, no. 8, pp. 3302–3316, 2021.

[55] "https://holtecinternational.com/2017/08/31/peening-to-fortify-multi-purpose-canisters-against-stress-corrosion-cracking-enters-production-following-intensive-rd-effort/." .

[56] M. John, A. M. Ralls, M. Misra, and P. L. Menezes, "Understanding the Mechanism of Stress Corrosion Cracking Resistance in Stainless Steel Welds Subjected to Laser Shock Peening without Coating for Nuclear Canister Applications," *J. Mater. Eng. Perform.*, vol. 33, no. 8, pp. 3957–3977, 2024.

[57] Y.-R. Yoo, S.-H. Choi, and Y.-S. Kim, "Effect of Laser Shock Peening on the Stress Corrosion Cracking of 304L Stainless Steel," *J. Manuf. Sci. Eng. Trans. ASME*, vol. 144, no. 6, pp. 1–21, 2022.

[58] Y. Sano *et al.*, "Retardation of crack initiation and growth in austenitic stainless steels by laser peening without protective coating," *Mater. Sci. Eng. A*, vol. 417, no. 1–2, pp. 334–340, 2006.

[59] S. Prabhakaran, A. Kulkarni, G. Vasanth, S. Kalainathan, P. Shukla, and V. K. Vasudevan, "Laser shock peening without coating induced residual stress distribution, wettability characteristics and enhanced pitting corrosion resistance of austenitic stainless steel," *Appl. Surf. Sci.*, vol. 428, pp. 17–30, 2018.

[60] R. Sundar *et al.*, "Mitigation of Stress Corrosion Cracking Susceptibility of Machined 304L Stainless Steel Through Laser Peening," *J. Mater. Eng. Perform.*, vol. 25, no. 9, pp. 3710–3724, 2016.

[61] A. Sharma, J. Song, D. Furfari, S. R. Mannava, and V. K. Vasudevan, "Influence of Laser Shock Peening and Ultrasonic Nanocrystal Surface Modification on Residual Stress, Microstructure, and Corrosion–Fatigue Behavior of Aluminum 7075-T6," *Metall. Mater. Trans. A Phys. Metall. Mater. Sci.*, vol. 54, no. 11, pp. 4233–4252, 2023.

[62] E. Maleki, O. Unal, M. Guagliano, and S. Bagherifard, "The effects of shot peening, laser shock peening and ultrasonic nanocrystal surface modification on the fatigue strength of

Inconel 718," *Mater. Sci. Eng. A*, vol. 810, no. February, p. 141029, 2021.

[63] U. S. N. R. COMMISSION, "POTENTIAL CHLORIDE-INDUCED STRESS CORROSION CRACKING OF AUSTENITIC STAINLESS STEEL AND MAINTENANCE OF DRY CASK STORAGE SYSTEM CANISTERS," 2010.

[64] E. D. Larsen, A. D. Watkins, T. R. Mcjunkin, D. P. Pace, and R. J. Bitsoi, "Remote Welding, NDE and Repair of DOE Standardized Canisters," *Idaho Natl. Lab.*, vol. 5th Intern, 2006.

[65] K. A. Ross, P. Mayur, B. Gwalani, T. J. Montoya, E. Karasz, and R. F. Schaller, "Cold Spray for Mitigation and Repair of Spent Nuclear Fuel Dry Storage Canisters," *Prep. US Dep. Energy M3SF-21PN010207032 PNNL-32917 SAND2022-6663 O*, 2022.

[66] H. Yeom, T. Dabney, N. Pocquette, K. Ross, F. E. Pfefferkorn, and K. Sridharan, "Cold spray deposition of 304L stainless steel to mitigate chloride-induced stress corrosion cracking in canisters for used nuclear fuel storage," *J. Nucl. Mater.*, vol. 538, p. 152254, 2020.

[67] D. J. Barton, V. S. Bhattiprolu, G. B. Thompson, and L. N. Brewer, "Laser assisted cold spray of AISI 4340 steel," *Surf. Coatings Technol.*, vol. 400, no. July, p. 126218, 2020.

[68] R. Nikbakht *et al.*, "Cold Spray and Laser-Assisted Cold Spray of CrMnCoFeNi High Entropy Alloy Using Nitrogen as the Propelling Gas," *J. Therm. Spray Technol.*, vol. 31, no. 4, pp. 1129–1142, 2022.

[69] P. Coddet, C. Verdy, C. Coddet, F. Debray, and F. Lecouturier, "Mechanical properties of thick 304L stainless steel deposits processed by He cold spray," *Surf. Coatings Technol.*, vol. 277, pp. 74–80, 2015.

[70] B. Dikici, H. Yilmazer, I. Ozdemir, and M. Isik, "The Effect of Post-Heat Treatment on Microstructure of 316L Cold-Sprayed Coatings and Their Corrosion Performance," *J. Therm. Spray Technol.*, vol. 25, no. 4, pp. 704–714, 2016.

[71] Y. Xie, M. P. Planche, R. Raoelison, H. Liao, X. Suo, and P. Hervé, "Effect of Substrate Preheating on Adhesive Strength of SS 316L Cold Spray Coatings," *J. Therm. Spray*

Technol., vol. 25, no. 1–2, pp. 123–130, 2016.

[72] M. Villa, S. Dosta, and J. M. Guilemany, "Optimization of 316L stainless steel coatings on light alloys using Cold Gas Spray," *Surf. Coatings Technol.*, vol. 235, pp. 220–225, 2013.

[73] X. Meng, J. Zhang, J. Zhao, Y. Liang, and Y. Zhang, "Influence of Gas Temperature on Microstructure and Properties of Cold Spray 304SS Coating," *J. Mater. Sci. Technol.*, vol. 27, no. 9, pp. 809–815, 2011.

[74] X. M. Meng, J. B. Zhang, W. Han, J. Zhao, and Y. L. Liang, "Influence of annealing treatment on the microstructure and mechanical performance of cold sprayed 304 stainless steel coating," *Appl. Surf. Sci.*, vol. 258, no. 2, pp. 700–704, 2011.

[75] B. Al-Mangour, R. Dallala, F. Zhim, R. Mongrain, and S. Yue, "Fatigue behavior of annealed cold-sprayed 316L stainless steel coating for biomedical applications," *Mater. Lett.*, vol. 91, no. 2013, pp. 352–355, 2013.

[76] K. Spencer and M. X. Zhang, "Optimisation of stainless steel cold spray coatings using mixed particle size distributions," *Surf. Coatings Technol.*, vol. 205, no. 21–22, pp. 5135–5140, 2011.

[77] R. Cortés *et al.*, "Effect of processing conditions on the mechanical performance of stainless steel cold sprayed coatings," *Surf. Coatings Technol.*, vol. 394, no. May, p. 125874, 2020.

[78] S. Adachi and N. Ueda, "Wear and corrosion properties of cold-sprayed AISI 316L coatings treated by combined plasma carburizing and nitriding at low temperature," *Coatings*, vol. 8, no. 12, 2018.

[79] B. Al-Mangour, R. Mongrain, E. Irissou, and S. Yue, "Improving the strength and corrosion resistance of 316L stainless steel for biomedical applications using cold spray," *Surf. Coatings Technol.*, vol. 216, pp. 297–307, 2013.

[80] A. M. Ralls *et al.*, "Tribological and Corrosion Behavior of High Pressure Cold Sprayed Duplex 316 L Stainless Steel," *Tribol. Int.*, vol. 169, no. February, p. 107471, 2022.

[81] D. Christoulis, M. Jeandin, E. Irissou, J.-G. Legoux, and W. Knapp, “Laser-assisted cold spray (LACS),” in *Laser-assisted cold spray (LACS)*, 2012.

[82] C. M. Roper, A. Heczel, V. S. Bhattiprolu, T. Kolonits, J. Gubicza, and L. N. Brewer, “Effect of laser heating on microstructure and deposition properties of cold sprayed SS304L,” *Materialia*, vol. 22, no. February, 2022.

[83] W. A. Story, D. J. Barton, B. C. Hornbuckle, K. A. Darling, G. B. Thompson, and L. N. Brewer, “Laser assisted cold spray of Fe–Ni–Zr oxide dispersion strengthened steel,” *Materialia*, vol. 3, no. September, pp. 239–242, 2018.

[84] B. E. T. Roper *et al.*, “Microstructure Evolution in 304L Stainless Steel Cladding Produced by Additive Friction Stir Deposition,” *Metallogr. Microstruct. Anal.*, vol. 13, no. 1, pp. 174–180, 2024.

[85] O. G. Rivera *et al.*, “Microstructures and mechanical behavior of Inconel 625 fabricated by solid-state additive manufacturing,” *Mater. Sci. Eng. A*, vol. 694, no. March, pp. 1–9, 2017.

[86] H. Beladi, E. Farabi, P. D. Hodgson, M. R. Barnett, G. S. Rohrer, and D. Fabijanic, “Microstructure evolution of 316L stainless steel during solid-state additive friction stir deposition,” *Philos. Mag.*, vol. 102, no. 7, pp. 618–633, Apr. 2022.

[87] E. Farabi, S. Babaniaris, M. R. Barnett, and D. M. Fabijanic, “Microstructure and mechanical properties of Ti6Al4V alloys fabricated by additive friction stir deposition,” *Addit. Manuf. Lett.*, vol. 2, no. January, p. 100034, 2022.

[88] International Stainless Steel forum, “ISSF_Stainless_Steel_in_Figures_2021.” 2021.

[89] J. Campbell, “issf__The Stainless Steel Family – An Overview,” *PetroSkills*, vol. 32, no. 0, pp. 1–5, 2014.

[90] M. Shirdel, H. Mirzadeh, and M. H. Parsa, “Microstructural Evolution During Normal / Abnormal Grain Growth in Austenitic Stainless Steel,” vol. 45, no. October, pp. 5185–5193, 2014.

[91] G. Suresh *et al.*, “Effect of Laser Surface Melting on the Microstructure and Pitting Corrosion Resistance of 304L SS Weldment,” *Metall. Mater. Trans. B Process Metall. Mater. Process. Sci.*, vol. 48, no. 5, pp. 2516–2525, 2017.

[92] American Iron and Steel Institute, “Welding of Stainless Steels and Other Joining Methods,” *Aisi*, pp. 1–46, 1988.

[93] S. Krishnan, J. Dumbre, S. Bhatt, E. T. Akinlabi, and R. Ramalingam, “Effect of Crystallographic Orientation on the Pitting Corrosion Resistance of Laser Surface Melted AISI 304L Austenitic Stainless Steel,” no. 4, pp. 246–249, 2013.

[94] J. Stewart and D. E. Williams, “The initiation of pitting corrosion on austenitic stainless steel: on the role and importance of sulphide inclusions,” *Corros. Sci.*, vol. 33, no. 3, 1992.

[95] D. G. Enos and C. R. Bryan, “Understanding the Risk of Chloride Induced Stress Corrosion Cracking of Interim Storage Containers for the Dry Storage of Spent Nuclear Fuel: Residual Stresses in Typical Welded Containers,” 2015.

[96] M. Bray, A. Cockburn, and W. O’Neill, “The Laser-assisted Cold Spray process and deposit characterisation,” *Surf. Coatings Technol.*, vol. 203, no. 19, pp. 2851–2857, 2009.

[97] B. Li, Y. Jin, J. Yao, Z. Li, Q. Zhang, and X. Zhang, “Influence of laser irradiation on deposition characteristics of cold sprayed Stellite-6 coatings,” *Opt. Laser Technol.*, vol. 100, pp. 27–39, 2018.

[98] J. Yao, Z. Li, B. Li, and L. Yang, “Characteristics and bonding behavior of Stellite 6 alloy coating processed with supersonic laser deposition,” *J. Alloys Compd.*, vol. 661, pp. 526–534, 2016.

[99] R. Lupoi, A. Cockburn, C. Bryan, M. Sparkes, F. Luo, and W. O’Neill, “Hardfacing steel with nanostructured coatings of Stellite-6 by supersonic laser deposition,” *Light Sci. Appl.*, vol. 1, no. MAY, pp. 1–6, 2012.

[100] E. O. Olakanmi, M. Tlotleng, C. Meacock, S. Pityana, and M. Doyoyo, “Deposition mechanism and microstructure of laser-assisted cold-sprayed (LACS) Al-12 wt.%Si

coatings: Effects of laser power," *Jom*, vol. 65, no. 6, pp. 776–783, 2013.

[101] E. Irissou, J. G. Legoux, A. N. Ryabinin, B. Jodoin, and C. Moreau, "Review on cold spray process and technology: Part I - Intellectual property," *J. Therm. Spray Technol.*, vol. 17, no. 4, pp. 495–516, 2008.

[102] J. Chen and B. Young, "Stress-strain curves for stainless steel at elevated temperatures," *Eng. Struct.*, vol. 28, no. 2, pp. 229–239, 2006.

[103] R. Morgan, P. Fox, J. Pattison, C. Sutcliffe, and W. O'Neill, "Analysis of cold gas dynamically sprayed aluminium deposits," *Mater. Lett.*, vol. 58, no. 7–8, pp. 1317–1320, 2004.

[104] R. S. Mishra, P. S. De, and N. Kumar, *Friction Stir Welding and Processing*. 2014.

[105] K. Anderson-Wedge *et al.*, "Characterization of the fatigue behavior of additive friction stir-deposition AA2219," *Int. J. Fatigue*, vol. 142, no. January 2020, p. 105951, 2021.

[106] P. S. Prevey, "X-RAY DIFFRACTION X-RAY DIFFRACTION RESIDUAL STRESS TECHNIQUES," in *Metals Handbook. 10. Metals Park: American Society for Metals*, no. 513, 1986, pp. 380–392.